



GIS-Based Infrastructure Management System for Optimized Response  
to Extreme Events of Terrestrial Transport Networks



# **Dynamic Risk-based Predictive Models**

## **D5.1**

February 2021 (V1.0)

**PUBLIC**



This project has received funding from the European Union's Horizon 2020 research and innovation programme under grant agreement No. 769255.



# SAFEWAY

GIS-BASED INFRASTRUCTURE MANAGEMENT SYSTEM  
FOR OPTIMIZED RESPONSE TO EXTREME EVENTS OF  
TERRESTRIAL TRANSPORT NETWORKS

**Grant Agreement No. 769255**

## Dynamic Risk-based Predictive Models

WP 5

PREDICTIVE MODELS

|                          |   |
|--------------------------|---|
| <b>Deliverable ID</b>    | <b>D 5.1</b>                                |
| <b>Deliverable name</b>  | <b>Dynamic Risk-based Predictive Models</b> |
| <b>Interim Del. name</b> | <b>Infrastructure Predictive Models</b>     |
| Lead partner             | UMINHO                                      |
| Contributors             | NGI, TØI, UCAM, IMC                         |

**PUBLIC**

### PROPRIETARY RIGHTS STATEMENT

This document contains information, which is proprietary to the SAFEWAY Consortium. Neither this document nor the information contained herein shall be used, duplicated or communicated by any means to any third party, in whole or in parts, except with prior written consent of the SAFEWAY Consortium.

## SAFEWAY Project Synopsis



According to European TEN-T guidelines, due consideration must be given to the risk assessments and adaptation measures during infrastructure planning, in order to improve resilience to disasters. SAFEWAY's aim is to design, validate and implement holistic methods, strategies, tools and technical interventions to significantly increase the resilience of inland transport infrastructure. SAFEWAY leads to significantly improved resilience of transport infrastructures, developing a holistic toolset with transversal application to anticipate and mitigate the effects extreme events at all modes of disaster cycle:

1. **"Preparation"**: substantial improvement of risk prediction, monitoring and decision tools contributing to anticipate, prevent and prepare critical assets for the damage impacts;
2. **"Response and Recovery"**: the incorporation of SAFEWAY IT solutions into emergency plans, and real-time optimal communication with operators and end users (via crowdsourcing and social media);
3. **"Mitigation"**: improving precision in the adoption of mitigation actions (by impact analysis of different scenarios) together with new construction systems and materials, contributing to the resistance & absorption of the damage impact.

SAFEWAY consortium has 15 partners that cover multidisciplinary and multi-sectorial business fields associated with resilience of transport infrastructure in Europe: national transport infrastructure managers & operators, a main global infrastructure operator, partners able to provide various data sources with large coverage in real time, comprehensive ITC solutions, and leading experts in resilience, risk databases, remote sensing-based inspection, and decision systems based on predictive modelling.

SAFEWAY will carry-out 4 real case studies distributed through 4 countries, linked to 5 corridors of the TEN-T Core Network. SAFEWAY has as main expected impacts:

1. at least 20% improvement in mobility; and
2. at least 20% lower cost of infrastructure maintenance.

### LEGAL NOTICE

The sole responsibility for the content of this publication lies with the authors. It does not necessarily reflect the opinion of the European Union. Neither the Innovation and Networks Executive Agency (INEA) nor the European Commission are responsible for any use that may be made of the information contained therein.



## Document Information

|                            |   |   |
|----------------------------|---|---|
| <b>Document Name</b>       | Dynamic Risk-based Predictive Models  |   |
| <b>Version No.</b>         | V1.0  |   |
| <b>Report date</b>         | 28/02/2020  |   |
| <b>Number of pages</b>     | 202   |   |
| <b>Lead Author</b>         | Monica Santamaria (UMinho), Erica Arango (UMinho), Fereshteh Jafari (UMinho), Hélder Sousa (UMinho) |   |
| <b>Other Authors</b>       | Unni Eidsvig (NGI),<br>Farrokh Nadim (NGI),<br>Luca Piciullo (NGI),<br>Ingar Haug Steinholt (NGI),  | Ronny Klæboe (TØI),<br>Johanna Ludvigsen (TØI),<br>Georgios Hadjidemetriou (UCAM),<br>José Matos (UMinho),<br>Maria Morais (UMinho) |
| <b>Other Contributors</b>  | Nikola Tanasic (IMC),<br>Rade Hajdin (IMC)  |   |
| <b>Dissemination level</b> | Public  |   |

## Document History

| Ver. | Date       | Description   | Authors   | Checked by   |
|------|------------|---|---|--|
| 0.1  | 15/06/2020 | Creation of the deliverable, structure, and ideas of contents | M. Santamaria (UMinho)  | Unni Eidsvig (NGI)   |
| 0.2  | 10/11/2020 | Preliminary draft version of the deliverable                  | M. Santamaria (UMinho)  | Nikola Tanasic (IMC)   |
| 0.3  | 22/12/2020 | Draft for review by SAFEWAY partners                          | M. Santamaria (UMinho)<br>E. Arango (UMinho)<br>F. Jafari (UMinho)<br>G. Hadjidemetriou (UCAM)<br>R. Klæboe (TØI) | Unni Eidsvig (NGI),<br>S. Cuerva Navas (Ferrovial)<br>B. Riveiro (UVigo)   |
| 0.4  | 01/31/2021 | Updated draft for review by SAFEWAY partners                  | All authors   | Unni Eidsvig (NGI),<br>Farrokh Nadim (NGI),<br>S. Cuerva Navas (Ferrovial) |

|     |            |               |             |                    |
|-----|------------|---------------|-------------|--------------------|
|     |            |               |             | B. Riveiro (UVigo) |
| 1.0 | 02/28/2021 | Final version | All authors | B. Riveiro (UVigo) |

## Document Approval

| Ver. | Name              | Position in project | Beneficiary | Date       | Visa |
|------|-------------------|---------------------|-------------|------------|------|
| 1.0  | Dr. Belén Riveiro | Project Coordinator | UVIGO       | 04/03/2021 | BR   |
|      |                   |                     |             |            |      |



## Executive Summary

The scope of this deliverable is to provide a framework for dynamic risk-based predictive models for transportation networks. First, an overview of the most common predictive models for forecasting the future condition of transportation infrastructures is presented. These models were built upon performance indicators available in large databases. Then, the possibility of updating the predictive models based on new collected information from different sources of data was introduced into the framework through Bayesian inference procedures.

Moreover, it was addressed how the occurrence of sudden events, i.e. natural and human-made events, affect the transportation network performance. In this way, a risk-based framework which enables the understanding of the effect of hazards on infrastructure assets and the associated consequences for the network was adopted. The framework is also endorsed by local and real time data to refine the risk estimation. Accordingly, return periods of extreme events and its magnitude were used to assess the direct impacts on road and railway infrastructures at both asset and network level. Additionally, two approaches were presented to facilitate the quantification of indirect impacts arising from the disruption of the transportation service and its duration, together with a review of all the socioeconomic costs associated to both road and railway disruptions.

Finally, the time-dependent factors influencing the risk assessment of transportation networks were analysed. Essentially, expected changes in the return period of hazards due to climate change were examined, with focus on floods and wildfires. Thus, direct impacts for future scenarios were assessed. Additionally, time variant socioeconomic attributes which affect the indirect impacts such as the status of a population and traffic demands were reviewed for the development of consequence models. Consequently, the proposed framework introduced in the present deliverable enables a dynamic risk assessment of transportation networks.

## Table of Contents

|   |            |
|---|------------|
| <b>Executive Summary .....</b>                              | <b>8</b>   |
| <b>Table of Contents .....</b>                              | <b>9</b>   |
| <b>Glossary of Terms.....</b>                               | <b>11</b>  |
| <b>1. Introduction .....</b>                                | <b>12</b>  |
| 1.1 Scope .....   | 13         |
| 1.2 Outline of the deliverable .....                        | 14         |
| <b>2. Overview of predictive models.....</b>                | <b>15</b>  |
| 2.1 Available databases for predictive models.....          | 16         |
| 2.1.1 Roadway and railway bridges database .....            | 16         |
| 2.1.2 Pavements database.....                               | 20         |
| 2.1.3 Rail tracks database .....                            | 21         |
| 2.1.4 UK database .....                                     | 22         |
| 2.2 Deterministic Models.....                               | 23         |
| 2.3 Stochastic Models.....                                  | 24         |
| 2.3.1 Markov Chains Model .....                             | 24         |
| 2.3.2 Collaborative Gaussian Process Regression .....       | 28         |
| 2.4 Dynamic Predictive Models .....                         | 33         |
| 2.4.1 Reliability Analysis.....                             | 34         |
| 2.4.2 Analytical Degradation Models .....                   | 38         |
| 2.4.3 Case study: application example .....                 | 43         |
| <b>3. Dynamic Risk-based Predictive Models .....</b>        | <b>57</b>  |
| 3.1 System boundaries .....                                 | 58         |
| 3.2 Hazard assessment .....                                 | 60         |
| 3.2.1 Characterization from existing flood hazard maps..... | 63         |
| 3.2.2 Statistical analysis of flow discharge data .....     | 65         |
| 3.2.3 Flow discharge from hydrologic modelling .....        | 70         |
| 3.2.4 Real-time data .....                                  | 71         |
| 3.3 Infrastructure performance functions .....              | 72         |
| 3.4 Consequences to infrastructure network.....             | 74         |
| 3.4.1 Crowd sourcing data .....                             | 74         |
| <b>4. Fragility functions for flood hazard.....</b>         | <b>76</b>  |
| 4.1 Bridge fragility functions .....                        | 76         |
| 4.1.1 Bridge failure modes in a flooding event.....         | 78         |
| 4.1.2 Definition of bridge classes for SAFEWAY pilot.....   | 84         |
| 4.1.3 Intensity Measure .....                               | 89         |
| 4.1.4 Treatment of uncertainties .....                      | 89         |
| 4.1.5 Time-dependent fragility assessment.....              | 90         |
| 4.1.6 Damage states and bridge functionality .....          | 92         |
| 4.1.7 Example of bridge fragility function .....            | 93         |
| 4.2 Road fragility functions .....                          | 99         |
| 4.3 Roadway embankment fragility functions .....            | 100        |
| 4.4 Railway embankment fragility functions .....            | 101        |
| <b>5. Assessment of direct impacts .....</b>                | <b>103</b> |
| 5.1 Assessment of direct impacts at asset level .....       | 103        |
| 5.2 Assessment of direct impacts at network level .....     | 105        |
| 5.2.1 Methodology .....                                     | 105        |
| 5.2.2 Application and results.....                          | 110        |

|           |  |            |
|-----------|--|------------|
| <b>6.</b> | <b>Assessment of indirect impacts .....</b>  | <b>115</b> |
| 6.1       | Simplified assessment of probability of flooding and duration of service disruption<br>116 |            |
| 6.1.1     | Probability and consequence classes .....  | 116        |
| 6.1.2     | Workflow for the assessment .....  | 117        |
| 6.1.3     | Methodology for the assessment of consequences and ranking of risk.....                    | 118        |
| 6.1.4     | The GIS analyses .....   | 119        |
| 6.1.5     | Results of the assessment .....  | 119        |
| 6.2       | Assessment of service disruption through traffic models.....                               | 123        |
| 6.2.1     | Building the road network .....  | 123        |
| 6.2.2     | Generate the traffic .....   | 123        |
| 6.2.3     | Recognizing more critical scenarios .....  | 124        |
| 6.2.4     | Road traffic model .....   | 124        |
| 6.2.5     | Scenarios .....  | 124        |
| 6.2.6     | Results .....  | 126        |
| 6.3       | Socioeconomic costs of roadway infrastructure disruptions .....                            | 129        |
| 6.4       | Socioeconomic costs of railway infrastructure disruptions .....                            | 131        |
| 6.4.1     | Goods characteristics.....   | 132        |
| 6.4.2     | Just-in-time delivery requirements .....   | 132        |
| 6.4.3     | Quick response demands .....   | 132        |
| 6.4.4     | Future Economic calculations .....   | 133        |
| 6.5       | Dynamic Economic Calculation Tool .....  | 133        |
| 6.6       | Number of 100-year floods between 2021-2100.....   | 134        |
| 6.7       | SAFEWAY enhancement for analysing resilience policies .....                                | 135        |
| <b>7.</b> | <b>Projections of long-term consequences .....</b>   | <b>137</b> |
| 7.1       | Dispersion of future hazards .....   | 137        |
| 7.1.1     | Change in return period of hazards due to climate change.....                              | 137        |
| 7.1.2     | Identification and review of hazard maps including climate change projections<br>141       |            |
| 7.1.3     | Future exposure of transportation system .....   | 143        |
| 7.1.4     | Modelling of direct flood damage in future climate .....                                   | 145        |
| 7.2       | Population models .....  | 148        |
| 7.2.1     | Future impacts are more heavily discounted .....   | 148        |
| 7.2.2     | Monte Carlo modelling of economic indicators .....   | 149        |
| 7.2.3     | Diminishing returns of investments .....   | 149        |
| 7.2.4     | Demographic change in Europe.....  | 149        |
| 7.2.5     | Predicted population change in demonstration area .....                                    | 152        |
| 7.3       | Time-variant consequence models.....   | 153        |
| <b>8.</b> | <b>Conclusions .....</b>   | <b>154</b> |
|           | <b>Acknowledgements .....</b>  | <b>156</b> |
|           | <b>References .....</b>  | <b>157</b> |
|           | <b>Appendices Content.....</b>   | <b>173</b> |
|           | • Appendix 1: Deterministic Models .....   | 174        |
|           | • Appendix 2: Stochastic Models .....  | 173        |
|           | • Appendix 3: Fragility Functions.....   | 173        |
|           | • Appendix 4: Population Changes.....  | 200        |

## Glossary of Terms

|                      |  |
|----------------------|--|
| Predictive model     | Predictive modelling is a technique that uses mathematical and computational methods to predict an event or outcome. The model is used to forecast an outcome at some future state based upon changes to the model inputs.   |
| Deterministic models | Deterministic models are dependent on a mathematical or statistical formula. The output of this model is expressed by deterministic values that represent the average predicted outcome, i.e., no randomness in the input nor the output is considered.  |
| Stochastic models    | Stochastic models are used to represent the dynamics of physical processes that evolve over time according to random phenomena.  |
| PI                   | Performance Indicator(s) is/are metric(s) that define qualitatively and/or quantitatively the condition state an asset.  |
| Reliability          | Structural reliability is a measure of the capability of a structure to operate without failure when put into service.   |
| Hazard               | A dangerous phenomenon resulting from a natural process or a human activity, which triggers a condition that may cause loss of life, injury or other health impacts, property damage, loss of livelihoods and services, social and economic disruption, or environmental damage.   |
| Consequence          | The outcomes or potential outcomes arising from the occurrence of an adverse event, expressed qualitatively or quantitatively in terms of monetary loss, disadvantage or gain damage, injury or loss of life. Consequences could be characterised as direct and indirect. Direct consequences refer to a physical destruction of exposed elements, and indirect consequences stem from related impacts that this destruction has on the functionality of elements. |
| Failure              | General term to refer to a different type of failures such as structural failure or functional failure (unavailability). Due to slow (deterioration) and sudden (e.g., natural hazard) processes, damages may occur that result in additional failure modes. These are quasi-permanent or transient situations that violate code specifications or owner's/operator's provisions. Here included are situations that might compromise public perception of safety.  |
| Fragility curve      | Fragility curves are functions that describe the probability of failure, conditioned on the load, over the full range of loads to which a system might be exposed. The probability of failure could also encompass probability of exceeding predefined damage states.  |
| Risk                 | Measure of the probability and severity of an adverse effect to life, health, property, economic activities or the environment. Quantitatively, Risk = Hazard · Potential Worth of Loss. This can be also expressed as "Probability of an adverse event times the consequences if the event occurs" (ISSMGE TC32, 2004)  |
| Resilience           | The ability of a system to resist, adapt to and recover from the effects of a hazard in a timely and efficient manner, including through the preservation and restoration of its essential basic structures and functions through risk management.   |

## 1. Introduction

A successful asset management system highly depends on determining the optimum intervention actions that assure structural safety, serviceability and reliability, while maintaining the lowest investment of financial costs related to available management budget and associated resources. In order to achieve this, one of the keys of asset management systems are predictive models that allow to forecast, for different time periods, the performance of the asset taking into account both the resistance of the asset itself, as well as the demand values the asset is exposed to. Hence, the subsequent modules regarding the time and the extent of the maintenance actions needed, depend entirely on the deterioration/performance model established, the load/demand values, the consequences triggered in case of failure, and the costs related to each type of intervention.

Following Bukhsh and Stipanovic (2020), the maintenance expenditure ranges from 50% to 70% with respect to the overall life cycle cost of a structure. These outlays of maintenance are even higher in case of sudden break-down and rearrangement of scheduled activities. Predictive maintenance seeks to prevent these asset failures completely and aims at lower maintenance costs and higher reliability and availability. As mentioned in Karimzadeh and Shoghli (2020), predictive approaches for maintenance management provide optimal long-term planning capability and integrate risk management into asset maintenance planning. Furthermore, they allow for more accurate condition prediction of transportation assets, as knowledge about time, location and extent of foreseen failures help asset owners and managers to be prepared to implement associated interventions to prevent those failures. One of the major limitations of using reactive maintenance is the lack of such information. Therefore, reactive maintenance activities are expected to take longer than initially anticipated and may be relatively more expensive. This means that, for reactive management, budget allocation and coordination of maintenance resources are poor. In contrast, proactive maintenance prevents most of the failures and enables asset owners to manage maintenance actions. In addition, the proactive strategy improves the reliability of the performance of transportation assets by avoiding failures. Although being asset-dependent, according to estimations by Marshall Institute (2020), the reactive approach costs companies up to 5 times more than proactive types of maintenance, where predictive modelling is included.

Moreover, predictive methods let asset managers anticipate and perform inspection and maintenance actions based on available information, allowing for a more efficient allocation of budget resources since a preventive procedure implementing a series of regular periodic actions with specified time intervals may result in unnecessary maintenance works. Lastly, these management strategies should also consider the fact that several infrastructure assets may be simultaneously affected as a result of extreme natural or human-made hazards.



---

Even though these events have a low probability of occurrence, the costs associated with various infrastructure assets becoming non-operational are large, for both infrastructure owners and users. In this sense, management strategies must be established considering all potential economic losses, as well as social and environmental impacts. Accordingly, risk-based predictive models have been implemented in this deliverable aiming at supporting optimal decisions for transportation networks.

The impact of predictive models on the SAFEWAY project corresponds to a better definition of the performance of the assets for different maintenance expectance times attending to several conditions such as performance of the assets based on deterioration models, demand based on population changes, and external load changes either due to different frequency or intensity. Although, the involved asset managers already have a condition-based assessment for management and intervention planning, the quantitative impact analysis of the predictive models will be assessed within the improved management system and intervention planning considering their use.

## **1.1 Scope**

This deliverable comprises the main results obtained by implementation of deterministic and stochastic predictive models, as well as the framework detailing for a dynamic risk-based model, whereby real-time data and time-variant factors are introduced. The models are based and validated in databases retrieved from different SAFEWAY partners.

The databases and associated assets are described, and validation of the models is made for the assets with more substantiated data. Therefore, special attention was given to bridges (both roadway and railway) and pavements. Based on different demand scenarios, such as flood events with different return periods (changing periodicity and intensity), the performance of the transportation assets is assessed through the use of fragility functions, and respective consequences are estimated. The key performance indicators of the analysed system are given in terms of impact, both direct and indirect, assuming different traffic scenarios and socioeconomic conditions. Long-term consequence projections are also made assuming variability on the demand and exposure, and on population demographics.

This report ultimately describes the framework for predictive modelling implementation within an asset management system. This will allow for an initial validation of the procedure using existing databases and highlighting both the possibility of updating the results by different methods and inspection information. Moreover, its application is possible for extension on the long-term prediction of consequences by assuming different variability levels.

---

## 1.2 Outline of the deliverable

One of the main objectives of this deliverable is to provide a framework for dynamic, risk-based predictive modelling. In order to do so, the deliverable is organised as follows. First, an overview of the most common predictive models for forecasting the future condition of transportation infrastructures is presented in Chapter 2. Subsequently, the possibility of updating the predictive models based on new collected information is introduced into the framework through Bayesian inference procedures. The updated condition is then used to assess the probability of failure of the infrastructures when exposed to natural hazard events. Chapters 3 and 4 present the framework for asset performance determination based on dynamic risk-based predictive models and determination of fragility curves.

Based on the prior results, the direct and indirect consequences resulting from the failure of the infrastructures are estimated in order to quantify the risks. This is presented in Chapters 5 and 6. Considering the time-dependent characteristics of traffic demands and population growth, projections of long-term consequences are evaluated in order to obtain dynamic risk-based predictive models in Chapter 7.

Finally, conclusions are given with respect to the obtained results as well as its applicability within the overall concept of the SAFEWAY project.

## 2. Overview of predictive models

Transportation infrastructure assets deteriorate as a result of several threats such as exposure to adverse environmental and climatic conditions, natural and man-made hazards. Moreover, changing load demands due to e.g., increasing traffic volumes resulting from population and economic growth, poor quality of construction materials, or insufficient maintenance, may accelerate infrastructure deterioration. Therefore, infrastructure managers have the challenge of defining optimal maintenance, rehabilitation, and replacement actions to guarantee the functionality of their vulnerable infrastructure systems. To achieve this goal, it is essential to reliably assess the condition of infrastructure assets and accurately predict their deterioration over their service life.

Several condition assessment tools to estimate asset's damage have been developed over the years such as visual surveys, probing, non-destructive techniques (NDT) and structural health monitoring (SHM) (Faleschini, Zanini and Casas Rius, 2019). The damages found are communicated through performance indicators (PIs), which are metrics that define qualitatively and/or quantitatively the condition state of assets. Faleschini et al (2019) classified the PIs in two main categories: operational and research indicators. The former indicators are based on a qualitative scale adopted, where one value is defined as the new condition, and the remaining values represent a deviation from the new condition. Conversely, research indicators are based on a quantitative evaluation of the structural safety of the assets, i.e., computing the probability of failure for a given limit state.

Due to the differences among PIs, numerous predictive models have been developed. Many applications use operational PIs, i.e., condition ratings, due to the large amount of assets that transportation agencies must manage, which poses a challenge to implement research indicators. Applications of predictive models based on condition ratings is extensive and include (but is not limited to): deterministic models (e.g. Morcoux 2011), stochastic models (e.g. Denysiuk et al. 2016), artificial intelligence techniques (e.g. Burgueño, Zhe, and others 2008; Bu et al. 2014), Bayesian networks (e.g. Zhang and Marsh 2019), and Petri nets (e.g. Le and Andrews 2016). Among them, deterministic and stochastic Markov models are the most frequent predictive models used in current Infrastructure Management Systems (Mirzaei *et al.*, 2014). In this section, deterministic and stochastic models were implemented and validated with real case studies. Given the limitations exhibited by stochastic Markov models, a methodology involving collaborative Gaussian Process Regression (GPR) was proposed (Hadjidemetriou, Xie and Parlikad, 2020).

Finally, in the last part of this section, a methodology is elaborated to introduce structural reliability as PI to assess the condition of infrastructures together with the possibility of updating the measured condition based on data from remote monitoring technologies. This methodology based on a more quantitative indicator is encouraged, as the implementation of deterioration models based on operational PIs suffer from several shortcomings including a significant subjective variability of the condition ratings assigned by different inspectors, which makes it difficult to

observed the true state of the infrastructure and predict its deterioration reliably (Santamaria Ariza *et al.*, 2020).

## 2.1 Available databases for predictive models

Infraestruturas de Portugal, S.A. (IP) is a public company managing the largest stock of assets in Portugal. IP manages more than 15.000 km of roads, 2.600 km of railways, more than 7.500 bridges and many sub-systems as signalling, catenary or power supply (Morgado *et al.*, 2019).

IP's asset portfolio is mainly comprised by the following asset types:

- Rail network: earth retaining structures, bridges, tunnels, tracks, switches and crossings (S&C), signalling systems, catenary, and power supply installations;
- Road network: pavements, bridges (including overpasses, culverts, underpasses, cattle creeps, viaducts, pedestrian crossings, and tunnels).

Asset management systems were developed and implemented during the last ten to fifteen years for road pavements and bridges (both road and rail). For the remaining asset types, regular inspections were carried out, but only to define short- to medium-term activities without implementing a formal asset management system.

Given that IP resulted from a merger process between the former road network infrastructure manager (EP -Estradas de Portugal) and the former rail network infrastructure manager (REFER - Rede Ferroviária Nacional), different performance indicators were defined to assess the condition of each asset type. Efforts have been done recently to harmonize the performance indicators across multiple assets to better communicate and support decision making (Morgado *et al.*, 2019). Nevertheless, the databases continue to maintain the asset specific performance indicators, which are described in the following sections and are used for the development of the predictive models.

### 2.1.1 Roadway and railway bridges database

IP's Bridge Management System, SGOA, is a decision support tool implemented since 2006 with the main goal of prioritising interventions. The SGOA is comprised by an inventory module which collects data regarding the assets; an inspection module which collects data from principal, routine and sub-aquatic inspections and assess the damages; and a maintenance, repair, rehabilitation, and replacement module for planning short-term intervention plans (IP, 2017).

Principal inspections are performed with a frequency of 5-6 years by qualified engineers through a close visual observation to each bridge component in order to assess the bridge safety. Generally, roadway bridges comprise the components enumerated in Figure 1, where number 1) refers to the complete infrastructure; 2) wing walls; 3) slopes; 4) abutment; 5) bearing devices; 6) piers; 7) deck; 8) kerb; 9) parapet; 10) guardrails; 11) sidewalk; 12) pavement; 13) drainage system; and 14) expansion joints. Accordingly, based on the inspection findings, a condition state (CS) for each bridge component is assigned, and consequently a global CS is assigned to the bridge. Table 1 presents the CS scale used for roadway bridges. The obtained CS defines the urgency of the intervention to be conducted.

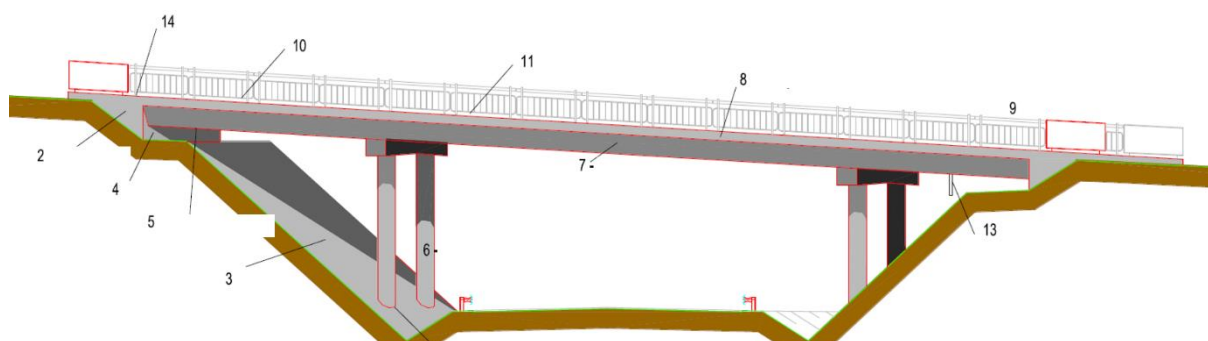


**Figure 1. Main components of roadway assets (source: Infraestruturas de Portugal, S.A.)**

**Table 1. Performance indicators used for the condition of roadway bridges (source: Infraestruturas de Portugal, S.A.)**

| Condition State | Description  | Action   |
|-----------------|--------------|--|
| 0               | Excellent    | Repair is no required  |
| 1               | Very Good    | Some repair is required  |
| 2               | Good         | Non-priority repairs are necessary   |
| 3               | Satisfactory | Materials quality or their execution appears is poorer. The deficient operation, with special importance in the durability of the infrastructure. The intervention can be carried out between 3 to 5 years.  |
| 4               | Deficient    | The start of the intervention in the short term (2 years) must be specified. It is verified that the quality of the materials or their execution is more defective in function with importance in the durability and behaviour of the infrastructure.    |
| 5               | Bad          | The start of the intervention must be specified urgently or in the short term (advisable 1 year and a maximum of 2 years). The need for a reinforcement/rehabilitation project must be specified. Road traffic restriction measures must be implemented. |

Railway bridges generally comprise the same components as roadway bridges but differ in the deck slab, as the railway deck is composed of rail tracks, sleepers, and

ballast. As previously mentioned, the CS scale used for railway bridge components slightly differs from roadways as shown in Table 2.

**Table 2. Performance indicators used for the condition of railway bridge components (source: Infraestruturas de Portugal, S.A.)**

| Condition State | Definition  | Action                                     |
|-----------------|---|--|
| 0               | Normal operating state                                | -  |
| 1               | Existence of defects that do not affect the operation | No long-term corrective action             |
| 2               | Probable or latent failure status                     | Corrective action in the medium term       |
| 3               | Imminent failure state                                | Corrective action in short- to medium-term |
| 4               | Failure state   | Immediate corrective action                |

On the other hand, routine inspections are conducted every two years, intercalated between principal inspections. During this type of inspections, a Maintenance State (MS) indicator is evaluated. This indicator may adopt two different states, namely "Priority" or "Non-priority", which represents the urgency of maintenance activities for each bridge component. Basically, the "non-priority" indicator is characterized by maintenance activities which do not have to be carried out in the short-term, while the "priority" indicator comprises maintenance needs that should be performed immediately, as they can compromise the bridge and user's safety.

Finally, sub-aquatic inspections are carried out with a frequency of maximum 5 years, ideally associated with the principal inspections. It should be noted that the frequency of the inspections is also governed by the condition state of the asset. In general terms, if the CS assigned for the asset is equal or higher than 3, the next principal inspection should be performed within 1-3 years depending on the surveillance regime defined, i.e. strengthen surveillance (CS=3), or high surveillance (CS $\geq$ 4) (IP, 2017).

The roadway database for the SAFEWAY pilot comprises inspection records from 221 different assets by the year 2019. The earliest inspections date from 2006, covering a span of approximately 13 years. As the principal inspections are performed every 5-6 years, most of the assets have 2 records. Moreover, some bridges were recently built, resulting in a lower number of available inspections. Similarly, the railway database comprises inspections records from 168 assets by the year 2019. In this case, the earliest inspections date from 2000, covering a span of approximately 19 years. Thus, most of the assets have 3 records (see Table 3). In addition to recording the CS, both databases contain information about the assets such as structure type, year of construction, number of spans, asset

length and width, and deck material. Table 3 summarizes some relevant information about the distribution of bridges according to selected attributes.

**Table 3. Distribution of bridges according to selected parameters**

| Structure Type                                       | Construction Year |     | Deck Material |     | Ro | Ra                  |     |    |    |    |
|--|-------------------|-----|---------------|-----|----|---------------------|-----|----|----|----|
|  | Ro                | Ra  | Ro            | Ra  |    |                     |     |    |    |    |
| Culvert  | 59                | 66  | 1850-1900     | 4   | 47 | Reinforced Concrete | 163 | 92 |    |    |
| Pedestrian Crossing                                  | 2                 | 20  | 1900-1920     | 2   | 4  | Masonry             | 31  | 48 |    |    |
| Bridge   | 34                | 27  | 1920-1940     | 9   | 4  | Metallic            | 27  | 28 |    |    |
| Overpass   | 48                | 25  | 1940-1960     | 1   | 9  |                     |     |    |    |    |
| Underpass  | 27                | 29  | 1960-1980     | 10  | 3  |                     |     |    |    |    |
| Cattle Creep   | 26                | (-) | 1980-2000     | 123 | 33 |                     |     |    |    |    |
| Tunnel   | 1                 | (-) | 2000-2020     | 43  | 22 |                     |     |    |    |    |
| Viaduct  | 24                | 1   | NA            | 29  | 46 |                     |     |    |    |    |
| Condition States                                     |                   |     |               |     |    |                     |     |    |    |    |
|  | Roadway           |     |               |     |    | Railway             |     |    |    |    |
|  | 1                 | 2   | 3             | 4   | 5  | 1                   | 2   | 3  | 4  | 5  |
| Deck – Reinforced Concrete                           | 192               | 102 | 14            | 5   | 2  | 110                 | 51  | 1  | 27 | 4  |
| Deck – Masonry                                       | 14                | 36  | 10            | 4   | 0  | 22                  | 55  | 4  | 47 | 7  |
| Deck – Metallic                                      | 7                 | 5   | 1             | 0   | 0  | 32                  | 23  | 1  | 18 | 0  |
| Abutments  | 284               | 120 | 28            | 3   | 2  | 241                 | 114 | 3  | 42 | 13 |
| Bearing Devices                                      | 144               | 39  | 5             | 2   | 0  | 84                  | 0   | 32 | 6  | 3  |
| Expansion Joints                                     | 115               | 66  | 23            | 11  | 0  | 55                  | 7   | 0  | 0  | 0  |
| Piers  | 181               | 38  | 9             | 1   | 0  | 84                  | 22  | 0  | 10 | 0  |
| Slopes   | 279               | 105 | 25            | 6   | 0  | 304                 | 30  | 2  | 8  | 3  |
| Wing Walls   | 266               | 113 | 19            | 8   | 1  | 208                 | 101 | 4  | 40 | 7  |
| Ro = Roadway;<br>Ra = Railway;<br>NA = Not available |                   |     |               |     |    |                     |     |    |    |    |



From Table 3 it can be observed that there is a low number of very low condition ratings in comparison with the number of available mid-condition ratings. Also, it should be noted that the CS from both roadways and railway assets were harmonized into 5 states, in order to enable their direct comparison in the development of stochastic predictive models (Chapter 2.3). To this end, condition states "0" and "1" from roadway assets were merged into a CS "1", as both states (excellent and very good) are very similar and are comparable with the definition of the best CS from railways (normal operating state). Furthermore, some filtering was performed to both databases in order to remove inconsistencies before its implementation in the stochastic predictive models. For instance, records without CS were removed, along with cases where an improvement in the CS was observed. This latter effect can be attributed to maintenance actions, or condition assessment inaccuracy due to the inherent subjectivity of inspectors during the visual inspection technique (as further discussed in Santamaria Ariza et al. (2020).

### 2.1.2 Pavements database

IP's Pavement Management System, SGPav, was developed between 2003 and 2007. The first network-wide inspections were performed in 2007, and the frequency of inspections has been annual since then (Morgado *et al.*, 2019).

The database provided by IP contains 311 km of pavements within the flood case study and 119 km of the fire case. Those pavement lengths are divided in sections of 100 m. and classified according; First, type of road such as principal routes, complementary routes, national roads, secondary national roads and regional roads<sup>1</sup>. Second, type of region such as Leiria, Coimbra or Santarem. And third, these sections are also classified according to the annual average daily traffic (AADT). The database incorporates other information such as the identification of each section within the National Highway Plan; year of construction, with some sections built since 1972 and Km descriptions (initial and final). The main pavement sections include annual inspections from 2012 to 2018, in which inspections are consigned as each of the components shown in Eq. 1 and provide information regarding maintenance process apply as well. Finally, it is important to highlight that the quality index of the complete sections depends on the average of all the corresponding 100 m sections.

The quality evaluation methodology used within SGPav is based on a Quality Index (QI), which characterizes the pavement condition as a function of several parameters collected for a given network stretch. The QI is based on the PSI value (Present Serviceability Index), through information obtained by AASTHO. The QI is obtained by the Eq. (1)

$$QI_t = 5 e^{-0.0002030 IRI_t} - 0.002139 R_t^2 - 0.03 C_{3t}^{0.5} \quad (1)$$

<sup>1</sup> *Itinerários Principais (IP), Itinerários Complementares (IC), Estradas Nacionais (EN), Estradas Nacionais secundarias (End), Estradas regionais (ER)*



Where:

$IRI_t$ : Pavement longitudinal irregularity in year  $t$  (mm/km)

$R_t$ : Road depth average in year  $t$

$C_{ct}$ : Cracked area coefficient in year  $t$  ( $m^2/100m^2$ )

QI can be measured in a range from 0 to 5, where 5 means the pavement has not suffered any alteration. Otherwise, the QI is divided into 4 levels according to the distribution shown in Table 4.

**Table 4. Performance indicators used for the condition of pavements**

| Qualitative scale  | QI          |
|--------------------|-------------|
| Good               | 4.50 - 3.50 |
| Satisfactory       | 3.49 - 2.50 |
| Requires attention | 2.49 - 1.50 |
| Unsatisfactory     | 1.49 - 0.50 |

The deterministic models (Chapter 2.2) were built from a set of filtered data according to the classifications mentioned above (type of road, type of region and AADT). These filters were applied in order to eliminate missing, duplicate or active data with important maintenance actions and obtain a reliable data set for deterioration models. It is important to mention that into the AADT classification there are three different ranges  $AADT < 2500$ ,  $2500 < AADT < 7500$  and  $AADT > 7500$ .

### 2.1.3 Rail tracks database

Currently, there is no management system implemented for rail tracks. However, condition-based inspections are performed continuously. Track inspection is performed using the EM-120, a self-propelled car, which measures the track geometric parameters, such as gauge changes, longitudinal level, cross-level, track alignment and cant, through a laser measurement system (Morgado *et al.*, 2019). The condition estate is classified according to EN 14363, which provides a track geometry limits QN1, QN2 and QN3 (see Table 5). The quality index is obtained at each 200 metres.

The information provided by IP contains three types of data, track characteristics, time and inspection data. First, the track characteristics concern those aspects inherent to the railway track, being subdivided into (i-1) line track location and (i-2) velocity class attributed by the asset manager. Second, the time data concern the (ii-1) last year of renovation that was assumed as the year zero (due to the non-possibility of knowing the construction date) and (ii-2) inspection year that corresponds to the time when the measurements of data were made. Finally, the

inspection data concerns the type of track measurements that were made during each year of inspection (e.g., track geometric parameters).

**Table 5. Performance indicators used for the condition of rail tracks (source: Infraestruturas de Portugal, S.A.)**

| Designation | Limits  | Action state  |
|-------------|---|---|
| QN1         | $\leq$ Alert limit                                  | Sections in perfectly normal operating conditions, there is no need to plan for additional maintenance.   |
| QN2         | $>$ Alert limit,<br>$\leq 1.3 * \text{alert limit}$ | Sections are in normal operating conditions. However, the need to plan maintenance actions should be evaluated, in the context of the short-term plan of the asset management plan.   |
| QN3         | $> 1.3 * \text{alert limit}$                        | Sections that are in a deficient operating situation, without necessarily jeopardizing the sequestration. However, more pressing maintenance actions should be planned, in the context of the short-term plan of the asset management plan. |

Taking into account that information, the data are clustered assuming that the non-influence of the line track location for the track degradation. Consequently, it is applying a cluster regarding the velocity class and the type of track. Due to the existences of segments with different dates of last year of renovation, sub-groups are created according to that date (last year of renovation). Moreover, based on the time of each inspection year since the last year of renovation it was assumed the time after last renovation (e.g., 2 years) to be used for the evaluation of the degradation of the provided data over the time, in both sub-groups and analyse groups.

#### **2.1.4 UK database**

The methodology proposed based on Collaborative Gaussian Process Regression (Chapter 2.3.2) could not be applied to the IP's dataset since there were limited inspection data for every bridge. Another dataset was provided by a large transport infrastructure owner in the UK. The dataset consists of inspection records of several bridges across the UK maintained by the organisation. Bridges undergo regular inspections every three or four years. Maintenance is recommended when the condition is lower than predefined threshold values. Each bridge component is rated independently based on the infrastructure owner's internal specifications.

The PI used by the organization for the assessment of bridges corresponds to a condition index, which ranges from 100 to 0, with 100 indicating perfect condition. Different infrastructure owners use different condition indices. However, the presented prediction methodology applies to any bridge element, rated by any infrastructure owner.

## 2.2 Deterministic Models

Deterministic predictive models establish an empirical formula for the relationship between the factors affecting infrastructure deterioration and the measured condition. The output of a deterministic model represents the average predicted condition, with no probabilities involved. Several research studies have applied these deterministic methods such as straight-line extrapolation, linear, non-linear, and stepwise regressions, and curve-fitting techniques to model infrastructure deterioration (e.g. (Bolukbasi, Mohammadi and Arditi, 2004; Morcous, 2011; Tolliver and Lu, 2012; Lu, Wang, and Tolliver, 2019)).

To develop regression models, a correlation analysis was initially carried out as an attempt to reveal the strength of the relationship between the PI of an asset component and the variables that more significantly influence its condition (explanatory parameters). Different regressions were implemented to the pavements and rail tracks database. It was necessary to apply different clusters for each database due to a large amount of data. Those clusters were considered as mentioned in section 2.1. For instance, in the pavement database, the filters considered among other were road type, region type, and AADT. After verifying that it does not follow a normal distribution, through Spearman's coefficient (using BMI SPSS software) a weak correlation was found between the quality index and the variables considered. Details of this procedure can be found in Appendix 1. Table 6 shows the correlation results. The table shows a minimum level of correlation between QI and the other variables. However, the Spearman  $\rho$  values are less than 0.3, indicating a minimum dependence for these variables with QI.

**Table 6. Spearman correlations between Quality Index and other variables**

|   | <b>Correlation coefficient</b> | <b>Sig. (2-tailed)</b> | <b>N</b> |
|---|--------------------------------|------------------------|----------|
| Inspection Year   | -0,004                         | 0,601                  | 20270    |
| ADTT  | 0,085**                        | 0,000                  | 20270    |
| ADT   | 0,101**                        | 0,000                  | 20270    |
| Year built  | -0,143**                       | 0,000                  | 20061    |
| Age at inspection   | 0,117**                        | 0,000                  | 20061    |
| Type of road  | -0,243**                       | 0,000                  | 20270    |
| Region  | -0,225**                       | 0,000                  | 20270    |
| ** Correlation is significant at the level 0,01 (2-tailed). |                                |                        |          |

Consequently, the degradation model considered the quality index as a dependent variable and the Age at inspection as an independent variable. Posterior, model regressions were applied and compared regarding  $R^2$  value, in order to select the model that best fits with the data. The degradation models for the national road (EN) in the Leiria region and an annual average daily traffic of less than 2,500, is shown in Figure 2.

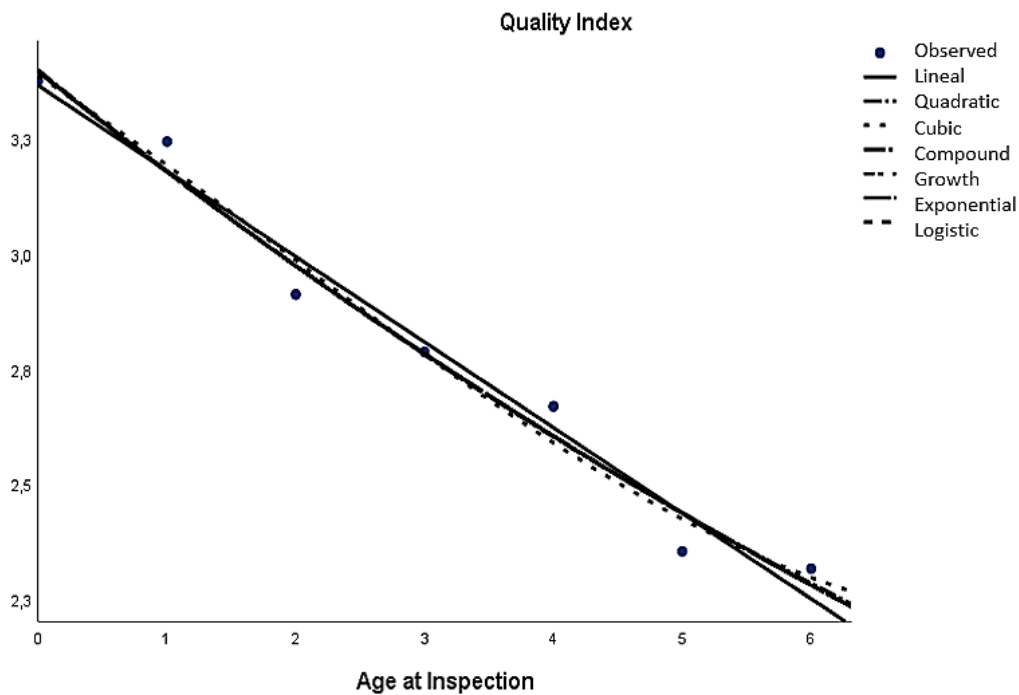


**Figure 2. Model regressions for National roads in Leiria and AADT<2500**

The complete regressions and information for the databases are available in Appendix 1.

## 2.3 Stochastic Models

### 2.3.1 Markov Chains Model

The Markov chain (MC) approach is the most widespread stochastic deterioration modelling technique that has been used for predicting the performance of infrastructures. MC models capture the uncertainties and randomness of the deterioration process by accumulating the probability of transition from one condition state to another over multiple discrete time intervals (Morcoux, 2011).

Generally, discrete-time Markov Chain is used assuming a constant interval between inspections. The implementation of such model simplifies the mathematical formulation and its computation in order to get the performance prediction curve. In these cases, the transition between states is defined by computing the transition matrix  $P^{\Delta t}$ , which is typically an upper triangular matrix with null values below the main diagonal to simulate the natural degradation of the bridge component:

$$\mathbf{P}^{\Delta t} = \begin{bmatrix} p_{11} & p_{12} & \dots & p_{1n} \\ \mathbf{0} & p_{22} & \dots & p_{2n} \\ \vdots & \vdots & \vdots & \vdots \\ \mathbf{0} & \mathbf{0} & \dots & p_{mn} \end{bmatrix}^{\Delta t} \quad (2)$$

Where  $p_{ij}$  corresponds to the transition probability between the state  $i$  and  $j$  from instant  $t$  to  $t + \Delta t$ .

However, in many cases, the assumption behind this model does not correspond to reality, i.e., the inspections do not occur in uniform intervals. During the last two decades, the scientific community has done some improvements to the original Markov-Chain leading to the implementation of new models into the infrastructure management systems, namely continuous-time versions to efficiently consider the actual interval between inspections.

In the continuous time Markov Chain, the transitions between states occur in a structured manner. Assuming that the chain is in a particular state  $i$  at time  $t = 0$ , the length of time (sojourn time) spent in the initial state  $i$  must have the memoryless property according with one of the Markov properties. The main Markov property states that the next state only depends on the current state and not on the past sequence. During a continuous time process, the time between system state changes has an exponential distribution that depends only on state  $i$  (Sánchez-silva and Klutke, 2016).

From the mathematical point of view, when intervals are not regular, the transition matrix  $\mathbf{P}$  is related to a new matrix known as the intensity matrix  $\mathbf{Q}$  through the following differential equation (Denysiuk *et al.*, 2016):

$$\frac{\delta}{\delta x} \mathbf{P} = \mathbf{P} \mathbf{Q} \quad (3)$$

Where  $\mathbf{P}$  is the transition matrix and  $\mathbf{Q}$  is the intensity matrix. The intensity matrix  $\mathbf{Q}$  represents the instantaneous transition probability between state  $i$  and the state  $j \neq i$ . In each time interval, the condition state of the component only can advance for the higher adjacent condition state. Thus, the elements of  $\mathbf{Q}$  are null except for the main diagonal and the diagonal above.

$$\mathbf{Q} = \begin{bmatrix} -\theta_1 & \theta_2 & \dots & \mathbf{0} \\ \vdots & \ddots & \ddots & \vdots \\ \mathbf{0} & \dots & -\theta_i & \theta_i \\ \mathbf{0} & \dots & \mathbf{0} & \mathbf{0} \end{bmatrix} \quad (4)$$

The Equation (3) is known as the Chapman-Kolmogorov equation, and its solution allows to compute the transition matrix for any time interval  $\Delta t$  from the following expression:

$$\mathbf{P} = e^{\mathbf{Q} \Delta t} \quad (5)$$

In order to start the process of building Markov model is necessary a historical record of condition states assigned during inspections. From a previous analysis of

the database, the initial estimate of matrix  $Q$  is computed through the following equation:

$$\theta_i = \frac{n_{ij}}{\sum \Delta t_i} \quad (6)$$

Where  $\theta_i$  represents the transition rate between the adjacent states,  $n_{ij}$  is the number of elements that moved from state  $i$  to state  $j$ , and  $\sum \Delta t_i$  is the sum of the time intervals between observations for which initial state is  $i$ .

The results obtained from the application of the Markov Chains predictive model to the roadway and railway databases described in Chapter 2.1.1, can be found in the Appendix 2. As an example, from the results, Figure 3 presents the performance prediction of railway bridge decks where it is possible to identify a similar degradation after a 75-year period for different deck materials, with a slightly higher deterioration observed for metallic decks. Additionally, Figure 4 compares the prediction for the same bridge component, namely abutments, for both transportation modes. It can be observed from this figure, as well from the results obtained for other bridge components (in Appendix 2), that components associated with the railway network achieve higher condition states at the end of the period of analysis. This phenomenon might be associated with the age of railway assets which are in general older than roadway assets (as can be verified from the year of construction in Table 3). Furthermore, the amount of historical data for railway assets is higher when compared with roadway assets, given that for the majority of railway assets the condition states started to be assigned since 2000, while for roadway assets the first condition states were assigned since 2007.

Finally, for some components, it can be seen from the obtained performance prediction curves that the degradation is not very strong at the end of the studied period. This effect can be attributed to the fact that maintenance actions are done every 15 months in all the bridges, including a general cleaning of the structure (e.g. cutting of vegetation), cleaning and lubrication of the bearings, unblocking and cleaning of the drainage system and maintenance of special equipment such as anti-seismic hydraulic devices (Silva, 2019). Therefore, this minor maintenance activities are likely to delay the degradation processes, which is evidenced in the prolonged sojourn times at the same condition state.

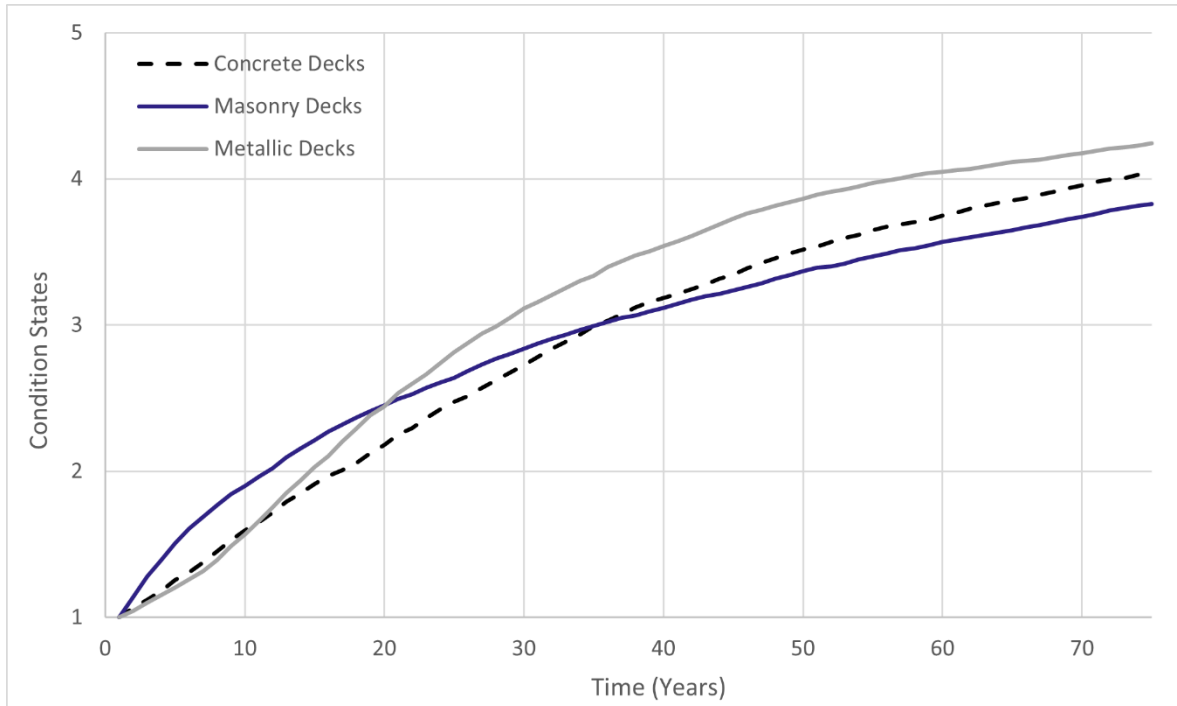


**Figure 3. Performance prediction of bridge decks through MC models**

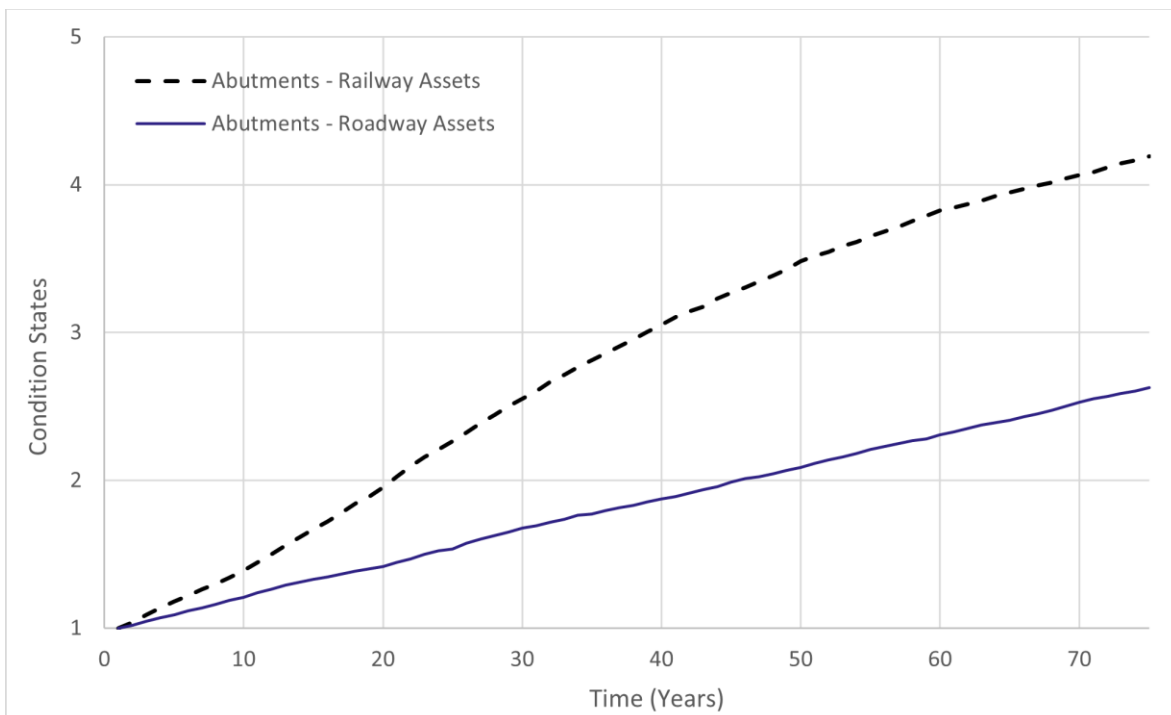


**Figure 4. Performance Prediction of bridge abutments through MC models**

### 2.3.2 Collaborative Gaussian Process Regression

Presented herein is a prediction model for failures in bridge elements, using collaborative Gaussian Process Regression (GPR). GPR is a non-parametric and data-driven regression technique that generates a stochastic distribution of functions, mapping the inputs to corresponding outputs for a given dataset. A major benefit of GPR is that it can quantify the confidence of the predictions (Alvarez, Rosasco and Lawrence, 2011). Applications of GPR include Lithium-ion battery health estimation (Richardson, Osborne and Howey, 2017) and learning the dynamics of robotic arms (Bocsi *et al.*, 2011).

GPR is selected for bridge condition prediction because of the low frequency of bridge inspections. Since the bridges are inspected once in several years, their deterioration process cannot be continuously tracked. Moreover, bridges undergo timely maintenance activities, and thus uninterrupted inspection records from their new to failed states are rare. GPR is capable of extrapolating such scattered inspection information to unrecorded health states, and of generating a distribution of functions that describe bridge deterioration throughout their lifetime.

GPR assumes a joint multivariate normal distribution for all outputs in a dataset. The output for any given input data point is the marginal normal distribution at that point. The marginal distribution for each input point is Gaussian, characterised by the mean and standard deviation. The mean is the predicted value of the output, and the standard deviation is a measure of confidence. A higher standard deviation implies lower confidence. The marginal distribution for unknown points is predicted based on their similarity with the known points from the training dataset. Depending on the application, the similarity is calculated, using various kernel functions that have larger values for points lying closer to one another and smaller values for those far apart (Rasmussen, 2004). The maths described here were extracted from Rasmussen (Rasmussen, 2004). For the input space  $X$ , the corresponding function is estimated as follows:  $f: X \rightarrow \mathfrak{R}$  from the input space to the reals.  $f$  is a Gaussian process, if for any vector of inputs  $x = [x_1, x_2, \dots, x_n]^T$  such that  $x_i \in X$  for all  $i$ , the vector of outputs  $f(x) = [f(x_1), f(x_2), \dots, f(x_n)]^T$  is Gaussian distributed. GPR is specified by a mean function  $\mu: X \rightarrow \mathfrak{R}$ , such that  $\mu(x)$  is the mean of  $f(x)$  and a covariance/kernel function  $k: X \times X \rightarrow \mathfrak{R}$  such that  $k(x_i, x_j)$  is the covariance between  $f(x_i)$  and  $f(x_j)$ . We say  $f \sim GP(\mu, k)$  if for any  $x_1, x_2, \dots, x_n \in X$ ,  $[f(x_1), f(x_2), \dots, f(x_n)]^T$  is Gaussian distributed, with mean  $[\mu(x_1), \mu(x_2), \dots, \mu(x_n)]^T$  and  $n \times n$  covariance/kernel matrix  $K_{xx}$ , Eq. (7).

$$K_{xx} = \begin{bmatrix} k(x_1, x_1) & k(x_1, x_2) & \cdots & k(x_1, x_n) \\ k(x_2, x_1) & k(x_2, x_2) & \cdots & k(x_2, x_n) \\ \vdots & \vdots & \vdots & \vdots \\ k(x_n, x_1) & k(x_n, x_2) & \cdots & k(x_n, x_n) \end{bmatrix} \quad (7)$$

GPR sequentially evaluates the covariance for neighbouring points using a kernel function, followed by calculating their corresponding marginal distributions. As the granularity of neighbouring unknown points is increasing, it approaches a continuous domain and eventually is equivalent to a function with the domain of all possible input values. Despite poor scalability due to the computations involved, GPR models can be optimised and achieve a satisfactory trade-off between fitting



the data and smoothing. GPR is therefore a favourite solution for problems with small regression datasets (Chapados and Bengio, 2007).

For the presented problem, the methodology for bridge element condition prediction can be separated into the following main phases: (i) clustering of similar bridges and pooling of their data together; and (ii) application of GPR to fit functions to data. Clustering similar bridges (phase 1) leads to a more descriptive record. For the reasons explained before, a single bridge would not have enough data describing its deterioration. To cluster similar bridges, features that govern the deterioration process are identified. Such features might be intrinsic like bridge material, mileage, or span count, or extrinsic like local weather conditions or traffic. The hypothesis is that bridges with common features are bound to deteriorate similarly. Such collaborative deterioration modelling has been presented as a successful solution to the problem of the lack of local data in recent literature (Palau *et al.*, 2018). Within a cluster, the inspection records corresponding to different ranges of bridge health conditions are concatenated together and a common training dataset is attained. This dataset consists of a time-series of inspections starting from the best inspected health state in the cluster and finishing with the worst.

It should be noted that if there is a requirement for bridges to have multiple or all of their features similar to be in the same cluster, then the cluster size will be significantly reduced. In the extremity, this would be representative of the case where the bridges in a cluster are required to be identical and we would fall back to the original problem of data scarcity. On the other hand, lenient clustering would cause the bridges to be too different (with their deterioration rate being different too) and undermine the purpose of clustering. Work in progress focuses on finding a trade between strict and lenient clustering. An automated algorithm will be able to identify the sweet spot, where a cluster holds enough data to be modelled confidently. In the presented case study, clustering is based on the material of bridge decks. There were four different materials and thus four clusters. Clustering was based on only one feature due to the lack of extensive data. This feature (i.e., material) was selected because it the major influencer amongst the available features, according to bridge engineers of the organisation, which provided the data.

Next (Phase 2), GPR is used to predict values for unknown data points. Since the bridge health deteriorates over time, we need a decreasing mean value function for the GPR priors. This is different from conventional applications where the mean is usually zero, or a constant value. The mean value for regression is calculated by fitting a straight line using a least square fit. Using this mean value and random covariances, a prior distribution of functions is generated. This distribution is updated according to the data from the previous step, with exponential kernel (8) calculating covariances for unknown data points:

$$k(x_a, x_b) = \sigma^2 \exp\left(\frac{-(x_a - x_b)^2}{2 * l^2}\right) \quad (8)$$

where  $l$  =characteristic length

$\sigma^2$  =signal variance

$(x_a, x_b)$  =points for which covariance is calculated

Analyses for the two clusters (amongst the four available clusters) with the highest number of data points (71 points for both) are presented here. To concatenate the data points within clusters, the average rates of deterioration were used as references, assuming the deck to be aged zero at condition index 100.

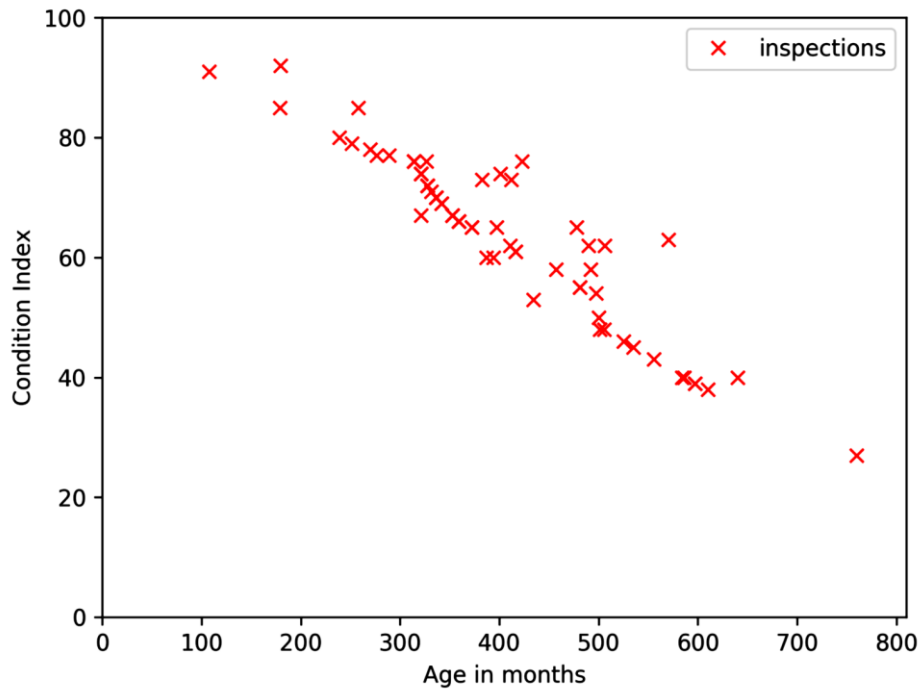


**Figure 5. Plot obtained after concatenating data points from cluster 1**

For example, the bridge age for condition index 99 would be calculated using the average rate of deterioration between the indices 100 and 99. This is followed until condition index 0. For consecutive inspections within a cluster, the first inspection was marked on the plot with y-axis value equal to its health index, and x-axis value as the corresponding reference age. For the next inspection, y-axis value was its new condition index and x-axis value was its previous age plus the time since previous inspection. Eventually, a plot with condition index on the y-axis and age on the x-axis was obtained. An example for such a plot for one of the clusters is shown in Figure 5, where the red cross-marks are individual data points.

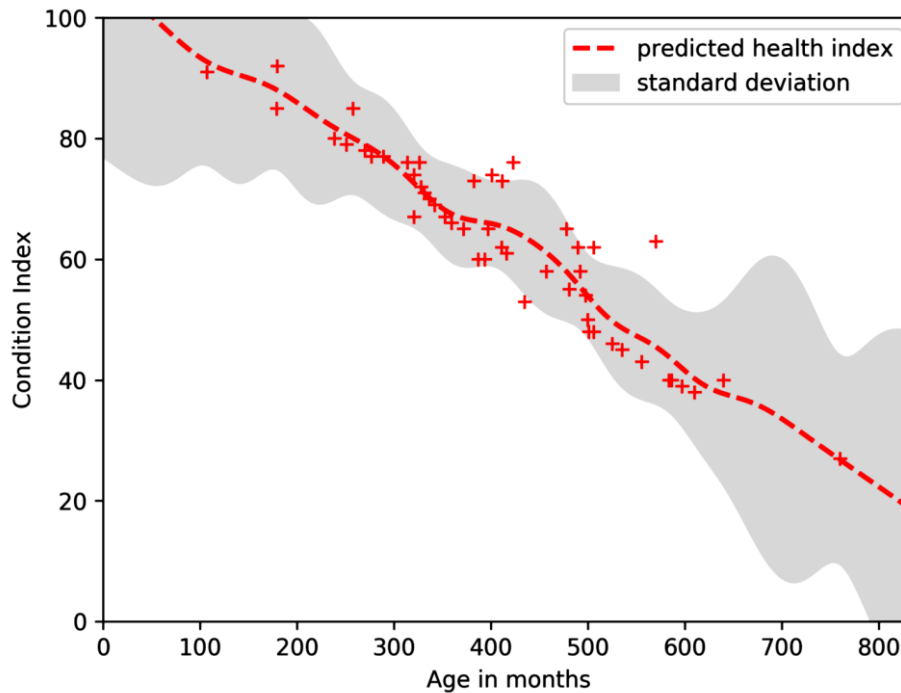


**Figure 6. Posterior distribution of functions for cluster 1**

In Phase 2, GPR was applied for fitting distributions of functions to individual clusters. A straight line was first fit to obtain prior mean values, followed by calculating posterior distribution of the functions. Exponential kernel function with characteristic length ( $l$ ) equal to 45 and signal variance equal to 100 was found suitable for calculating the covariance matrix of the clusters. Posterior distribution for the cluster in Figure 5 is shown in Figure 6, where the red dotted line represents the posterior mean and the grey region shows the standard deviation. Figure 7 displays the same technical plot for cluster 2. Certain ambiguities can be seen in these plots, for example the data points corresponding to different bridges Figure 6 and Figure 7 are not exactly similar. This is due to the fact that only a single feature, i.e., the deck material, was used as the basis for identifying the clusters. The clustering step can be further improved, depending on the application, if more features are incorporated while clustering the bridges.

Summarising, the condition of a bridge deck, which has never been maintained and it is characterised by common features as the clusters, can be estimated based on its age using the plots in Figure 6 and Figure 7. The red line is the predicted value, and the grey region is the confidence of prediction. The quality of the prognosis was evaluated using 5-fold cross validation, with 80% of data being used for training and 20% of data being used for testing, in each run. The data points (i.e., actual condition values) consisting the testing set were compared with the predicted values (i.e., red line in Figure 5 and Figure 6), which were calculated by the model using the training set. The mean absolute error was equal to 8%. Additionally, the narrower the grey region Figure 6 and Figure 7, the more confident the prediction is and vice versa. As it can be observed from the plots, the presence of more and closely located data points causes more confident predictions. Moreover, for the conditions where we do not have any historical

inspection data, the confidence of predictions is very low. For example, the standard deviation of predictions is very high after  $t = 650$  in Figure 6. In such situation, it is recommended for the infrastructure owner to resort to a conservative maintenance plan and observe the bridge deterioration more frequently.

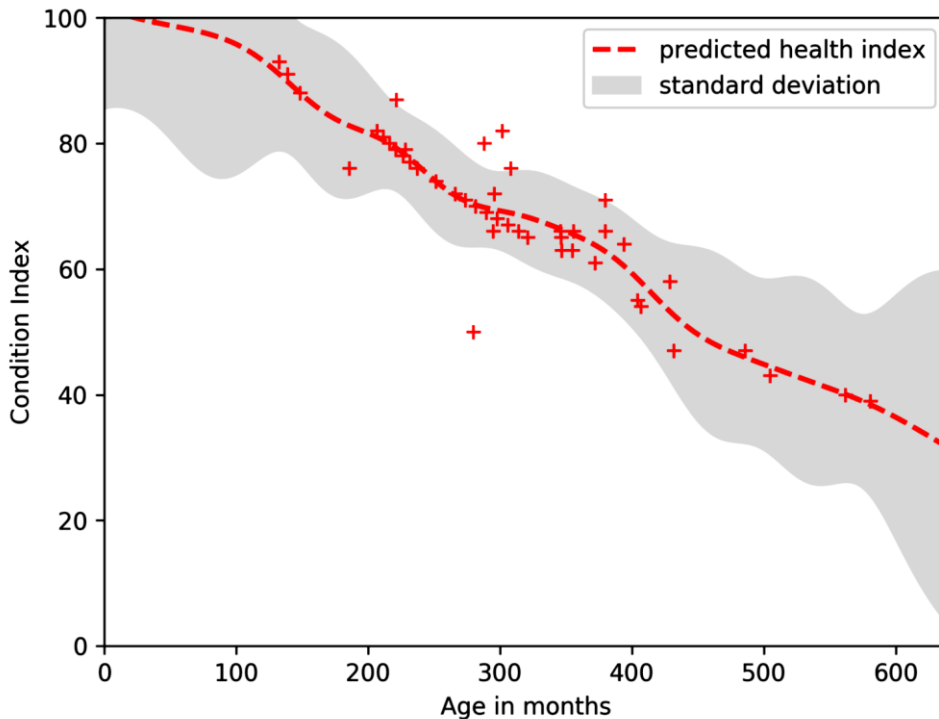


**Figure 7. Posterior distribution of functions for cluster 2**

The proposed collaborative GPR-based model was applied to a case study, with several significant outcomes being extracted. Firstly, most of the data from bridge inspections are concentrated within 80 to 40 condition index range. In the examined cluster, very few bridges have inspection records for very fragile conditions due to a safety threshold, set by the organisation. A bridge element must be repaired or replaced if its condition index is below 40. The repair or maintenance strategy is based on the type of element and existing defects. Secondly, the proposed method of clustering similar bridges to expand the dataset is deemed applicable since the rates of deterioration are nearly constant and the standard deviation tight within the cluster. Moreover, when GPR was applied for combined data of all bridges, the grey region was more spread out. Thirdly, there are some outliers, but GPR can understand the common behaviour and fit a distribution of predictor functions. It can be observed in both Figure 6 and Figure 7 that the grey region narrows down where the concentration of data points increases near the mean and broadens in the presence of the outliers indicating less confidence in the predictions.

---

## 2.4 Dynamic Predictive Models

Structural reliability has developed rapidly and has become widely accepted among researchers and owners over the past decade providing valuable information about the structural condition of infrastructures. Taking into account that bridges are critical components of the road infrastructure, bridge failure or collapse can have adverse consequences for the economy and the environment and even the life and physical integrity of society (Chang and Song 2016).

Reliability, considered one of the most important key performance indicators, is associated based on the uncertainty, loads, and strength of the structure. The procedure is carried out from the ultimate limit states (moment and shear load capacities) using design and construction information. This deterministic approach is based on individual components analysis in which the structure capacity is defined when any of the components reaches its maximum capacity (Czarnecki and Nowak, 2006).

It is worth mentioning that applying reliability assessment requires a great effort in terms of information from the design phase or previous maintenance activities. However, a bridge management system is normally assessed by observable damage recorded during inspections, resulting in a qualitative measure, called a condition rating, condition state, condition class, along with others. The inspection results are generally stored in databases, while information from the design phase such as load combinations, safety factors are generally not stored. Even after maintenance interventions, where there is relevant information on safety and serviceability, it is not stored either. Also, in most cases when stored on paper, the stored information is lost due to negligence or accidents.

Authors such as Rade Hajdin, Casas, and Matos (2019) mention that the optimal procedure would be to change from condition rating to reliability index, thus move on from a qualitative measure to a quantitative key performance indicator. Since condition rating is not a measure that can easily be correlated with bridge safety, serviceability, or reliability, another option should be considered for integrating both measures. Nevertheless, there is a gap in terms of procedures to incorporate the information obtained from visual inspections into a reliability assessment. Moreover, to define optimal maintenance, rehabilitation, and replacement strategies for bridge networks, it is necessary to consider the deterioration predictions as well. Therefore, the reliability model must be constantly updated according to the current state of the bridge throughout its useful life.

This section describes an assessment methodology for existing infrastructures health based on the system reliability. To show the methodology effectiveness, a time-reliability analysis, and an update are developed based on the inspection results of one bridge of the Portugal case study (SAFEWAY, 2019c). It should be noted that this approach can be applied to any type of structure or material, as long as the necessary information is available from both design and inspection on the state of deterioration.

## Reliability Updating Methodology

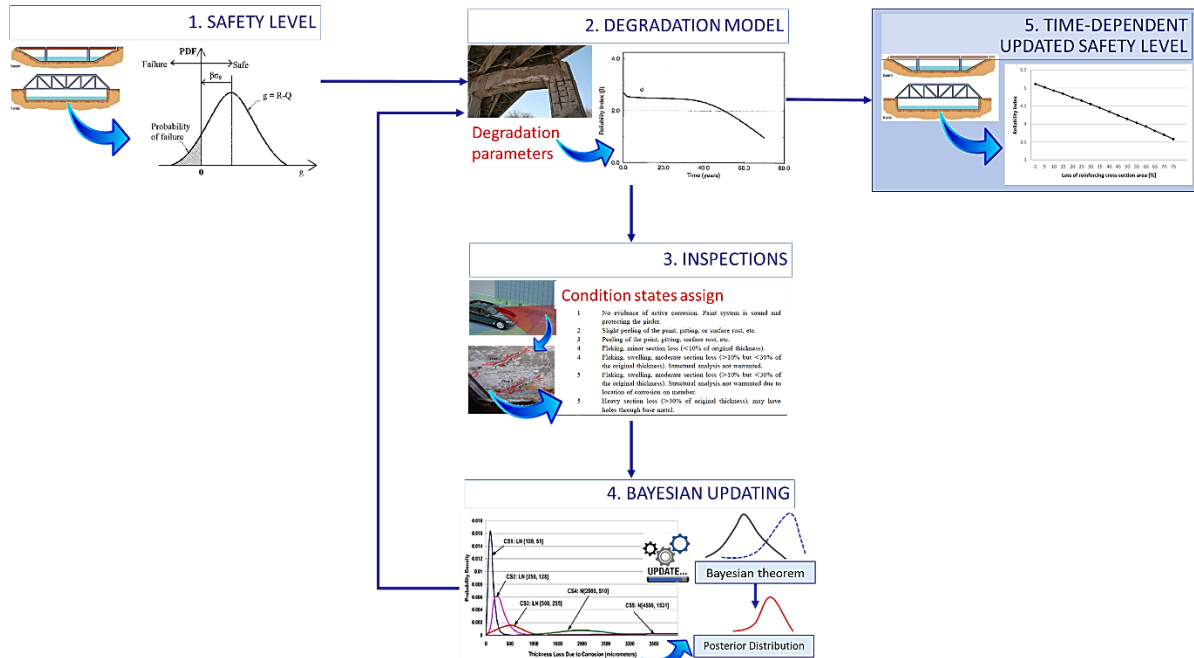


**Figure 8. The proposed framework for bridge reliability updating**

The methodology consists of 5 main steps, as shown in Figure 8. First, the initial reliability level calculation. Second, incorporation of degradation models. Third, inspection records. Fourth, translation from condition ratings to probabilistic terms and Bayesian updating. And finally, after the previous steps, obtaining the time-dependent updated reliability level. Each of these steps is explained in more detail below.

### 2.4.1 Reliability Analysis

There are several methods for reliability assessment. However, these methods differ regarding precision, required input data, and computational effort. There is also a differentiation concerning the range of application, as it may be suitable procedures for reliability analysis of individual components or complete structural systems (Czarnecki and Nowak, 2006).

The safety level will be assessed in terms of a reliability index ( $\beta$ ), defined as a function of the probability of failure. The reliability analysis is performed for the strength prediction models based on design code procedures, having account the use of yield capacity verifying when predicting ultimate moment or shear capacities for heavily corroded RC beams. The use of moment or shear capacities depends on the critical condition of elements and their influence over the whole infrastructure. The general form of the limit state function is expressed as (9):

$$g = R - Q \quad (9)$$

Where  $g$  is the limit state function;  $R$  is the resistance and,  $Q$  the load effect. If the function  $g \geq 0$ , the structure is safe, i.e., the load-bearing capacity of the assessed

structure is higher than the effects (stresses or internal forces) of the applied loads. Otherwise, when  $g < 0$  the structure is not safe (Nowak, 2004). Therefore, in terms of failure probability,  $P_f$ , is given when the probability that the limit state function reaches a negative value (Rakoczy and Nowak, 2013) as is show in Eq. (10).

$$P_f = P(R - Q < 0) = P(g < 0) \quad (10)$$

Moreover, the reliability index  $\beta$  is related to the probability of failure as Eq. (11):

$$\beta = -\Phi^{-1}(P_f) \quad (11)$$

Where  $\Phi^{-1}$  is the inverse standard normal probability distribution function.

#### 2.4.1.1 Resistance model

This methodology focuses on resistance prediction models based on the procedures specified in the design codes, which refer to the elastic limit. Therefore, shear and yield strength are verified by predicting the ultimate moment for the element. Another important aspect is that the analysis is considered according to the critical elements involved in the resistance system. Such as elements without which it is possible to guarantee the safety of the structure or those segments and/or structure elements where the damage has the greatest impact on safety and serviceability. In other words, vulnerable zones can be related to various failure modes.

The identification of critical elements can be mainly based on design concepts, which may be taken into account as conceptual weaknesses. For example, in a reinforced concrete bridge one of its critical elements is the girders. This is illustrated in Figure 9, where the conceptual weaknesses are marked with "CW" both at the element level and the cross-sectional level (e.g., in a prefabricated multicellular cross-section).

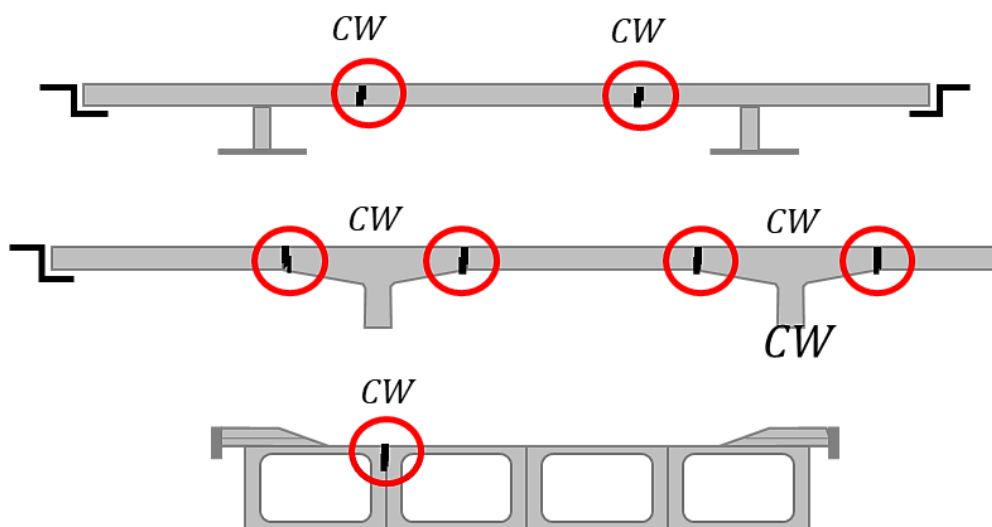


**Figure 9. Conceptual weaknesses for bridge systems, From (Hajdin, Kušar, Mašovic, et al. 2018)**



Another way to identify vulnerable areas is through inspection experience. On another hand, damage detected outside vulnerable areas can sometimes also incur failures, although it occurs only in cases where the extent of the damage is significantly greater than in vulnerable areas. Additionally, there are elements buried or embankment, which are difficult to access. But there are symptoms such as structure or embankment deflection/settlement that can indicate a hidden damage process. Therefore, an additional failure mode associated with the observed damage must be considered (Hajdin, Kušar, Mašovic, et al. 2018).

Returning to the example of a reinforced concrete bridge, where the most critical element is the beams. The yield strength is directly proportional to the section strength (and the capacity of the reinforcing bar), where ultimate flexural capacity ( $M_u$ ) of a singly reinforced RC beam can be expressed as Eq. (12) (ACI 318 2014):

$$M_u = A_s f_y \left( d - \frac{A_s f_y}{1.7 f'_c b} \right) \quad (12)$$

Depending on the concrete compressive strength ( $f'_c$ ), the effective depth ( $d$ ), beamwidth ( $b$ ), the yield stress ( $f_y$ ) and the cross-sectional area of reinforcement ( $A_s$ ). Meanwhile, the ultimate shear capacity of a girder with shear reinforcement ( $V_u$ ) comprises the shear capacities of the concrete ( $V_c$ ) and the shear reinforcement ( $V_s$ ) as is shown in Eq. 8, 9, and 10.

$$V_u = V_c + V_s \quad (13)$$

$$V_c = 0.17 \sqrt{f'_c} b d \quad (14)$$

$$V_s = n_v A_v f_y \quad (15)$$

Where  $n_v$  is the number of stirrups and  $A_v$  is the cross-sectional area of shear reinforcement (stirrup) (ACI 318 CODE, 2014).

It is worth explaining that in a system with components in a series configuration arranged, the system failure is conditioned by the failure of any member. Therefore, the component with the lowest reliability is the one that has the greatest effect on the reliability of the system. The best example for this is a chain, where all the rings are in series and if any of the rings break, the system fails. Thus, the weakest link dictates the chain strength in the same way that the weakest component/subsystem dictates the reliability of a series system. Whereas a system with its components distributed in parallel is at least as strong as its strongest member. Consequently, the system does not fail until all its members fail. As opposed to a series system, in a parallel configuration, the component with the highest reliability is the one that has the greatest effect on the reliability of the whole system (Estes, 1997).

The resistance capacity of a reinforced concrete section considers  $n$  number of reinforcing bars in a parallel system. Likewise, the total capacity of the structure can also be considered, with  $n$  number of beams in a parallel system. This principle can be applied to any infrastructure, considering the infrastructure as the sum of its most critical elements in a series-parallel system regardless of the type of material.



On the other hand, it is important to highlight that in this analysis some terms of the resistance model are treated as random variables. In which, a random variable is a function conceived in intervals on the axis of the real numbers (Nowak & Collins, 2013). The resistance represents the load-carrying capacity of the infrastructure according to the critical element evaluated, which is affected by uncertainties because of the variability in the strength of the materials, the dimensions, and the analysis procedures (Rakoczy and Nowak, 2013). The selection of the parameters to be considered as random variables (RVs) is performed considering previous knowledge and engineering judgment. Therefore, most of the terms for the expression shown in Eq.(12) or Eq. (13) can be treated as a probabilistic parameter such as concrete compressive strength ( $f'_c$ ), reinforcement yield strength ( $f_y$ ), and steel area ( $A_s$ ). Also incorporating an uncertainty model ( $\theta$ ) into the equations Eq.(12) and Eq. (13) (Estes and Frangopol, 1999).

#### 2.4.1.2 Load model

The load model considers the main components such as dead load, live load, dynamic load, environmental loads (temperature, wind, earthquake) among others (collision, braking). These charges are taken into account according to the availability of the information available in each case. It is worth mentioning that the load is described through a cumulative distribution function, including a bias factor (the relationship between the mean and the nominal value) and the variation coefficient, in order to consider the load variation (Czarnecki and Nowak, 2006).

The most common combination is normally dead and live load. Dead load involves gravity loading due to the self-weight of permanently attached structural and non-structural components. Meanwhile, live loads which depend on use and capacity due to those loads are translated to loads that vary over time, such as people or moving objects. In both cases, dead or live loads, the codes provide a calculation of equivalent loads for different types of structures, according to experience and accepted practice (Nowak 1995).

For instance, consider the load model for a bridge. In terms of dead load, maybe include the weight of the beams, deck slab, wear surface, barriers, sidewalks, and diaphragms, where applicable. In this case, the bias factor must also be included, which depends on the manufacture of the items considered as factory-made components or cast-on-site components (Nowak 2004).

Regarding live load for bridges, this is typically represented by a specifically designed truck, rail cargo, or military cargo. When this proposes fixed or constant variables are assumed such as the axle spacing and percentage of the total load per axle, while variables such as the gross vehicle weight or the transverse position of the truck within the roadway (curb distance) are assumed as random variables. Besides, the distribution factor (fraction of the total truckload per beam) may be included as well (Czarnecki and Nowak, 2006).

Dynamic loading is due to the same dynamic properties of the bridge, surface roughness, and the vehicle's suspension system. Defining dynamic load factor as the ratio of dynamic deformation (or deflection) and static deformation (deflection). A dynamic load factor can be conservatively assumed as 0.10 and the

coefficient of variation as 0.80 (Nowak 2004). An example of statistical parameters for the load model can be found in the available literature ( Nowak 1995; Estes and Frangopol 2003).

### 2.4.2 Analytical Degradation Models

Structures tend to deteriorate over time according to their materials. In the case of reinforced concrete, the poor durability of the concrete and especially the reinforcing steel corrosion has been identified as one of the major causes of the premature rehabilitation of reinforced concrete structures (Tuutti, 1982). During this time, the chloride ions are diffusing through the concrete cover until the steel surface and thereby initiate corrosion (Ma *et al.*, 2013), especially those infrastructures exposed to aggressive chloride environments. Corrosion-initiated can be present as a uniform reduction of steel area across the section or as localized corrosion pits along the length of the rebar (Higgins and Farrow, 2006) (Ghosh and Sood, 2016). Area reductions in the cross-section of the element can become significant, for instance, up to 80% loss of cross-section was observed in a 40-year-old Canadian bridge (Palsson and Mirza, 2002). There is also evidence to suggest that corrosion not only causes area loss but also results in the linear degradation of yield strength of reinforcing bars (Stewart, 2009; Jnaid and Aboutaha, 2016).

Taking into account the impact of environmental conditions, the curing of the concrete and the densification of the cement paste, the migration of chloride ions through the concrete can be represented. In this case, Fick's second law of diffusion is used through a semi-infinite solid medium, in which the corrosion onset time can be generically represented as Eq.(16) (Enright and Frangopol, 1998):

$$T_i = \left\{ \frac{x^2}{4k_e k_c D_{cl,0} (t_0)^{n_{cl}}} \left[ \text{erf}^{-1} \left( \frac{C_s - C_{Cr}}{C_s} \right) \right]^{-2} \right\}^{\frac{1}{(1-n_{cl})}} \quad (16)$$

Where,  $T_i$  is the corrosion initiation time (*years*),  $x$  is the concrete cover depth (*mm*),  $D_{cl,0}$  is the reference diffusion coefficient ( $\text{mm}^2/\text{year}$ ) determined from compliance tests,  $k_c$  is the curing factor,  $k_e$  is the environmental factor,  $t_0$  is the age of concrete in years when the compliance test is performed,  $n_{cl}$  is the age exponent that incorporates the densification of cement paste due to further hydration,  $C_s$  is the equilibrium chloride concentration at the exposed concrete surface,  $C_{cr}$  is the critical chloride concentration, and  $\text{erf}$  is the Gaussian error function.

Then assuming a continued steel area loss, the uniform corrosion model, equally around the cross-section with the residual cross-sectional area  $A_r^u(t)$  at time  $t$  calculated as Eq. (17).

$$A_r^u(t) = \frac{\pi \left[ D_0 - 2 \int_{T_i}^t r_{corr}(t_p) dt_p \right]^2}{4} \quad (17)$$

In which,  $D_0$  is the initial steel diameter before corrosion initiation ( $mm$ ),  $r_{corr}(t_p)$  is the time-dependent corrosion rate ( $mm/year$ ) calculated at  $t_p$  years since corrosion initiation as a function of  $i_{corr}(t_p)$  ( $\mu A/cm^2$ ) as Eq.(18).

$$r_{corr}(t_p) = 0.0116 \cdot i_{corr}(t_p) \quad (18)$$

Where  $i_{corr}(t_p)$  can be calculated as Eq. (19).

$$i_{corr}(t_p) = 0.85 i_{corr,0} t_p^{-0.29} \quad (19)$$

$i_{corr,0}$  is the initial corrosion rate ( $\mu A/cm^2$ ) calculated as a function of concrete cover depth ( $x$ ) and water-cement ( $w/c$ ) ratio, how is shown in Eq. (20).

$$i_{corr,0} = \frac{37.8 (1 - w/c)^{-1.64}}{x} \quad (20)$$

It is important to highlight that the value of concrete cover depth ( $x$ ) must be in  $mm$  for this equation (Ghosh and Sood, 2016).

Since corrosion causes area loss and it consequently results in the degradation of yield strength causing structural strength decrease. Du, Clark, and Chan (2005) mention that the reinforcing yield stress is reducing approximately linearly with corrosion loss as Eq. (21):

$$f_y(t) = \left[ 1.0 - \alpha_y \frac{A_0 - A(t)}{A_0} \cdot 100 \right] \cdot f_{y0} \quad (21)$$

where  $f_{y0}$  is the yield stress,  $A_0$  is the area of the uncorroded steel bar.  $A(t)$  is the area of corroded steel bar which changes with time, and  $\alpha_y$  is an empirical coefficient that depends on the material properties in a specific corrosive environment, assuming to be normally distributed with a mean of 0.009 and a standard deviation of 0.001. In this way, the section resistance (and the capacity of the reinforcing bar) is directly proportional to the yield capacity which is equal to the product of the yield stress and the cross-sectional area, both affected by corrosion. by bite.

On the other hand, To consider the corrosion penetration in the case of steel elements, the model developed by Albrecht and Naeemi (1984) will be implemented. This model predicts corrosion loss through a regression analysis of a database collected in the field. Where the corrosion penetration  $C(t)$  ( $\mu m$ ) at any time ( $t$ ) ( $years$ ) may be expressed as Eq. (22).

$$C(t) = At^B \quad (22)$$

In which  $A$  and  $B$  parameters are based on different environments such as rural, industrial, and marine environments, besides the type of steel. For more detailed information on parameters  $A$  and  $B$  see (Albrecht and Naeemi, 1984).

#### 2.4.2.1 Inspections

By taking the degradation models into account, the reliability index can be calculated at any time ( $t$ ), which allows identifying when the infrastructure is no longer considered safe. Since this analysis is based on a predictive model, periodic inspections are highly important in order to provide additional data regarding the structure state. It is not only to validate and update the models but to support decision-making about design, construction, maintenance; and structural intervention, made by infrastructure management over time. Inspection data can be used to update structural features, increasing the accuracy of the models (Hall, 1988). Therefore, at shorter intervals between inspections, the greater the reliability analysis confidence. Thus, providing a tool for evaluating the future condition and performance of structures, allowing adequate inspection and maintenance strategies to maintain reliability at an acceptable level (Ellingwood and Mori, 1993).

There are two main categories when it comes to in-service structural evaluation methods (Ellingwood, 2007). The first category corresponds to methods for detecting faults and measuring their extent. Typically, these methods are based on visual inspection, which makes it easier to identify surface defects than internal ones. However, this has some disadvantages, such as difficulty in accessing all parts of the structure for inspection or incorrect conclusions. On the other hand, the second category refers to the methods that indicate the strength in situ, either directly or indirectly. Given that the materials of the structures in service can vary considerably from the values assumed during the design stage, not considering these changes in the degradation model can lead to an erroneous reliability estimation. The methods implemented in this category may be non-destructive evaluation (NDE) (rebound hammers, ultrasonic pulse velocity measurements) or may involve local damage to the structure (tensile coupons, drilled cores, pull-out tests). It is worth mentioning that no category is uncertainty exempt in the degradation analysis.

There are also uncertainties associated with the inspection process itself, complicating the effects on structural performance (Ellingwood, 2007). Which arise from:

- Differences in codes and design standards for components of different ages.
- Lack of measurements and records in service.
- Temporal and spatial variations in-service loads.
- Models limitations to quantify time-dependent material changes and their contribution to structural capacity.
- Limitations in NDE technologies application.
- Deficiencies in existing rehabilitation and repair methods.

This is why an aging management approach developed within a framework of structural reliability is required. Consequently, there are different guidelines for infrastructure inspection practices, which differ considerably from country to country. But generally, the evaluation may be divided into phases. This implies a preliminary evaluation, a detailed investigation, expert evaluation, and, finally, an advanced evaluation, depending on the structural condition of the infrastructure

(Saviotti, 2014). Based on these phases, Omar and Nehdi (2018) classify the most relevant techniques for condition assessment into five different groups, as shown in Figure 10.

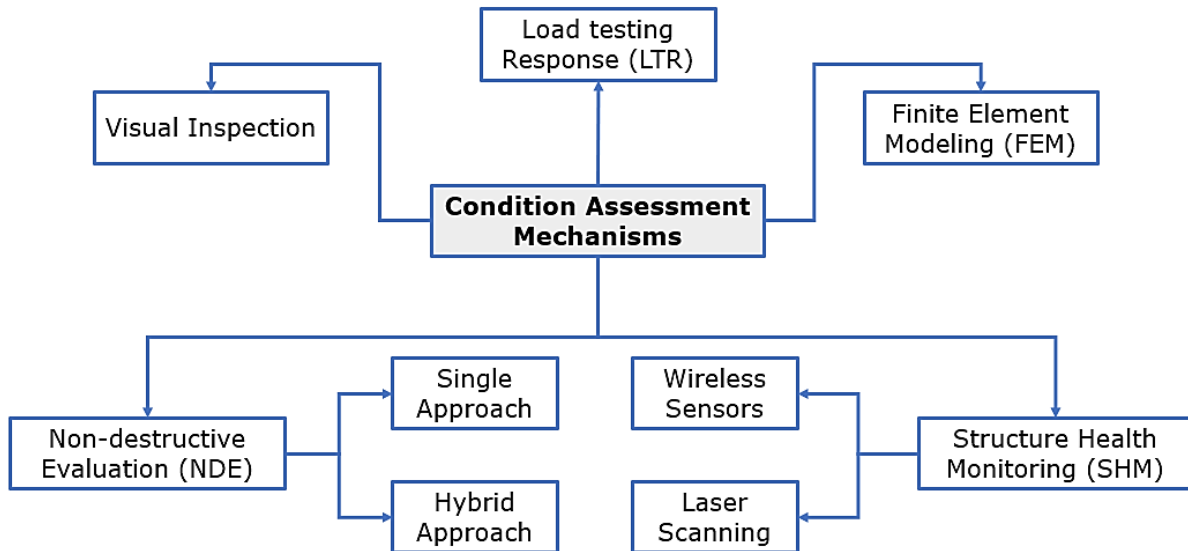


**Figure 10. Condition Assessment Mechanisms, from Omar and Nehdi (2018)**

However, there are still many limitations to the use of this type of evaluation and monitoring techniques of the state of infrastructures. Each of the mentioned categories has different scopes and limitations. For more detailed information on each of the categories refer to Omar and Nehdi (2018).

#### 2.4.2.2 Bayesian Updating

Bayesian updating techniques are very useful to combine inspection data of these parameters and prior information into a predictive model. Bayesian updating uses both the prior information and new inspection information to find the relative uncertainty associated with each (Frangopol and Estes, 1997).

Therefore, Bayesian statistics purpose is to represent the prior uncertainty about the model parameters with a probability distribution and update it with current data to provide a posterior probability distribution with parameters that contain a lower degree of uncertainty. Since from the Bayesian approach, any quantity whose real value is uncertain can be represented with probability distributions. Bayes' theorem, expressed in terms of probability distributions, appears as Eq. (23) (Lynch, 2007).

$$f(\theta|data) = \frac{f(data|\theta)f(\theta)}{f(data)} \quad (23)$$

Where  $f(\theta|data)$  is the posterior distribution of  $\theta$  parameter,  $f(data|\theta)$  is the data sampling density (which is proportional to the likelihood function, only differing by a constant that makes it a proper density function),  $f(\theta)$  is the prior parameter distribution and  $f(data)$  is the marginal probability of the data, computed as Eq. (24) for a continuous sample space.

$$f(\text{data}) = \int f(\text{data}|\theta)f(\theta)d\theta \quad (24)$$

The integral of the sampling density multiplied by the prior over the sample space  $\theta$ . This quantity is sometimes called the "marginal probability" for the data and acts as a normalization constant to make the posterior density suitable.

For instance, assuming an influencing parameter of strength described as a random variable  $\theta$ , believed to have a density function  $f'(\theta)$  where  $\theta$  is the parameter of that distribution (i.e., the deterioration model). On the other hand, in an inspection, there is a set of values  $x_1, x_2 \dots x_n$  that represent a random sample from a population  $x$  with underlying density function  $f(x)$  are observed and are fit to a new density function  $f(x_i)$  (i.e., the visual inspection results  $f(\text{data}|\theta)$ ). The updated or posterior density function  $f''(\theta)$  which uses both sets of information and provides the best use of both ( $f(\theta|\text{data})$ ) can be expressed as Eq. (25) (Estes & Frangopol 2003).

$$f''(\theta) = k L(\theta) f'(\theta) \quad (25)$$

where  $L(\theta)$  is the likelihood function and  $k$  is the normalizing constant. For the case where both  $f'(\theta)$  and  $f(x)$  are normally distributed, the posterior function  $f''(\theta)$  is also normally distributed and has the mean value and standard deviation, respectively, as Eq. (26).

$$\mu'' = \frac{\mu(\sigma')^2 + \mu'(\sigma)^2}{(\sigma')^2 + (\sigma)^2} \quad \sigma'' = \sqrt{\frac{(\sigma')^2(\sigma)^2}{(\sigma')^2 + (\sigma)^2}} \quad (26)$$

Where  $\mu, \mu'$  and  $\mu''$  are the mean values of the inspection results, the prior distribution, and the posterior distribution, respectively, and  $\sigma, \sigma'$  and  $\sigma''$  the standard deviations of those same distributions.

#### 2.4.2.3 Target reliability

There are three different outputs for reliability index use. First, it is the probability of failure itself, which also serves to determine which variables have the greatest influence on the structure reliability. Second, for a single structure, the reliability index can be directly compared to some target value depending on the structural type and failure mode, which is generally defined by design codes. And finally, for multiple structures, classification and prioritization of the infrastructures can be established in terms of their respective reliabilities and a target value. Although there is no absolute certainty regarding the reliability analysis, particularly concerning the probability of failure and the comparison of a target value. This procedure allows the judgment of the relative bridge safety concerning the inherent safety level of the code, expressed as a ratio. However, there are still gaps in the interpretation of a ratio that is close to unity (Lark and Flaig, 2005).

Different guidelines and codes present recommended values to be used in the design and assessment of infrastructures, such as JCSS publication and the standard ISO 13822.



### 2.4.3 Case study: application example

The selected bridge is located between Albergaria dos Doze-Alfarelos in central Portugal, crossing the Arunca river. The bridge is operating since 2005 and is part of the railway network of the Santarém/Leiria Region. It has four simply supported spans for a total length of 66.63 m. Regarding superstructure, the cross-section is a “H” shape in each direction, which consists of two beams of 1.35 m high and a 0.4 m slab that serves as a connection between both beams as shown in Figure 11.

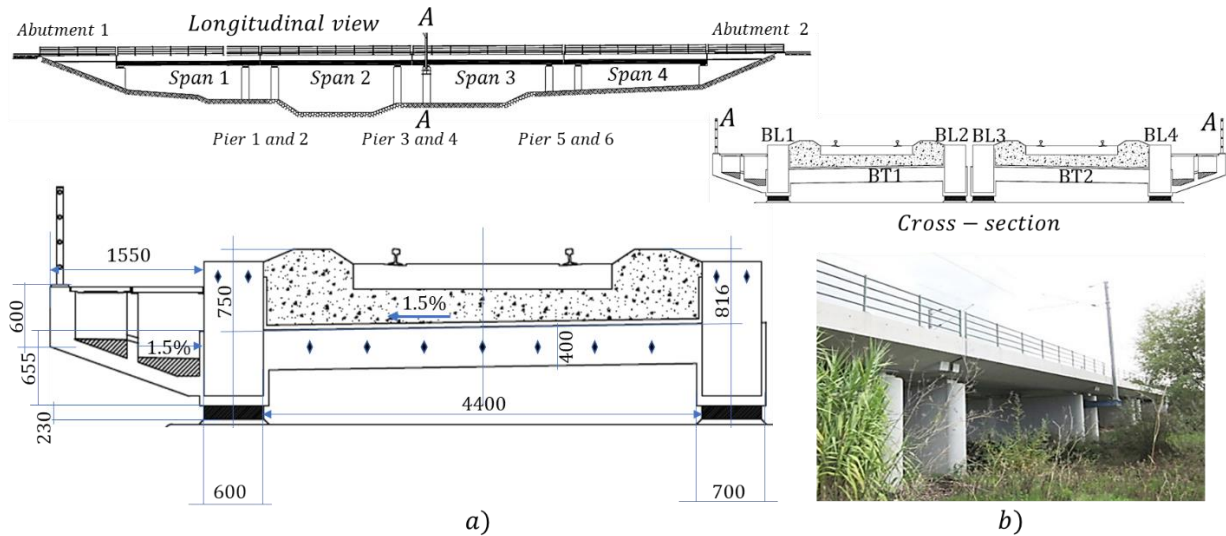


**Figure 11. Simões railway bridge. a) Deck cross-section detail. b) Lateral view. Source: Infraestruturas de Portugal**

It is considered that the critical elements are the simply supported beams of the superstructure. Therefore, they are established as the element that most influences the reliability of the entire bridge, that is, considering that the failure of the beams will cause the collapse of the bridge.

Likewise, it is important to mention that for the practical example, the bridge will only be analyzed for moment loading (flexural strength), focusing on the beams as a critical element. However, the methodology is applicable in the same way for the shear effects and for evaluating the reliability of all the bridge components needed for obtaining total structure reliability.

#### 2.4.3.1 Resistance model

The resistance model that represents the bridge load capacity is mainly affected by the uncertainties due to the variability in the materials resistance, dimensions, and the analysis procedures (Rakoczy and Nowak, 2013). Taking into account the above, the flexural strength for the entire section can be calculated as Eq.(27) (Santamaria *et al.*, 2019):

$$M_R = A_{s1}f_{s1}d_{s1} + A_{s2}f_{s2}d_{s2} + A_{s3}f_{s3}d_{s3} + A_{p1}f_{p1}d_{p1} + A_{p2}f_{p2}d_{p2} - A_{s4}f_{s4}d_{s4} - 0.85f_{cm}b\lambda^2x^2/2 \quad (27)$$

where  $A_{si}$  ( $i=1,\dots,4$ ) are to the total reinforcement steel positioned at  $d_{si}$  level;  $A_{pj}$  ( $j=1,2$ ) are the total prestressed steel positioned at  $d_{pj}$  level;  $f_{si}$  is the reinforcement steel strength at the particular fiber;  $f_{pj}$  is the prestressing steel strength at the particular fiber;  $f_{cm}$  is the mean concrete compressive strength;  $\lambda$  is the effective height of the compression zone equivalent to 0.8 for characteristic concrete strength less than 50MPa, and  $x$  corresponds to the neutral axis depth as is shown in Figure 12.

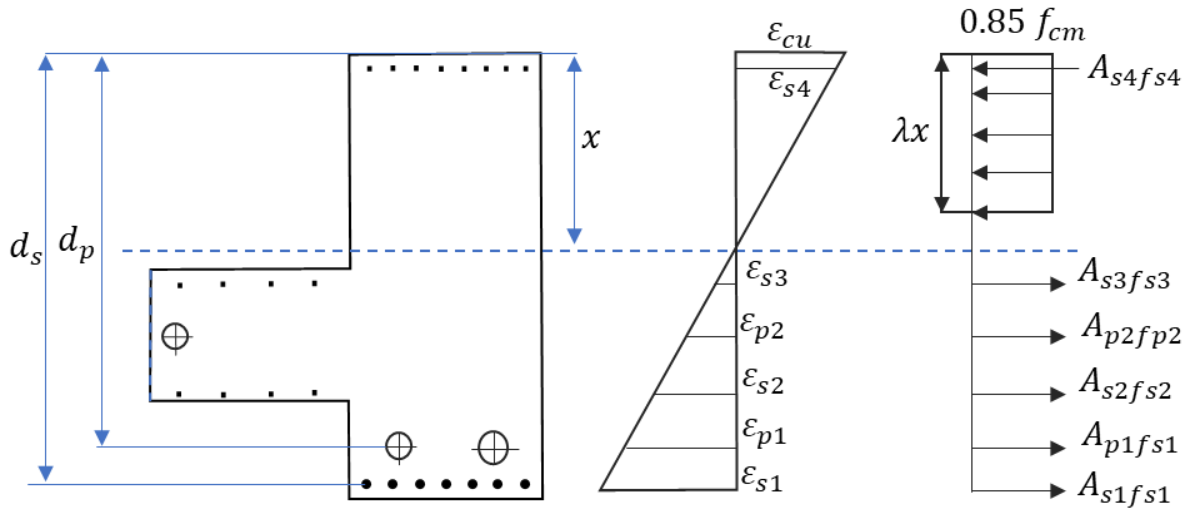


**Figure 12. Stresses and strains distribution in the cross-section**

Solving the static equilibrium of the entire section (i.e., compression and tensile forces equality) the depth of the neutral axis is found. Assuming that the extreme compression fiber reaches the maximum compression deformation ( $\varepsilon_{cu}=0.0035$ ) and the elastic limit of ( $\varepsilon_{si}=0.0028$ ;  $\varepsilon_{pi}=0.01$ ). Therefore, the flexural strength of the section is expressed as Eq. (28).

$$M_R = (1.32A_{s1} - 0.04A_{s4})f_y + \frac{E_s}{x}(0.0037A_{s2} + 0.0017A_{s3}) + \frac{E_p}{x}(0.0049A_{p1} + 0.0026A_{p2}) - E_s(0.0024A_{s3} + 0.0036A_{s2}) + E_p(0.0018A_{p1} + 0.0013A_{p2}) - 0.33 \times 1000^2 f_{cm} x^2 \text{ [N.m]} \quad (28)$$

Those parameters are considered as random variables (RVs) to estimate the flexural capacity and were selected from the most prominent of the scientific literature and engineering judgment as are presented in Table 7. RVs are assumed with normal distributions. The statistical characteristic such as the mean value and the coefficient of variance (CoV) were defined according to the probabilistic model code from the Joint Committee on Structural Safety (JCSS) (JCSS 2001) and the statistical analysis performed by Wisniewski, Ferreira, and Cruz (2006), based on experimental tests of materials produced in Portugal during the years 2000 and 2001.



**Table 7. Probabilistic parameters of RVs for the resistance model**

| Parameter                                  | Mean value                   | CoV (%) | Distribution |
|--|------------------------------|---------|--------------|
| Concrete compressive strength ( $f_{cm}$ ) | 43 [MPa]                     | 10      | Normal       |
| Reinforcement yield strength ( $f_y$ )     | 560 [MPa]                    | 5.4     | Normal       |
| Reinforcing steel young modulus ( $E_s$ )  | 200 [GPa]                    | 2       | Normal       |
| Prestressing steel young modulus ( $E_p$ ) | 195 [GPa]                    | 2       | Normal       |
| Steel area ( $A_s, A_p$ )                  | Nom. area [mm <sup>2</sup> ] | 2       | Normal       |
| Neutral axis depth ( $x$ )                 | 0.70 [m]                     | 5.6     | Normal       |
| Model uncertainties ( $\theta$ )           | 1.2                          | 15      | Lognormal    |

In this case, the neutral axis depth is considered as a random variable as well. Since  $x$  is a function of all random variables. Therefore, a set of 10.000 RVs values was generated using the Latin Hypercube sampling method (see Figure 13). Subsequently, the depth of the neutral axis is calculated for each pair of values and normal distribution is adjusted to determine its mean and coefficient of variance, as shown in Table 7.

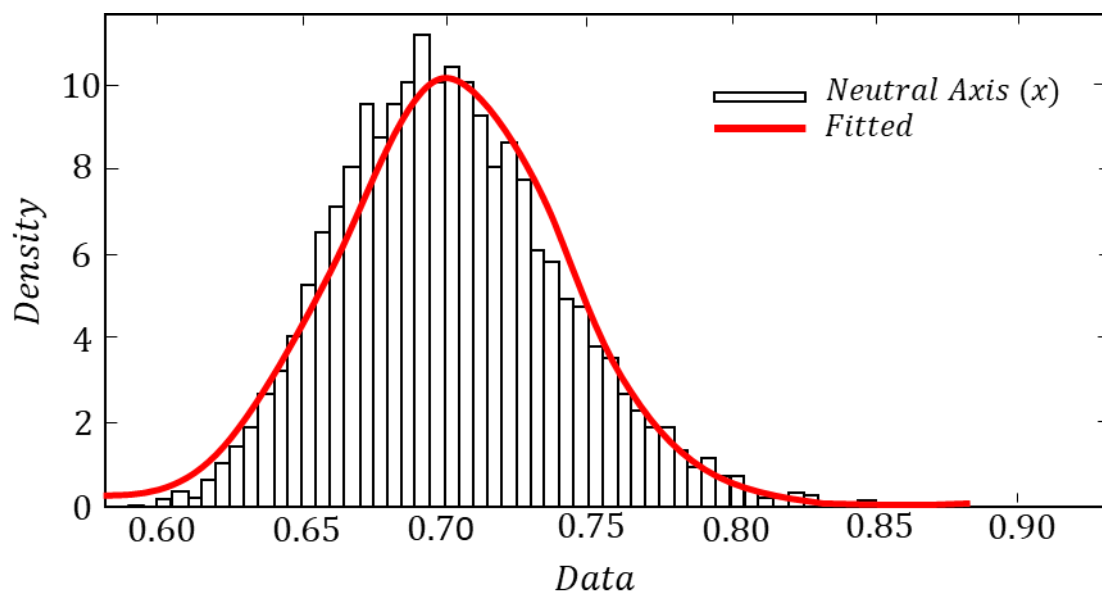


**Figure 13. Normal distribution fitted to the neutral axis depth**

### 2.4.3.2 Load model

For this analysis, it is considered that the bending moment is caused by the effect of the structure's weight, permanent loads, and loads from railway traffic. Therefore, the dead load is assumed as a normal distribution, with  $CoV = 0.10$ . This value of  $CoV$  is assumed due to the variability in terms of the dimensions and specific weight of the materials (e.g., concrete, ballast). On the other hand, the rail traffic load is considered according to the specifications of EN 1991-2 (CEN, 2003) with the Load Model 71 (LM71). This model includes 4 loads of 250 kN per axis, spaced 1.60 m from each other, and to two distributed loads of 80 kN/m spaced 0.80 m from the axle loads, as shown in Figure 14. The load was applied in the most critical position to obtain the maximum bending moment, i.e., the mean value of the axle loads (207 kN) and distributed load (63.4kN/m) in the most critical position of the beam. Furthermore, the characteristic values corresponding to the 98th percentile of the rail freight PDF following a normal distribution (Sustainable Bridges, 2007).

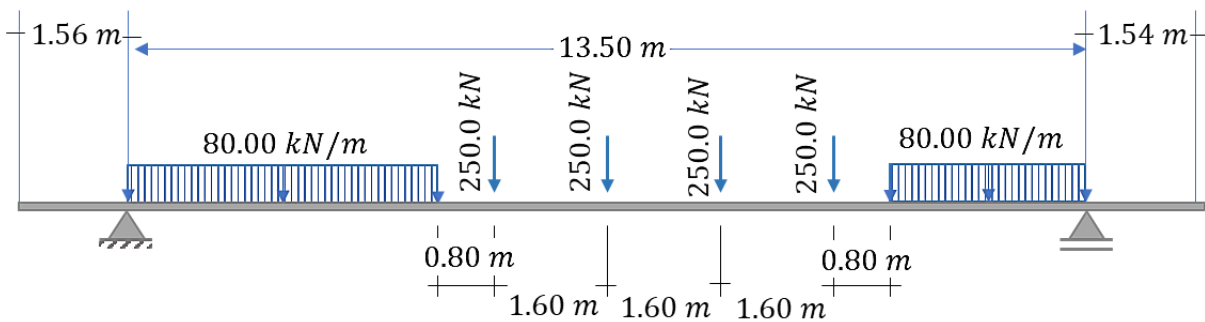


**Figure 14. Load Model 71: railway traffic loads in the critical position (CEN, 2003)**

Furthermore, a dynamic factor ( $\Phi$ ) is considered, which serves to consider the dynamic magnification of stresses and vibration effects in the structure due to the railway moving loads. The dynamic factor is a deterministic value calculated according to equation 6.5 of EN 1991-2 (CEN, 2003).

Finally, the acting bending moment for the load model is expressed as Eq. (29) and the overall parameters and their respective statistical information are summarized in Table 8.

$$M_Q = 21.58W_D + 9W_L + 14P_L \text{ [kN.m]} \quad (29)$$

**Table 8. Statistical parameters of the random variables for the load model**

| Parameter                                       | Mean         | CoV (%) | Distribution |
|---|--------------|---------|--------------|
| Self-weight and additional dead loads ( $W_D$ ) | 150.7 [kN/m] | 10      | Normal       |
| Railway traffic load ( $W_L$ )                  | 63.4 [kN/m]  | 10      | Normal       |

| Parameter                      | Mean       | CoV (%) | Distribution  |
|--------------------------------|------------|---------|---------------|
| Railway traffic load ( $P_D$ ) | 207.4 [kN] | 10      | Normal        |
| Dynamic factor ( $\Phi$ )      | 1.36       | -       | Deterministic |

### 2.4.3.3 Reliability evaluation

Once the resistance and load models have been determined, the flexural limit state is calculated from Eq. (28) and Eq. (29) as shown in Eq. (30).

$$g = \left[ (1.32A_{s1} - 0.04A_{s4})f_y + \frac{E_s}{\chi} (0.0037A_{s2} + 0.0017A_{s3}) + \frac{E_p}{\chi} (0.0049A_{p1} + 0.0026A_{p2}) - \frac{E_s(0.0024A_{s3} + 0.0036A_{s2}) + E_p(0.0018A_{p1} + 0.0013A_{p2}) - 0.33 \times 1000^2 f_{cm} x^2}{(21.58W_D + 9W_L + 14P_L)} \right] \times 10^{-3} \quad (30)$$

The defined limit state function is computed using the first-order reliability method (FORM). The obtained results indicate a reliability index of  $\beta = 5.11$  corresponding to a probability of failure of  $P_f = 1.609 \times 10^{-7}$ .

### 2.4.3.4 Acceptance criteria

The target values to compare the bridge reliability index are shown in Table 9. The present target reliability levels are retrieved from the Joint Committee on Structural Safety publication (JCSS 2001) and the standard ISO 13822, for the ultimate limit state and normal relative costs of safety measures. Note that the related reference period differs for each reference.

When comparing the reliability index obtained, if this is a value higher than the target values specified in the guidelines, then the Simões bridge can be considered safe in the ultimate limit state.

**Table 9. Target reliability levels for ultimate limit state**

| Consequences of failure   | Target reliability indices |                            |
|---|----------------------------|----------------------------|
|   | JCSS*<br>(JCSS 2001)       | ISO 13822**<br>(ISO, 2018) |
| Very low  | -                          | 2.3                        |
| Low   | 3.7                        | 3.1                        |
| Medium  | 4.2                        | 3.8                        |
| High  | 4.4                        | 4.3                        |
| * 1-year reference period<br>** standard period for safety e.g., 50 years |                            |                            |

### 2.4.3.5 Analytical Degradation Models

Since the bridge was commissioned in 2005, it has been inspected four times and some minor maintenance actions have been applied. However, the last available inspection (2016) found some cracking on the deck with water infiltration. This finding is not significant for the bridge performance in the short term, as it does not represent a failure scenario for long term maintenance. Nevertheless, this type of failure can trigger the onset of corrosion, which is one of the biggest sources of bridge deterioration.

Therefore, the equations described in section 2.4.2 are applied. Assuming a uniform area reduction in the bottom reinforcing rebar cross-section. Corrosion is not assumed in prestressed tendons because they have a thicker concrete cover (160 mm) bigger than ordinary reinforcing steel (30mm) and therefore corrosion is not governed by carbonation or chloride penetration through the concrete cover (Sustainable Bridges 2007). For this, the data of average temperature and relative humidity were assumed according to the information available in a meteorological station in the region of Coimbra, where the bridge is located (IPMA, 2020). Furthermore, an w/c ratio of 0.5 is assumed. The remaining random variables used in this section are shown in Table 10. After calculations, the reduction in cross-sectional area is obtained after the corrosion onset time, as shown in Figure 15.

**Table 10. Random Variables Used in Girders Reliability Analysis**

| Definition of Rvs                                       | Notation           | $\mu$                                  | $\sigma$               | Distribution | Reference                   |
|---|--------------------|--|------------------------|--------------|-----------------------------|
| Concrete cover depth                                    | $x$                | Dnom+0.8 mm                            | 3.6 mm                 | Normal       | (Vu and Stewart, 2000)      |
| Reference chloride diffusion coefficient                | $D_{cl,0}$         | 473.0 mm <sup>2</sup> /year            | 43.2 m <sup>2</sup> /s | Normal       | (Ghosh and Sood, 2016)      |
| Model uncertainty coefficient - Fick's law idealization | $X_1$              | 1                                      | 0.05                   | Lognormal    | (Choe <i>et al.</i> , 2008) |
| Environmental correction factor                         | $k_e$              | 2.92                                   | 11.0                   | Gamma        | (Ghosh and Sood, 2016)      |
| Correction factor for tests                             | $k_t$              | 0.832                                  | 0.024                  | Normal       | (Choe <i>et al.</i> , 2008) |
| Curing time correction factor                           | $k_c$              | a = 1.0, b = 4.0<br>p = 2.15, q = 10.7 |                        | Beta         | (Ghosh and Sood, 2016)      |
| Aging factor or age exponent                            | $\eta_{cl}$        | a = 0.0, b = 1.0<br>p = 17.2, q = 29.3 |                        | Beta         | (Ghosh and Sood, 2016)      |
| Chloride surface content regression parameter           | $A_{cs}$           | 7.76                                   | 1.36                   | Normal       | (Ghosh and Sood, 2016)      |
| Chloride surface  | $\varepsilon_{cs}$ | 0                                      | 1.11                   | Normal       | (Ghosh and Sood, 2016)      |

| Definition of Rvs               | Notation | $\mu$ | $\sigma$ | Distribution | Reference              |
|---------------------------------|----------|-------|----------|--------------|------------------------|
| content error term              |          |       |          |              |                        |
| Critical chloride concentration | $C_{cr}$ | 0.50  | 0.10     | Normal       | (Ghosh and Sood, 2016) |

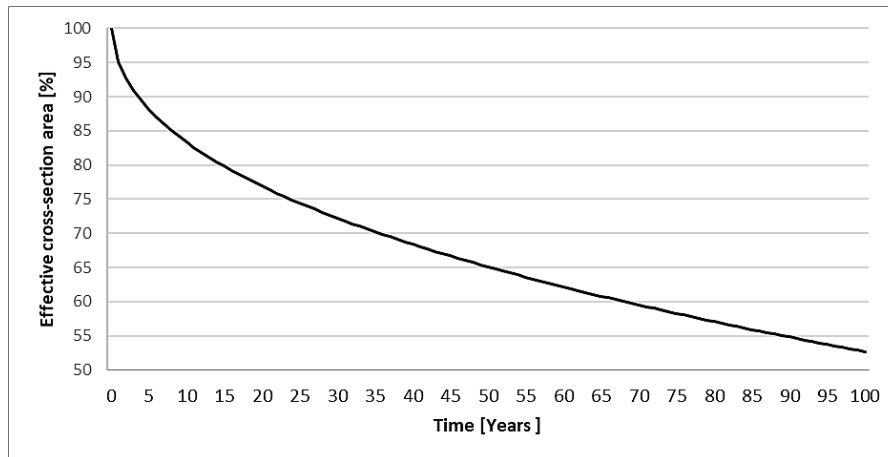


**Figure 15. Reinforcement area variation over time**

Additionally, in Figure 16 is possible to observe the directly proportional relationship between the reinforcement area reduction in the cross-section and the bearing capacity reduction of the bridge. It is important to highlight that in some cases the reliability indices are lower than the target values shown in Table 9.

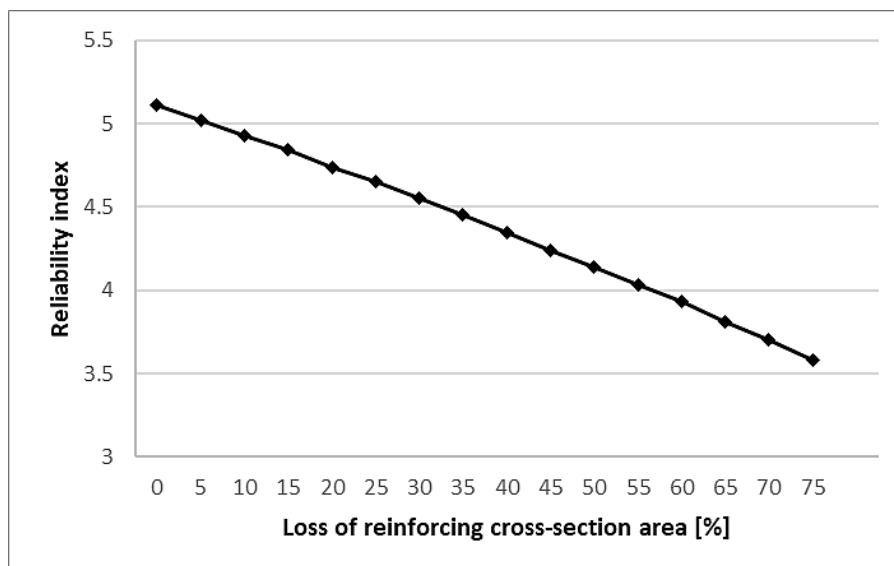


**Figure 16. Reliability index variation due to corrosion**

From this, it can be concluded that a loss of more than 40% of the cross-sectional steel area lowers the reliability indices below the target values. This percentage

could be reached after 65 years of bridge life, which is designed for a longer lifespan.

#### 2.4.3.6 Inspections

The inspection process will be based on the AASHTO Bridge Element Inspection Guide Manual (AASHTO, 2010), which serves as a resource for agencies to perform element level bridge inspections in the United States (US). This latter version replaced the AASHTO Guide to Commonly Recognized Structural Elements from 1994. It is a reference for standardized element definitions, quantity calculations, condition state definitions, element feasible actions, and inspection conventions (AASHTO, 2010). This manual consists of assigning a condition classification to the different elements of the bridge through visual inspections. Structural and non-structural elements are included (e.g., railings, joints). Moreover, different types of materials such as concrete, steel, or wood can be addressed. Inspections must be performed by a trained inspector who can classify each item in one of the specified condition states. For this case in which the beams are analysed as a critical element of the Simões bridge, the classification designated in element 110 shown in Table 11 must be taken into account.

**Table 11. AASHTO (2010) Suggested condition state ratings for Reinforced Concrete Girder / Beam**

| Condition State | Cracking  | Spalls / Delaminations/ Patched Areas                                 | Efflorescence                            | Load Capacity                              |
|-----------------|---|---|--|--|
| 1               | None  | None  | None                                     | No reduction                               |
| 2               | Narrow size and/or density  | Moderate spall or patch areas that are sound                          | Moderate without rust                    | No reduction                               |
|                 | < 0.0625 inches (1.6 mm)  | N/A   | Spacing Greater than 3.0 feet (0.33 m)   | NA   |
| 3               | Medium size and/or density  | Severe spall or patched area showing distress                         | Severe with rust staining                | No reduction                               |
|                 | 0.0625 – 0.125 inches (1.6 – 3.2 mm)  | Spall less than 1 inch (25 mm) deep or less than 6 inches in diameter | Spacing of 1.0 - 3.0 feet (0.33 – 1.0 m) | Surface white without build-up or leaching |
| 4               | The condition is beyond the limits established in condition state three (3) and/or warrants a structural review to determine the strength or serviceability of the element or bridge. |   |  |  |

| Condition State | Cracking               | Spalls / Delaminations / Patched Areas   | Efflorescence                        | Load Capacity                     |
|-----------------|------------------------|--|--------------------------------------|-----------------------------------|
|                 | >0.125 inches (3.2 mm) | Spall greater than 1 inch (25 mm) deep or greater than 6 inches in diameter or exposed rebar | Spacing of less than 1 foot (0.33 m) | Heavy build-up with rust staining |

However, there are some problems with using inspection data to update reliability. The first problem is that the condition state-assigned is equal to the entire beam length and does not offer an adequate beam identification regarding deterioration or damage. The element location is necessary due to, according to the location is possible to attribute the damage to the correct failure mode (i.e., if the damage is located near the beam centre, the moment limit state is the most affected). Another problem is regarding use the data effectively in reliability analysis because the data (i.e., thickness loss caused by corrosion) must be defined in probabilistic terms, which is not possible from a visual inspection.

Therefore, some conservative assumptions are made to provide a reliability assessment taking into account the information from the inspections. Consequently, to overcome the location problem, the procedure suggested by Hearn and Frangopol (1996) and Estes, ASCE, and Frangopol (1999) is adopted. It consists of inspection by segments following the AASTHO guidelines, assigning the conditions state in specific locations of the structure. In other words, the bridge is divided into small, easily definable segments and each segment is classified separately. To make this process easier, it is recommended to have a drawing of the structure as part of the inspection report (an example is shown in Figure 17). It is important to mention that subdividing the structure into several segments does not alter the work time required during the inspection. Just a preliminary time to develop the drawing.

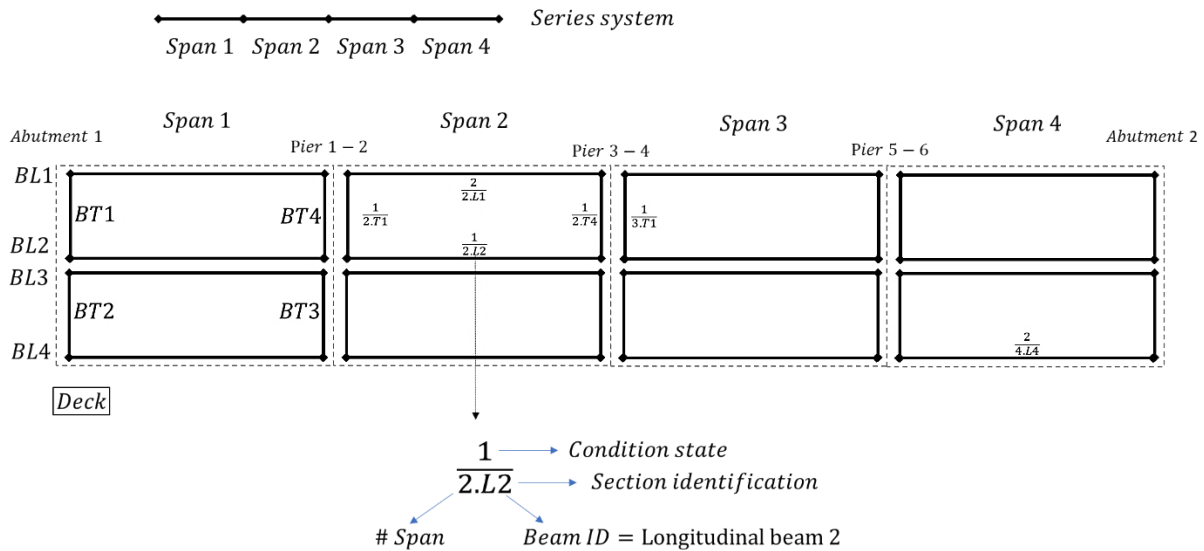


**Figure 17. Segment-based inspection reporting results for the superstructure**

Figure 17 presents a procedure example illustrated for the case study. However, the assigned condition states do not correspond to the actual ones. First, because the existing inspection reports were not developed with the procedure described here. Second, the most recent report is from 2016. Although it was possible to assign condition states in some bridge elements, as shown in Figure 18. These condition states were made based on the available visual inspection reports provide by “Infraestructuras de Portugal” and taking into account the descriptions in Table 11.

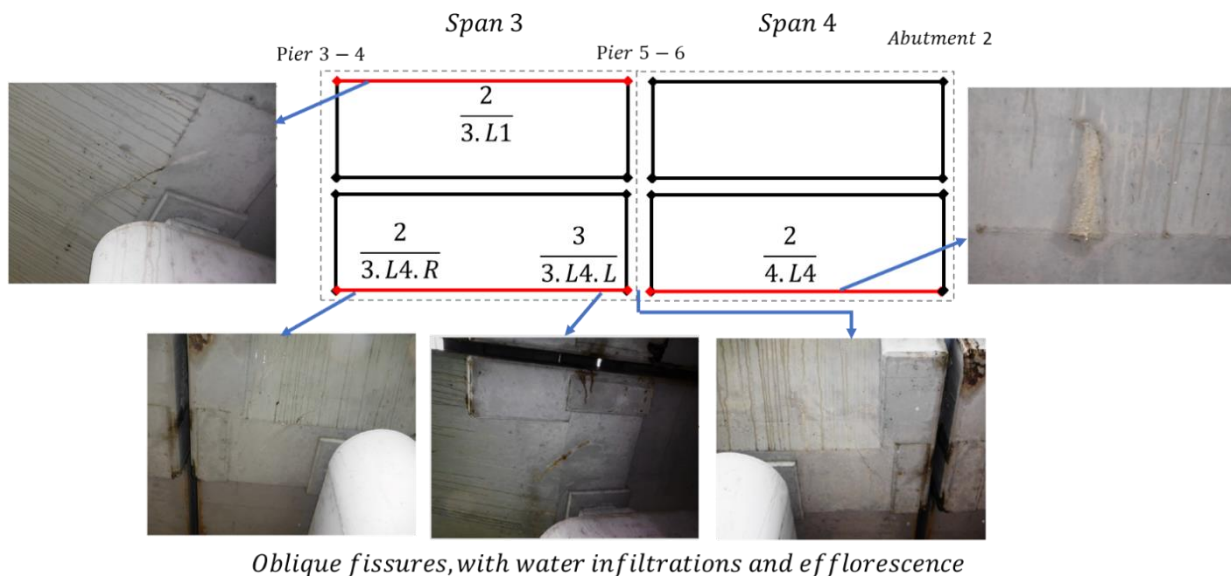


**Figure 18. Segment-based damaged identification from visual inspection reports (Source: Infraestruturas de Portugal) – Simões bridge girders**

After inspection, each beam segment may have different assigned condition states (e.g., 3.BL4, in which R corresponds to the right side and L to the left side). Therefore, a global beam condition state is assigned depending on the most critical



value received according to the reported failure mode (e.g., condition state 3 for BL4). However, the reported damages are not significant for the failure mode studied, which in this case corresponds to the bending moment.

On another hand, to refine the reliability calculation, it is necessary to know the parameters with the greatest influence on the structure reliability. Variables identification may be achieved through sensitivity analysis, which provides a measure of the importance of the variation coefficient of a specific parameter concerning the structure reliability. Subsequently, it is possible to apply the Bayesian updating to the predetermined distributions of the identified key parameters. Lark and Flaig (2005) have identified the main parameters that can influence the capacity of corroded RC beam are the corrosion loss of reinforcing bars, concrete cover, and strength. Since the only parameter that can be evaluated from a visual inspection is the concrete cover. For the next section, the example continues under the assumption that the deterioration identified in the inspections reports affects the failure mode by bending moment of the beams, specifically BL3, which is the most affected by corrosion and therefore greater probability of occurring concrete cover loss, reinforcement loss area and consequently capacity loss.

It is worth noting that SAFEWAY project aims to complement visual inspections with laser scanner (LiDAR-based systems) measurements, which are described in SAFEWAY (2019c). It is intended to identify damages such as those shown in Figure 19, developed by Isailović et al. (2020). Nevertheless, such inspection inputs were not available for this report.

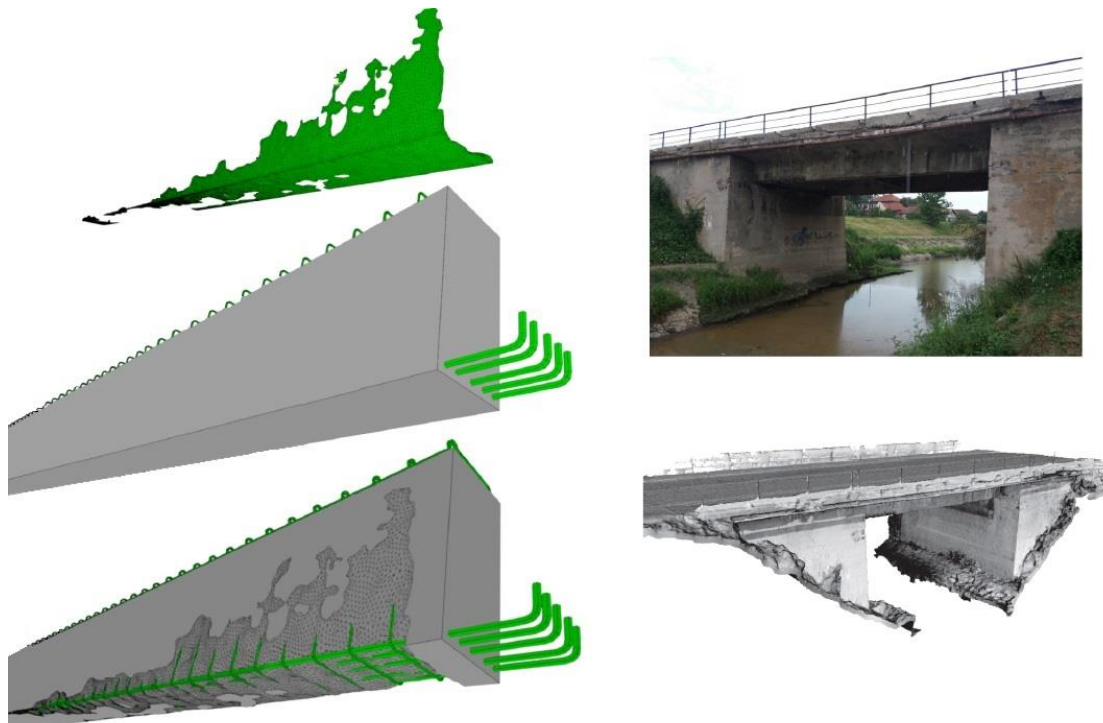


**Figure 19. Geometric representation of damage through Photogrammetry-based 3D point cloud. Adapted from: Isailović et al. (2020).**

#### 2.4.3.7.1. Condition states into probabilistic terms.

Condition states will be translated into probabilistic terms assuming that the condition states are linear over time and deterioration intensity values are normally distributed. The parameters such as mean value and standard deviation are determined by the component condition and the quality of the inspector (Estes and Frangopol 2003). Table 12 shown the condition state suggested to classify concrete cover in beams. This information is not part of the AASTHO manual specifications but is created based on it to quantify the observed concrete cover damaged. Since the experience of the inspector is also taken into account. Frangopol and Estes (1997) recommend considering three possible cases, inspectors qualified as very experienced, experienced, and inexperienced. Frangopol and Estes (1997) recommend considering three possible cases, inspectors qualified as very experienced, experienced, and inexperienced. Assuming the ratings provided by them are correct 95%, 85%, and 75% of the time respectively.

**Table 12. Assigned concrete cover loss from a Condition Index Inspection**

| Condition State | Description   | Section loss <sup>a</sup> |
|-----------------|---|---------------------------|
| 1               | No significant cracking areas, spalls/laminations exist or the area is 5% or less of the beam surface | 0 - 5 %                   |
| 2               | The cracking/spalls/delamination area is 10% or less of the beam surface                              | 0 - 10 %                  |
| 3               | Cracking/spalls/delamination area is more than 10% but less than 25% of beam surface                  | 10 - 25 %                 |
| 4               | Cracking/spalls/delamination area is more than 25% of beam surface                                    | > 25 %                    |

<sup>a</sup>Not part of the AASHTO definition - created to quantify the observed concrete cover damaged.

For instance, to build the probabilistic distribution of condition state 3 (CS 3). From Table 12 is possible to observe the range of concrete cover loss is from 10% to 25%, the mean value ( $\mu$ ) would be 17.5%. On another hand, and assuming that the inspector will classify the structure correctly 90% of the time the standard deviation  $\sigma$  can be computed as Eq. (31).

$$\sigma = \frac{(vm - \mu)}{\Phi^{-1}(EI)} = 5.9 \quad (31)$$

Where  $vm$  is the maximum value of the range,  $\mu$  the mean value,  $\Phi^{-1}$  is the inverse standard normal an  $EI$  is the inspector's experience. The mean value increases linearly until reaches a maximum value ( $vm$ ) of 25% concrete cover, where it will

remain until an inspector classifies the deck as condition state 4 in a future inspection (Estes, Foltz, and Mckay 2005).

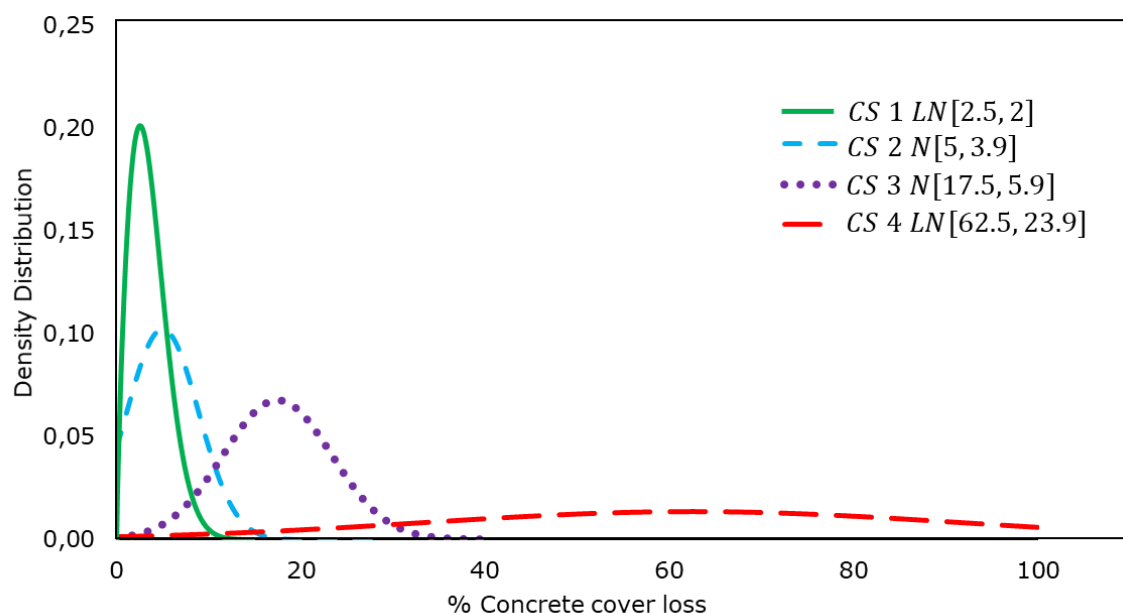


**Figure 20. Probability density distributions associated with condition state (CS) ratings for concrete cover loss**

All condition states are presented as a normal distribution except the first and last condition states, which are assumed to be lognormal, CS1 to reflect that the section will not increase in the area due to corrosion and CS4 to represent that the negative area is not possible for a cross-section (Estes and Frangopol, 2003). All probability distributions in Figure 20 were built assuming an inspector correctly assigns the condition states 90% of the time.

#### 2.4.3.7 Bayesian updating

The parameter under study (concrete cover) was initially specified as a random variable from the definition of the corrosion parameters in analytical models (see section 2.4.3.5, Table 10). From the inspection data, a condition state 3 is assumed for the longitudinal beam of the third spam (3BL see Figure 18), consequently, the concrete cover loss due to corrosion can be estimated and its reliability updated as is shown in Table 13. Other examples of Bayesian update techniques can be found at (Ang and Tang, 1975; Melchers and Beck, 2018).

**Table 13. Comparison of concrete cover results for 3BL based on Deterioration Model Prediction, Inspection Results, and Updated Posterior Distribution**

| Condition state | Cover $x$ (mm) | Model prediction |          | Inspection results |           | Posterior distribution |            |
|-----------------|----------------|------------------|----------|--------------------|-----------|------------------------|------------|
|                 |                | $\mu$            | $\sigma$ | $\mu'$             | $\sigma'$ | $\mu''$                | $\sigma''$ |
| 3               | 40             | 40,08            | 3,6      | 33                 | 5,9       | 38,16                  | 3,07       |

Note: Inspection results are based on a very experienced inspector.

$\mu$  and  $\sigma$  are the mean values and standard deviations for the respective distributions.

After obtaining the posterior distribution for the concrete cover, it is proceeded to update the degradation models (section 2.4.3.5). This is summarized in Figure 21, in which the area reduction of the reinforcing bars due to corrosion can be observed for the three cases (i.e., predictive model, inspection results, and with the information obtained from the Bayesian update).

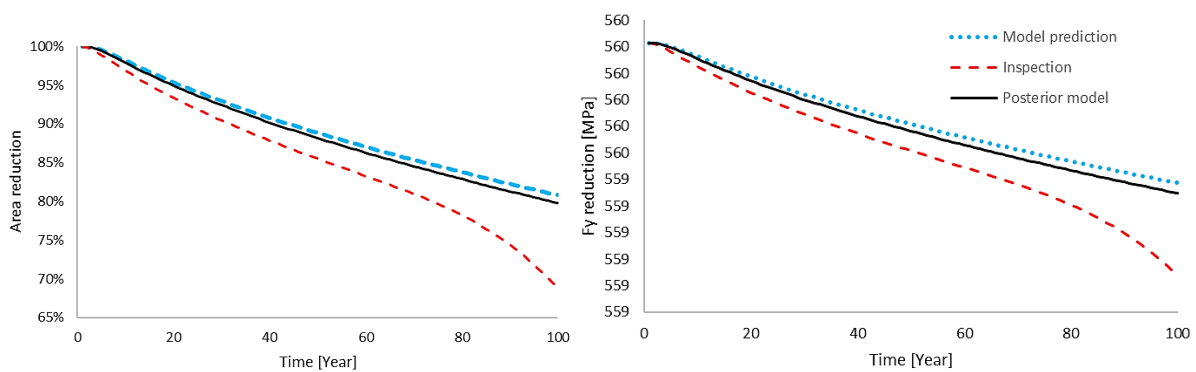


**Figure 21. Comparison of Area and Strength rebar reduction based on concrete cover model Prediction, inspection Results, and updated posterior distribution.**

With the information obtained from the Bayesian update, there is a difference in the area reduction of 0.12% and a difference of 3.9 MPa in the  $f_y$ . It means that without the parameter update the structural damage is underestimated. It should be noted that after updating the degradation models, the prediction of the reliability analysis over time must also be updated.

Finally, it should be highlighted that this methodology can be applied in the update of any of the parameters selected within the framework as random variables, as long as the information from inspections is available. It can also be applicable to any type of infrastructure or material.

### 3. Dynamic Risk-based Predictive Models

Managers of transport infrastructures have the continuous task to plan and execute interventions to guarantee the operational state of their networks, even in the aftermath of hazard events (Hackl *et al.*, 2018). As the resources available to managers to protect their infrastructures are limited, it is essential for managers to be aware of the probable consequences (i.e., risk) in order to set priorities and be resource-efficient (Eidsvig, Kristensen and Vangelsten, 2017).

A risk-based framework facilitates a rational and balanced approach for evaluating the effect of hazards on systems, possible failure modes, and associated consequences (Lounis and McAllister, 2016). A conceptual risk model for assessment of impacts to asset systems triggered by natural events was presented in SAFEWAY (2020). Nevertheless, there are many uncertainties involved in the estimation of risk, i.e., uncertainties in the hazard frequency and intensity; uncertainties in the infrastructure performance when subjected to the hazard; and uncertainties in the socio-economic impacts associated with the possible disruptions in the network; which can be reduced by means of observations to the system. Moreover, the risk might not be stationary into the future (Beven and Hall, 2014). Thus, a risk-based framework should account for the variability of the analysed system over time. For instance, the condition of the infrastructures deteriorates over their service life. Likewise, time-dependent socio-economic factors such as population growth (or decline) and future traffic demands affect the prediction of impacts. Therefore, an integrated framework for dynamic risk-based predictive models is herein proposed, whereby real-time data and time-variant factors are introduced.

The proposed framework is presented in Figure 22. The core of the framework is the three main components of a risk-based methodology, namely the hazard module, the infrastructure performance, and the quantification of possible consequences (represented with grey boxes). It can be observed that time-variant factors (represented with yellow boxes) are integrated in order to *i)* consider the actual condition of the infrastructure into the fragility assessment under the natural hazards; *ii)* address the dispersion of future hazards due to climate change projections; and *iii)* account for the actual population affected and the real traffic demands when computing the socio-economic impacts involved with the failure of the assets. Furthermore, real-time data (represented with green boxes) can be used for monitoring the hazard, monitoring the infrastructure condition, and provide crowd sourcing data. Monitoring the key indicators of hazard, e.g., the water level for flooding hazard, the uncertainties in the hazard magnitude/intensity can be reduced. Similarly, by means of monitoring the infrastructure using emerging digital technologies, e.g., remote technologies such as LiDAR systems, the uncertainties in defining the infrastructure condition can be reduced. Finally, crowd sourcing data can be used for traffic rerouting after hazard occurrences in order to reduce the impact of traffic-related consequences.

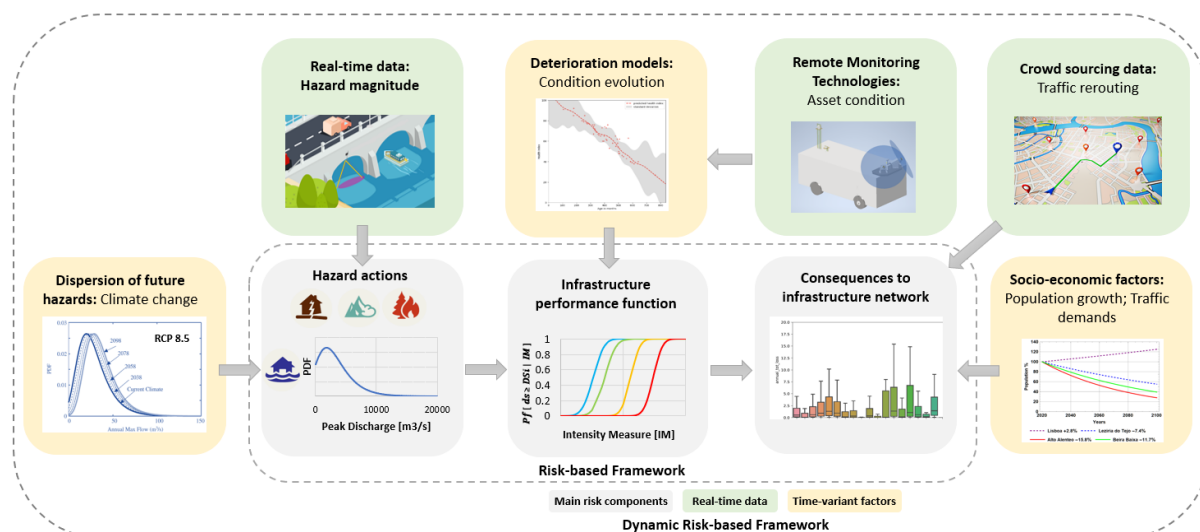


**Figure 22: Integrated framework for Dynamic Risk-based Predictive Models**

The proposed framework can be applied to any hazard or multiple hazards. In the context of the present deliverable, the methodology will be further detailed to roadway and railway infrastructures exposed to flooding hazard. Accordingly, the SAFEWAY pilot located in Santarém, Portugal, will be the focus of study. Nevertheless, it can be extended to other type hazards identified within SAFEWAY pilots (SAFEWAY, 2019a, 2019c).

In the following subchapters, an overview of the methodologies used for the assessment of the dynamic risk-based components are briefly presented. Section 3.1 defines the boundaries of the system to be analysed; Section 3.2 explains how the hazard module will be treated within SAFEWAY; Sections 3.3 and 3.4 give introductory remarks regarding the evaluation of infrastructure performance and the quantification of consequences, respectively. Both of these components will be further studied in the remaining chapters of this report.

### 3.1 System boundaries

One of the first steps in conducting a risk assessment is to define spatially and temporally the boundaries of the system that is going to be analysed (Adey *et al.*, 2016). Table 14 summarizes the system boundaries that were specified for the implementation of the proposed dynamic risk-based framework.

**Table 14. Definition of the system boundaries**

| Type of boundary   | Definition  |
|--------------------|---|
| Spatial boundaries | The spatial boundary of the system is shown in red in Figure 23. The following municipal councils from the Santarém district are at the considered boundaries of the case study: Abrantes, Almeirim, Alpiarça, Cartaxo, Chamusca, Constância, Entrocamento, Golegã, |

| Type of boundary    | Definition  |
|---------------------|---|
|                     | <p>Salvaterra de Magos, Santarém, Tomar, Torres Novas, and Vila Nova da Barquinha. The selected boundaries (red polygon) cover an area of approximately 1200km<sup>2</sup>.</p> <p>Besides the main watercourse, namely the Tagus river, the following watercourses relevant to the study area are included: Almonda, Alviela, Torto, and Zêzere rivers. The hazard corresponds to slow-onset flood events associated to these watercourses.</p> <p>The objects are comprised by roadway and railway bridges located over the selected watercourses, 10 road sections, and 6 rail sections; all within the spatial boundary from in Figure 23.</p> <p>The traffic model (Chapter 6.2) includes all the transportation network from the municipal councils within the spatial boundary from Figure 23. Thus, the transport related consequences correspond to the ones generated within this area.</p> |
| Temporal boundaries | <p>The risk will be assessed for several time periods, namely the current year 2020, and future scenarios at years 2030, 2040, 2050, and 2070.</p> <p>As proposed in the framework from Figure 22, the system representation is dynamic, i.e. the infrastructure performance evolves over time (degradation/improvement), as well as the socio-economic factors (e.g. traffic demands and population growth) which dominate the consequences.</p>   |

It should be noted that some assumptions were considered regarding the modelling and the response of the system. Consequently, some possible situations outside the considered system are not being modelled. For instance, some consequences could be generated outside the specified spatial boundary, and physical damage to other types of roadway and railway assets (e.g. culverts) could also occur.



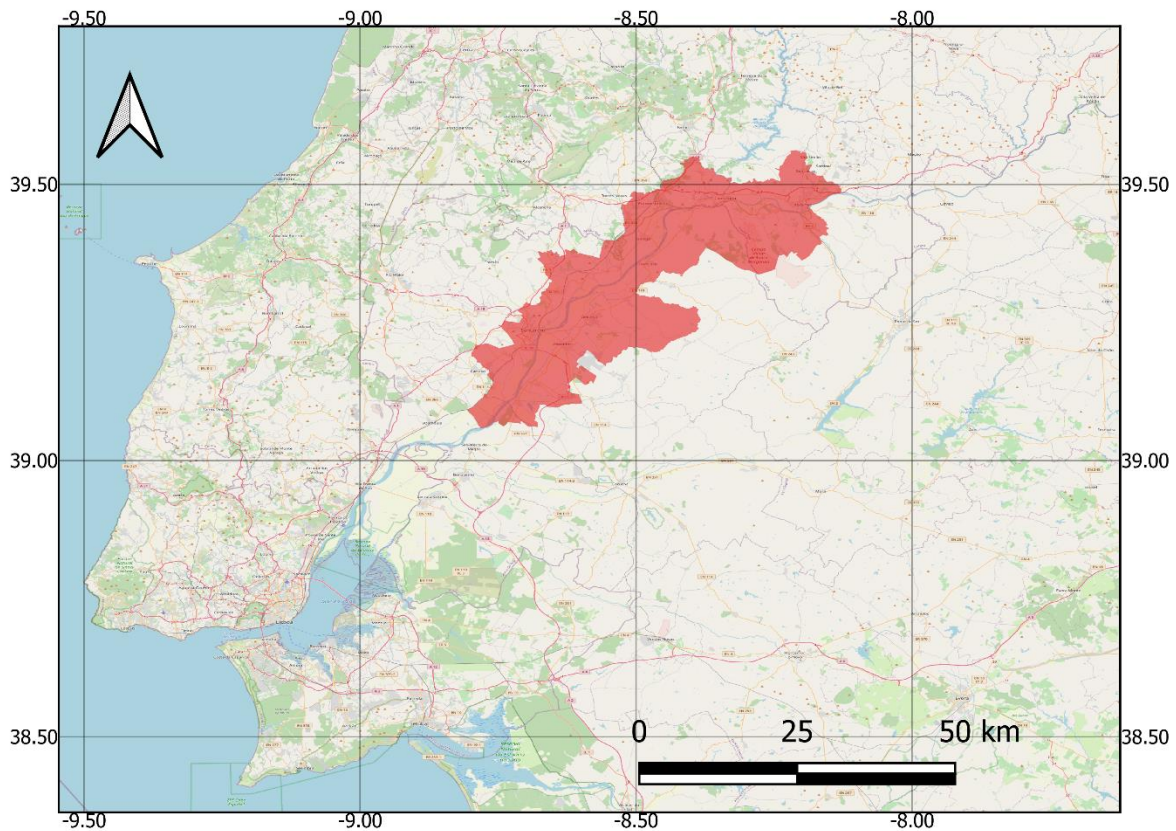


**Figure 23. Representation of the spatial boundary of the system analysed**

### 3.2 Hazard assessment

Floods are considered a major hazard in the Santarém demonstration site, as roads and railway infrastructures are placed along the basin of the Tagus River where slow-onset floods are particularly predominant (SAFEWAY, 2019c). The EU directive 2007/60/CE on the assessment and management of flood risks (DAGRI), established the need for elaborating hazard and risk maps for several return periods. Consequently, flood hazard (water depth, flux velocity, inundation boundary), consequence and risk maps were elaborated for Portugal for several return periods (20, 100, 1000 years) (APA, 2014). SAFEWAY (2019a) produced hot-spot maps for the Santarém region by overlapping the hazard maps with road and railway networks, so the most exposed areas of the transportation system were indicated.

The flood maps offer a first approximation of the flood inundation extent, water levels and flow velocities for the chosen probabilities of exceedance. However, they do not explicitly account for the multiple sources of uncertainty involved when deriving these maps, including topography data, estimated flood discharges for the chosen design event, choice of a hydraulic model, choice of model parameters (e.g. hydraulic roughness coefficients), and model assumptions (Beven, Leedal and McCarthy, 2014). Among these, it is recognized that the precision (or resolution) and accuracy of river channel and floodplains topography is one of the



most critical factors which influences the hydraulic modelling results (Casas *et al.*, 2006). Consequently, several studies have been carried out for evaluating the impact of the topographic data quality on the results of hydraulic models (for an overview refer to Md Ali, Solomatine and Di Baldassarre (2015)). The available flood maps for Santarém region were derived by using a digital elevation model (DEM) generated primarily from vectorial cartography (1:25000 scale) from 25 m contour intervals, complemented with data from the NASA global model derived from the Shuttle Radar Topography Mission (STRM), and at lower extent by LiDAR data available at specific areas (APA, 2014). This DEM resolution frequently provides a valuable source for large-scale flood studies, as it is able to simulate the flooding pattern and inundated area extent with reasonable accuracy. However, it has been found that the extent to which DEM resolution and accuracy influences the hydraulic outputs depends on the shape of the valleys and channel slope. Overall, small rivers with steeper channel slope, V-shaped valleys and urban land use are more influenced by DEM resolution and accuracy (i.e. contain larger errors) than flat channel slopes with deeper U-shaped valleys (Saksena and Merwade, 2015).

Therefore, in order to assess at asset level the flood hazard exposure within the SAFEWAY case study, the flowchart from Figure 24 is herein proposed. Essentially, based on the location of the exposed asset, and thus the river valley shape and channel slope, the decision whether to use or not the available flood hazard maps is taken. In the case they are employed, the uncertainties on the flood estimates at the asset location will be introduced by fitting a probability distribution with uncertainty intervals. Conversely, if the flood hazard maps are not used, the existence of flow discharge data at the site of interest should be verified. In case of flow data availability, flood frequency analysis should be performed, and the most appropriate probability distribution should be selected to describe the peak flow discharge with confidence intervals. In case of an ungauged site location, the peak discharges should be derived from hydrological models for each flood event. Then, a probability distribution will be fitted to the peak flow estimates with uncertainty intervals. If the site where the information is available does not correspond to the asset location, a transposition of flows is required. Finally, a hydraulic analysis is necessary to obtain the water depth and the flow velocity estimates to quantify the hydrodynamic load applied to the infrastructures. For this last step, the sources of hydraulic uncertainty should be also considered during the analysis (for further details see Lagasse *et al.* (2013)).

It should be pointed out that the flowchart from Figure 24 was proposed given the data availability constraints but could be replaced by a complete and detailed hydrologic-hydraulic modelling of the system defined in Section 3.1, with full consideration of the uncertainties involved in the modelling processes. However, this approach for the large system under analysis is very complex, time-consuming, and requires a large number of inputs which are usually unavailable especially with high accuracy (e.g. DEM models). Conversely, the alternatives included in the flowchart correspond to data which is usually readily available by national organizations in each country (such as the SNIRH and APA in Portugal), in order to comply with the EU directive 2007/60/CE demands.

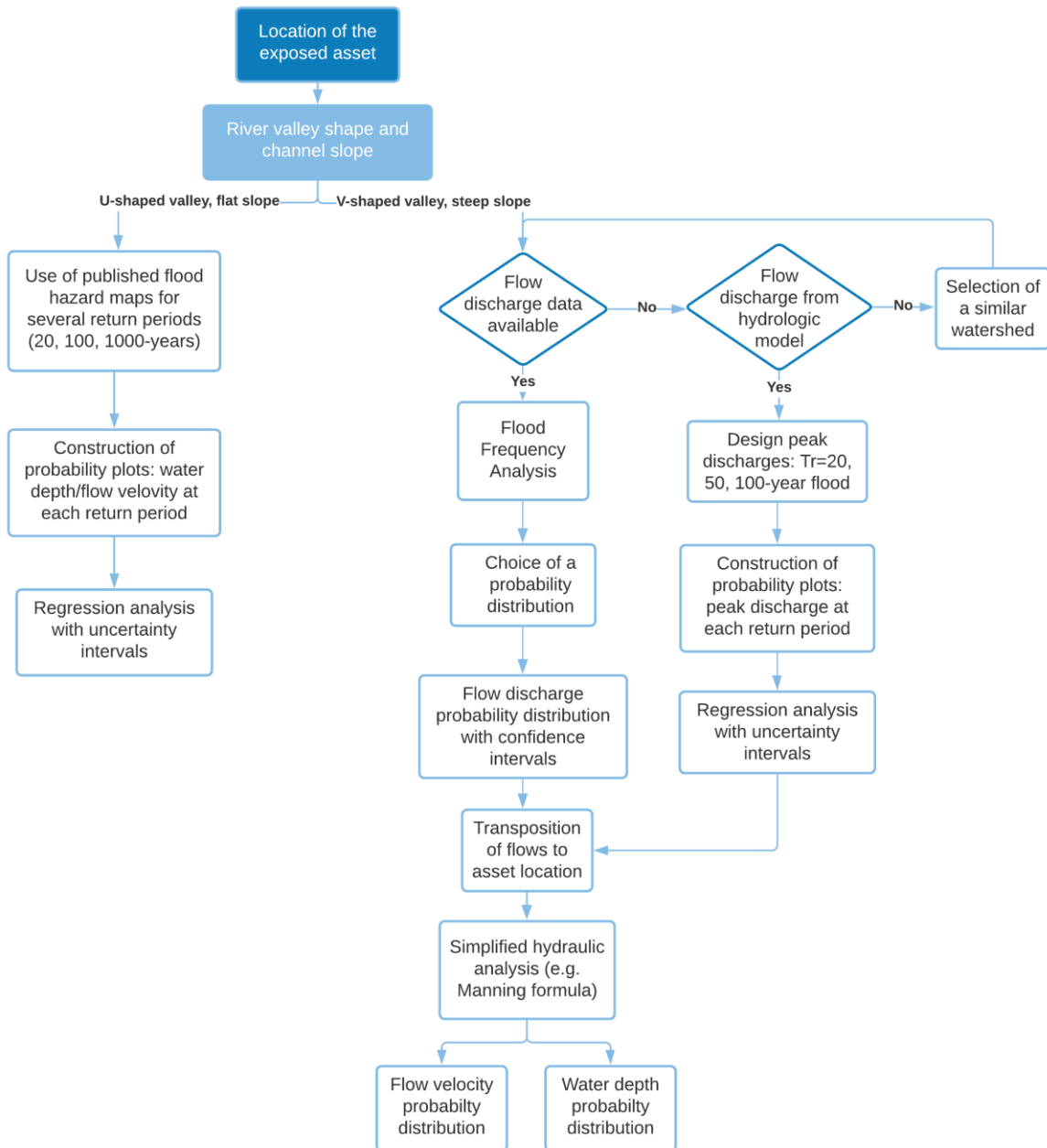


**Figure 24. Flowchart implemented to treat the flood hazard at asset level in SAFEWAY case study**

The following sub-chapters describe in more detailed the three main branches of the flowchart. It should be pointed out that the proposed flowchart is followed for a detailed analysis of each asset given its particular characteristics and the data availability for each case. However, if the scope of the analysis is at a network scale, the existing flood hazard maps may be directly applied as proposed in Sections 5.2 and Sections 6.1.

### 3.2.1 Characterization from existing flood hazard maps

As previously mentioned, flood hazard maps are subject to large amounts of uncertainties. Some of them are aleatory, i.e. related to the natural variability in the occurrence of floods, and others are epistemic, i.e. related to our limited knowledge about the hydrologic and hydraulic processes being modelled. Many studies have investigated the effect of these uncertainties on flood hazard predictions and have demonstrated that they can be significant. Therefore, methodologies and frameworks have been developed aiming at assessing these uncertainties reliably (refer to Beven and Hall (2014); Beven, Leedal and McCarthy (2014)).

The degree of detail regarding how to assess the uncertainty can vary from a qualitative expert judgement to a detailed analysis involving many runs of a hydraulic model accounting for various uncertain input factors. Detailed analysis are computationally expensive as the time for one simulation to run can take up to 50 minutes for fine resolution models for a basin of 2000km<sup>2</sup> (as reported by Savage *et al.* (2016)). For this reason, a trade-off between the use of models with coarser resolutions has been a research interest to optimize the computational time and perform a larger number of simulations, as well as conducting sensitivity analysis to understand which are the dominant sources of uncertainty and therefore reduce the number of uncertain inputs.

In this report, the intention was to express a confidence interval to the existing flood model predictions. Therefore, a qualitative analysis based on literature review was used to estimate the extent of the uncertainties. As this topic is relatively new, it is difficult to find a consensus regarding the importance of different sources of uncertainty and the appropriate assumptions for different types of application. Recently, Thomas Steven Savage *et al.* (2016) performed a global sensitivity analysis to investigate the influence of the spatial resolution, the Manning's friction coefficient parameters, the inflow hydrograph and the DEM resolution on the flood hazard predictions. It was found that the most influential factor for the average maximum water depth and the maximum flood extent were the boundary conditions, i.e. the river discharge. Even though there are limitations to extrapolate these findings to other locations, for different flood return periods, and for other predictions besides water depth such as flow velocity, it was assumed herein that the river discharge uncertainties are likewise the predominant source of uncertainty in the flood hazard predictions of this study. According to McMillan, Krueger and Free (2012), river discharges have been shown to be uncertain by at least  $\pm 10\text{--}20\%$  for medium or high (in-bank) flows and up to  $\pm 40\%$  for out of bank flows. Therefore, for the 20-year return period estimates (both water depth and flow velocity), an uncertainty of  $\pm 20\%$  was assumed; while for the 100- and 1000-year return period estimates, an uncertainty of  $\pm 30\%$  was considered. It should be noted that these uncertainties do not account for effects of climate change (refer to Section 7.1 for climate change considerations). These assumptions made will ultimately contribute to define if a more detailed analysis is justified or not.

Following Lagasse *et al.* (2013), a Lognormal distribution was assumed for water depth and flow velocity estimates for each return period. Thus, the estimates which correspond to the mean values were transformed to the logarithmic space, and

the lognormal standard deviations were obtained from the uncertainties previously defined. The expected values and standard deviations were input to Monte Carlo (MC) realizations for each variable per return period. Subsequently, a regression analysis was performed in order to provide extrapolations of the flood estimates for different return periods. To this end, probability plots were used to verify the adequacy of a specific theoretical distribution. These plots are designed by transforming the scale of the probability axis, so that a given distribution is represented by a straight line.

The water depth estimates at a specific asset location for each exceedance probability were plotted into a Gumbel probability plot, where it was evidenced that the variable is represented appropriately by this distribution as it is represented by a straight line (Figure 25). The results of the Gumbel regression with lower and upper bounds of the uncertainty interval representing the 5<sup>th</sup> and 95<sup>th</sup> percentiles are shown in Figure 25. Similarly, flow velocity exhibits the same behaviour as displayed in Figure 26.

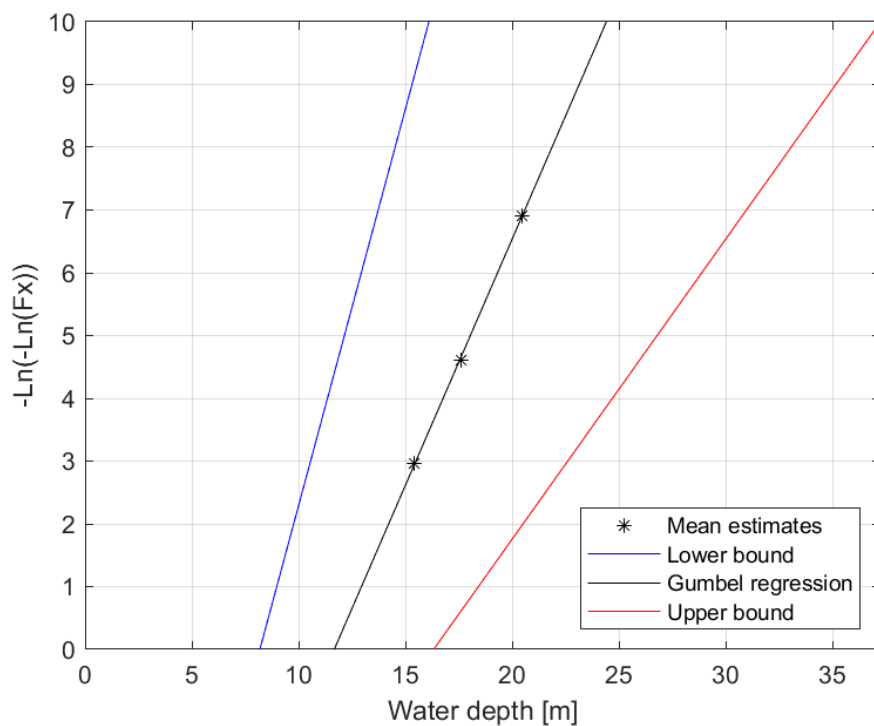


**Figure 25. Fitted Gumbel distribution for water depth with uncertainty intervals**

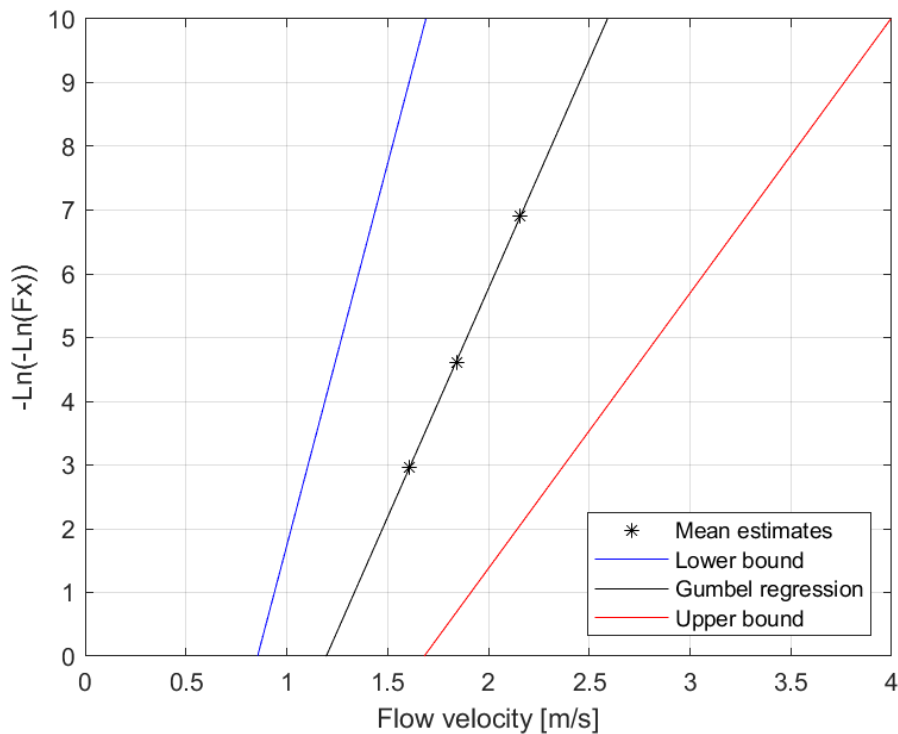


**Figure 26. Fitted Gumbel distribution for flow velocity with uncertainty intervals**

### 3.2.2 Statistical analysis of flow discharge data

One of the most widespread approaches for assessing the flood hazard consists of estimating the peak discharge for a given exceedance probability based on the statistical analysis of annual peak flows records. This method, frequently referred to as flood frequency analysis (FFA), is conditioned by the availability of flow data at the site of interest. That is, the accuracy of the estimated flood frequency curve depends on the records sample size, its representativeness, and the appropriateness of the chosen distribution (England Jr *et al.*, 2019).

On the main stretch of the Tagus River, there are three hydrometric stations, namely Tramagal, Almourol and Santarém/Ómnias (see Figure 27). Annual peak discharge data recorded at these stations are accessible free of charge through the website of the National Information System for Water Resources (SNIRH)<sup>2</sup>.

The data are available from 1974/1975 until the year when the stations were presumably discontinued, namely year 1999 for Santarém, year 2008 for Tramagal, and year 2017 for Almourol. However, some years of records are missing between these intervals, resulting into 25-30 years of records approximately. It should be noted that the complete period of records corresponds to the post-dam regimen. Therefore, the flow regime depends on the discharges of Alcántara and Cedillo dams in Spain, and Fratel, Pracana, Belver, and Castelo de Bode dams in Portugal (see Figure 27).

<sup>2</sup> <https://snirh.apambiente.pt/>

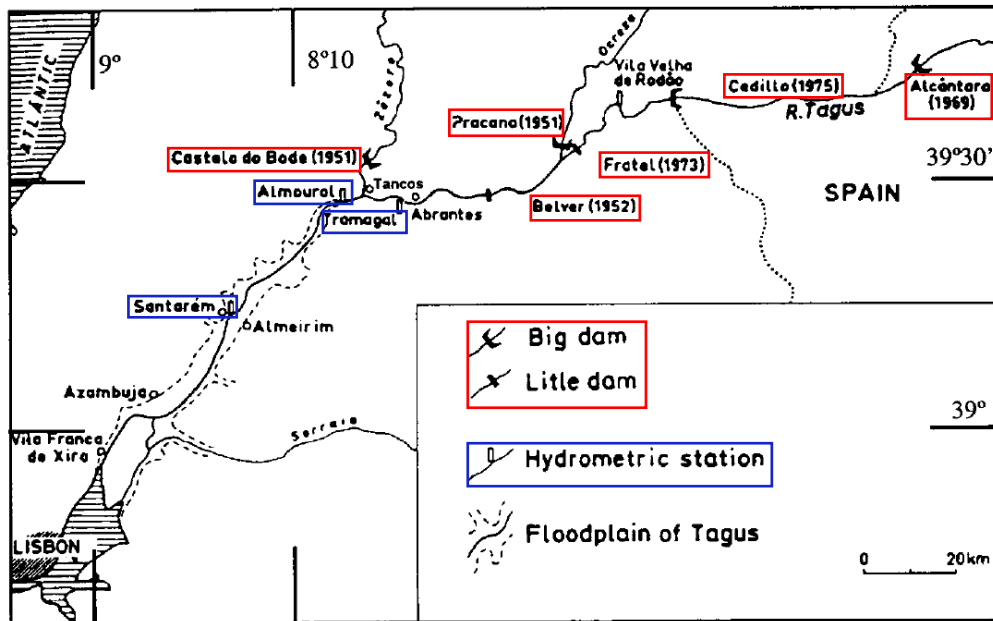


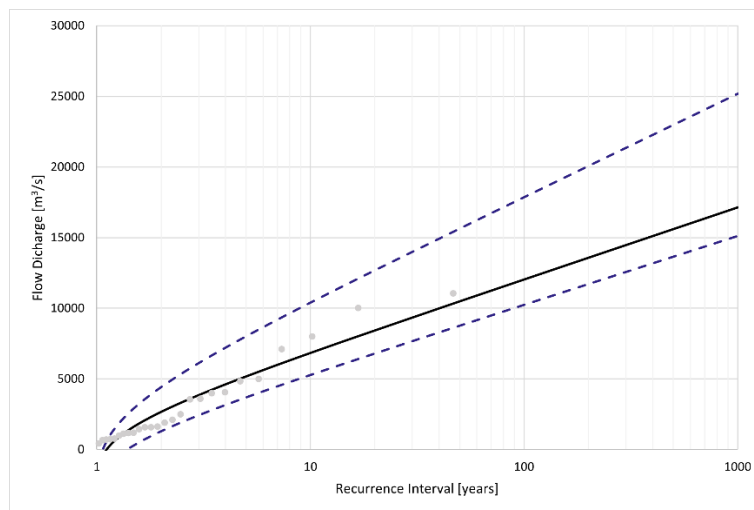
**Figure 27. Location of hydrometric stations: Tramagal, Almourol and Santarém/Ómnias (blue rectangles) and Spanish and Portuguese dams (red rectangles) (Azevêdo, Nunes and Ramos, 2004)**

The FFA analysis was performed following the Bulletin 17C methodology (England Jr *et al.*, 2019). In general terms, the procedure includes plotting positions; finding the best distribution that represents the extreme discharge flows at a given location; estimate the parameters of such distribution; methods to handle zero flows and potentially influential low floods; record extension for achieving a more representative sample if necessary; and confidence intervals for quantiles. It is worth noting that flood records describe a sequence of random natural events that do not fit any specific known statistical distribution. Thus, the distribution is usually selected based on different criteria such as goodness-of-fit statistics, e.g. Kolmogorov-Smirnov and Chi-squared tests, or national standardization such as the log-Pearson Type III distribution which is indicated for FFA in the US. Despite that there is no standardization proposed at Portuguese level, a Gumbel distribution is assumed to represent more appropriately the flow peak discharges as suggested by the Management Plan of the Tagus Hydrographic Region (PGRH-Tagus) (ARH Tejo, 2012). The method of moments was used to estimate the parameters of the Gumbel distribution. Record extension was not applied as the number of records is higher than the minimum recommended for FFA in Bulletin 17C (10 years), and also there are not nearby stations with longer time period of records. Gumbel probability plots and Chi-squared goodness of fit tests showed that the peak annual discharge, for all three stations can be reasonably well modelled by Gumbel probability distributions (see Figure 28).

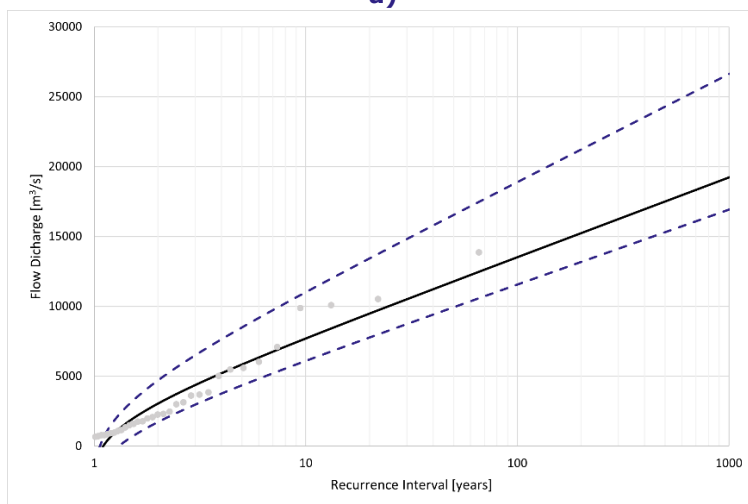
Finally, it is acknowledged that the obtained flood frequency curve is not an exact approximation, as the record of annual peak flows at a given location is a random sample of the underlying population of annual peaks. Then, to quantify the accuracy of this approximation, an interval which contains the population frequency curve with high degree of confidence is commonly constructed (usually

95% of confidence is used) (England Jr *et al.*, 2019). In this manner, the uncertainty in the flood event magnitude due to sampling variability is considered, yet conditional on the choice of a particular distribution.

Table 15 presents the results of the FFAs performed in the three hydrometric stations, as well as the 95% confidence limits of the estimated values. Recurrence intervals of 5-,20-,50-,and 100-years were selected to facilitate the comparison with the the PGRH-Tagus (ARH Tejo, 2012). The mean values reported for Tramagal and Ómnias/Santarém stations are very similar to those reported in the PGRH-Tagus; while the values for Almourol station are slightly different presumably because herein new records (from 2012-2017) were used. It can be observed that for smaller, i.e., more frequent events, the reliability of the discharge estimation is greater than for larger events (very wide confidence intervals). This is expected as the database of past events is sparse, i.e., only 25-30 years of records are available. Thus, there are significant uncertainties in the estimated river discharges obtained through this statistical approach. As more data becomes available, it is expected that the estimates improve and consequently the confidence intervals narrowed.

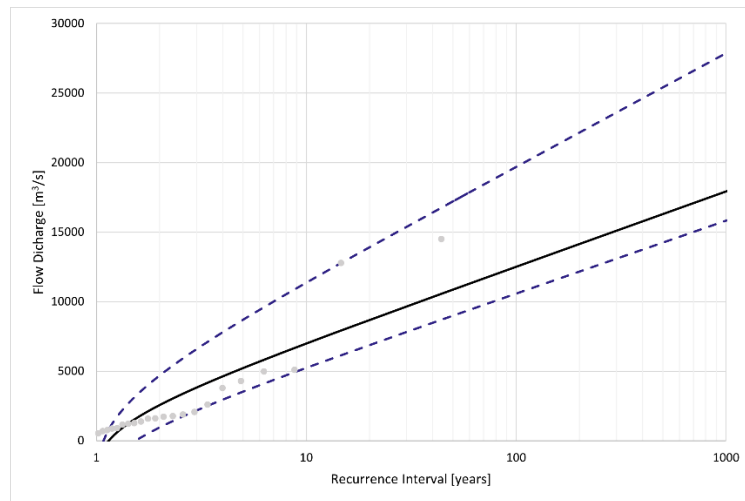


a)



b)





c)

**Figure 28. Flood frequency estimates with 95% confidence intervals for a) Tramagal station; b) Almourol station; c) Ómnias/Santarém station**

Finally, for purposes of quantifying the hydraulic loads on the infrastructures and predicting processes like scour, it is necessary to associate the flow discharge with the hydraulic parameters, i.e. the flow depth and velocity. To this end, HEC-RAS modelling (USACE, 2016), or more advanced 2-D or 3-D models can be performed. Yet, the Gauckler-Manning-Strickler formula can be considered for the hydraulic analysis under the assumption of uniform flow conditions (Manning *et al.*, 1890). Regardless of the method chosen for the hydraulic analysis, the estimation of the hydraulic parameters involves uncertainties such as *i)* model uncertainties due to the simplification of complex physical processes; *ii)* parameter uncertainties from the difficulty in estimating variables such as Manning's roughness coefficient; and *iii)* randomness due to the fluctuation of parameters over time such as changes to floodplain vegetation. Therefore, it is necessary to incorporate these sources of hydraulic uncertainty through e.g. MC simulation (see Lagasse *et al.* (2013)).



**Table 15. Flood frequency analysis for gauge stations along Tagus River**

| Recurrence interval (years) | Discharge (m <sup>3</sup> /s) |                |       |          |                |       |                   |                |       |
|-----------------------------|-------------------------------|----------------|-------|----------|----------------|-------|-------------------|----------------|-------|
|                             | Tramagal                      |                |       | Almourol |                |       | Ómnias (Santarém) |                |       |
|                             | Mean                          | 95% Confidence |       | Mean     | 95% Confidence |       | Mean              | 95% Confidence |       |
|                             |                               | Lower          | Upper |          | Lower          | Upper |                   | Lower          | Upper |
| 5                           | 5175                          | 3846           | 7869  | 5840     | 4500           | 8334  | 5224              | 3704           | 8517  |
| 20                          | 8430                          | 6309           | 13179 | 9478     | 7317           | 13864 | 8678              | 6279           | 14497 |
| 50                          | 10492                         | 7819           | 16596 | 11784    | 9052           | 17417 | 10868             | 7849           | 18348 |
| 100                         | 12038                         | 8940           | 19167 | 13511    | 10343          | 20089 | 12508             | 9013           | 21246 |

### 3.2.3 Flow discharge from hydrologic modelling

As previously mentioned, the selection of the FFA approach for assessing the flood hazard is conditioned by the availability of flow data at the site of interest. Then, another approach broadly applied consists of the physical modelling of the complete hydrological process of dendritic watershed systems. This method is frequently referred as rainfall-runoff modelling (Beven, 2011). The main limitation of this approach is the complexity and the need of good data such as a good digital elevation model, run-off coefficients, and rainfall data.

The PGRH-Tagus developed a HEC-HMS model, and the obtained results for the sub-basins included within the system boundaries are shown in Table 16. It should be noted that these values correspond to the outlet sections of the sub-basins. Thus, at the exact asset locations the discharges are transposed through the Meyer formula using the regionalization coefficients reported in the PGRH-Tagus (ARH Tejo, 2012).

**Table 16. Peak flow discharges obtained from hydrologic model** (ARH Tejo, 2012)

| Sub-basin        | Reference Section  | Discharge (m <sup>3</sup> /s) |            |            |             |
|------------------|--------------------|-------------------------------|------------|------------|-------------|
|                  |                    | T=5 years                     | T=20 years | T=50 years | T=100 years |
| Zêzere River     | Fábrica de Matrena | 476                           | 699        | 844        | 954         |
| Almonda River    | Outlet section     | 144                           | 220        | 269        | 306         |
| Alviela River    | Outlet section     | 375                           | 550        | 663        | 748         |
| Vala de Alpiarça | Outlet section     | 214                           | 326        | 398        | 453         |
| Ribeira de Muge  | Outlet section     | 187                           | 318        | 408        | 478         |

Using the same procedure described in Section 3.2.1, a regression analysis can be performed to the peak flow discharges from Table 16 in order to extrapolate them for different return periods and define lower and upper bounds of the uncertainty interval. Figure 29 depicts the results of the Gumbel regression with uncertainty intervals for the flow discharges from Almonda River.

Subsequently, for the quantification of the hydraulic loads on the infrastructures, the approaches described in the previous section can be also applied.

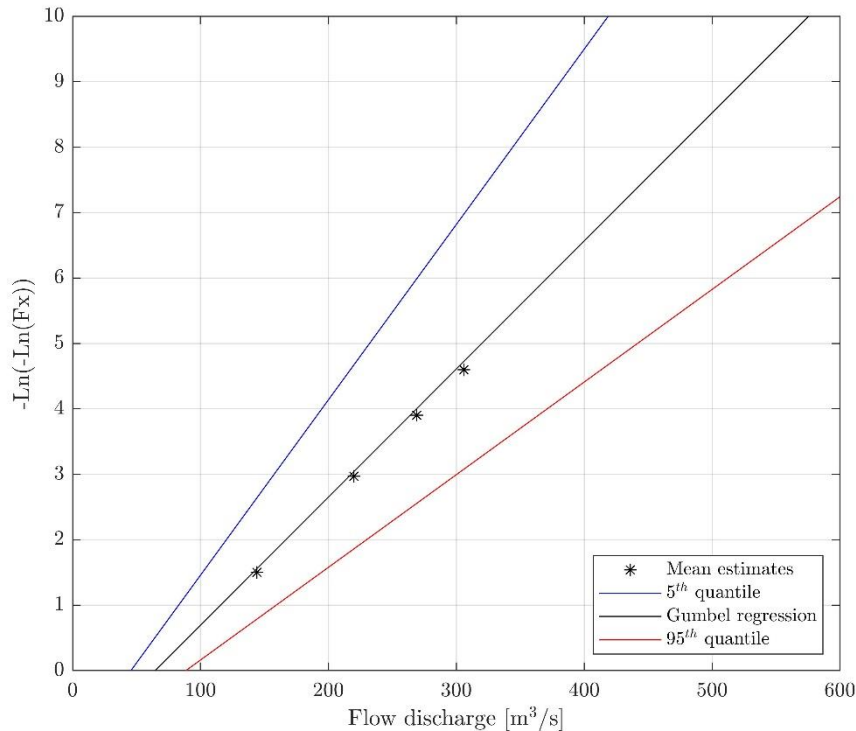


**Figure 29. Fitted Gumbel distribution for Almonda River discharges with uncertainty intervals**

### 3.2.4 Real-time data

As stated within the dynamic risk-based framework and demonstrated in the previous sub-chapters, the flood hazard assessment involves many epistemic and aleatory uncertainties. Therefore, monitoring systems can provide an input for updating existing hazard models. For instance, Crotti and Cigada (2019) installed different monitoring systems on a bridge over the River Po, Italy, namely an anemometer to measure wind intensity and directions, a hydrometer to measure water level, video cameras to check the debris accumulation upstream of the pier, and an echo sounder and a novel device called BLESS to measure the river bed level (scour). Moreover, monitoring systems provide a tool for early-warning systems (EWS), i.e. by adverting the occurrence of external loads that may compromise an infrastructure safety, and therefore giving an alarm for closing or evacuating certain areas in due time.

On the Santarém demonstration pilot, fiber Bragg grating (FBG) sensors will be installed on bridges along the Tagus River. This fiber optic sensing technology has been implemented before to perform real-time monitoring and early warning of natural hazards such as landslides, debris flows, land subsidence, earth fissures, among others (for a review refer to Zhu, Shi and Zhang (2017)). The application of FBG systems on SAFEWAY, will allow to implement two different levels of early warning procedures, namely a warning level and an alert level. In the former, the probability of failure is “moderate”, i.e. there is need for confirmation on the site

---

if the situation can become worse, and thus there is sufficient time to make this inspection. Conversely, for the alert level, there is a high probability of failure (e.g. overtopping is about to happen), so the road sections have to be closed and the traffic should be rerouted. Other types of activities besides inspection or closing the road could also be proposed based on the necessities and available responsive options.

### **3.3 Infrastructure performance functions**

The performance of transport infrastructures is based on its ability to resist the actions to which it is subjected. This performance has been commonly expressed through damage-, loss- or fragility functions (refer to SAFEWAY (2020) for a thorough overview). The choice of the type of functions to be used depends on the type of analysis that is intended, i.e. the scope, the level (asset level or network level) and the type of consequences to be analysed.

For the case of linear transportation infrastructures, vulnerability functions are useful for quantifying the functionality loss due to a given hazard intensity (refer to Chapter 5.2). For the case of infrastructure assets with complex failure modes such as bridges, fragility functions are frequently constructed to communicate the probability of exceeding an undesirable limit state for a given intensity of the hazard (refer to Argyroudis et al. (2019)). A limit state defines the boundary between two different damage conditions often referred to as damage states (DS) (Pitilakis, Crowley and Kaynia, 2014). The damage is measured through engineering demand parameters (EDPs), which represent a structural response to assess the performance of a component. Different damage criteria exist depending on the asset and hazard type. Based on a qualitative approach, a common classification may be defined as: No damage, minor, moderate, extensive, or complete damage (see Figure 30). The selection of the number of DS is usually related with the functionality loss and repair duration (D'Ayala *et al.*, 2015).

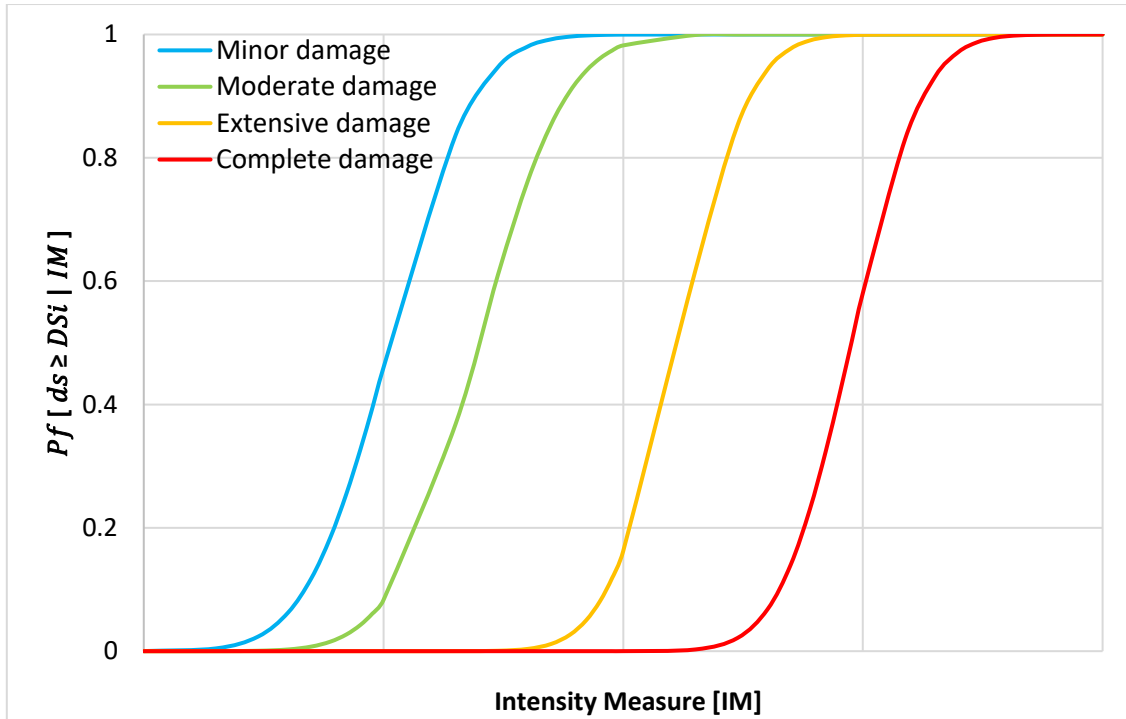


**Figure 30. Example of fragility functions**

Fragility functions are often described by a lognormal probability distribution function as (Pitilakis, Crowley and Kaynia, 2014):

$$P_f[ds \geq DS_i | IM] = \Phi \left[ \frac{1}{\beta_{tot}} \ln \left( \frac{IM}{IM_{mi}} \right) \right] \quad (32)$$

Where  $P_f$  denotes the probability of being at or exceeding a damage state,  $DS_i$ , for a given hazard intensity level defined by the intensity measure  $IM$ ,  $\Phi$  is the standard cumulative probability function,  $IM_{mi}$  is the median threshold value of the hazard intensity measure  $IM$  required to cause the  $i_{th}$  damage state, and  $\beta_{tot}$  is the lognormal standard deviation, which describes the total variability associated with the fragility curve. Generally, there are three primary sources of uncertainty namely uncertainty in the capacity,  $\beta_C$ , uncertainty in the demand,  $\beta_D$ , and uncertainty in the definition of damage states,  $\beta_{DS}$ . Thus, assuming the uncertainties are stochastically independent and lognormally distributed, the total variability can be obtained as (Pitilakis, Crowley and Kaynia, 2014):

$$\beta_{tot} = \sqrt{\beta_C^2 + \beta_D^2 + \beta_{DS}^2} \quad (33)$$

The selection of the appropriate  $IM$  is related to the adopted hazard model, the typology of the asset, the considered damage modes and the method of fragility analysis (Argyroudis *et al.*, 2019). The fragility assessment of different asset infrastructures exposed to the flood hazard is thoroughly studied in Chapter 4.

### 3.4 Consequences to infrastructure network

The occurrence of natural or human-induced hazards may trigger consequences to transportation infrastructure networks. The assessment of probable consequences is essential, so infrastructure managers can make informed decisions about the execution and prioritization of different risk-reducing interventions (Lam and Adey, 2016). The consequences are diverse and generally depend strongly on the specific characteristics of the hazard as well as the location where it occurs and the assets which are exposed (JCSS, 2008). As a general rule, consequences should be assessed in regard to loss of human lives and injuries, damages to the qualities of the environment and economic losses. An overview of monetisation of different consequence types was given in SAFEWAY (2019b) and SAFEWAY (2020).

Consequences of hazard events are frequently classified as direct, i.e. as caused directly by the event including casualties, injuries, and damage to infrastructure; and indirect, resulting from the unavailability of the impaired transport infrastructure, e.g. additional travel time and travel distance, and the loss of access to certain areas (Erath, 2011). A more detailed description of direct and indirect consequences is presented in Chapter 5 and Chapter 6, respectively. Moreover, consequences depend on the economic activities and population situation at future times. This variation of the socio-economic factors for the computation of the indirect consequences is addressed in Chapter 7.

#### 3.4.1 Crowd sourcing data

Vehicle monitoring systems or more in general road users monitoring systems have evolved during last two decades from traditional roadside equipment-based monitoring systems towards floating vehicle monitoring systems, resulting in various types of data and network coverage. The number and diversity of sensors present in vehicles are continuously increasing, giving an opportunity to obtain insights on the vehicle surroundings based on data gathered by those sensors. The produced floating car data (FCD) are quite different compared to the roadside equipment-based data. FCD has in principle a wide area coverage, so covering all roads where vehicles are moving. It is also producing speeds and instead of number of vehicles, travel times. This information can be valuable for the condition assessment of certain assets on the road infrastructure (e.g. pavement, lane markings, traffic signs, protective barriers, overpasses, etc.). The connectivity capabilities of modern vehicles also allow to evaluate mobility conditions more efficiently and to establish ways of communication with the drivers and infrastructure operators to trigger actions consequently. Alternatively, it is based on a less than 100% sample size, because not all vehicles are producing FCD and are connected to a cloud service. On the other hand, these systems are relatively cheap, the costs are partly paid by the users as they are buying their smartphone or satnav and they are also paying a subscription fee for the traffic service, in a one-off when buying the Satnav or by a monthly licence fee.

The growing availability of smart devices with advanced sensors has increased the opportunities for citizen science applications for empirical monitoring. This type of monitoring can provide more specific and actionable guidance for improving road network resilience and disaster management in different areas with diverse environmental and socio-economic conditions. Few empirical approaches are

available for evaluating road network vulnerability or resilience in real disaster events. The existing approaches are primarily based on simulation models, predicting the potential degradation of network performance in hypothetical hazardous conditions (Taylor, Sekhar and D'Este, 2006; Miller-Hooks, Zhang and Faturechi, 2012). However, the actual performance of road networks in real hazard events is dynamic and complex, dependent on not only physical network properties (e.g. topology, road type and capacity), but also environmental (e.g. weather and topography) (Pregolato, Ford, Glenis, *et al.*, 2017) and human factors (e.g. mitigation, emergency management and individuals' travel behaviour) (Zheng and Ling, 2013; Jacobsen, Leiren and Saarinen, 2016). Empirical observations of road network performance are needed to validate the predictions of the theory-based models and unravel the complex interplays among the various factors.

Crowdsourcing strategies have also been exploited to confront safety issues in road work zones, with the aim on obtaining richer information about the situation surrounding these areas. A method to analyse post-event impact of road works was developed by TTI (Pesti and Brydia, 2017), based on data gathered with Bluetooth probe tracking technology, using readers that automatically identify individual vehicles by matching Bluetooth MAC addresses. Travel time delays are quantified, as well as traffic queue length, to assess the deployment of queue warning systems and the best start time for lane closures. The feasibility of using connected vehicle data, crash data and geometric data from on-board installed LiDAR is addressed in (Mekker *et al.*, 2018) to analyse congested conditions upstream of work zones and trigger alerts to infrastructure operators via a real-time queue alert system.

Throughout the developed world, road agencies acquire the data used to manage traffic on their roads from roadside sensors such as induction loops, radar or cameras – a monitoring infrastructure, which is costly and requires ongoing maintenance. Increasingly, step-by-step in a low pace, they are supplementing data from these sensors or even seeking to replace them altogether with FCD generated by mobile devices moving on their network. In this way they are moving towards integrated usage of FCD data in their daily traffic management business.

## 4. Fragility functions for flood hazard

The assessment of the physical damage that transport infrastructures will experience when exposed to a given intensity of the flood hazard is of paramount importance to define the direct and indirect impacts on the transportation system functionality. SAFEWAY (2020) presents a thorough explanation of different methods for the development of fragility curves, namely judgemental, empirical, analytical and hybrid approaches. Moreover, an extensive review on available fragility functions for different hazard types and infrastructure assets was elaborated. However, it was concluded therein that the availability of such functions was limited, and there is a need for developing new functions and updating existing ones in order to consider various natural events and related failure modes. Therefore, this subchapter elaborates a quantitative, yet straightforward procedure for fragility assessment of bridges exposed to flood hazards to be applied at network scale and therefore be adopted on the SAFEWAY case study. Furthermore, fragility functions for other type of transport infrastructure assets namely roads, roadway and railway embankments, are reviewed to be adopted on the SAFEWAY case study.

### 4.1 Bridge fragility functions

Published literature on fragility functions for bridges exposed to flood hazard are less common than for other natural hazards such as earthquakes. The HAZUS methodology for estimating losses due to flood hazard (Hanus-MH, 2013) proposed bridge failure probabilities for different flood return periods as a function of the scour potential, waterway adequacy and span type, which are available attributes within the FHWA bridge inventory database. The failure probabilities and associated losses were defined by expert judgement as no comprehensive database of bridge damage due to flood hazard was identified. Moreover, the focus was only given to bridge foundation failure.

On the other hand, some efforts have been done recently to assess the combined effect of flood-induced scour on the seismic fragility of bridges by analytical approaches (e.g. Dong, Frangopol, and Saydam (2013); Ganesh Prasad and Banerjee (2013); Yilmaz, Banerjee, and Johnson (2018)). However, these studies account for the scour as an aggravated condition for the seismic fragility, rather than as a collapse failure mechanism itself. Conversely, Tanasić, Ilić, and Hajdin (2013) developed fragility functions for multiple span RC bridges supported on shallow foundations, where pier sinking was assumed as the bridge failure mechanism as a result of the degradation of the bearing capacity of the soil beneath the foundation during the scouring event. Also, D'Ayala et al. (2015); Hackl et al. (2018) obtained fragility curves for bridges that could fail as a result of local scour, assuming the failure as the probability of reaching certain scour depth thresholds.

It can be observed that the research focus has been given to foundation failure during extreme flood events, i.e. scour damage, while other types of failures can be also present, namely deck or pier failure due to hydraulic pressures (Mondoro and Frangopol, 2018). In this regard, (Turner, 2016) analysed the deck failure



induced by hydrodynamic lift forces to develop fragility curves for eight bridges. Also, Kim et al. (2017) constructed flood fragility curves for a bridge, considering multiple failure modes due to local scour, deterioration due to corrosion and increased hydrodynamic pressure due to debris accumulation. However, these research efforts are very case specific and time-consuming (involving finite element modelling), which hinders the possibility of implementing them at a network level scale, i.e., for a large portfolio of assets.

Therefore, a methodology for construction of flood fragility curves for a portfolio of bridges is proposed herein aiming at *i*) overcoming the fact that observations (i.e., damage records) are usually insufficient to construct empirical flood fragility curves for bridges; *ii*) providing a more accurate estimation based on an analytical approach rather than a pure judgemental approach; *iii*) accounting for different bridge failure modes. The general methodology is illustrated in Figure 31, where it should be highlighted that the key step is the definition of bridge classes among the bridge stock. Bridges within the same class are expected to perform in the same way, i.e., share the same predominant failure mode so that a single limit state equation can be used to construct representative fragility curves for the class. To this end, an analysis of the characteristics of the bridge and the watercourse is needed in order to define the scenario induced by the flood and the possible associated failure modes. This analysis is thoroughly explained in the next subsection. Then, the classes defined for the SAFEWAY bridge stock are presented, and the damage limit state equations to be used for these classes are proposed. Lastly, the remaining sections are dedicated to the justification of the selection of the intensity measure to represent the flood hazard, the definition of the bridge functionality after the occurrence of each damage state, the treatment of uncertainties, and the possible degradation factors to be considered to construct time-dependent fragility curves. To demonstrate the methodology, an illustrative example from SAFEWAY case study is presented at the end of this section.

It should be noted that the approaches proposed herein can be validated with experimental data and observations in the aftermath of hazard events.

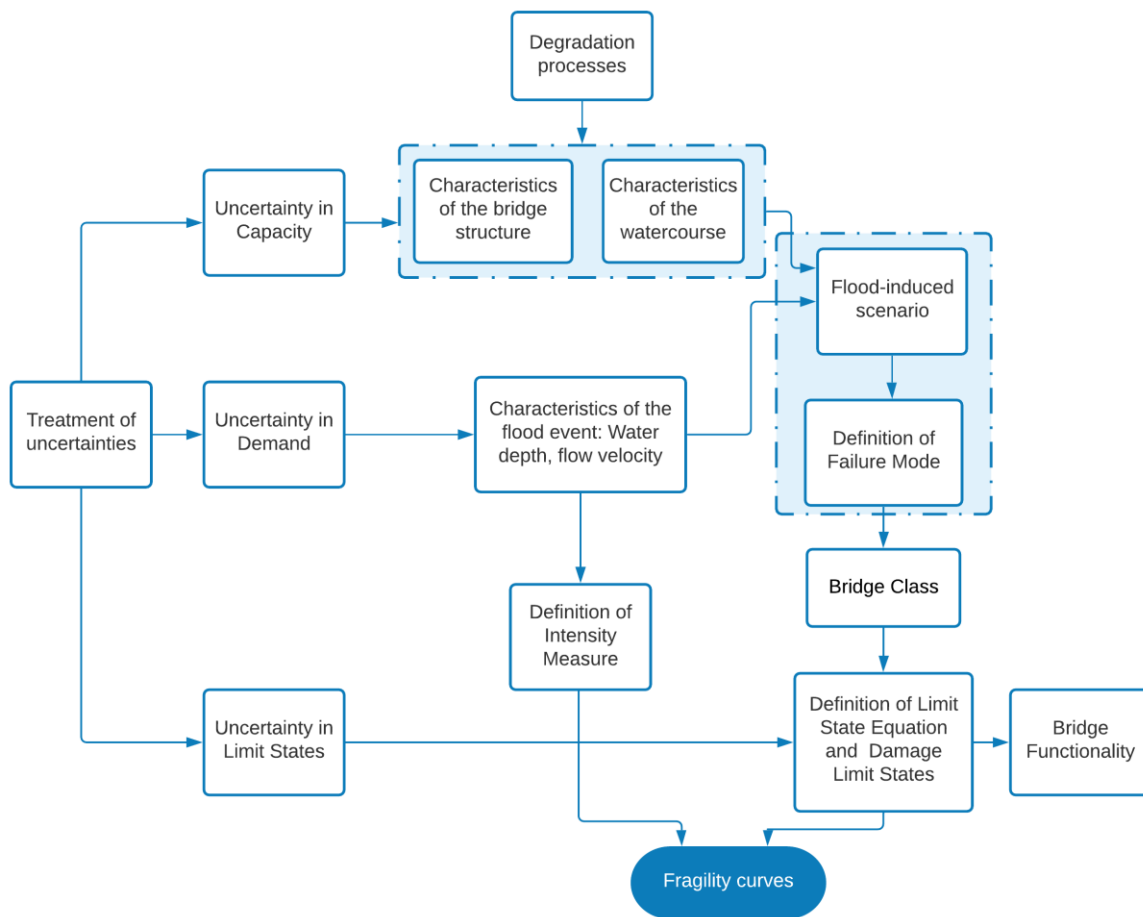


**Figure 31. Methodology for construction of flood fragility curves for a portfolio of bridges**

#### 4.1.1 Bridge failure modes in a flooding event

Failure can be defined as complete or partial damage of bridge components leading to a reduction of the bridge functional performance. A relatively large number of failure modes can be identified since each bridge component may fail differently when exposed to an extreme flood event. Birdsall and Hajdin (2008) identified five different failure scenarios in which a flood can cause partial or complete failure of a bridge. These failure scenarios may be grouped into three flood-induced scenarios, namely bridge overtopping, scour at bridge foundations or hydraulic overloading as depicted in Figure 32. Essentially, if the characteristics of the flood conducts to bridge overtopping, a roadway/railway might be buried, a superstructure might fail horizontally, or the superstructure-substructure connection might fail. Similarly, the bridge might fail due to the undermining of its foundations, if the characteristics of the streambed material subjected to the flow conditions result in scour on bridge foundations. Finally, bridge piers might fail horizontally if the hydraulic loading exerted are beyond the design loads, e.g., when exacerbated by debris accumulation.

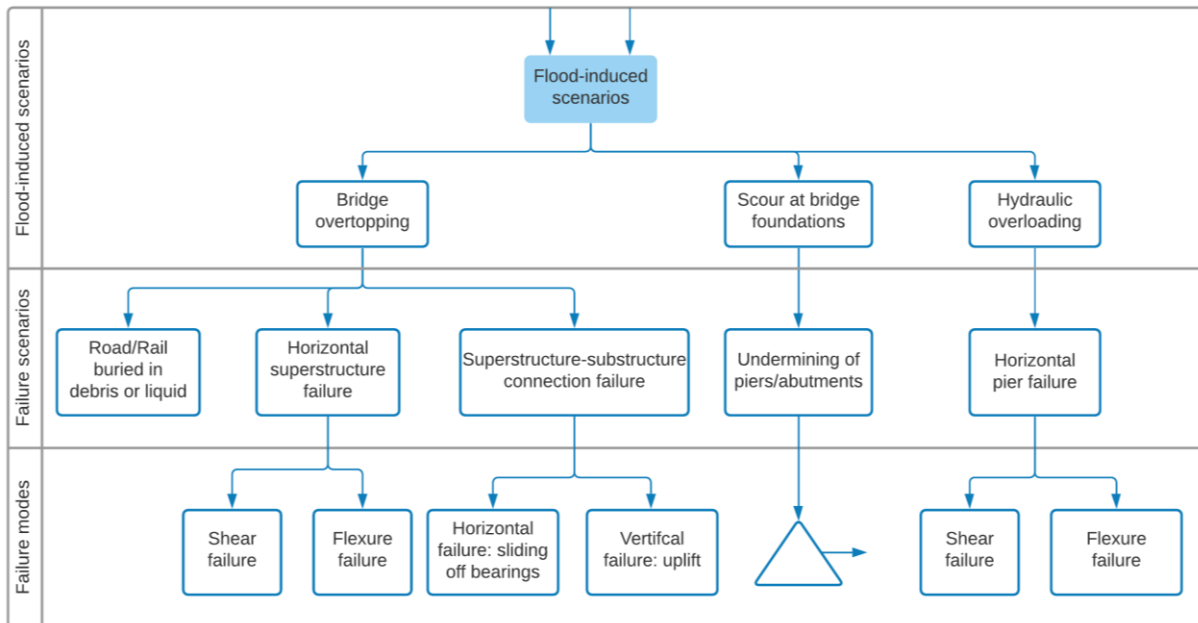


**Figure 32. Bridge failure scenarios induced by the flood event**

The occurrence of a particular flood-induced scenario depends on the characteristics of the bridge structure, the watercourse, and the flood event, as shown in Figure 31. Table 17 summarizes all the necessary data to be collected and analysed in order to define the most probable scenario. This list is adapted from the factors proposed by (Lamb *et al.*, 2017) to be considered when assessing scour risk to bridges. These factors allow to evaluate not only if scour is a problem for the structure under analysis, but also if bridge overtopping or hydraulic overloading might take place and cause a bridge failure.

It should be noted that factors such as channel modification (e.g. due to dredging) or the presence of floating debris, are sometimes considered as causes of failure (Benn, 2013). However, both factors are known to affect bridge structures by intensifying scour depths and/or hydraulic loadings. Therefore, they are not assumed as additional bridge failure scenarios, but as relevant factors to predict the scour extent and quantify the hydraulic load magnitude.

**Table 17. Input data for the definition of the flood-induced scenario (adapted from (Lamb *et al.*, 2017))**

| Group                                   | Factors  | Comments  |
|---|--|---|
| Characteristics of the bridge structure | <ul style="list-style-type: none"> <li>Structure type and span</li> <li>Foundation type and depth</li> <li>Construction date</li> <li>Scour history and protection</li> <li>Flow constriction at the bridge</li> </ul> | Information to be retrieved from bridge inventory database and inspection reports |

| Group                              | Factors   | Comments  |
|------------------------------------|---|---|
| Characteristics of the watercourse | <ul style="list-style-type: none"> <li>• Bed material</li> <li>• Stability of the watercourse</li> <li>• History of weir removal and sand/gravel extraction</li> <li>• Debris accumulation potential</li> </ul> | Information to be retrieved from bridge inventory database, inspection reports, and maps, aerial photographs, and survey data to define debris potential (or debris hazard map if available). |
| Characteristics of the flood event | <ul style="list-style-type: none"> <li>• Flow velocity</li> <li>• Water depth</li> </ul>  | Information to be retrieved from hazard maps at the bridge location (or through the flowchart from Figure 24)   |

Finally, it can be observed from Figure 32 that each of the failure scenarios can conduct to different bridge failure modes (FMs). For instance, bridge piers subjected to high water pressures could fail in a shear or a flexure failure mode. Similarly, the superstructure-substructure connection could fail horizontally, i.e., sliding-off bearings failure mode, or vertically, i.e., uplift failure mode. Nevertheless, the definition of bridge FMs due to scour at bridge foundations is represented in Figure 32 as a triangle (transfer symbol), as it requires a large discretization of many other parameters involved as it will be discussed in the following.

Briaud et al. (2011), defined four typical bridge FMs due to scour namely big scour hole, settlement and rotation of the pier, loss of the deck, and loss of the pier. However, these FMs are defined based on observed damages and do not explain how the failure develops. On the other hand, Van Leeuwen and Lamb (2014) introduced the resistance of multiple bridge components by dividing the failure mechanisms as secondary mechanisms resulting from primary mechanisms. Essentially, scour can undermine shallow foundations or cause destabilisation of deep foundations through erosion of the riverbed; this can lead to settlement or tilting of piers/abutments, or tilting of group of piles (primary mechanism), which in turn might result in structural damage to superstructure, or deck sliding or falling off abutments/piers due to differential settlements or tilting of supports (secondary mechanism) (see Table 18).

Fundamentally, the possible FMs due to scour are governed by the combined resistance of a soil-bridge system. Tanasić (2015) elaborated this concept for the case of multiple span RC bridges supported on shallow foundations. The soil resistance to local scour is governed by the soil erodibility and its geotechnical properties: internal angle of friction, cohesion and self-weight; while the bridge resistance is governed by its ability to redistribute the internal forces due to the removal of supporting soil at bridges substructures. Therefore, the bridge resistance depends on the following aspects:

- Bridge geometry, material properties, quantities/detailing of reinforcement
- Type and detailing of bearings, joints between superstructure and substructure, and dilatations
- Elements' (deteriorated) condition

From this work, it was found that the lowest resistance to local scour is exhibited by bridges with no horizontal restraint on the top of the affected substructure. Conversely, in presence of horizontal restraint, the superstructure capacity and adjacent substructure are relevant for the ultimate bridge resistance. This highlights the importance of defining the failure modes for each bridge type.

More recently, COST TU1406 Action (Hajdin, Kušar, *et al.*, 2018) developed a comprehensive failure mode analysis for girder/frame bridges and masonry arch bridges exposed to local scour at substructures. The main FMs types identified are presented in Table 18. This table summarizes the possible bridge FMs in a flooding event defined by different research works for various bridge types. It can be observed that FMs differ significantly among masonry arch bridges and RC bridges, and between bridges supported on shallow and deep foundations. Moreover, it can be noted that there is no full agreement between the possible FMs defined for the same type of bridges among different research works (e.g. (Lin *et al.*, 2014; Kim *et al.*, 2017)).

**Table 18. Possible bridge failure modes in a flooding event for different bridge types**

| Type of Bridge   | Flood-induced scenario       | Failure modes  | Reference   |
|--|------------------------------|--|---|
| Girder/frame bridges supported on shallow/deep foundations | Local scour at substructures | FM1: Pier or abutment settlement due to loss of support, leading to structural damage to superstructure or deck<br>FM2: Pier or abutment tilting (or tilting of group of piles for deep foundations), leading to superstructure or deck falling off pier or abutment         | Van Leeuwen and Lamb (2014)                               |
|  | Hydraulic loading            | FM3: Piers, abutments or footings damaged by hydraulic loading, possibly aggravated by debris accumulation<br>FM4: Superstructure or deck sliding off supports due to hydraulic or debris loading or collision<br>FM5: Superstructure or deck damaged by collision of debris |   |
| Masonry Arch bridges                                       | Local scour at substructures | FM1: Fragmentation of a pier<br>FM2: Symmetrical, in-plane failure mode<br>FM3: Non-Symmetrical, in-plane failure mode<br>FM4: Fragmentation of an abutment<br>FM5: Out-of-plane failure and spandrel wall displacement  | R. Hajdin, Kušar, et al. (2018)<br>Zampieri et al. (2017) |
| Girder/frame bridges supported on shallow foundations      | Local scour at substructures | FM1: Loss or serious damage of substructure leading to deck failure<br>FM2: Tilting/rotation of substructure not restrained by the superstructure<br>FM3: Settlement of substructure restrained by the superstructure  | R. Hajdin, Kušar, et al. (2018)                           |

| Type of Bridge                        | Flood-induced scenario                               | Failure modes  | Reference                    |
|---------------------------------------|--|--|------------------------------|
|                                       |  | FM4: Loss or serious damage of substructure, no deck failure   |                              |
| Bridges supported on deep foundations | Local scour at substructures and hydrodynamic forces | FM1: Loss of soil bearing capacity (insufficient penetration for friction piles, undermine of pile tip for end bearing piles)<br>FM2: Buckling of piles<br>FM3: Lateral failure (pushover failure, structural hinging or kick-out of foundations)<br>FM4: Torsional failure due to skew flow | C. Lin et al. (2014)         |
| Bridges supported on deep foundations | Local scour at substructures and hydrodynamic forces | FM1: Lack of displacement ductility of bridge piers and piles<br>FM2: Steel reinforcement rupture of bridge piers and piles<br>FM3: Deck loss due to relative displacements  | Kim et al. (2017)            |
| Girder bridges                        | Deck overtopping                                     | FM1: Transverse failure<br>FM2: Uplift failure   | Mondoro and Frangopol (2018) |
|                                       | Hydrodynamic forces on pier                          | FM3: Flexural and axial failure of bridge pier<br>FM4: Shear failure of bridge pier  |                              |
|                                       | Scour at pier foundation                             | FM5: Flexural and axial failure of pile group  |                              |



#### **4.1.2 Definition of bridge classes for SAFEWAY pilot**

Conducting an asset-specific fragility model for a large portfolio of assets would be a far too time-consuming and computationally expensive task. Therefore, it was proposed in SAFEWAY (2020) to categorise the assets into classes and apply a fragility function describing a representative asset type and its failure mode.

The classes are defined initially by grouping bridges having similar structural characteristics and comparable characteristics of the watercourse (Figure 31). Then, following the analysis presented in Figure 32, the key assumption is that all bridges within the same class are expected to have the same predominant failure mode when subjected to the same flood-induced scenario.

It should be pointed out that complete data of the assets was not available. Some information was albeit obtained from geo-information systems, inspection reports and other available datasets. The unavailability of high-quality data for the proper understanding of bridge performance is a current issue shared by many countries and highlighted by many researchers (Hajdin, Casas and Matos, 2019; Pregnolato, 2019). This issue was tackled herein by using the available information from actual bridges and making assumptions in absence of reliable data for the purpose of illustration and demonstration of the methodology.

The results of the definition of Classes for the case study are presented in Table 19. Bridges belonging to Class I and Class II correspond to multiple span and single span masonry arch bridges, respectively, which constitute a significant proportion of the bridge inventory in the case study. These structures are typically founded on shallow footings (usually of unknown depth) or on timber piles, which given their environmental exposure and due to ageing might be severely weakened. Even though there is no information available regarding the soil characteristics to define their vulnerability to scour, it is recognized that masonry arch bridges are extremely vulnerable to this phenomenon due to their rigid behaviour which does not allow significant settlements (Zampieri *et al.*, 2017). Accordingly, scour at bridge foundations was defined as the flood-induced scenario for both classes, and the predominant failure mode was defined in accordance with Hajdin, Kušar, *et al.* (2018).

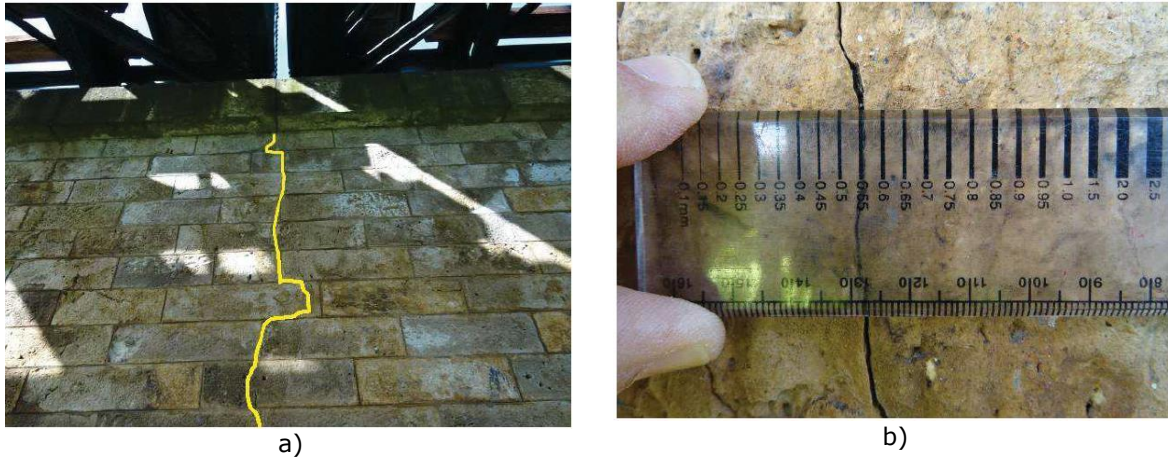
Bridges within Class III correspond to a particular type of bridges found along the Tagus river, which are of great geographical importance since they communicate municipalities located on the riverbanks. These bridges are characterized by having multiple spans (with total spans between 400-600m), masonry wall piers, steel truss structures for the deck, and were built between 110-150 years ago. The foundation of these type of bridges consists of a deep prolongation of the piers until reaching a soil stratum with sufficient capacity, i.e. loads are transferred by direct bearing to dense soil. From geotechnical surveys conducted during the last decade, it has been found that some of the bridge piers within this class were founded on soils with insufficient bearing capacity. Moreover, these surveys revealed the presence of coarse sands in the upper soil layers, which renders the bridge susceptible to scour. In fact, during sub-aquatic inspections, scour has been found in several piers, reaching depths up to 1.5m (Figure 33a). As a countermeasure, the riverbed has been protected with rock fill layers around piers. However, during subsequent inspections, it is evidenced the displacement or

“washed away” of the protective fills (Figure 33b). Given these conditions, scour is considered a relevant threat for the bridge safety, acknowledging the fact that deep foundations are by design considered to be more resistant to this phenomenon. However, the loss of supporting lateral soil, together with the fact that the bridge piers are founded on weak soils, and the presence of a significant water pressure over the pier during flood events (water depths reach approximately 12-14m during a 100-year flood), this scenario could lead to instability of the pier and thus to the collapse of the complete bridge (as exhibited by the Hintze Ribeiro bridge collapse (Sousa and Bastos, 2013)).



**Figure 33. Presence of local scour in bridges within Class III**

Class IV bridges have a similar structural type to Class III, i.e. steel truss structures for the deck supported on masonry abutments and wall piers and were built approximately 130 years ago. One of the main differences relies on the characteristics of the watercourse, as the river channel sections for the bridges within this class are smaller (as shown in the reference figure of the class in Table 19). According to available drawings, the abutments are supported on timber piles, which given the year of construction of the bridge are expected to be in an advanced state of deterioration. This hypothesis is also founded on existing crack patterns which have been evidenced during principal inspections, and presumably correspond to differential settlements (see Figure 34). Consequently, the occurrence of scour at bridge abutments could represent a potential threat, as the timber piles might not be able to withstand the unsupported pile height and might exceed their buckling capacity leading to the abutment failure.

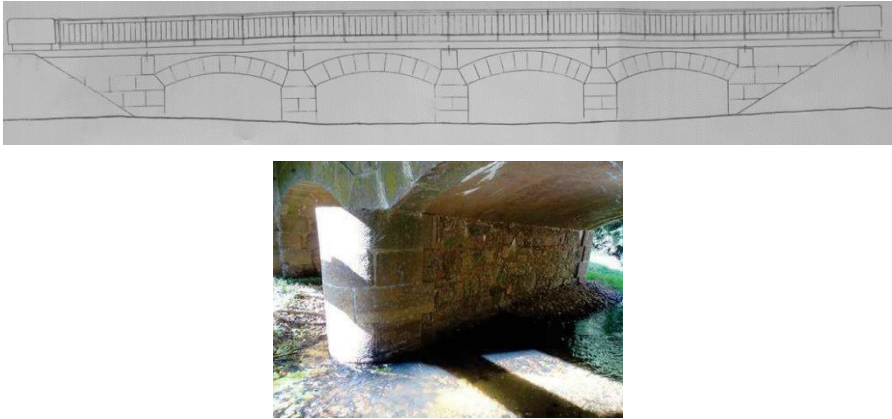



**Figure 34. Presence of cracking at bridge abutments within Class IV**

Finally, Class V corresponds to multiple span RC integral bridges with deep foundation. Bridges within this class are localized at watercourses with V-shaped valleys (as shown in the reference figure of the class in Table 19). Given these conditions and the characteristics of the flood events, Class V bridges could be subjected to rather hydraulic overloading or bridge overtopping scenarios. However, as the connection between superstructure-substructure is monolithic, it is not expected that significant physical damages would take place during overtopping as it is in the case for simply supported structures (as studied in Mondoro and Frangopol (2018)). Conversely, hydraulic overloading, probably exacerbated by debris accumulation due to the watercourse characteristics, could lead to a pier flexural/shear failure mode.

It should be noted that only the most likely flood-induced scenario and the expected predominant failure mode were defined for each class, acknowledging that more than one scenario could occur, and/or multiple failure modes can develop in different bridge elements. For instance, bridge overtopping is also likely to happen in Class I bridges. Under this scenario, some research has been done to investigate the reduction in the load-carrying capacity of fully flooded masonry arch bridges (e.g.(Hulet, Smith and Gilbert, 2006)). Thus, combining both failure modes at bridge system level would be required (as proposed by (D'Ayala *et al.*, 2015)). However, the approach herein proposed seeks to identify the most probable scenario and the most likely failure mode, and it is presumed that the probability of any other failure mode is negligible.

**Table 19. Bridge Classes defined for SAFEWAY case study**

| Class    | Structural System  | Flood-induced scenario      | Predominant failure mode  | Example bridge within the class   |
|----------|--|-----------------------------|---|---|
| Class I  | Multiple span masonry arch bridges founded on shallow footings | Scour at bridge foundations | Local pier scour leading to a symmetrical (or not symmetrical), in-plane failure mode |    |
| Class II | Single span masonry arch bridges founded on shallow footings   | Scour at bridge foundations | Fragmentation of abutment due to local scour  |  |



| Class     | Structural System  | Flood-induced scenario      | Predominant failure mode                         | Example bridge within the class |
|-----------|--|-----------------------------|--|---------------------------------|
| Class III | Multiple span steel truss bridges supported on masonry piers | Scour at bridge foundations | Instability of bridge piers due to local scour   |                                 |
| Class IV  | Multiple span steel truss bridges supported on masonry piers | Scour at bridge foundations | Abutment failure due to buckling of timber piles |                                 |
| Class V   | Multiple span RC integral bridges, deep foundation           | Hydraulic overloading       | Pier flexure/shear failure                       |                                 |

### 4.1.3 Intensity Measure

The most frequent intensity measures to describe the flood hazard magnitude for fragility analysis are the peak flow discharge and velocity, flood height (water depth) and scour depth. Nevertheless, it can be argued that the latter does not represent the loading of the hazard but a consequence of the flood event. Lamb et al. (2017) applied a formal process of expert elicitation to explore the relevant factors when assessing scour risk and to derive bridge failure probabilities conditional of flood event severity for different scenarios. Within the scope, the loading conditions for a scour fragility function was also discussed. Debris load and other four factors related to hydraulic conditions during a flood event were preferred, including duration of high flow and flood flow, flood flow return period, and flow velocity, which are intrinsically linked. Among them, the flood return period (or alternatively, the exceedance probability) is considered a more abstract measure of the load intensity, as it is flexible in regard of the methods applied to define a flood event and estimate its probability, and more standardised regardless of the physical scale of the system (e.g., channel width and depth). For these reasons, the flood return period is herein adopted as the intensity measure for the development of the flood fragility functions.

### 4.1.4 Treatment of uncertainties

As briefly mentioned in Section 3.3, there are three primary sources of uncertainty when assessing the fragility of an infrastructure subjected to a hazard action: uncertainty in the capacity,  $\beta_C$ , in the demand,  $\beta_D$ , and in the definition of damage limit states,  $\beta_{DS}$  (Figure 31).

The uncertainty in the capacity is associated to the structure and soil parameters such as the geometric and mechanical properties, and to the uncertainty due to structural modelling simplifications, i.e. the soil-structure capacity variability. The uncertainty in the demand was largely discussed in Section 3.2 for the flood hazard and represents the variability of the hydraulic actions on the structure for each return period. Additionally, the model uncertainty associated to the accuracy of existing methodologies to estimate water pressures or predict flood-induced phenomena such as scour should also be considered (Lagasse *et al.*, 2013). Lastly, the uncertainty in the damage limit states is related to the fact that the thresholds specified for each damage state are not known (Argyroudis *et al.*, 2019).

Given all the different sources of uncertainty involved in the development of fragility curves, it is acknowledged that a proper treatment of uncertainties is a challenge. Thus, it is important to determine appropriate distributions to model each random variable in the limit state-equations and find their parameters, i.e. mean and standard deviation. Based on the probability distribution parameters, sampling approaches such as the Latin Hypercube or MC techniques, can be used to generate random combinations of the uncertain parameters. By means of decreasing the computational cost of the statistical sampling and the number of simulations, sensitivity analyses can be used to investigate which are the most significant parameters on the performance of the infrastructure and thus reduce the number of uncertain inputs (e.g. (Yilmaz, Banerjee and Johnson, 2018)).

Finally, real-time data and monitoring techniques as proposed in the framework from Figure 22, could assist at reducing the uncertainties and provide means for updating fragility functions in order to represent more reliably the response of infrastructures to the hazard events.

#### 4.1.5 Time-dependent fragility assessment

As mentioned in Chapter 2, transportation infrastructure assets deteriorate as a result of exposure to adverse environmental and climatic conditions, ageing, changing load patterns, among other factors. This time-dependent deterioration effects can significantly increase the fragility of the of bridge components over time (Argyroudis *et al.*, 2019).

There are different deterioration mechanisms that can develop in the asset structural elements, earthworks and streambed material. For concrete structural elements, corrosion of reinforcing steel is one of the main causes of loss of structural resistance. Corrosion is usually modelled by reducing the cross section area of reinforcement as a function of time (see Figure 35), and secondary effects such as cracking and spalling of concrete, loss of bond strength, among others, should be also considered to investigate the total loss of structural strength due to corrosion (Ghosh and Padgett, 2010).

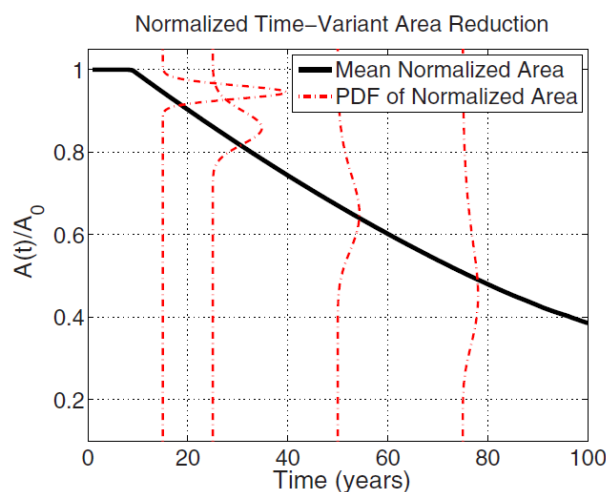


**Figure 35. Time-variant area of the concrete element reinforcement** (Ghosh and Padgett, 2010)

Likewise, corrosion also affects steel bearings, anchor bolts and keeper plates, which results in reduced stiffness and reduced ultimate strength in the bearing assemblies. Ghosh & Padgett (2010) derived the ultimate lateral strength for fixed bearings in the longitudinal direction affected by corrosion (see Figure 36).

Bridge substructure can also be affected by different deterioration mechanisms. For instance, during an underwater inspection, it was found that the I-10 Bridge over the Jourdan River in Mississippi, USA, supported on friction steel piles, had an average of approximately 50% of steel pile cross section loss as a result of severe corrosion. Due to the reduced cross section the web and flanges of the piles



had buckled locally. The corrosion was originated due to significant scour that exposed the steel piling (Avent and Alawady, 2005).

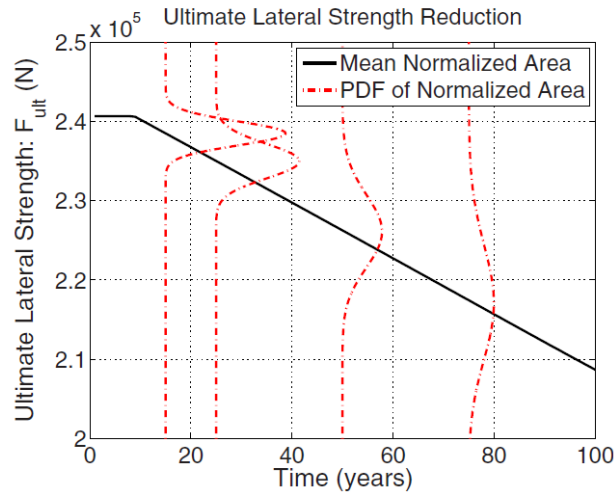


**Figure 36. Reduction of ultimate lateral strength of fixed bearings due to corrosion of anchor bolts** (Ghosh and Padgett, 2010)

On the other hand, scour has been also regarded as a history-dependent and time-dependent phenomenon. In other words, bridges are exposed during their service life to multiple floods, some of which exceed the discharge corresponding to the design return period, while some correspond to a very low return period, but still capable of causing scour. These latter events of minor intensity may not result in the critical scour depth being exceeded, but may cause partial erosions which accumulate as a consequence of multiple floods and may lead to bridge failures (Tubaldi *et al.*, 2017). For instance, the cause of collapse of the Malahide viaduct on the railway line from Dublin to Belfast on 21 August 2009 was reported as the result of a combination of factors including the accumulative scouring action over a long time period, and the inappropriate inspection and maintenance activities (Benn, 2013).

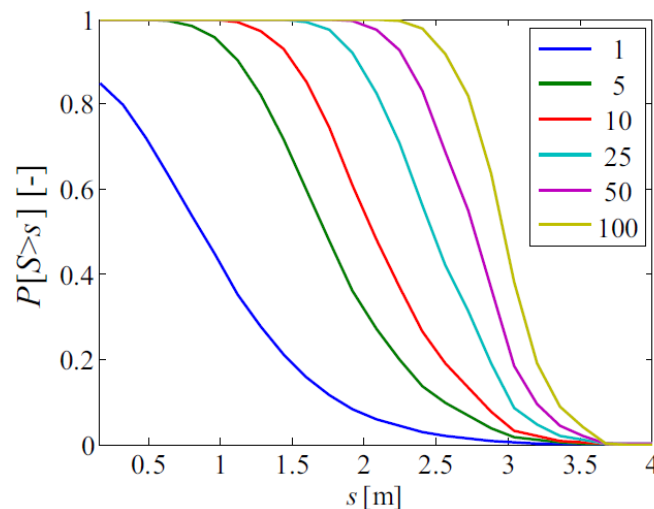


**Figure 37. CCDF of the scour depth at different times of observation T (from 1-100 years)** (Tubaldi *et al.*, 2017)

#### 4.1.6 Damage states and bridge functionality

As stated in Section 4.1.1, failure can be defined as complete or partial damage of bridge components leading to a reduction of the bridge functional performance. As such, the number of bridge damage states is variable, moving from none to extensive, or complete collapse. Each damage state is associated to a level of functionality loss, which is defined by the traffic capacity of the infrastructure, i.e. from full service to completely closed to traffic. Intermediate functionality levels are usually defined as load restrictions, only one lane open, speed restrictions, or emergency access only. These levels have been defined based on observed data from past hazard events (Hazus-MH, 2013), or data collected from expert opinion. Additionally, each damage state can be associated to an estimated duration of the repair operations, i.e. a restoration time, and to a repair cost. Table 20 summarizes the findings from an expert-based survey done within the INFRARISK research project (D’Ayala *et al.*, 2015), where four damage states were defined and the expected functionality losses, downtime durations and repair costs (as a percentage of the replacement cost) were estimated. These values support a roughly quantification of direct and indirect consequences. However, there is no full agreement yet in the literature (nor in practice) regarding these estimates, as they vary significantly among different hazards and bridge structure types. Nevertheless, efforts have been done recently to provide systematic data to relate damage levels to repair decisions and traffic closures for different natural hazards (refer to Section 5.1).

**Table 20. Functionality loss of different damage states according to INFRARISK expert-based survey (D’Ayala *et al.*, 2015)**

| Damage State                 | Functionality loss | Duration    | Costs    |
|------------------------------|--------------------|-------------|----------|
| DS1: Slight damage           | -                  | -           | -        |
| DS2: Minor structural damage | 0%-25% (speed)     | 1-90 days   | 0%-20%   |
| DS3: Extensive damage        | 100% closed lanes  | 60-120 days | 20%      |
| DS4: Collapse                | 100% closed lanes  | 90-150 days | 20%-100% |

#### 4.1.7 Example of bridge fragility function

Based on the methodology proposed in Figure 31, a fragility function is herein constructed for bridges within Class I, i.e. multiple span masonry arch bridges founded on shallow footings. Although this is a realistic example, some information was not available. Therefore, some assumptions were made for the purpose of illustration of the methodology.

In most approaches found in the literature, failure of bridges on shallow foundations is assumed to occur when the predicted local scour depth reaches the foundation base, which has been demonstrated to be a conservative assumption for multiple span RC girder bridges (Tanasić, 2015) as well as for masonry arch bridges (Zampieri *et al.*, 2017). Consequently, it is important to identify the maximum scour depth and extent (i.e., the geometry of the scour cavity) beneath the foundation level that the soil-bridge structure may withstand before collapse (see Figure 38). This limit might be found by assuming a rigid plastic behaviour of the soil and bridge elements and applying the upper bound theorem of the theory of plasticity (see (Tanasić, 2015)), or by a soil-bridge structure finite element model. For instance, Zampieri *et al.* (2017) elaborated a soil-bridge structure finite element model of a masonry arch bridge in order to analyse the scour layout able to induce a collapse mechanism. To this end, increasing local scour profiles (symmetric and not-symmetric) were applied through the removal of soil elements. This loss of supporting soil due to the erosional process conducted to vertical settlements for the symmetric scour layout and combined vertical-rotational settlements for the not-symmetric layout. As expected, with the increase of local scour, settlement values become significant leading to cracking phenomena at the arch intrados and extrados, and finally to rigid block sliding failure.

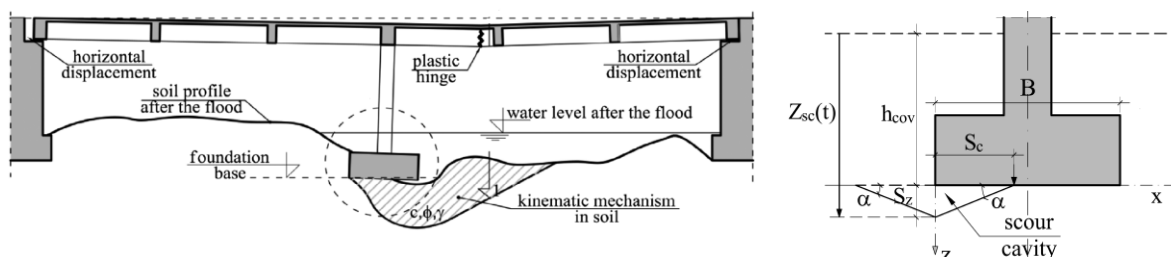


**Figure 38. Maximum scour cavity that a soil-bridge structure may withstand adapted from (Tanasić and Hajdin, 2018)**

In order to conduct the fragility assessment of bridges within this class, a four-span masonry arch bridge was considered as representative of the typical layout of arch bridges with short to medium span length found in the demonstrative pilot. The geometry of the bridge is shown in Figure 39. It should be noted that the dimensions, bridge materials and soil characteristics do not correspond exactly to any actual bridge. It is assumed that the soil corresponds to an alluvial deposit mostly granular, with coarse sands loosely cohesive.

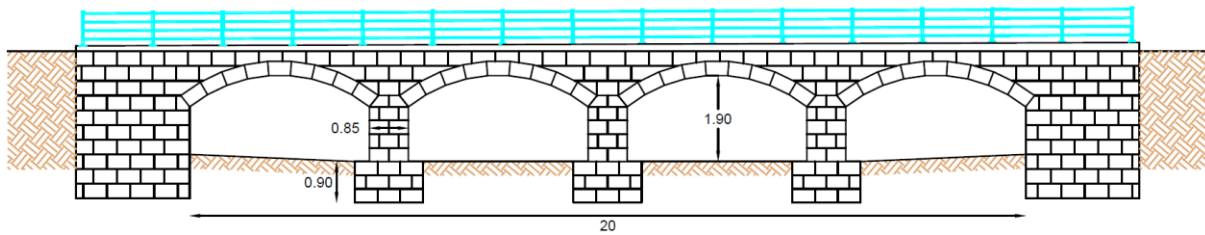
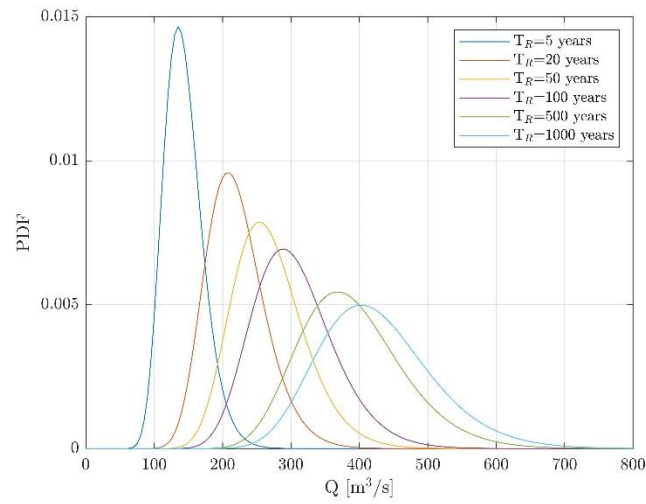


**Figure 39. Representative masonry arch bridge for Class I**

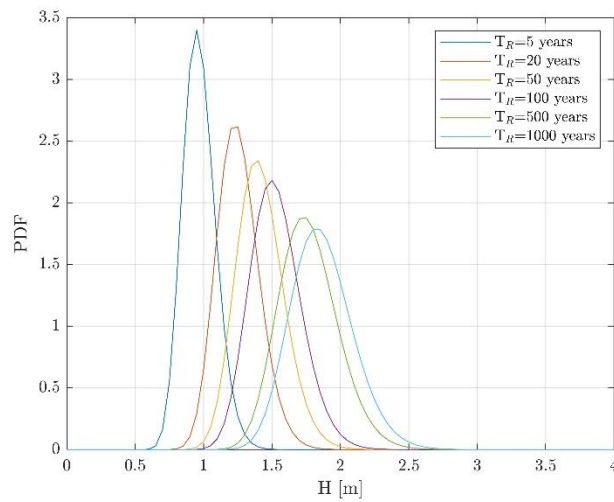
Considering that finite element models are computationally expensive to carry out probabilistic analysis and even more to perform fragility analysis which describe the probability of failure over a range of loads, discontinuity layout optimization (DLO) which is a numerical limit analysis technique is used herein as a less costly but powerful computational alternative (Smith and Gilbert, 2007). DLO is an upper bound method that has been recently used for verifying the safety of masonry arch bridges (Gilbert *et al.*, 2019), which is incorporated in the LimitState:GEO software, freely available for academic use (<http://www.limitstate.com>). However, as limit analysis-based methods are founded on plasticity theory, their aim is to estimate the collapse load of a structure. Thus, the masonry arch bridge is analysed only in relation to its ultimate damage state. If the interest is to define and investigate intermediate damage states (as shown in 4.1.6), finite element analysis would be required.

Masonry units were modelled using a rigid material model, and masonry joints were modelled using a Mohr–Coulomb model with zero cohesion and an angle of friction derived from the coefficient of friction. A Mohr–Coulomb model was also considered for the backfill and the foundation soil. The material properties used in the analysis, i.e. masonry compressive strength, unit weights for each material, and internal friction angles can be found in Appendix 3. The probability distributions selected to describe each variable are also provided, following the suggestions from previous research works (Moreira *et al.*, 2016). The bridge dimensions are considered deterministic as these uncertainties can be effectively reduced by means of LiDAR technologies for acquiring the external geometry of the bridge in its current condition (Conde *et al.*, 2020). It is worth to mention that a sensitivity analysis can be performed before the probabilistic analysis in order to select the most influent input variables and consequently reduce the computational effort of these analyses.

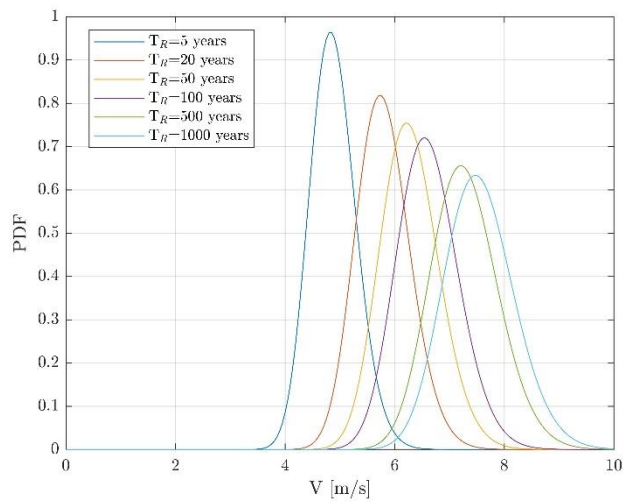
The bridge is assumed to be located at the outlet section of Almonda River. Then, the Gumbel distribution fitted to the flow discharges from Figure 29, is used herein to quantify the hydraulic loads on the masonry arch bridge. To this end, the Gauckler–Manning–Strickler formula is considered for the hydraulic analysis under the assumption of uniform flow conditions (Manning *et al.*, 1890). Probability distributions for the hydraulic parameters, i.e. manning roughness coefficient and channel slope are adopted from Lagasse *et al.* (2013) (refer to Appendix 3). From the hydraulic analysis, the water depth and flow velocity are determined for each return period and are fitted to a Lognormal probability distributions. Figure 40 depicts the PDF functions of the flow discharge, water depth and flow velocity for the 5-, 20-, 50-, 100-, 500-, and 1000-year return periods.



a)



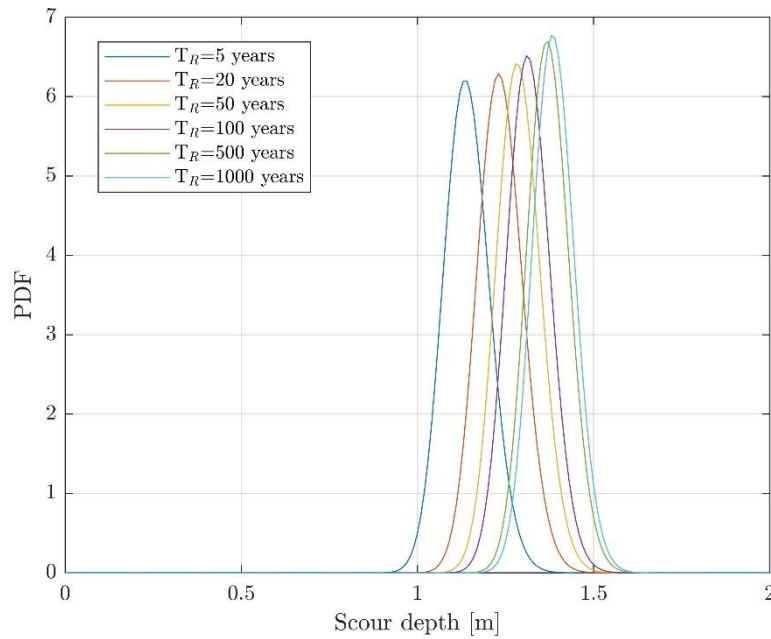
b)



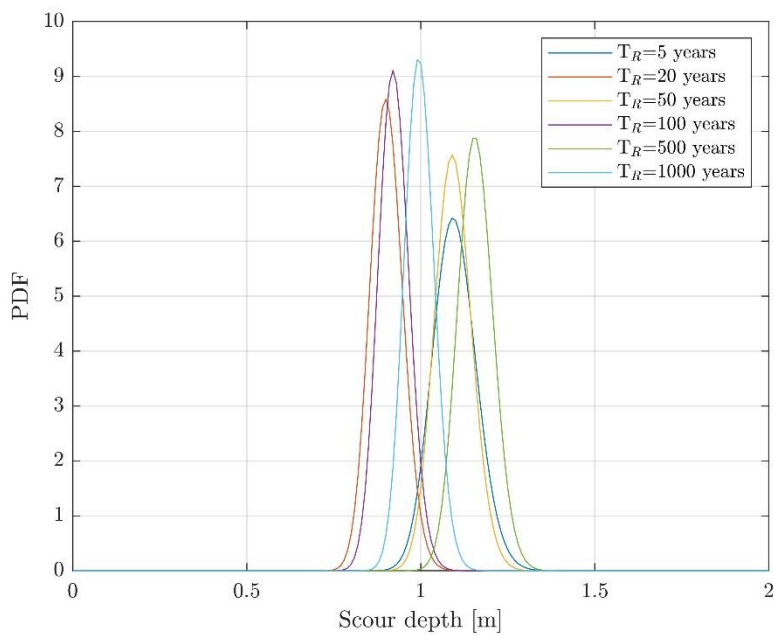
c)

**Figure 40. PDF functions of the a) flow discharge, b) water depth and c) flow velocity for the 5-, 20-, 50-, 100-, 500-, and 1000-year return periods.**

Based on the hydraulic loads and the soil characteristics, local scour at a bridge pier is investigated. It is worth noting that the contribution from contraction scour and long-term degradation could be also added to obtain the total scour. Nevertheless, local scour is commonly the ultimate cause of bridge failures during extreme flooding events (Sheppard and Renna, 2010). Thus, only local scour is considered and its depth is estimated following the FDOT methodology (Sheppard and Renna, 2010).



a)



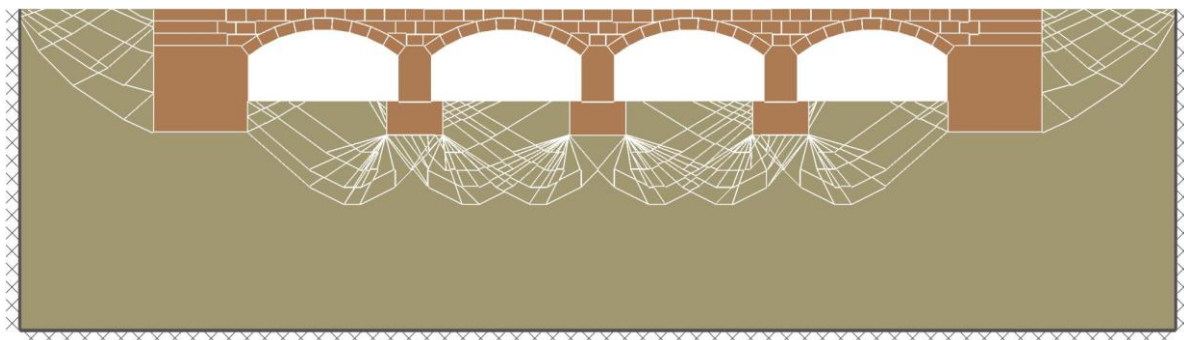
b)

**Figure 41. PDF function of the local scour depth a) without model uncertainties, b) with model uncertainties after (Lagasse et al., 2013)**

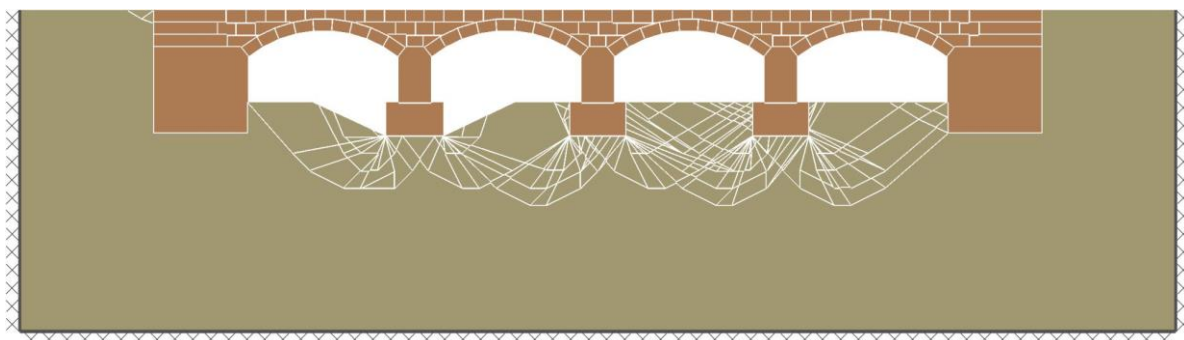


Figure 42a shows the PDF functions of the estimated local scour depths for the 5-, 20-, 50-, 100-, 500-, and 1000-year return periods. It can be observed that the scour depths do not vary significantly among the return periods studied. This effect is evidenced as the FDOT methodology is not too sensitive to the hydraulic conditions as shown by previous studies when testing the performance of scour predictions (refer to (Yang *et al.*, 2019)). This epistemic uncertainty associated with the accuracy of the FDOT method to predict scour can be considered through the application of bias factors with a coefficient of variation obtained from the ratio of observed scour with predicted scour as suggested by Lagasse *et al.* (2013). The application of these factors to the scour estimates results in the PDF functions from Figure 42b. It can be seen that the inclusion of this model uncertainty leads to the scour depth for a return period of 5-years being higher than the scour depth for a 100-year return period. This effect occurs due to the large coefficient of variation of the bias factor and reflects the need for a better assessment and understanding of the epistemic uncertainties associated to scour predictions. Therefore, the scour estimates without model uncertainties are employed for the fragility assessment of the masonry arch bridge under study.

Figure 43 shows the masonry arch bridge modelled in LimitState:GEO (LimitState, 2019) for the no-scour condition (Figure 43a), scour due to a 5-year flood (Figure 43b), and scour due to a 1000-year flood (Figure 43c). For modelling the geometry of the scour cavity, the experimental results from Vijayasree *et al.* (2019) were followed. It should be noted that a symmetrical in-plane failure mode is assumed, as the water flow is aligned with respect to the pier plan orientation (if skewed, the expected failure mode would be not-symmetrical).

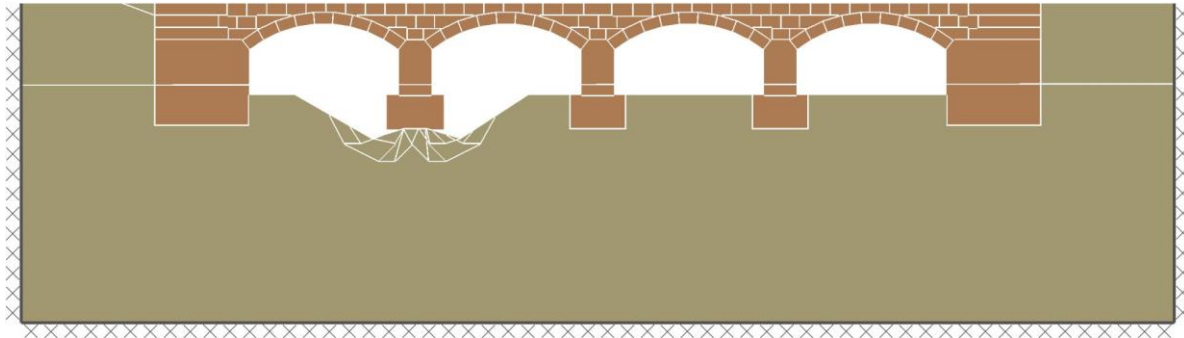


a)



b)





c)

**Figure 42. DLO model of the masonry arch bridge in LimitState:GEO (LimitState, 2019): a) no scour condition, b) scour due to a 5-year flood, c) scour due to a 1000-year flood**

An adequacy factor, which is defined as the factor by which specified loads must be increased in order for the system to reach a collapse state, was obtained in LimitState:GEO for each intensity measure (return period) after modelling the corresponding conditions, i.e. the scour cavity and hydrodynamic load conditions. Subsequently, the probability of failure was computed using the first order reliability method (FORM).

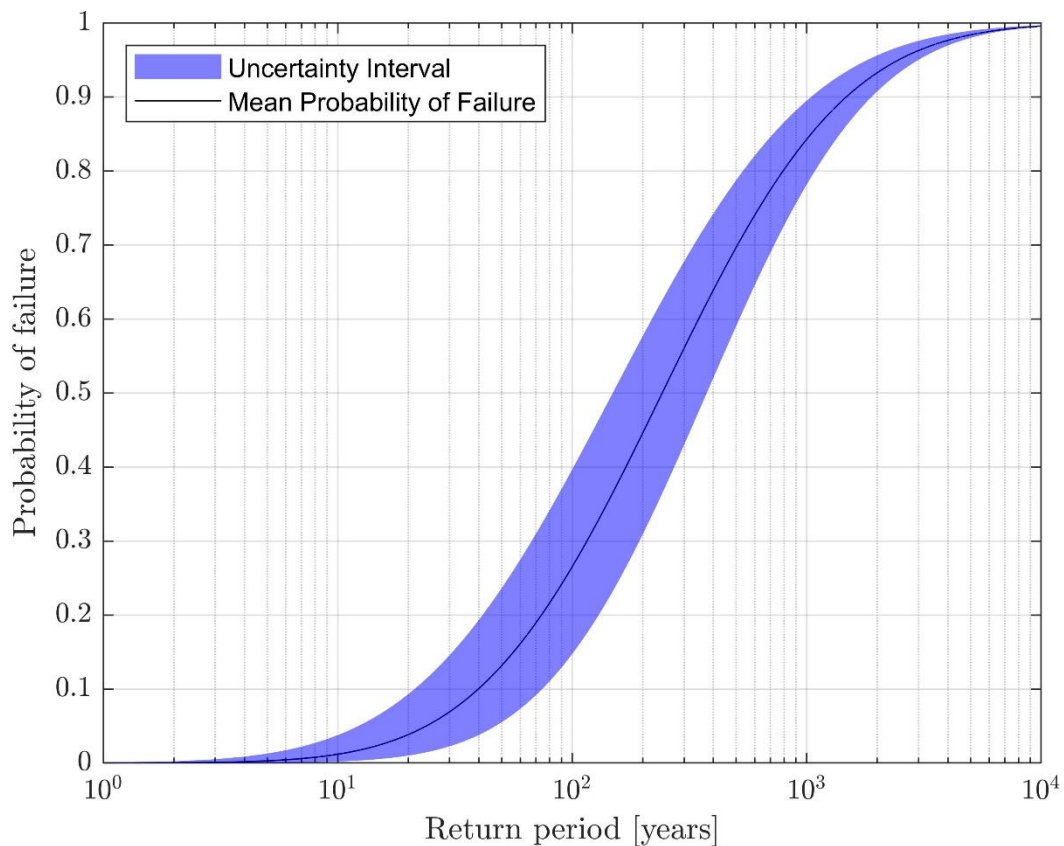


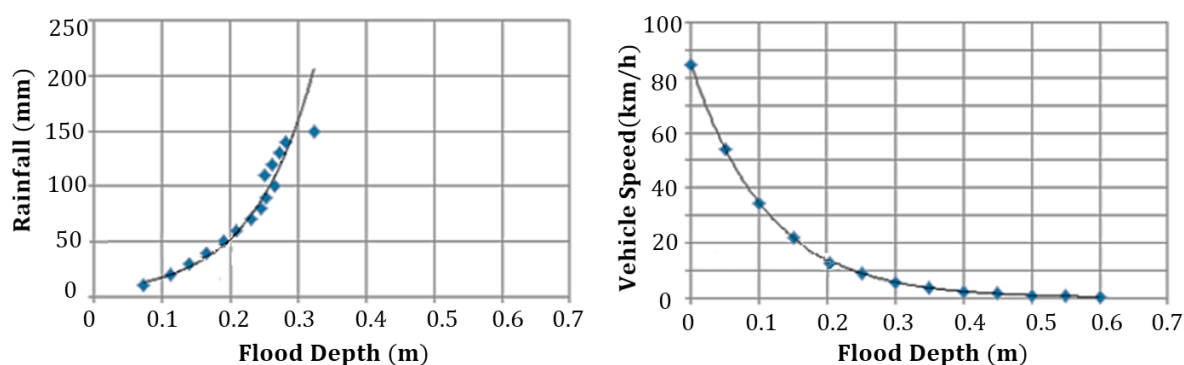
**Figure 43. Fragility functions for Class I bridges**

The obtained fragility curve with uncertainty bounds is shown in Figure 43. As previously mentioned, the curve was constructed for the ultimate limit state. Thus, the bridge functionality associated to this damage level is 100% loss of service. It should be noted that in this example the degradation processes were not yet included. However, time-dependent fragility functions as described in Section 4.1.5 can be obtained by introducing the reduction in the compressive strength of the masonry units due to deterioration, as well as the accumulation of scour as a consequence of multiple floods. These effects will be addressed in future work.

## 4.2 Road fragility functions

Floods can manifest over hours or days. This exposure (daily or hourly) can have a temporary or definitive impact on the loss of road functional capacity. Especially flash floods (which start as a result of heavy rains) are the predominant cause of weather-related disruptions in the transport sector (DfT 2014a). This problem seriously affects the road network in urban areas, where there is a large number of impermeable surfaces. Therefore, when excessive rains occur, large surface water flows cause drains to exceed their capacity and consequently increases the economic and social effects.

Currently, there are insufficient studies regarding the relationship between adverse weather (rains and floods) and traffic flow and congestion. In SAFEWAY (2020) simple and sophisticated models for the evaluation of mobility on roads are described. Among them, the simplest approach consists of assuming two scenarios. One in which the road is fully operational and the other in which the road is completely blocked, which would allow defining a threshold for the depth of the water on the road by comparing the two scenarios. Meanwhile, more sophisticated approaches address the capacity reduction or the reduction of the vehicle speed according to the water depth. Among other studies, Lam et al. (2013), proposed an equation to estimate vehicle speed/density under various rainy conditions. Pregolato, et al. (2017) propose a relationship between the standing water depth and the vehicle speed, identifying that a road is impassable when a water level of 30 cm is reached. From these investigations, Lee (2017), develop a traffic interruption map taking into account the rain-flood depth curves and the vehicle speed-flood curves as shown in Figure 44.



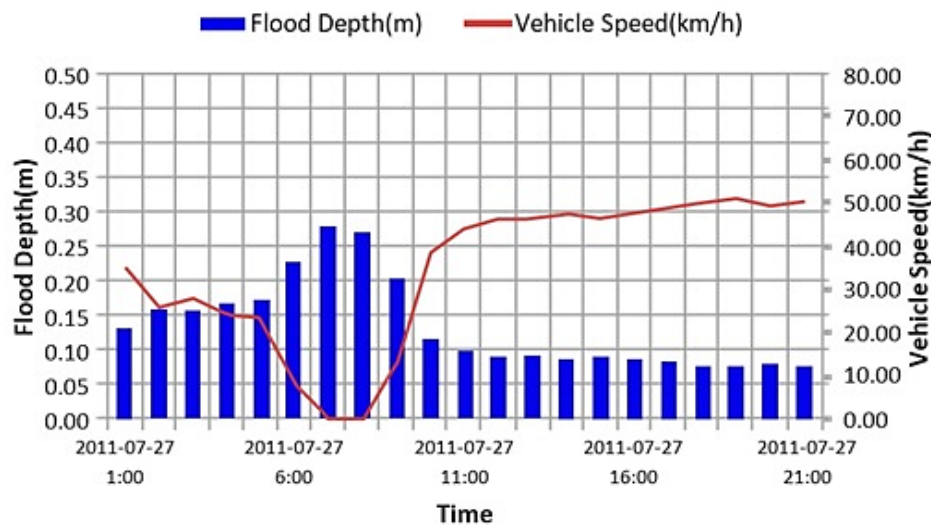


Figure 44. Rainfall–depth–vehicle speed relation. From: Lee (2017)

### 4.3 Roadway embankment fragility functions

Floods can often cause damage to transportation systems. Damage ranging from natural landslides to damage to slopes and embankments due to scour processes is a relevant failure mechanism in transportation infrastructure (Benn, 2013; Van Leeuwen and Lamb, 2014).

It is relatively difficult to derive fragility functions for geotechnical assets, such as road slopes and embankments, due to their inherent heterogeneity. However, McKenna *et al.*, (2021) proposed an approach for fragility functions derived to predict the displacement, and therefore the damage of a road over a granular embankment that is subject to flooding. The fragility evaluation is provided through numerical simulations, considering parameters drained of the soil materials, for a gradually increased water table, followed by scouring hole development at the toe of the embankment slope.

The curves construction process consists of five main stages. First, perform numerical analysis to increase the intensity of hazards including slope/embankment and foundation soil, and imposed hazard effects (i.e., water table and scour due to flooding). Second, define the damage states based on the range of preset measurement values. Third, plot the intensity measure against the corresponding damage measure and use the best-fit regression to derive the probabilistic data (i.e., the median) of the threshold intensity measure at each damage state. Fourth, uncertainty values calculation of the components and subsequent combinations to calculate the total uncertainty values. Finally, the normal logarithmic cumulative distribution function is calculated, using the values obtained in the previous steps to derive the fragility curves. Those fragility curves proposed by the authors are shown in Figure 45.

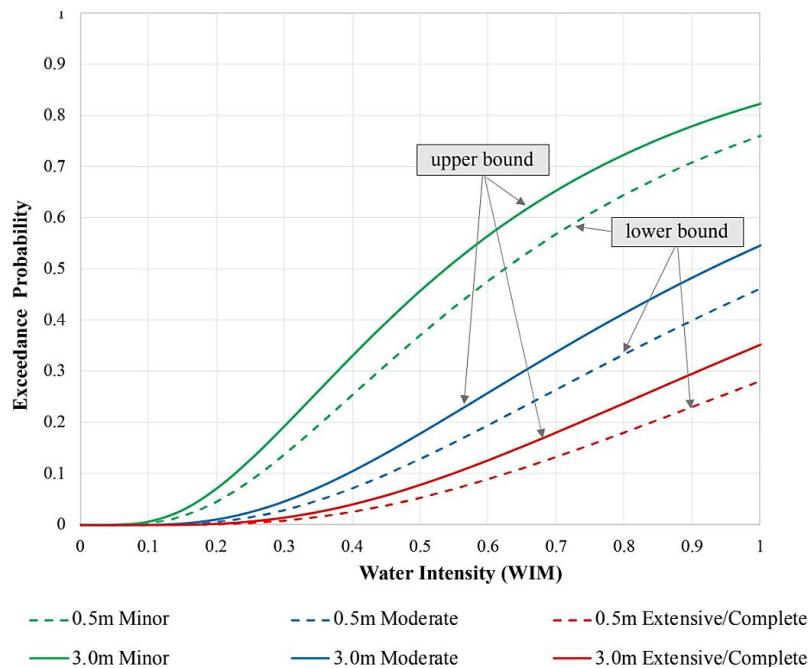


**Figure 45. Fragility functions for roadway embankment scour (McKenna *et al.*, 2020)**

Moreover, McKenna *et al.* (2020) recommended these fragility functions for use in the design processes, as they provide information for the performance of assets under various hazards considering different levels of design of hazard magnitudes and frequencies.

#### 4.4 Railway embankment fragility functions

Railways are significantly vulnerable when rail tracks are inundated or overtopped, given that a short section of track being washed out causes the entire railway system to experience delays. The most common failure mechanisms of rail tracks due to flood overtopping are scouring of the embankment fill which supports the rail tracks and/or scouring of the ballast. (Tsubaki *et al.*, 2016) developed fragility curves based on railway scour damage recorded during two flood events. The upstream flood water level was used as the intensity measure for the fragility curves, and the damage states defined were “no damage”, “ballast scour”, and “embankment scour”. Figure 46 displays the obtained fragility curves for ballast scour, embankment scour, and the combination of ballast and embankment scour. The overtopping water depth,  $\Delta h$ , corresponds to the difference between the upstream flood water level  $H$  and the elevation of the railway track,  $z$ , i.e.,  $H = z + \Delta h$ . Ballast scour was fitted to a normal fragility curve, while embankment scour and the combination of ballast and embankment scour were fitted to log-normal fragility curves.

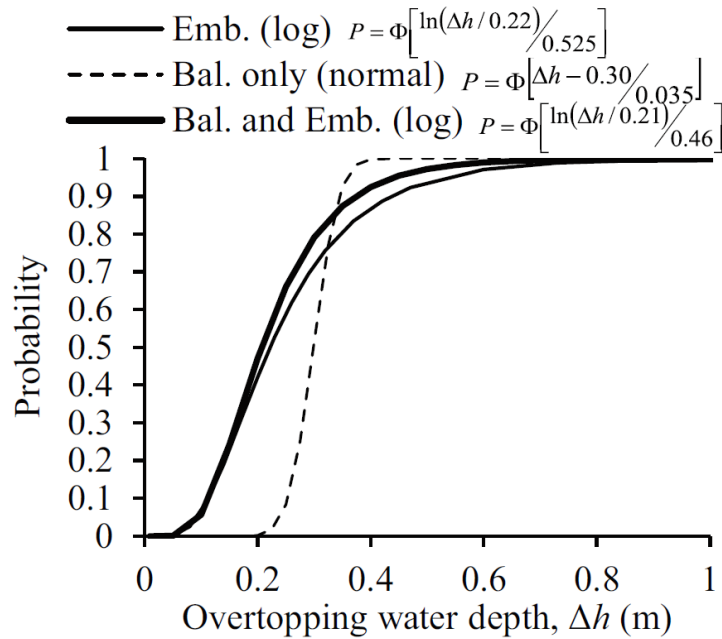


**Figure 46. Fragility curves for ballast scour (Bal. only), embankment scour (Emb.), and ballast and embankment scour (Bal. and Emb.) from (Tsubaki et al., 2016)**

Given that the type of records used for the development of ballast and embankment fragility curves are not available at the Santarém case study, the aforementioned fragility curves from literature will be implemented on the application for SAFEWAY.

## 5. Assessment of direct impacts

### 5.1 Assessment of direct impacts at asset level

After the occurrence of extreme hazard events, infrastructure assets which experienced physical damages must be repaired to restore the complete functionality of the transportation system. As mentioned in Section 4.1.6, these intervention costs are a function of the damage level attained by the infrastructure and may be expressed as a percentage of the replacement cost, or by absolute costs in e.g., euros per m<sup>2</sup>. Even though most of available studies focus on seismic damage and post-hazard disruptions, some surveys have been recently carried out to associate bridge damage caused by flood-induced scour to repair decisions, repair costs, functionality loss, and closure times. For instance, Hackl *et al.* (2018) estimated the restoration costs composed of a fixed part, i.e. site setup, and a variable part, i.e. per m<sup>2</sup> of reconstruction material, from the survey conducted by D’Ayala *et al.* (2015). The estimated values are shown in Table 21 in Swiss franc (CHF) adjusted to 2017 price levels. However, the repair actions are not clearly stated for each damage state and thus it is difficult to extrapolate these values to other applications.

**Table 21. Functionality loss and restoration costs for bridge scour according to (Hackl *et al.*, 2018)**

| State                | Functionality loss        | Fixed costs<br>[CHF] | Variable costs<br>[CHF/pier] |
|----------------------|---------------------------|----------------------|------------------------------|
| S0: Operational      | -                         | -                    | -                            |
| S1: Monitored        | -                         | 16,000               | 24,000                       |
| S2: Capacity reduced | 20% reduction in capacity | 30,000               | 40,000                       |
| S3: Closed           | 100% closed lanes         | 48,000               | 64,000                       |

On the other hand, Misra *et al.* (2020) have recently conducted an online survey to experts in the field of roadway and bridge inspection and repair, to characterize post-hazard restoration planning. Flood-related damages to bridge components were related to repair decisions, repair time, traffic closure decisions and closure times, as summarized in Table 22. These data can be used to develop statistical models to construct restoration functions, which are important for the quantification of indirect consequences (see further details in Section 6).

It is worth mentioning that current efforts are being done to collect surveys from a pool of experts to define restoration tasks after flood-induced damages and loss of functionality of bridges, in order to enable the quantification of the resilience of

bridges and transportation networks in the UK (refer to Mitoulis and Argyroudis (2021)).

**Table 22. Bridge repair and closure actions after flood-related damages (Misra *et al.*, 2020)**

| Damage state | Description  | Repair decision  | Repair time (days)                         | Bridge closure action  | Bridge closure duration (days)             |
|--------------|--|--|--|--|--|
| BS1          | Scour at abutment leading to piles being exposed   | No action (0%)<br>Repair (79%)<br>Replace component (11%)<br>Replace bridge (5%)<br>NA (5%)  | Mean (21.7)<br>Median (14)<br>COV (1.31)   | No action (16%)<br>Complete closure (63%)<br>Partial closure (21%)     | Mean (15.7)<br>Median (14)<br>COV (0.98)   |
| BS2          | Scour at column base leading to exposed foundation | No action (26%)<br>Repair (63%)<br>Replace component (0%)<br>Replace bridge (0%)<br>NA (11%) | Mean (21.6)<br>Median (10)<br>COV (1.95)   | No action (53%)<br>Complete closure (23.5%)<br>Partial closure (23.5%) | Mean (12.6)<br>Median (0)<br>COV (1.89)    |
| BS3          | Scouring leading to settlement at pier             | No action (0%)<br>Repair (0%)<br>Replace component (42%)<br>Replace bridge (25%)<br>NA (33%) | Mean (194.3)<br>Median (165)<br>COV (0.77) | No action (0%)<br>Complete closure (100%)<br>Partial closure (0%)      | Mean (158.1)<br>Median (150)<br>COV (0.84) |

NA= Not answered



## 5.2 Assessment of direct impacts at network level

In this section, the risk has been evaluated measuring the probability and severity of an adverse effect (ISSMGE Glossary of risk management terms) to linear transportation infrastructures, considering direct, material impacts.

### 5.2.1 Methodology

#### 5.2.1.1 Risk calculation

We performed a quantitative risk analyses based on the formulations of Varnes (1984) and Fell et al. (2005), where the frequency of the event, the probability of reaching the element at risk, the vulnerability (i.e., degree of loss) and costs of rehabilitation have been considered.

For the risk evaluation, Equation (34) was considered (Kaplan and Garrick, 1981; Varnes, 1984):

$$R = H \times V \times E \quad (34)$$

where the risk is calculated as a combination of hazard (H), vulnerability (V) and element exposed (E). Three different flood scenarios were assessed, each one representing different return periods and flood intensities. The exposed length of infrastructure was evaluated per each territorial unit with a geometric analysis carried out in GIS. The vulnerability term, V, was evaluated as a function of the flood category that affect a railway/road. We used fragility curves from literature where 3 different ranges have been identified for the V of linear infrastructures: lower, mean, upper (Table 25).

To evaluate the annual loss, the formula from Fell *et al.* (2005) was considered (Equation (35)). The calculation considers the costs for total rehabilitation (C) of a railway/road, the vulnerability of the linear infrastructure classified in three different ranges as a function of the category of flood depth, and the conditional probability of impacting a line in a given region. The formulation has been applied for a range of floods frequencies (see Table 24). The expected annual loss is calculated by the summation of all plausible flood scenarios.

$$\text{Annual loss (M€)} = P(F) \times P(i | \text{flood}) \times C \times V \quad (35)$$

Where  $P(F)$  is the frequency of flooding,  $P(i | \text{flood})$  is the probability of line exposure (affected / tot) in a given region,  $C$  is the total rehabilitation value of railway/road in a region [M€] (cost per unit m \* tot meter), and  $V$  is the vulnerability of the element at risk to flooding.

**Table 23. Probability classes and flood scenarios used in the assessment**

| Verbal description of probability | Return period | Representative flood scenario used in analyses |
|-----------------------------------|---------------|--|
| Neglectable                       | < 3 years     | No loss  |
| Low                               | 3-30 years    | 10-yr  |
| Medium                            | 30-300 years  | 100-yr   |
| High                              | >300 years    | 500-yr   |

### 5.2.1.2 Concept

The practical approach applied to evaluate the expected annual loss and the risk of damage is described in Figure 47. Open access databases on natural hazards have been collected from different online sources (SAFEWAY; 2019a). The linear infrastructure database has been obtained from Open Street Map (OSM). Hazard and linear infrastructure maps were overlapped in a GIS environment to assess the exposure of the assets in different scenarios. The administrative region was chosen as the minimum territorial unit for our analyses. It is important to mention that one can apply this procedure even for a smaller territorial unit, such as the municipal border. The approach illustrated in Figure 47 is applicable for a variety of natural hazards. In the following sections, river flood has been considered as the natural hazard for carrying out our analyses. In a quantitative flood risk assessment all plausible floods need to be considered. In this assessment, three different flood scenarios are assessed, each one representing a different return periods and flood intensities as indicated in Table 24.

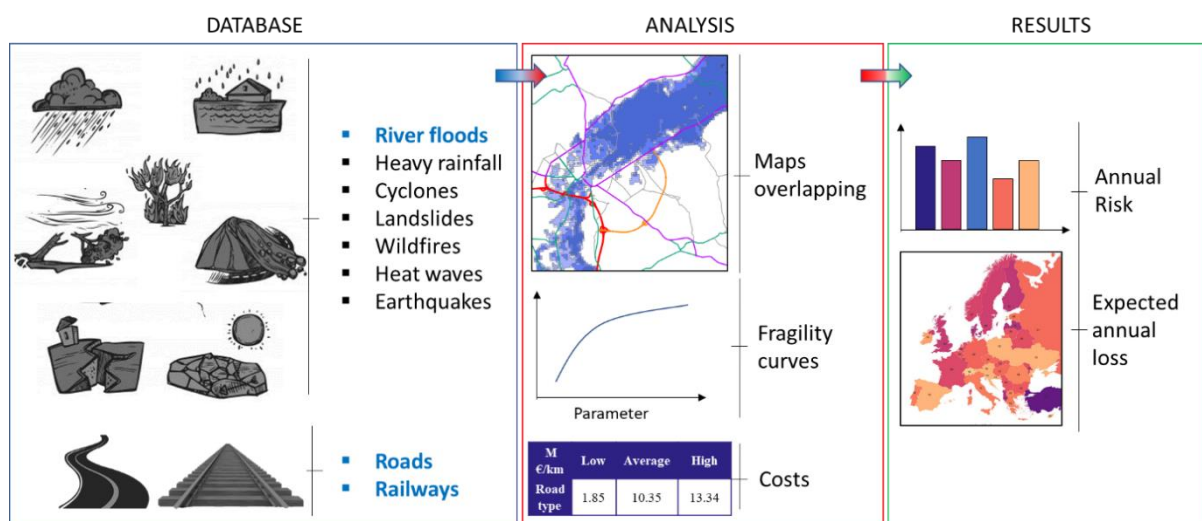


**Figure 47. Overview of the analysis steps for this assessment**

### 5.2.1.3 Vulnerability evaluation

Vulnerability relations are used to express the degree of physical loss/material damage to an asset. The vulnerability for roads and railway has been defined considering the vulnerability relations available in literature. The Swiss road authorities provide guidelines for assessment of material damage of roadways caused by flooding. The guidelines relate the damage degree of the road segment to the intensity of the flooding. The criteria for classification into intensity classes are described in Table 24. As a function of the flood depth, 3 different vulnerability classes were defined: low, medium, high. For each vulnerability class, lower, mean, and upper bounds of vulnerability were defined (Table 25). As vulnerability is dependent on the flow velocity, the estimates found in FEDRO (2012), were divided into either static ( $v < 1\text{m/s}$ ) or dynamic flooding ( $v > 1\text{m/s}$ ). Upper bounds were picked in accordance with the dynamic case, while the mode reflects the static case.

**Table 24. Classification of intensity of flooding (Bundesamt für Strassen ASTRA, 2012)**

| Flood intensity class | Quantitative description of intensity for flooding                     | Explanation  |
|-----------------------|--|--|
| Low                   | $h < 0.5\text{ m}$ (or $v \cdot h < 0.5\text{ m}^2/\text{s}$ )         | $h$ : flow depth<br>$v$ : flow velocity  |
| Medium                | $0.5 < h < 2\text{ m}$ (or $0.5 < v \cdot h < 2\text{ m}^2/\text{s}$ ) | For static flooding ( $v < 1\text{m/s}$ ) the intensity class is distinguished from flow depth only, i.e. the first part of the criteria will always be the strictest one. |
| High                  | $h > 2\text{ m}$ (or $v \cdot h > 2\text{ m}^2/\text{s}$ )             |  |

**Table 25. Vulnerability relations adapted from Bundesamt für Strassen ASTRA (2012) and Oberndorfer, Sander and Fuchs (2020)**

| Class  | Vulnerability (Degree of loss of road segment) |       |             |
|--------|--|-------|-------------|
|        | Lower bound                                    | Mean  | Upper bound |
| Low    | 0  | 0,001 | 0,05        |
| Medium | 0,001  | 0,01  | 0,05        |
| High   | 0,01   | 0,1   | 0,35        |

### 5.2.1.4 Rehabilitation cost estimation

The rehabilitation cost for road types and railway were estimated considering references from literature. Specifically, for railways, the "Assessment of unit costs of rail projects" (Attina *et al.*, 2018) has been considered. The rehabilitation cost has been defined as construction works mainly related to improvement work that are conducted to reinstall the design characteristics of an existing line (e.g. design speed, capacity, etc.) which has worsened in quality (Attina *et al.*, 2018). To consider possible uncertainties we have defined three ranges for the rehabilitation costs: lower, average and upper bound. The values are presented in Table 26.

**Table 26. Rehabilitation cost values for railways.**

| Rail costs     | Low<br>[M €/km] | Mean<br>[M €/km] | High<br>[M €/km] |
|----------------|-----------------|------------------|------------------|
| Rehabilitation | 1,55            | 3,1              | 4,81             |

The cost for roads is also taken from literature. The estimation of average construction costs for motorways in Europe is based on numbers of construction costs and total costs for motorways reported in (ECA, 2013). The motorway construction costs (Table 27) is also in accordance with numbers reported by an Austrian economy magazine for highways <https://www.derstandard.at/story/2292578/oesterreichs-autobahnen-kommen-teuer>

For assessment of construction costs for other road types, we assumed similar relationship between motorways – trunk roads and local roads as for the indicative total road infrastructure cost reported in Doll, van Essen and others (2008). Those costs indicate the annual depreciation of the investment, so we chose not to use directly those values, but to consider the relations between the different road types.

Assessment of construction costs encompass construction costs for motorways, primary roads, trunk roads and local roads. Local roads include secondary and tertiary roads. A summary of the construction costs applied in the assessment is provided in Table 27.

**Table 27. Construction costs for roads (ECA, 2013)**

|                            | Low<br>[M €/km] | Average<br>[M €/km] | High<br>[M €/km] |
|----------------------------|-----------------|---------------------|------------------|
| Highways,<br>Primary roads | 1.41            | 7.9                 | 10.1             |
| Trunk roads                | 0.12            | 0.6                 | 0.66             |
| Local roads                | 0.06            | 0.42                | 0.81             |

### 5.2.1.5 Montecarlo simulations and uncertainty

To handle the uncertainty of the vulnerability and the costs expressed from Table 25 to Table 27, a Monte Carlo simulation was conducted in order to estimate the expected annual loss. To sample values for the cost and vulnerability, it was necessary to specify a distribution associated with the values specified in the tables. To associate a distribution with the suggested bounds we have applied the Beta-PERT distribution. The Beta-PERT distribution is more centred around its mode, and less sensitive to extreme min or max values compared with the triangular distribution. For more details, see Oberndorfer, Sander and Fuchs (2020). However, also for the Beta-PERT distribution due to the skewness of the upper and lower bounds in comparison with the mean, the associated distribution, applying the mean as a mode, will only partly reflect the specification of the mean value. In Table 28 the associated mean and median values of the Beta-PERT distribution associated with Table 25, are displayed. In particular the low intensity category is highly skewed, due to the large discrepancy between static and dynamic flooding.

**Table 28. Associated mean and median values for the Beta-PERT distribution associated with the given vulnerability parameters in Table 25.**

|        | Mean   | Median |
|--------|--------|--------|
| Low    | 0.0090 | 0.0070 |
| Medium | 0.0152 | 0.0138 |
| High   | 0.1267 | 0.1200 |

As for the vulnerability estimates, a Beta-PERT distribution with the given values as min, mode and maximum has been applied for the cost from Table 26 and Table 27. The same considerations as above regarding the skewness of the mean applies to the sampled values. However, the mean cost is more centred than the mean vulnerability.

When sampling the numbers for vulnerability and cost, it is necessary to make some assumption regarding the dependency of the random variables. In the given simulation we assumed that cost and vulnerability could be sampled independently for each type of structure, within each region. It is well worth noting that assumptions regarding independence may have a considerable impact on the estimate, and further that it is likely to underestimate the uncertainty. In the below results we applied 1000 simulations to generate the statistics.

---

## 5.2.2 Application and results

### 5.2.2.1 The GIS procedure and preliminary results

The roads and railways used in the analysis were downloaded from Open Street Map. Polygons defining administrative units originates from the NUTS 2016 datasets provided by Eurostat (<https://ec.europa.eu/eurostat/web/gisco/geodata/reference-data/administrative-units-statistical-units/nuts>). Raster datasets defining the flooded areas were downloaded from the Joint Research centre data catalogue, representing flooding with return periods 10, 100 and 500 years.

The analyses were performed using vector data as input, therefore the flood maps needed to be converted to polygons. During this process, the flood depths were reclassified into 5 classes. The intersection between the transportation infrastructure (roads and railways), and the flooded areas were computed using the Identity tool. The input features (roads/railways) or portions thereof that overlap flooded areas will get the attributes of the flooded areas, including the flood depth. The same method was used to intersect roads and railways with administrative units. In this way, the two-line datasets with roads and railways contains all the attributes needed (length of segment, flood depth, administrative unit, and road type for roads).

Statistics could then be extracted from the roads for each combination of road type and return period, and from railways for each return period. In GIS we evaluated the percentage of infrastructures exposed to flood for each region as a function of the three different scenarios analysed and the flood depth categories. Figure 48 shows the percentage of highway, primary roads and railway exposed to different return period flood scenarios. In this case, the flood categories have been aggregated. A comparison between highway and railway for the same flood scenario (i.e., 10 years return period) shows that in general, railways are more exposed to flooding than highways and primary roads.



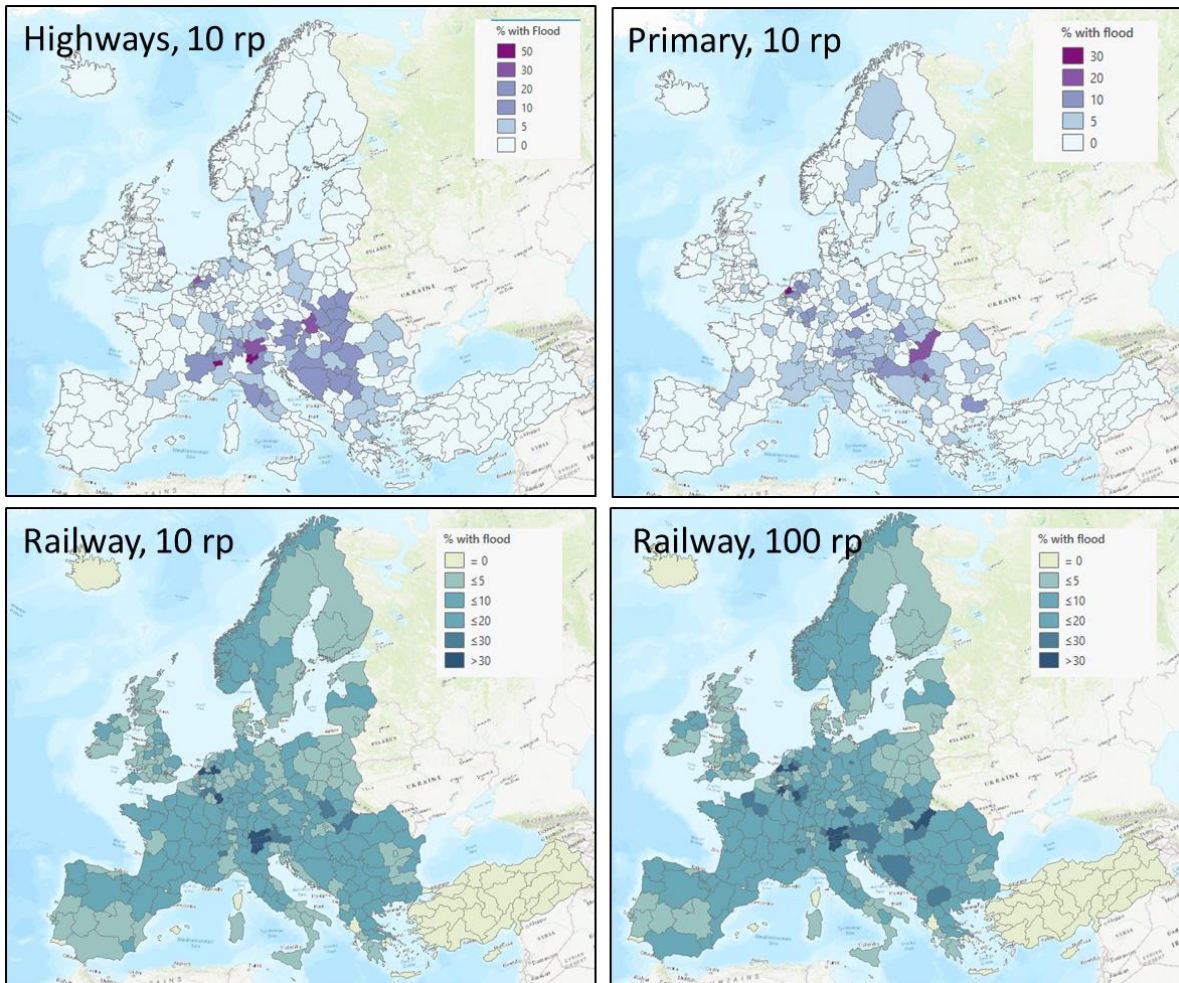


**Figure 48. Flood exposure of roads and railways in Europe**

However, it is also possible to show the exposed infrastructures dividing among the different categories of flood depth. Figure 49 to Figure 52 show the results aggregating the exposition to flood depth on national bases. The national abbreviations refer to the ISO3166-1 country codes. In Slovakia (SK) we can see that almost 20% of highway are exposed to a 10-year return period flood scenario. Considering the primary roads with a 10-years return period flood scenario Serbia (RS), Netherlands (NL) and Bosnia (BH) have more than 10% of exposed road. The results for railways considering the same flood scenario show an exposure in the range 10-20% for Austria (AT), Bosnia (BH), Lichtenstein (LI), Macedonia (MK). With Bosnia and Macedonia with 10% or railway exposed to more than 2 meters flood depth.



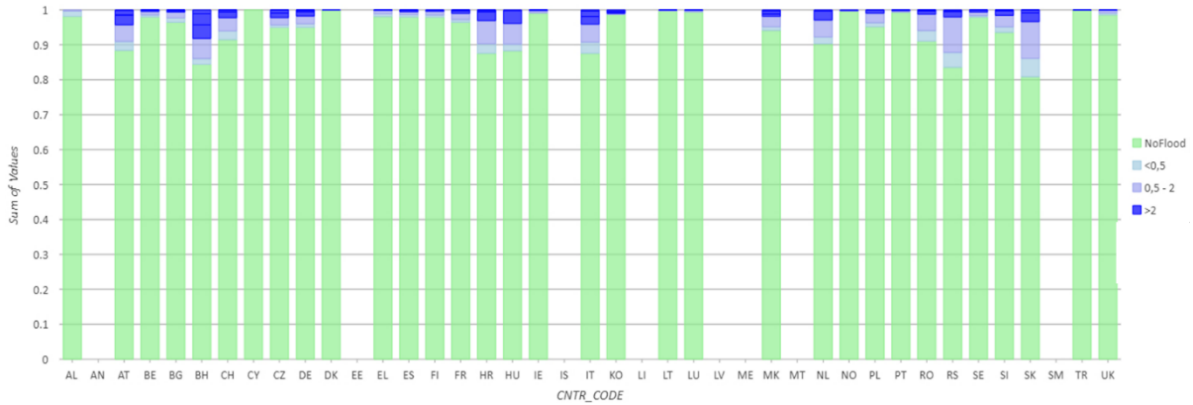


**Figure 49. Flood exposure of roads (Highway) for the 10-year return period flood scenario – as a function of flood depth categories**

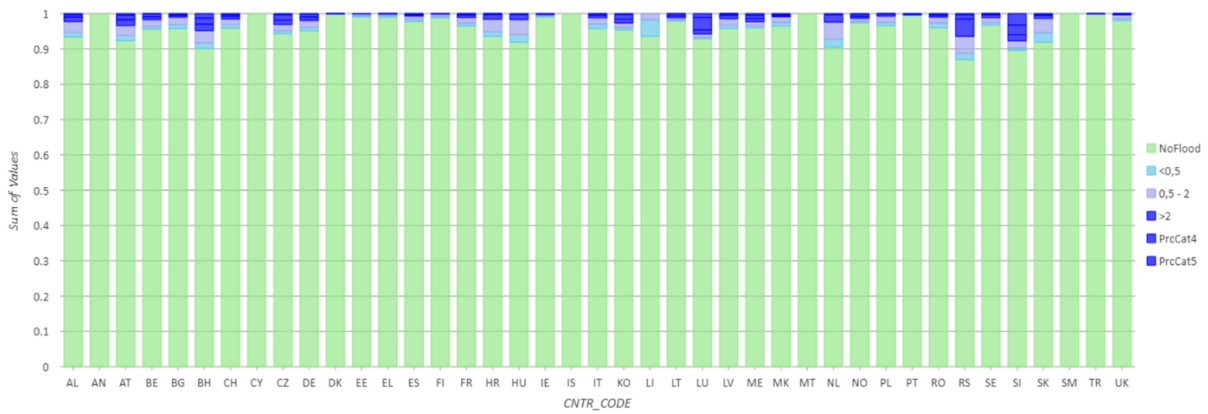


**Figure 50. Flood exposure of roads (Primary) for the 10-year return period flood scenario – as a function of flood depth categories**

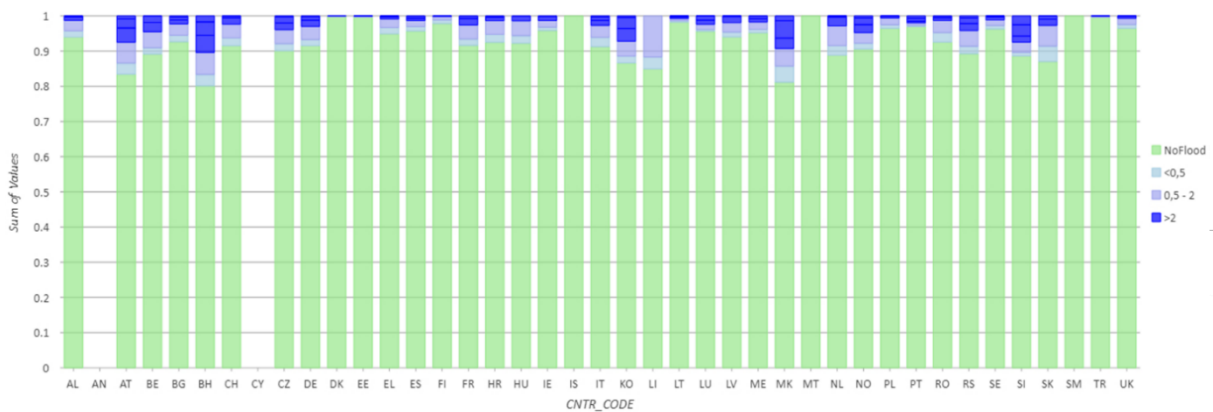
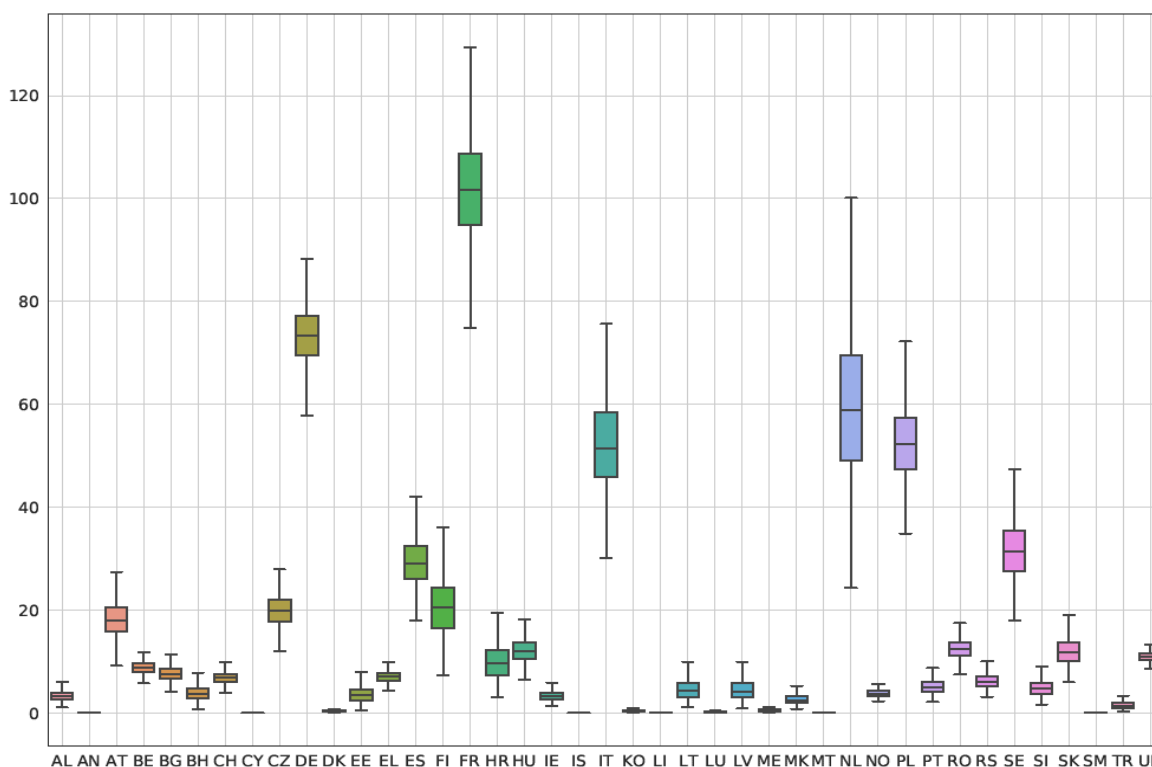


**Figure 51. Flood exposure of railway for the 10-year return period flood scenario – as a function of flood depth categories**

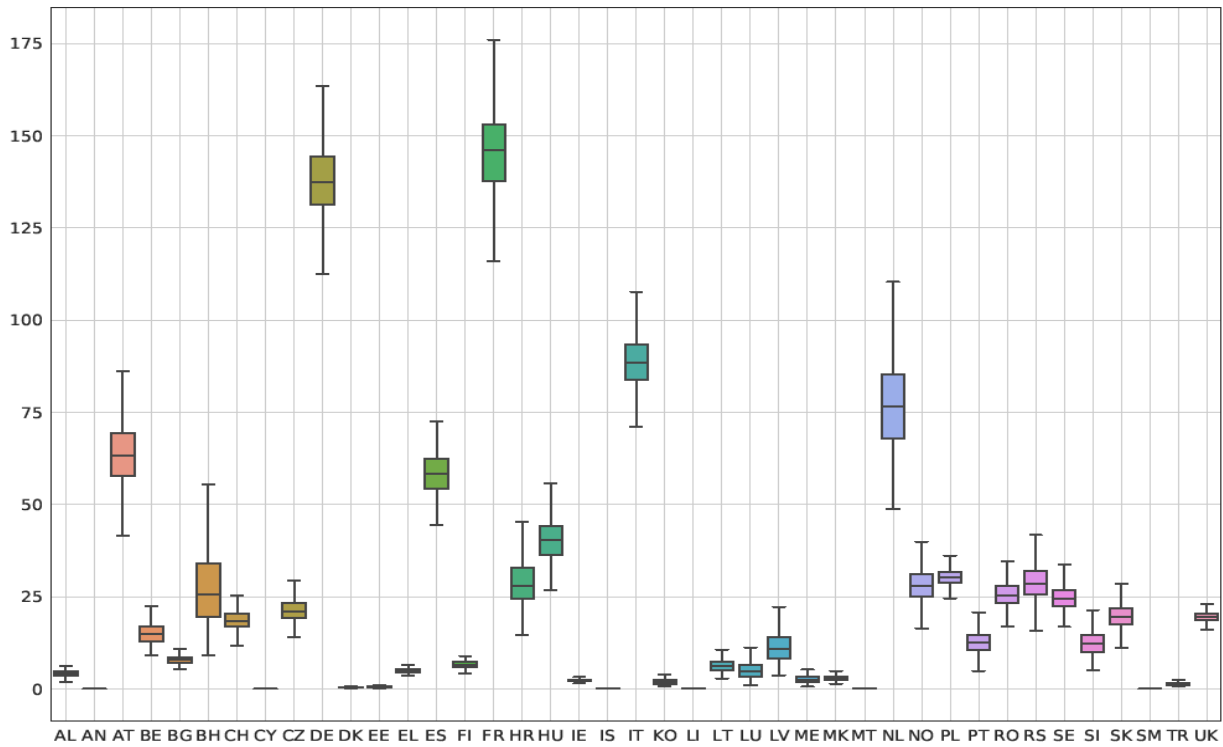
### 5.2.2.2 Description of the results

Figure 52 shows the results of the risk assessment in terms of probability of damage and annual loss for railways, aggregating the three different flood scenarios analysed. The results have been presented in box-and-whiskers plots, representing the median, the quartiles (25 and 75), the caps and the whiskers. The median annual loss for railway is lower than 50 M€ for most of the nations. However, Germany (DE) and France (FR) have respectively, around 75 and 100 M€ as median expected annual loss.

Figure 53 depicts the annual total loss for roads, grouping together highway, trunk, primary, secondary and tertiary roads. Germany (DE), France (FR), Italy (IT) and Netherlands (NL) show the largest ranges of expected annual loss. France has a median value of ca. 140 M€, Germany of 135 M€ and Italy around 85 M€.



**Figure 52. Results of the risk assessment for railways, per country, in terms of expected annual loss in M€.**



**Figure 53. Results of the risk assessment for roads, per country, in terms of expected annual loss in M€.**

## 6. Assessment of indirect impacts

The key aspect for the quantification of indirect impacts is the assessment of the disruption of the transportation service. The service disruption could occur directly from the natural event, e.g. floodwater on a road, or could occur from the physical damage to an asset, e.g. collapse of a bridge. In the former case, functional vulnerability functions could be used to describe the functionality loss due to a given hazard intensity. For the latter case, a more detailed analysis is needed among the asset physical damage, its degree of functionality loss, and the service disruption introduced at the network level. To this end, transportation traffic models are needed to support this type of analysis. In this chapter, both possibilities are examined. Firstly, a simplified assessment of indirect impacts of flooding is performed, by assessing the probability and duration of service disruption. Afterwards, a traffic model for the demonstration pilot is constructed for an accurate quantification of the functionality of the network after the failure of infrastructure components.

Moreover, disruptions of the transport infrastructure also have extraordinary consequences for an industry, terminal, service centre, among others, due to massive failures, single access roads being cut off, or critical links made unusable. These consequences need to be assessed reliably (e.g. see (Molarius *et al.*, 2012; Ludvigsen and Klæboe, 2014; Frauenfelder *et al.*, 2017)), in order to increase the resilience of transportation systems.

An example of indirect damages that often occur in the Tagus basin consists of closed roads, i.e. cut-off over a period of one or more weeks by flooding (see Figure 54). Given the strategic importance of the Tagus valley to agriculture and groundwater resources within Portugal, such events have led to economic consequences, as well as harmful social and health conditions (Santos *et al.*, 2020).



**Figure 54. Isolation of Reguengo de Alviela due to flood event during April/2013. Photo: A terceira Dimensão (<http://portugalfotografiaaerea.blogspot.com/2013/04/cheias-do-rio-tejo.html>)**

## 6.1 Simplified assessment of probability of flooding and duration of service disruption

Transportation infrastructure systems connect businesses and support supply chains and services and offer accessibility to vital resources for daily activities and in emergency circumstances (Faturechi and Miller-Hooks, 2015). Flooding (or other extreme events) may lead to a disruption of the transportation service, with social and economic consequences. The indirect impacts of flooding address consequences of the service disruption for the users. Indirect impacts are therefore of wider scale and with longer incidence in time than direct impacts.

The scope of the study is to analyse motorways affected by flooding in Portugal. Portugal has about 3,000 km of motorways. The simplified assessments in this section aims to support the assessment of the economic impact on the society induced by disruption in the transportation service, focusing on user costs. The indirect economic impacts depend on various components: the composition of the traffic, time values related to the users, the duration of the closure, the quality and capacity of the alternative routes and the traffic amount. In this subchapter, the focus is on the assessment of:

- Probability of a service disruption
- Duration of a service disruption



**Figure 55. Flood damage and service disruption of road the Algarve region in Portugal.**  
Photo: Sky News (<https://news.sky.com/story/one-dead-as-severe-flooding-hits-portugal-10341035>)

### 6.1.1 Probability and consequence classes

In the same manner as for the material consequences (Section 5.2), the quantitative flood risk assessment for indirect consequences need to consider all plausible floods. Table 23 outlines the three different flood scenarios applied in the assessment, as well as the range of probabilities covered by each scenario. In the simplified assessment described in this subsection, the duration of the service

disruption is the only consequence parameter considered. The criteria for subdivision into duration classes (Table 29) are chosen according to duration values used in the Swiss model for risk assessment of roads affected by natural hazards (Bundesamt für Strassen ASTRA, 2012). Ideally, the highest duration class should have been divided into two classes, e.g. by entering a distinction between closure lasting between one week and one month and longer than one month. Such a division would, however, require modification and expansion of the vulnerability relationships used, which is outside the scope of this study.

**Table 29. Duration classes used in the assessment**

| Verbal description of service disruption | Duration of service disruption |
|--|--------------------------------|
| Neglectable                              | < 1/2 hour                     |
| Short                                    | 1/2 hour – 12 hours            |
| Medium                                   | 12 hours – 1 week              |
| Long                                     | ≥ 1 week                       |

### 6.1.2 Workflow for the assessment

For assessment of disruptions in transportation networks due to flooding, a challenge is how to treat multiple service disruptions within one link. Here the term link expresses the connection between two locations that are part of a larger network and within which no diversion roads are available.

The analysis is conducted at a regional scale and is performed within a GIS environment. The following procedure for assessment of the probability and duration of a service disruption is applied in the analysis:

- Subdivide the road network into links. Within each link there are no opportunities for detours. Material damage within the link could lead to a service disruption in the transportation network. If there are more locations with potential material damage within one link, it should only be counted as one service disruption.
- Perform analyses for flooding with different return periods, in this case 10-year, 100-year and 500-year. For each return period:
  - Identify the exposed part of the transportation infrastructure
  - Categorise flood depth into flood intensities: low, medium and high, according to Table 24.
  - If the assessment indicates a material damage that could lead to service disruption at more than one location within the same link, the



maximum flood intensity per link will be applied in the further analysis.

- To assess the duration of the service disruption within one link, a relation between intensity and duration of service is applied (Table 30).

### 6.1.3 Methodology for the assessment of consequences and ranking of risk

In the assessment of the consequences, a relation between flood intensities and duration of road closure from (Bundesamt für Strassen ASTRA, 2012) is applied (Table 30). Criteria for subdivision into low, medium and high intensity for flooding are shown in Table 23. The duration of the service disruption is, through the use of the same intensity classes as for material damage, related to the damage degree caused by the flooding and not to the duration of the flooding event.

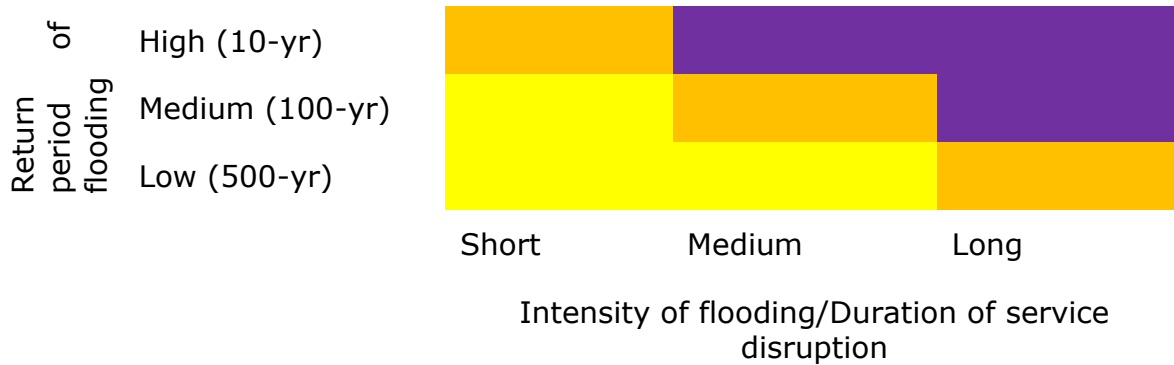
**Table 30. Average downtime (duration of service disruption) for roads after natural, gravitational events (Bundesamt für Strassen ASTRA, 2012).**

| Verbal description of intensity | Average downtime/duration of service disruption after natural event for roads (ASTRA; 2012) |
|---------------------------------|---|
| Low                             | 1 hour (1/24 day)   |
| Medium                          | 1 day   |
| High                            | 1 week (7 days) or more   |

The flood risk for the exposed links was analyzed as a function of the return period of the flooding, the flood intensities and the expected duration of service disruption. The risk is categorised into 3 levels: Low (yellow), medium (orange) and high (violet) in accordance with Table 31. Since the duration of the downtime is the only consequence parameter, Table 31 expresses a simplified risk ranking and must be regarded as an intermediate result of the risk assessment. The ranking of the risk may change with other factors such as traffic amount, the composition of the traffic, the increase of travel distance and the quality and capacity of the alternative routes. For quantification of the consequences, also time costs and other costs stemming from the increased travel distance are considered. The reader is referred to Section 6.3 for assessment of the socioeconomic costs of interruptions of roadway transportation.



**Table 31. Definition of risk levels. The colours were chosen to create a strong visual distinction between the risk levels in the resulting map.**



#### 6.1.4 The GIS analyses

In the GIS analysis, the data sets used for the road network were downloaded from Open Street Map. Flooding data from the Joint Research centre data catalogue was applied.

In order to count the number of road segments/links affected by flooding, a system for subdivision of the road network into links needed to be established. In general, each road segment should be continuous between intersections. On the other hand, it was not considered feasible to split a motorway link at intersections between a motorway and minor roads. The solution was to group the road segments into 3 classes: Motorway, trunk roads and other roads. Each class was handled separately, to define continuous road segments between intersections.

For each return period (10, 100 and 500 years), the flooded areas were divided into 3 intensity classes based on water depth: 0-0.5m, 0.5-2m and above 2m (i.e. according to Table 23). Nine new attributes were added to the road dataset – one for each combination of return period and intensity class of the flooding (Table 31). Finally, each attribute was set to 1 where the road segment intersected a corresponding flooded area.

#### 6.1.5 Results of the assessment

The procedure for subdivision into links resulted in a total of 7292 motorway segments in Portugal, when all motorway segments shorter than 100 m length were excluded<sup>3</sup>. Of these, 6220 were less than 1 km long.

The analysis shows that 184 motorway segments potentially could be affected by flooding. Table 32 provide statistics on the resulting risk levels. Figure 56 presents the risk map for the whole of Portugal. A majority of the potentially affected motorway segments are in the highest risk class.

<sup>3</sup> The procedure for subdivision into links resulted in a large number of short road segments, especially around complex intersection and roundabouts. These were considered irrelevant for the analyses and therefore excluded,

**Table 32. Distribution of risk levels for the exposed motorway segments**

| Number of motor way segment | Risk level |        |      |
|-----------------------------|------------|--------|------|
|                             | Low        | Medium | High |
|                             | 27         | 28     | 129  |

The analysis does not take into account the dimensioning of the road and assumes that all of the assessed flood scenarios will lead to a service disruption. This is a conservative assumption. A more realistic assumption is that the road is dimensioned at least for the 10-year flood and hence that the 10-year flood will not lead to a service disruption. Figure 57 shows the results of the analyses if the consequences of the 10-year flooding is excluded. However, even in this modified analysis, a majority of the potentially affected road segments are associated with the highest risk class.

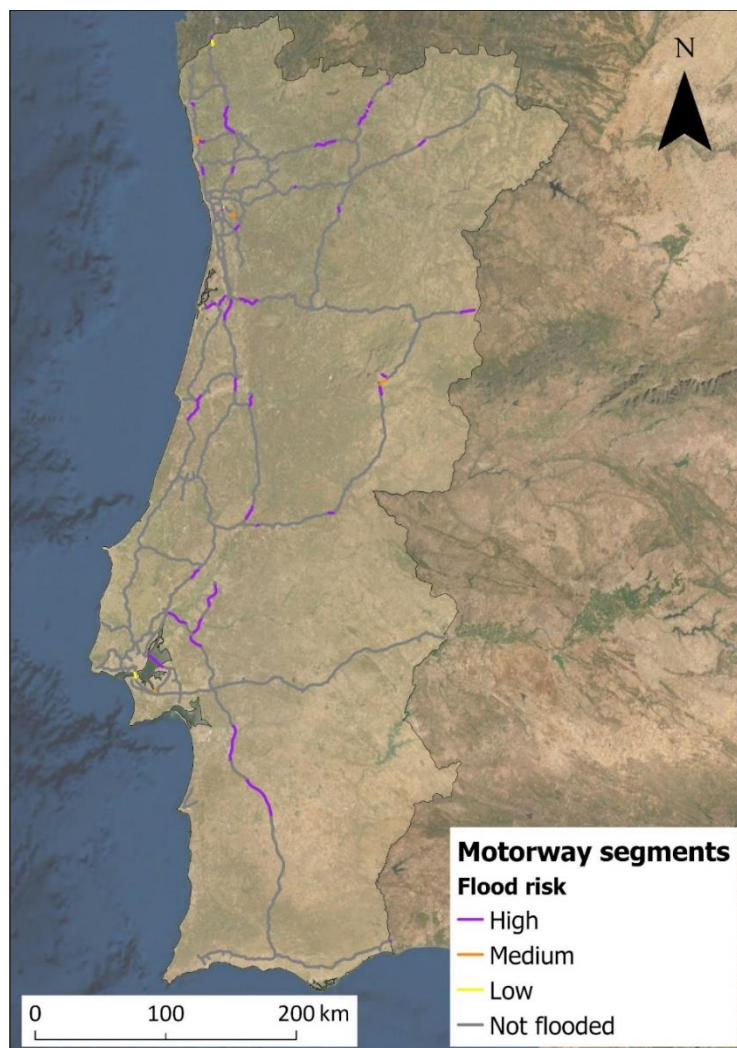


**Figure 56. Simplified flood risk ranking (In accordance with Table 32) with regard to indirect impacts.**

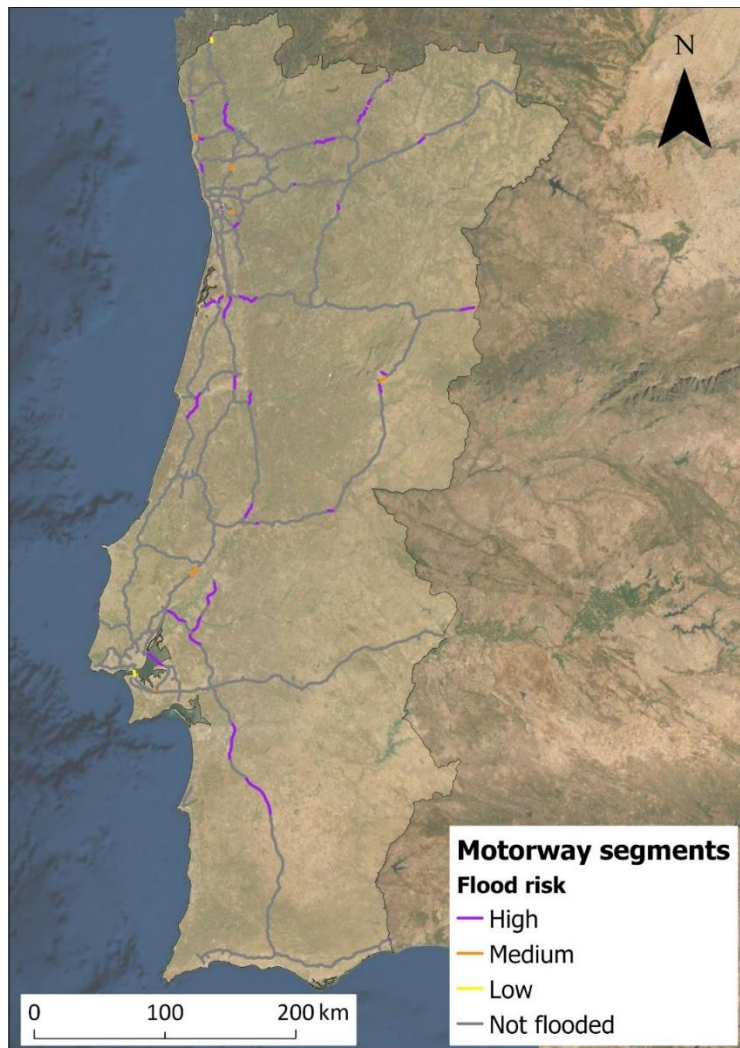


**Figure 57. Simplified flood risk ranking (In accordance with Table 32) with regard to indirect impacts, excluding 10-yr flooding.**

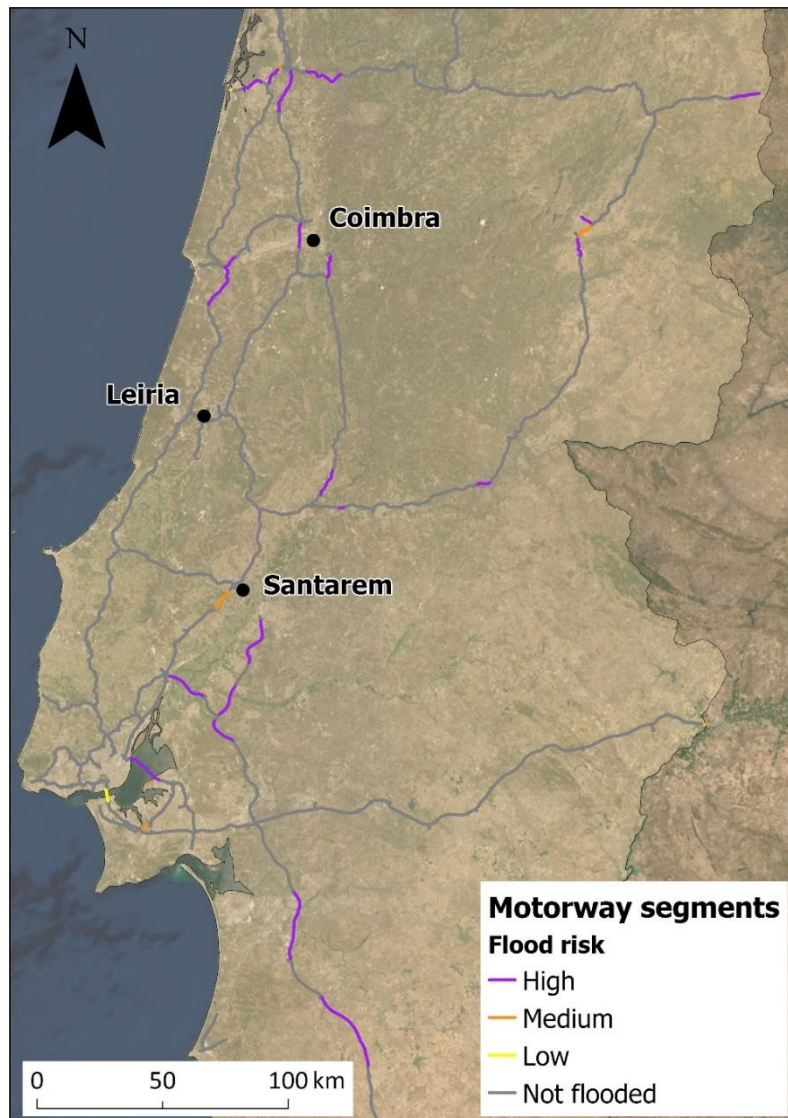


**Figure 58. Zoom-in of Figure 57, at the Portuguese Demonstration sites.**

The results of this assessment could be applied for a more detailed ranking and quantification of the risk, by considering also traffic amount, the composition of the traffic, the increase of travel distance and the quality and capacity of the alternative routes. In addition, time costs and other costs stemming from the increased travel distance are to be considered in a quantification of the economic consequences (Section 6.3).



## 6.2 Assessment of service disruption through traffic models

Traffic models allow the simulation of transportation systems to inform the design process, by representing the stretches of roads (links, and their nodes), users, and users' routing. In many researches the flood impacts on traffic have been approached using simple mathematical models (Penning-Rowsell *et al.*, 2005), or macroscopic traffic models (Suarez *et al.*, 2005; Chang *et al.*, 2010). None of these methods consider the dynamics of the transportation system, rerouting whilst a street is closed, or the dynamics of the flooding event. These methods represent a static system, which uses homogeneous aggregated traffic flows. Currently, modelling and simulation tends to be focused on transport network scale analysis rather than small scale vehicle-water interactions.

All traffic models consist of two main components, traffic supply and traffic demand. Traffic supply describes the capacity of the infrastructure. Traffic demand represents the behaviour of consumers of transport services and facilities. The transport modelling simulates how these two components interact over time and space. With a microscopic modelling technique, the trips could be computed for both rail and road modes in the transport network. There are several reasons to adopt a micro-simulation technique for assessment the indirect impacts of flood. First, a micro-simulation technique facilitates a more detailed representation of the traffic processes. Second, microscopic transport modelling simulates every single vehicle in the transport system. Third, it is capable of modelling different transport modes and driving behaviours. Fourth, microscopic traffic models can simulate the dynamics of the flood propagation both spatially and temporally. Finally, a comprehensive representation of congestions and the intermodal description of different vehicle types could be achieved by microscopic traffic models (Pyatkova *et al.*, 2019).

Once the traffic model runs with the flooding information, the differences between the traffic model results under normal conditions and flooded conditions yield the actual flood impacts induced to road and rail networks. The flood impacts on the transport system could be expressed in speed, travel delays, additional travelled distance, additional fuel consumption, and additional noise emissions.

### 6.2.1 Building the road network

Every traffic simulation requires a road network. The application netconvert is used to create a network which can be used by the simulation software, SUMO (Krajzewicz *et al.*, 2012). Currently, the model uses the traffic network of the whole region of Santarem, Portugal. This network has been achieved from traffic authority of Portugal (IP) and later on modified for the applications in SUMO.

### 6.2.2 Generate the traffic

After having generated a network, it still needs some kind of description about the vehicles. This is called the *traffic demand*. Before starting to generate the traffic demand, one should take the following nomenclature in account: A "trip" is a vehicle movement from one place to another defined by the starting edge (street), the destination edge, and the departure time. A "route" is an expanded trip, which means that a route definition contains not only the first and the last edge, but all

edges the vehicle will pass. SUMO needs routes as input for vehicle movements. There are several ways to generate routes for SUMO. Since our available input data, from IP, is in the format of Origin-Destination-Matrices (or O/D matrices), they have to be converted to trips. Using a special command trip tables from O/D matrices could be computed. This command assumes the matrices to be coded as amounts of vehicles that drive from one district or traffic assignment zone (TAZ) to another within a certain time period. Since the generated trips must start and end at edges, a mapping of TAZ to edges would be required. After creating the TAZ files, it is time to assign the shortest or optimal path routing to establish a route between the origin and the destination of each trip.

### **6.2.3 Recognizing more critical scenarios**

Floodwater reduces speeds or stops entirely traffic flows according to the usability of assets. Disruption types (100% closed, 50% closed, reduced speed 50%, no freight, one lane closed, no disruption), relates usability of assets to safe driving speed. For the flooded scenarios, the network properties of a link are modified according to this relationship, and traffic parameters recalculated for this perturbed state. Subsequently, journey travel time will increase in comparison with the baseline scenario. The validation of the traffic model would be achieved by comparing the model results with IP's traffic model results. Due to the large number of scenarios, just critical ones with the most additional travel time for traffic flows could be validated by IP.

### **6.2.4 Road traffic model**

First of all, it is necessary to mention a tip regarding the road network of the pilot zone and that is the large number of one-directional roads that limits the options of rerouting, just because drivers may not be allowed to make a U-turn before the flooded section of a road. It is worth noting that since the road network and the attributes of the roads are necessary inputs for doing the simulation, the effect of the roads direction has been seen in the modelling.

After defining the road network, trip definition which is central to traffic demand modelling has been done. A trip is defined with beginning time, starting position (origin) and end position (destination). With a microscopic modelling technique, the trips must be computed for each vehicle in the network.

After the trips were defined, a route assignment model computed the most likely routes to connect origins and destinations. This model was represented by a stochastic user equilibrium and was run 20 times iteratively to minimize the cost function of travel time for each trip and each vehicle. Thus, the travel times of vehicles were computed as interacting participants of the travel system, rather than assuming they were travelling in isolation. The main hypothesis in this approach was that drivers have a perfect knowledge of the traffic system, which can be expected for commuter traffic.

### **6.2.5 Scenarios**

Broadly speaking, the exposed infrastructure assets can be identified by geographical coincidence of the hazard maps with road and railway networks. This

is a prerequisite to define the possible simultaneous failures and other combinations of failures in the network. As previously mentioned, this task was performed in SAFEWAY (2019a). Then, the processed traffic model is used as a tool to compare the base scenario, when all the network links are active and there is no flood disruption, with different disruption scenarios, when some network links are closed due to the flooding. For illustration purposes, one disruption scenario for light vehicles was simulated. The definition of this scenario was based on damage surveys from flood events occurring on the Santarém region, which were provided by the National Authority of Civil Protection<sup>4</sup> from Portugal. This disruption scenario is shown in Figure 59.

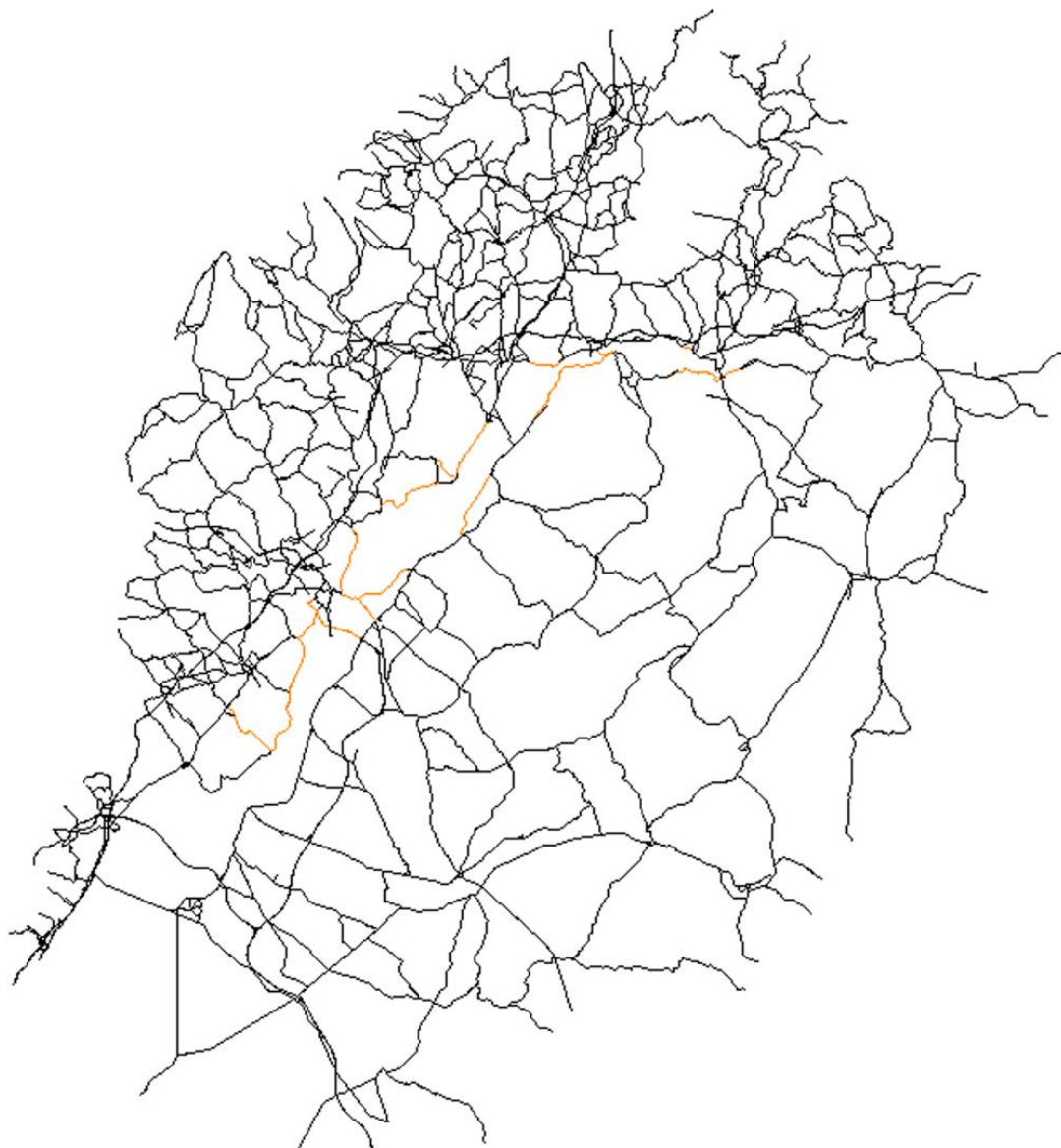


**Figure 59. Closed links at the proposed disruption scenario**

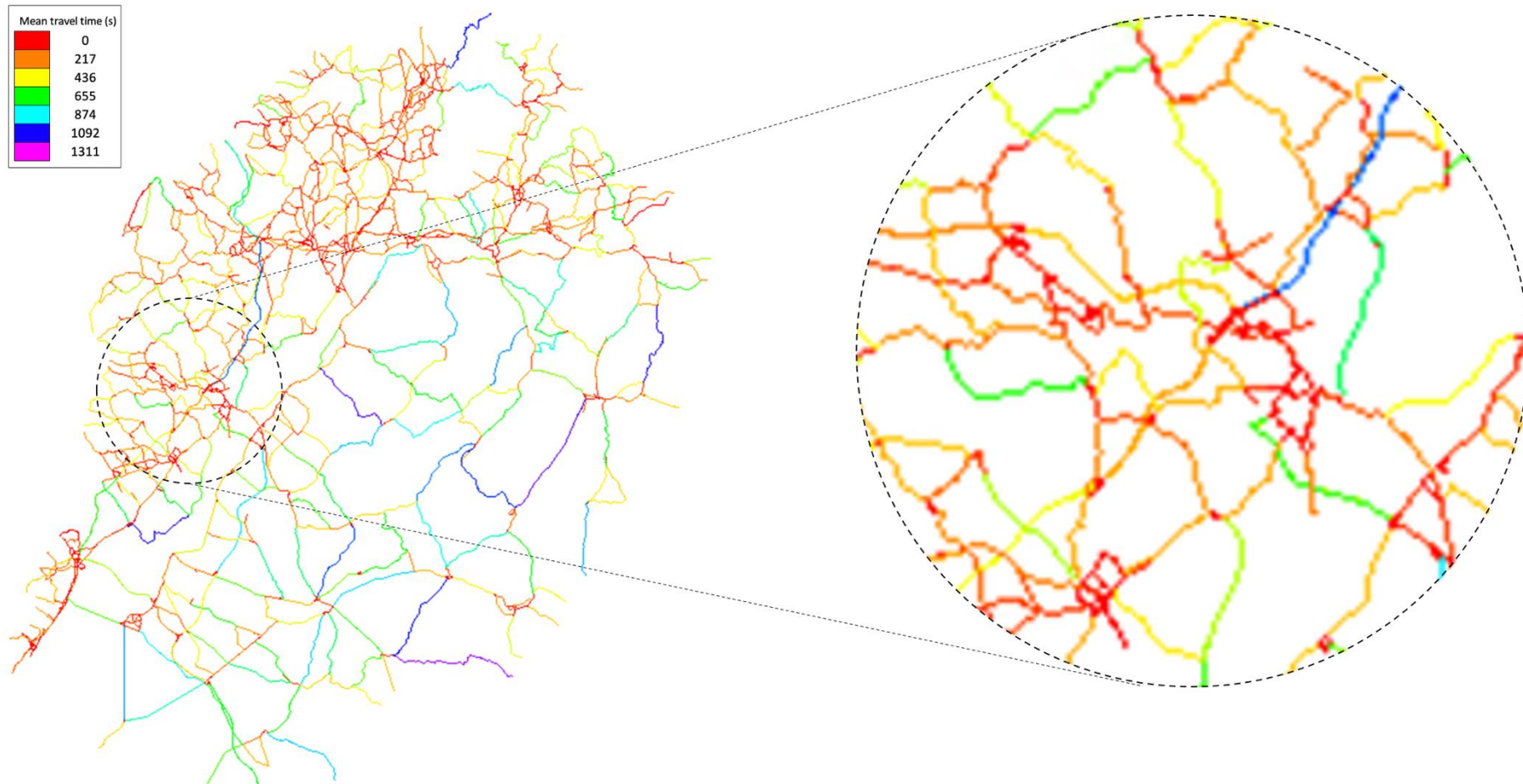
<sup>4</sup> <http://www.prociv.pt/>



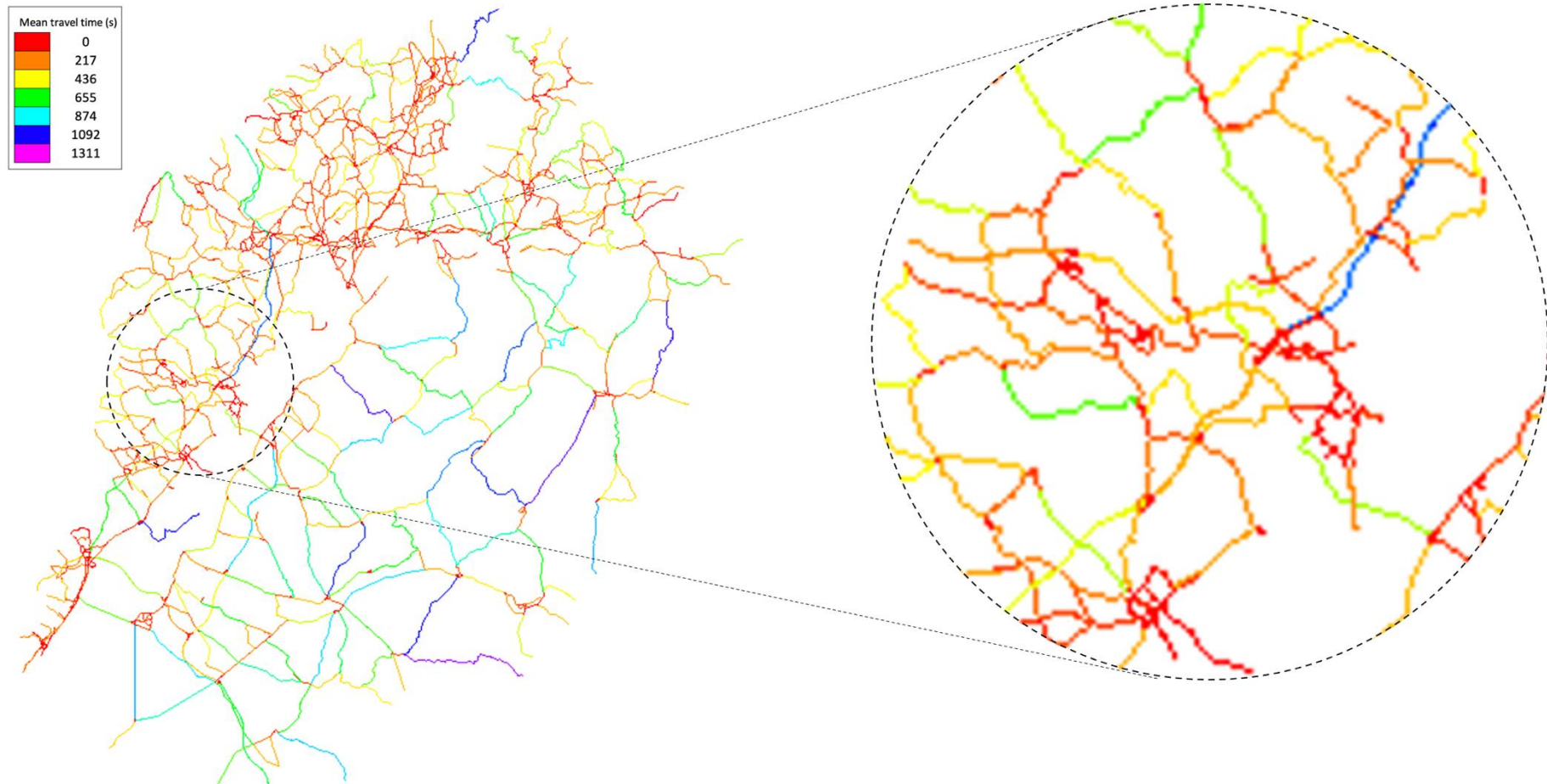
### 6.2.6 Results

Figure 60 and Figure 61 show the results for light vehicles travel time for each edge during a day. These figures are showing a pair maps of the average travel time for the normal and the flooded conditions. By comparing the colour of edges in these both maps, the edges with different travel time in different conditions can be recognised. The location of roads that received a travel time addition by flooding and closure of some edges, can be seen in the zoomed circular part. For example, the street in the upper part of the zoomed picture has been changed from yellow in the base scenario to the green in the flooded scenario which is showing the increasing of travel time in that street.

It should also be noted that these travel time values are equal to the time needed to pass the edge. Note that this is just an estimation based on the mean speed, not the exact time the vehicles needed. The mentioned mean speed is equal to the mean speed on the edge within the reported interval. Note that this is an average over time and space (space-mean-speed), rather than a local average over the vehicles (time-mean-speed). Since slow vehicles spend more time on the edge, they will have a proportionally bigger influence on average speed.



**Figure 60. Model results for edges average travel time during a weekday for light vehicles in base scenario**



**Figure 61. Model results for edges average travel time during a weekday for light vehicles in a flood disruption scenario**

### 6.3 Socioeconomic costs of roadway infrastructure disruptions

Rerouting will cause private and professional drivers to spend more time and travel longer to bypass the damaged area(s). This increases the time and operation costs of travel and external damage costs (noise, local air pollution, global emissions, road wear, queuing and accidents) associated with the increases in traffic flows. Goods will be delayed, causing problems to the supply chains up and down-stream.

Socioeconomic costs of roadway infrastructure disruptions involve:

1. Time costs (private and professional drivers, public transport users, costs of delays in delivery and/or reduced speed of delivery)
2. Fuel costs
3. Local air pollution: NO<sub>x</sub>, PM<sub>10</sub> (combustion and road wear, brakes and tire) and SO<sub>2</sub>
4. Global air pollution (costs per CO<sub>2</sub> ton-equivalents)
5. Noise
6. Road wear
7. Costs of accidents

Unit costs (last stage of Figure 62) differ between different areas and for different types of population, and local estimates will be preferred. Where these are not available from Portuguese infrastructure managers, estimates from international studies will be considered.

Building on recent work on marginal costs associated with surface transport, Rødseth *et al.* (2019) has recently undertaken a major project deriving the marginal external costs associated with road and rail traffic in Norway. This work implements the sequence of calculations according to stages in the effect chain (see Figure 62) (SFT, 2005). We provide a short description below for illustrative purposes. Note that this description is not complete since the calculations are built on many sub-studies.

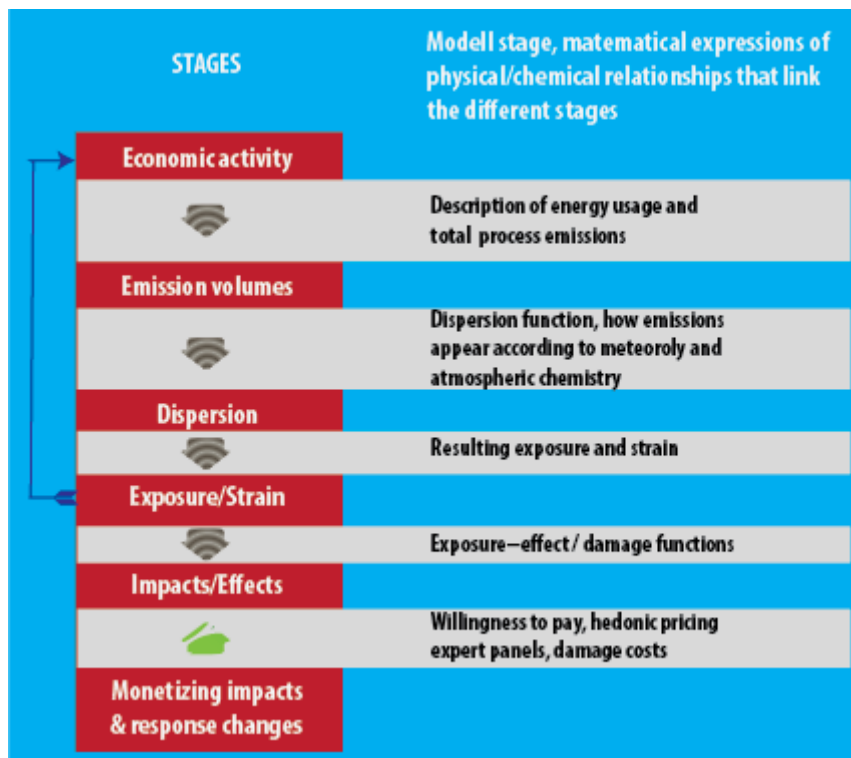


**Figure 62. Chain of effects used for calculating external costs in the Norwegian study (SFT, 2005)**

External costs of air pollution are based on the HRAPIE project - Health risks of air pollution in Europe (WHO, 2013), complemented with findings from previous Norwegian projects (Rosendahl, 2000).

A matrix of road types, vehicle types, and speed distributions are used to calculate emissions from road traffic and marginal changes in emissions given an extra vehicle (Holmgren and Fedoryshyn, 2015). The Handbook Emission Factors for Road Transport (HBEFA) provides emission factors according to fuel type, vehicle class, speed, and other parameters (see [www.hbefa.net](http://www.hbefa.net)). Particles are produced as part of the combustion processes, but are also the product of road-wear, tire particles, and debris from brakes.

The relationships between the emissions on the road network in major cities have been linked to the measured concentrations of NO<sub>2</sub>, PM<sub>10</sub> from combustion, and PM<sub>10</sub> from road dust particles. It is thereby possible to link emission changes to changes in population exposure.

The consequences of changes in the exposure to pollution in the form of particles PM<sub>10</sub> are split into short-term (acute) and long-term consequences. Acute impacts encompass premature deaths, hospitalization, upper and lower respiratory tract diseases by children, days with activity limitations. Chronic impacts are in the form of premature deaths due to lung and heart myocardial diseases, premature deaths due to lung cancer, children bronchitis, adult chronic obstructive pulmonary disease (COPD). The different endpoints are given as changes in hospital days, number of persons affected, increased exposure and the costs of these changes are applied given the number of people that are affected.



Nitrogen oxides are produced during the combustion processes. Depending on the ozone levels there are atmospheric-chemical processes depending on sunlight convert  $\text{NO}_2$  to  $\text{NO}_x$  and vice versa. Chronic effects of  $\text{NO}_2$  are premature deaths due to myocardial infarction and lung-diseases, children developing bronchitis. Acute effects are the number of people dying one year too early, number of hospital days, and an increase in the number of people highly annoyed by air pollution emissions (Amundsen, Klæboe and Fyhri, 2008; Klæboe, Amundsen and Fyhri, 2008).

$\text{CO}_2$  costs are built upon IPCC calculations of future costs depending on the chosen ambition to limit the temperature increase, which at the moment is 1.5 degrees according to the Paris agreement (IPCC, 2013).

Accident costs are based on a methodology by Lindberg (2005). Therein the number of accidents and the consequences are related to the traffic volumes. In situations with more than one transport mode, the costs are allocated according to responsibility for the accident.

External noise costs are based on very recent estimates of the health consequences from WHO (Guski, Schreckenber and Schuemer, 2017; Basner and McGuire, 2018; Van Kempen *et al.*, 2018) with exposure effect calculations also from Miedema and Oudshoorn (2001). The costs are calculated based on the number of people who become highly annoyed, are highly sleep disturbed and are at increased risk for myocardial infarction. In addition, there is a cost associated with life quality impacts of those who are moderately annoyed and subject to noise disturbances and restrict behaviours due to noise, but do not fall under the category of being highly annoyed. The life-quality reduction costs are based on willingness to pay. These costs are calculated in DALY (disability adjusted life years) and converted to monetary values. The Norwegian estimates build on detailed information on vehicle composition, day, evening, and night-time traffic flows, and affected populations in each time period from Norwegian transport authorities as well as knowledge about the proportion of the Norwegian population in different age groups who are disabled or die from myocardial heart disorders.

#### **6.4 Socioeconomic costs of railway infrastructure disruptions**

With respect to external cost the effect chain method is applied (Figure 62). The mix of locomotives and number of daily wagon-km for different stretches was used as input in the Norwegian work (Rødseth *et al.*, 2019).

With respect to passenger services, time costs for public rail transport users can be used to assess the cost of delays. This is often split between commuting trips, and leisure trips.

For goods, the cost of delays will depend on the type of goods (Ludvigsen *et al.*, 2012) and the consequences up and down-stream along the supply and demand chains.

It should be also considered that rerouting possibilities for goods transported by rail may be limited, necessitating transfer of goods from rail to road.

#### **6.4.1 Goods characteristics**

Some goods deteriorate as regards the value at destination if their transit time exceeds certain time limits. This pertains to perishable goods with shelf-time of only few days or hours whose utility may suffer from delivery tardiness. Some other goods such as fresh food and drinks may deteriorate in terms of “looks” if they stay longer in transit. Finally, some solid, powder and fluid chemicals carried in tankers may “settle” and/or change consistency after prolonged transit. Still some other materials can become hazardous due to chemical reactions released by longer time lapses between departures and arrivals and/or motions under transit. Still some other types of liquids may solidify in tank containers making discharge more difficult and/or expensive. In addition, some other types of cargo such as newspapers lose their inherent value composed of time-constrained information newness. As reported later, cargo’s consistency can also change as a consequence of longer than allowed exposure to adverse atmospheric conditions such as very low or high temperatures.

#### **6.4.2 Just-in-time delivery requirements**

Transport operators who deliver goods under just-in-time quality regime do typically carry components to manufacturing or assembly plants or materials needed for processing industries. In some cases, these operations may need time-precise deliveries of several loads per day. Since the continuity of these production processes can easily be jeopardised in the event of late arrivals, delivery times of just-in-time consignments are usually very precisely specified. Disruptions of flow movements with the consequent arrival delays impose thus legal and financial penalties on transport operators, consignors and manufacturers. Some high-value retailers which deal with medical and/or healthcare articles usually require just-in time delivery not only because of the risks of material decay or utility spoilage, but because of high costs of inventory and low stocks held at medical depots.

#### **6.4.3 Quick response demands**

Transport operators who handle deliveries of food, drinks or other high-value manufactured goods into retail trade segments often operate on orders from:

- Manufacturers or other suppliers delivering directly to individual retail outlets
- Manufacturers or other suppliers delivering into regional delivery centres (RDCs). Some of these “Quick response” deliveries of goods with little or no inventory stock are also being held by secondary distribution outlets and retailers.
- Logistics operators working under dedicated contracts for major retailers responsible for deliveries of consolidated loads from RDCs to individual retailer outlets
- Logistics operators contractually hired by shipping lines to perform overland transfer of large volumes of overseas and/or international cargo between European gateway ports and national and/or regional distribution hubs.



Since all four types of delivery are very time sensitive, retail deliveries to RDCs are often “booked in” for unloading at an agreed time. Extreme time sensitivity allows only for small windows of variability to be built around the booked supply time with high statutory penalties for late arrivals. In this context, lengthy supply time disruptions caused by weather hazards disintegrate the entire pipeline inventory and may disturb stock availability at, at least, two upstream supply chain echelons: wholesalers and retailers.

Another case where the supply network disruption may be quite critical arises from quite a common practice where consignor sends very late notice of the precise content of orders. For example, a retailer may transmit the order electronically at midnight, for delivery at RDC by mid-morning. In such cases the time available to a supplier to undertake order processing, picking of goods, checking loading, documentation and dispatch may be very tight, placing considerable strain on warehousing and transport operations. Again, abrupt punctuation of material flow between manufacturing plant and/or warehouse and a RDC may result in stock out and/or production downtime.

#### **6.4.4 Future Economic calculations**

Given a project horizon of 2020-2100, current unit values need to be adjusted according to future values of time, future energy costs and future energy efficiency of the vehicles and vehicle fleet mix. European Commission (EC) has a policy of phasing out fossil fuel vehicles from 2030. Given a higher percentage of Electric and Hybrid technologies, local air pollution from combustion will be reduced, while dust emissions from road wear, tires and brake pads, and noise (mainly from tires) is expected to be much the same. There may be regional differences in the speed with which new technologies are adopted and the phasing out older generation vehicles.

There are currently no reliable predictions of how vehicle fleet composition will change over time, so simplifying assumptions need to be made. Given the project’s strategic focus and the uncertainty of exactly when one or more flooding events will occur in the future, it is the trend of how the disruption costs will change in the future that is important and the most likely future costs.

### **6.5 Dynamic Economic Calculation Tool**

When deciding on resilience enhancement policies, the certain cost of the proposed investments, future upkeep and periodic maintenance must be balanced against the possible but uncertain benefits of avoiding or reducing the socio-economic impacts of one or more future natural or man-made hazard events.

This balancing is difficult since there are many uncertainties with respect to the sizes of the future costs and benefits, the efficacy of the implemented measures, changes in future prices, the valuation of future benefits, contextual factors, and the size of the population and values of future affected assets at the time the hazard occurs.

In the HOSANNA project (<http://greener-cities.eu>) a dynamic calculation tool for estimating the costs and benefits used Monte Carlo simulations to visualize the confidence bands of economic indicators given the many input and outcome

uncertainties. By applying uncertainty functions, an additional benefit is that when updated estimates of future costs and benefits do not deviate too much from the values used for the calculations, it is not necessary to rerun the analyses, since this type of deviations are already incorporated in the uncertainties. The calculations become more robust.

However, the tool used in Hosanna only dealt with fixed alternatives and did not contain any method for dealing with uncertain future events. The tool was also built using software tools that were modern and innovative at that time but are abandoned and/or obsolete up to date.

In SAFEWAY, the Hosanna tool for Monte Carlo simulations to undertake economic analyses taking into account the uncertainties of inputs and outputs has been simplified, modernized and augmented with a stochastic module. In the stochastic module the occurrence of future natural hazard and man-made hazard events are simulated, and the economic analyses performed depending on the simulated occurrences of the stochastic events. By repeating the analyses 1000 or more times, it is possible to visualize the expected mean economic results, and their confidence bands.

## 6.6 Number of 100-year floods between 2021-2100

Even in the simplest case where the chance of a 100-year flooding event is constant (1% per year), running 10000 simulations illustrates that the number of floods in the period from 2021 to 2100 varies as described by a Poisson process:

$$P(X = x) = \frac{e^{-\mu} \mu^x}{x!} \quad x \geq 0 \quad (36)$$

Since we have 79 years with probability 1/100 the parameter  $\mu$  becomes 0.79 and the expected number of floods in the 79-year period also 0.79.

The simulations show that in about 46 % of the runs there are no floods, and consequently no benefits of any investment. In 36 % of the cases there are a single 100-year flooding, in 14% there are two floods, while in 3.7 % we have three floods and in somewhat less than 1% of the cases do we have as many as four 100-year floods within the 69-year period.

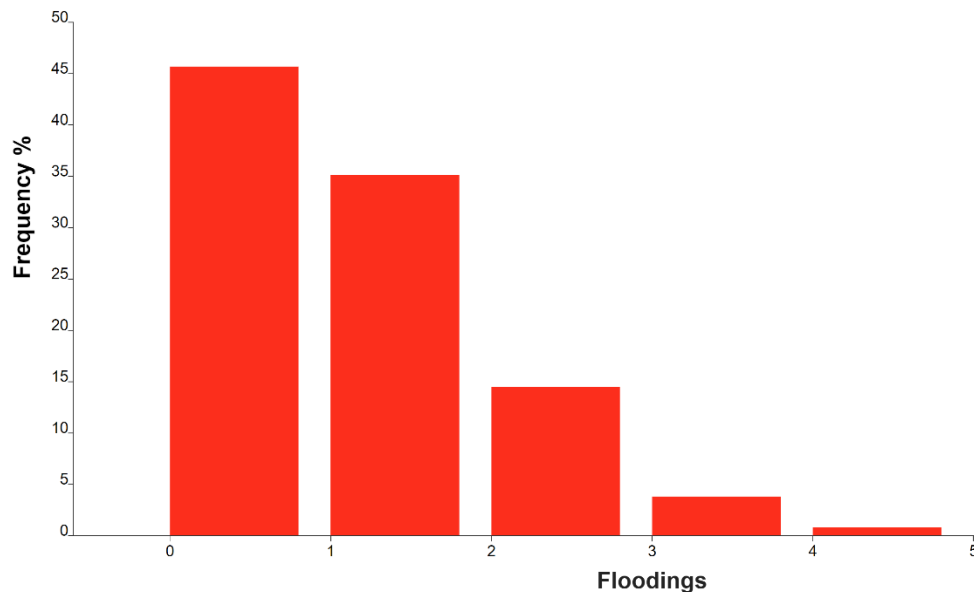


**Figure 63. Number of 100-year floods within the period [2021-2100]. Results from 10000 simulations.**

Not only does the number of floods vary, but also exactly when in the 79-year period they occur. The timing of each event is important for the socio-economic analyses of costs and benefits. Distant future costs and values are discounted more heavily than costs that are immediate or close in time. With a discount rate of 6% the present value of 1€ that occurs 40 years in the future (2060) is less than 0.10€, since 40 years of discounting results in a present value that is 9.7% of the future cost or benefit:

$$PV = \frac{1}{(1 + 6\%)^{40}} = 9.7\% \quad (37)$$

When the consequences are of the same size each year in the future, it is not too difficult to calculate the average present value. However, the size of the future damages is not constant but affected by the efficacy of resilience measures, and the accumulated benefits of resilience policies, or – if no policies are in place –, the accumulated adverse consequences of neglecting necessary upkeep and maintenance. The socio-economic consequences also depend on the location and size of the future population, land use, built up areas and asset values at the time of occurrence as well as contextual factors. Consequently, a more sophisticated approach is needed.

## 6.7 SAFEWAY enhancement for analysing resilience policies

By developing and implementing a SAFEWAY enhancement of the HOSANNA approach, future stochastic events are taken into account allowing us to perform economic analyses of the costs and benefits of measures that prevent, reduce or mitigate the impacts of future floods causing infrastructure damages, disruption or service degradations (slower speed, detours, bottlenecks, delays).

---

The tool achieves this by running the Monto Carlo simulations in two steps. In the first step the occurrences of single or multiple discrete events are triggered for each consecutive year according to one or more discrete probability distributions where the parameters may increase or decrease over time.

These distributions may be derived from the previous modelling of infrastructure damages based on climate change, precipitation, hydrological modelling, and fragility curves of the assets that are affected and/or other approaches.

Given the simulated occurrences of one or more future hazards, the second step simulates the compound impacts of the uncertainties of the different input and outcome factors on the resulting economic decision support indicators.

## 7. Projections of long-term consequences

According to the reports of the Intergovernmental Panel on Climate Change, IPCC, the increasing sea surface temperature has a significant effect on the rainfall, which is expected to increase at global scale (IPCC, 2013). Nevertheless, decreasing trends in rainfall are also expected at regional and local scales, such as in the case of the Iberian Peninsula (Portela, Espinosa and Zelenakova, 2020). However, rainfall amounts are projected to become more clustered into extreme rainfall events, and therefore extreme runoff indicators such as the 100-year daily peak flow will probably increase in basins such as Tagus (Alfieri *et al.*, 2015).

In this chapter, the projection of future hazards for the pilot area, as well as the situation and conditions of the population affected by these future occurrences, are investigated in order to analyse the long-term impacts.

### 7.1 Dispersion of future hazards

There are two different main strategies for assessment of future hazard with respect to climate change:

- Modification of the already produced hotspots maps in WP2 (reported in SAFEWAY (2019a) by making considerations about change in the return periods due to climate change.
- Overlay of future hazard maps (including effect of climate change, projected at 30- and 50-years timespan), with the locations of the infrastructure. Within this alternative, it is common to also develop and present maps that express the change in the spatial distribution of the hazard as well as exposure to the hazard.

#### 7.1.1 Change in return period of hazards due to climate change

Predictions of the change in spatial and temporal characteristic of a hazard due to climate change involve significant uncertainties. The uncertainties in climate projections are related to 1) uncertainty in future anthropogenic emissions, 2) natural climate variations, and 3) climate models. The first type of uncertainty is usually taken into account by using 2 or 3 emission scenarios. An emission scenario is typically characterised by Representative Concentration Pathway (RCP), which is a greenhouse gas concentration (not emissions) trajectory adopted by the IPCC. The pathways describe different climate futures, all of which are considered possible depending on the volume of greenhouse gases (GHG) emitted in the years to come. Four pathways – labelled RCP2.6, RCP4.5, RCP6, and RCP8.5 – were used for climate modelling and research in the IPCC Fifth Assessment Report (AR5) in 2013 (IPCC, 2013). The RCPs are labelled after a possible range of radiative forcing values in the year 2100 (e.g. RCP8.5 means a radiative forcing value of 8.5 W/m<sup>2</sup>). In most climate change impact studies since the publication of AR5, the RCP8.5 scenario is considered as the base case.

The second and third types of uncertainties are to some degree taken into account by giving prediction intervals for the metric of interest (e.g. average temperature in summer months, average annual precipitation, etc.) based on ensembles of

several model calculations. The climate change models are steadily being improved, but for some metrics, there is still a wide range of varying predictions from different models. One should also keep in mind that uncertainties mentioned above, span only a part of the total uncertainty when it comes to predicting the climate change impact.

Because of all these uncertainties, it is challenging to develop reliable hazard maps that are valid in say 50 or 100 years from now. A simplified approach that is examined in this section attempts to use the hazard maps developed for different return periods for a give hazard based on today's conditions but revise the return period such that they reflect the impact of climate change.

We start off with an example related to hazard maps for flooding. Climate change will affect high and low flows of large rivers around the globe. To what extent extreme flows will change differs from one region to another. The website (<https://www.climatechangepost.com/>) cites the paper by Blöschl *et al.* (2019), which concludes that the annual maximum river flow is changing across Europe, probably due to climate change. According to that study, increasing autumn and winter rainfall has resulted in increasing floods in north-western Europe; while decreasing precipitation and increasing evaporation have led to decreasing floods in southern Europe; and decreasing snow cover and snowmelt, resulting from warmer temperatures, have led to decreasing floods in eastern Europe.

In small catchments in southern Europe, however, local short-duration convective storms with high intensities are more relevant for flood generation than the long-duration storms that produce floods in medium and large catchments. These local convective storms are expected to increase in a warmer climate, which means that floods in small catchments may have actually increased in southern Europe despite the decreased annual precipitation.

The flood changes that have been identified are broadly consistent with climate model projections for future decades, suggesting that climate-driven changes are already happening. The observed trends for mean annual flood discharge may reflect changes in more extreme floods as well, such as the 100-year flood discharge, which is often the key design criterion in flood risk management.

In study of climate change impacts in Norway, Norwegian Centre for Climate Services (NCCS) assessed the future changes in flood magnitudes (the mean, 200- and 1000-year flood) for 115 catchments using RCM simulations, a catchment-based hydrological model and an extreme value analysis of the simulated discharge. Changes in the 200-year flood between a reference period, 1971-2000 and a future period, 2071-2100 are illustrated in Figure 64 (NCCS, 2017). There are large regional differences in the projected changes across Norway, with median ensemble projections ranging from -44% to +56% for the daily-averaged flood magnitude.

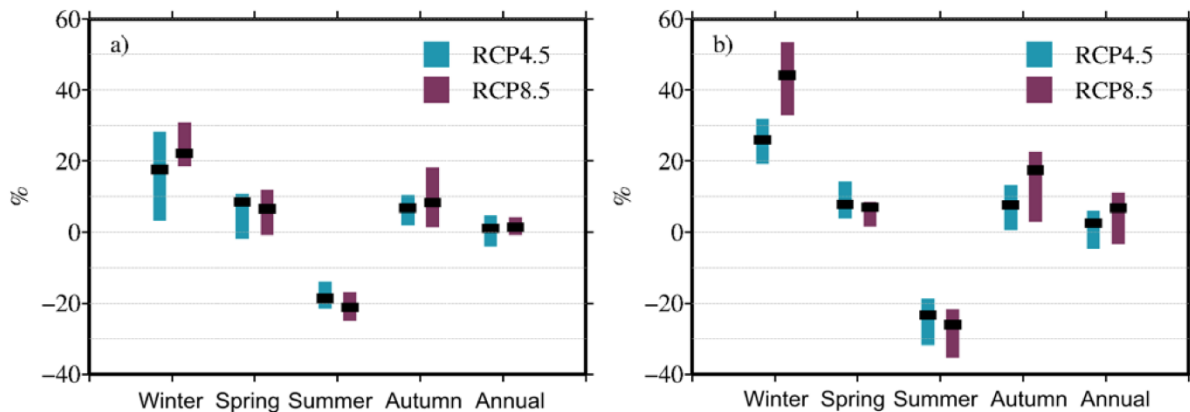


**Figure 64. Relative changes (%) in seasonal and annual runoff for Norway from 1971-2000 to a) 2031-2060 and b) 2071-2100 for emission scenarios RCP4.5 (blue) and RCP8.5 (red). Median projections are marked as a black solid line, while low and high projections are marked by the lower and upper ends of the boxes (NCCS, 2017).**

Using the observed and projected changes as related to flood generating processes in different regions and catchment types in Norway, (NCCS, 2017) recommended three “climate factor” categories for different catchments in Norway:

- 0 % for large rivers where snowmelt is the dominating flood generating process in today’s climate. This implies that design flood estimates can be based on up-to-date river flow observations.
- 20% or 40 % increase in the design flood estimates in all rivers dominated by rain floods and in small rivers responding quickly to heavy rain events. This implies adding 20% or 40% to the estimated design flood discharge (200- and 1000-year flood).

The type of recommendations given about are typical for climate change impact reports. These reports make predictions of relative change in seasonal and annual runoff (e.g. Figure 64) or make statements such as "the 100-year flood today is expected to happen once every 20 years in 2070-2100". To translate such statements into return period for flood hazard maps, one can assume a Gumbel distribution for the maximum annual flood in a region. The Gumbel distribution (Generalized Extreme Value Distribution Type-I) is often used to model the distribution of the maximum (or the minimum) of a number of samples of various distributions, for example the distribution of the maximum level of a river in a particular year. It is useful in predicting the probability that an extreme earthquake, flood or other natural event will occur. The cumulative distribution function for the Gumbel distribution is defined by:

$$F(x) = e^{-e^{(x-\mu)/\beta}} \quad (38)$$

where  $\mu$  is the location parameter and  $\beta$  is the scale parameter. The expected value of  $x$  is  $E(x) = \mu + \gamma \cdot \beta$  where  $\gamma$  is the Euler-Mascheroni constant ( $\gamma \approx 0.5772$ ) and the standard deviation of  $x$  is  $\sigma_x = \beta \cdot \frac{\pi}{\sqrt{6}} \Rightarrow \beta \approx 0.78\sigma_x$ .



Assuming that the annual maximum flood has a Gumbel distribution, the return period of flood of intensity "x" corresponds to  $1/[1 - F(x)]$ , where  $F(x)$  is calculated from Equation (38). Assuming further that the coefficient of variation (COV, defined as standard deviation divided by mean value) of the Gumbel distribution does not change in the future climate regime, one could derive the conversion factors listed in Table 33 for typical return periods of flood hazard maps. One could also translate statements such as "the 100-year flood today is expected to happen once every 20 years in 2070-2100" into the relative increase in the annual maximum flood intensity, as shown in Table 34.

**Table 33. Changes in return period for hazard maps due to climate change impact.**

| Increase/decrease in maximum annual flood due to climate change | Return period for present day hazard map (years) | Equivalent future return period for the same hazard map (years) |
|---|--|---|
| 10%   | 100  | 55  |
|   | 200  | 95  |
|   | 1000   | 330   |
| 30%   | 100  | 25  |
|   | 200  | 37  |
|   | 1000   | 83  |
| 50%   | 100  | 16  |
|   | 200  | 21  |
|   | 1000   | 38  |
| -10%  | 50   | 95  |
|   | 100  | 235   |
|   | 200  | 590   |
| -30%  | 50   | 1120  |
|   | 100  | 7050  |

**Table 34. Changes in return period for hazard maps due to climate change impact.**

| Return period for present day situation (years) | Return period for the same flood in a future climate regime (years) | Increase/decrease in maximum annual flood due to climate change |
|---|---|---|
| 100   | 20  | 39%   |
|   | 50  | 12%   |
|   | 500   | -16%  |

Compared to floods, assessing the impact on climate change on forest fires is much more challenging and uncertain. Large wildfires, with burned areas > 500 hectares, can be characterized by the climate and weather conditions that cause them. Climatic conditions over a time scale of seasons to years determine the amount of fuel that feed these fires. Weather conditions in the days or weeks prior to the onset of a fire change the fuel moisture state of especially the fine fuel and litter, and hence their flammability. On a shorter time scale, hourly and daily meteorological variables control fire ignition and propagation.

The number of wildfires in recent years has been particularly large in central and northern Portugal and in north-western Spain. However, in previous decades, burnt area has been decreasing in Spain and central Portugal (<https://www.climatechangepost.com/>). Only in northern Portugal burnt area has been increasing. What is different in northern Portugal? According to references cited in [climatechangepost.com](https://www.climatechangepost.com/), the answer is not related to climatic conditions. In the Mediterranean, the dynamics of fire regimes is driven mainly by human factors, such as changes in land cover, population, and fire management practices.

With the present state of knowledge and considering all the uncertainties involved in predicting forest fires, it is not possible to isolate the impact of climate change on forest fire hazard from all other drivers of this hazard.

### **7.1.2 Identification and review of hazard maps including climate change projections**

A review of hazard maps including climate change was conducted. In particular, the search was directed towards downloadable data at European level that can be opened in a GIS environment. Data from the RAIN project and the INTACT project were found particularly relevant in this context.

**The RAIN project** (Risk Analysis of Infrastructure Networks in response to extreme weather, <http://rain-project.eu/>) was funded in the EU programme FP7-SECURITY - Specific Programme "Cooperation": Security. The topic was SEC-2013.2.1-2 - Impact of extreme weather on critical infrastructure – Capability Project. The main aim of the project was to provide a framework for the identification of critical infrastructure assets impacted by extreme weather events and to propose a solution to minimise the impacts. The project also dealt with the influence of climate change in the frequency and intensity of different natural

hazards: windstorms and heavy precipitation, winter weather and forest fires, and coastal and river floods. The RAIN project report D2.5-"*Present and future probability of meteorological and hydrological hazards in Europe*" ([http://rain-project.eu/wp-content/uploads/2016/09/D2.5\\_REPORT\\_final.pdf](http://rain-project.eu/wp-content/uploads/2016/09/D2.5_REPORT_final.pdf)) presents analyses on the probability of hydro-meteorological hazard occurrence. Projections of changes have been carried out considering two climate scenarios (RCP 4.5 and RCP 8.5). These two scenarios correspond to those adopted by the Intergovernmental Panel on Climate Change in its 5th fifth Assessment Report (AR5). Two forecasted time 2021 - 2050 and 2071- 2100, were compared to simulations of the past period 1971-2000 for the two emission scenarios RCP 4.5 and RCP 8.5. The analyses have been based on datasets of observations, atmospheric reanalyses and regional climate models, although several other datasets were used for analyses of floods. Pan-European gridded data sets of the probability of occurrence of river floods, coastal floods, heavy precipitation, windstorms, heavy snowfall, blizzards, crown snow load, freezing rain, forest fires, thunderstorms, hailstorms, tornadoes and convective wind gusts under present and future climate are available as gridded databases at this link: <https://data.4tu.nl/repository/collection:ab70dbf9-ac4f-40a7-9859-9552d38fdccd>

**The INTACT project** "On the Impact of Extreme Weather on Critical Infrastructures" has received funding from the European Union Seventh Framework Programme (FP7/2007-2013) under grant agreement n° FP7-SEC-2013-1-606799. The topic was SEC-2013.2.1-2 - Impact of extreme weather on critical infrastructure – Capability Project. The project dealt with the resilience of critical infrastructures (CI) to Extreme Weather Events (EWE), such as heat waves, hurricanes, flooding and droughts. The main aim of INTACT was to reduce the risks caused by extreme weather by providing information, methods, tools and examples of good practices to support governments and managers of critical infrastructures. The project evaluated the hazard changes due to climate change in the following decades. Work Package 2 of INTACT aimed to identify and define appropriate Extreme Weather Indicators (EWIs) to characterise the relevant meteorological critical factors for analysing present and future climate projections.

The INTACT project was focusing specifically on four types of extreme weather:

- Temperature extreme
- Precipitation extreme (also including snowfall)
- Wind extreme
- Complex extreme (including 2 different parameters among temperature, precipitation and wind)
  - o Combined temperature and precipitation extreme
  - o Combined temperature and humidity extreme

Most of the Extreme Weather Indicators considered in INTACT were defined following the recommendations of the CCI/CLIVAR/JCOMM Expert Team on Climate Change Detection and Indices (ETCCDI).

### 7.1.3 Future exposure of transportation system

Hotspot-maps for future hazards in Portugal considering wildfires and floods have been produced considering the gridded database, for future climate, developed in the RAIN project (see section 7.1.2). For the area of analysis, the location of different road and railway assets has been provided by IP. This information has been overlapped with road and railway shapefiles (from OSM database) and gridded data sets of the probability of occurrence of river floods in future climate (from RAIN database). This database contains the information on the water depth in metres for a flood event with a return period of 10-, 30-, 100-, 300-, and 1000-years, for 100 m resolution. The simulations obtained for two future time periods (2021 - 2050 and 2071- 2100) have been compared to the ones obtained for the past period 1971-2000. The IPCC emission scenario RCP 8.5 was considered. The increment of the flood water depth compared to the past, has been calculated for three return periods: 10-, 100-, and 1000-years. Figure 65 and Figure 66 show the water depth increment for the long-term period (2071-2100) in the scenario RCP 8.5, respectively for road and railway assets. The map shows the influence of climate change in the intensity of river floods and highlights the different assets that may be potentially exposed in the future. A complete catalogue is presented in SAFEWAY (2019a).

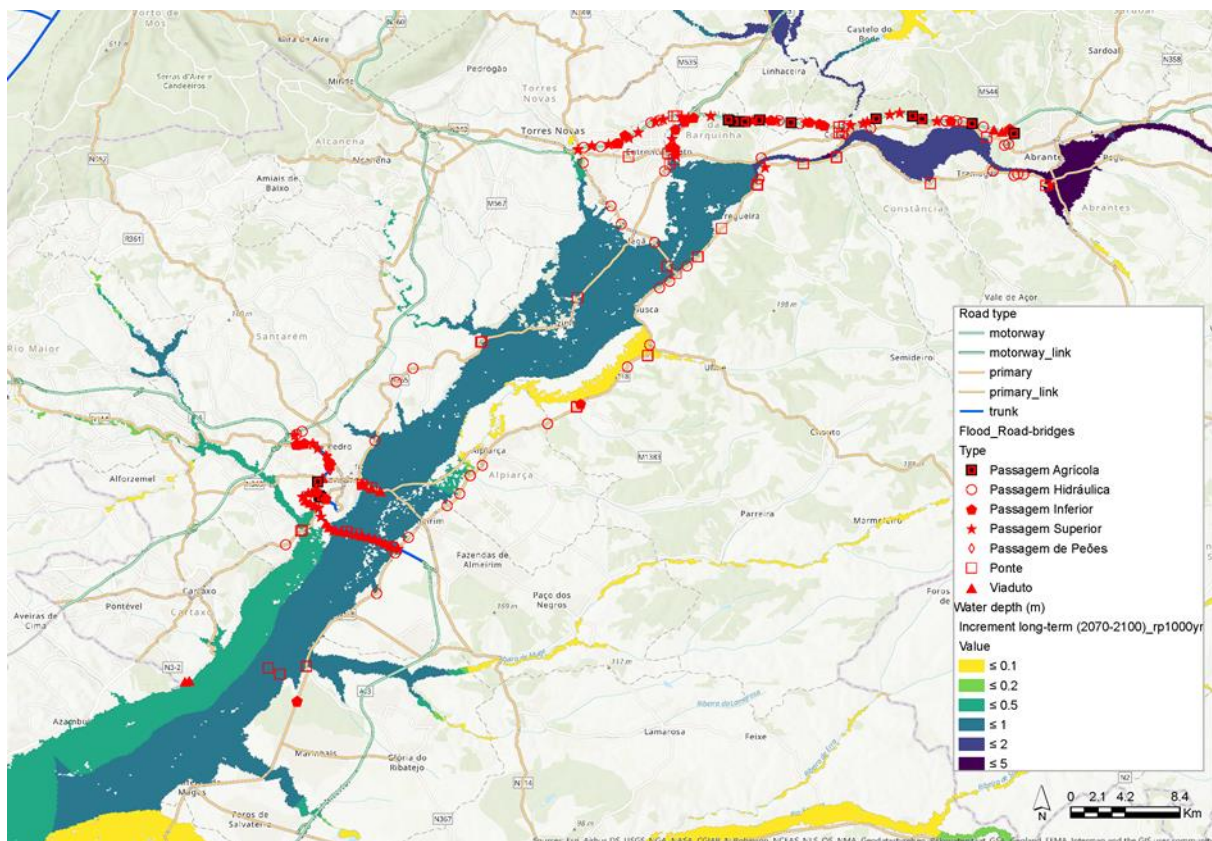


**Figure 65. Changes in flood pattern due to climate change. Hot-spot map for road assets considering the water depth increment in a long-term period (2071-2100) in a scenario RCP 8.5 for a flood return period of 1000 year.**



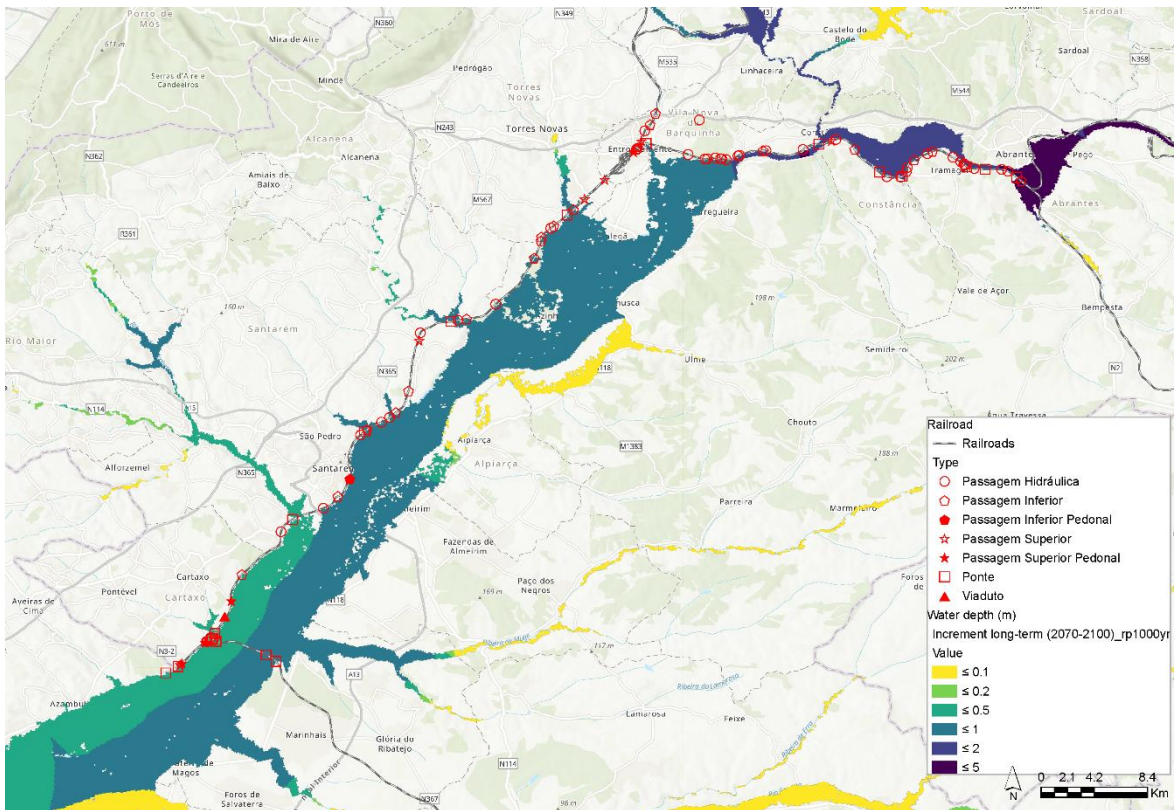


**Figure 66. Changes in flood pattern due to climate change. Hot-spot map for railway assets considering the water depth increment in a long-term period (2071-2100) in a scenario RCP 8.5 for a flood return period of 1000 year.**

The D2.5 report from the RAIN project highlights the influence of climate change in the frequency of future forest fires as well. A general increase of forest fires will be observed due to the raise of summertime temperatures, especially in Mediterranean areas (Mouillot, Rambal and Joffre, 2002; Bedia *et al.*, 2014), with the RCP 8.5 scenario. The Canadian Fire Weather Index, FWI (Van Wagner, Forest and others, 1987) has been considered to assess the future probability of forest fire. This index is composed by six components describing moisture of organic layers at different depths and predicting the rate of fire spread and the frontal fire intensity. Two thresholds,  $FWI > 20$  and  $FWI > 45$ , have been considered, respectively, for cool climate regionals and Mediterranean regions (Moriondo *et al.*, 2006). The difference between the daily probability of FWI exceedance in future climate 2071-2100 and past reference period 1971-2000, have been calculated with the purpose of providing the exceedance variation probability. This obtained database has been overlapped with road and railway tracks (from OSM) in Portugal. The threshold  $FWI > 45$  has been considered in this case. Figure 67 provides an example of the exceedance probability variation of the  $FWI > 45$  in the future climate period 2071-2100 in Portugal (between Coimbra and Leiria provinces) in the RCP 8.5 scenario.

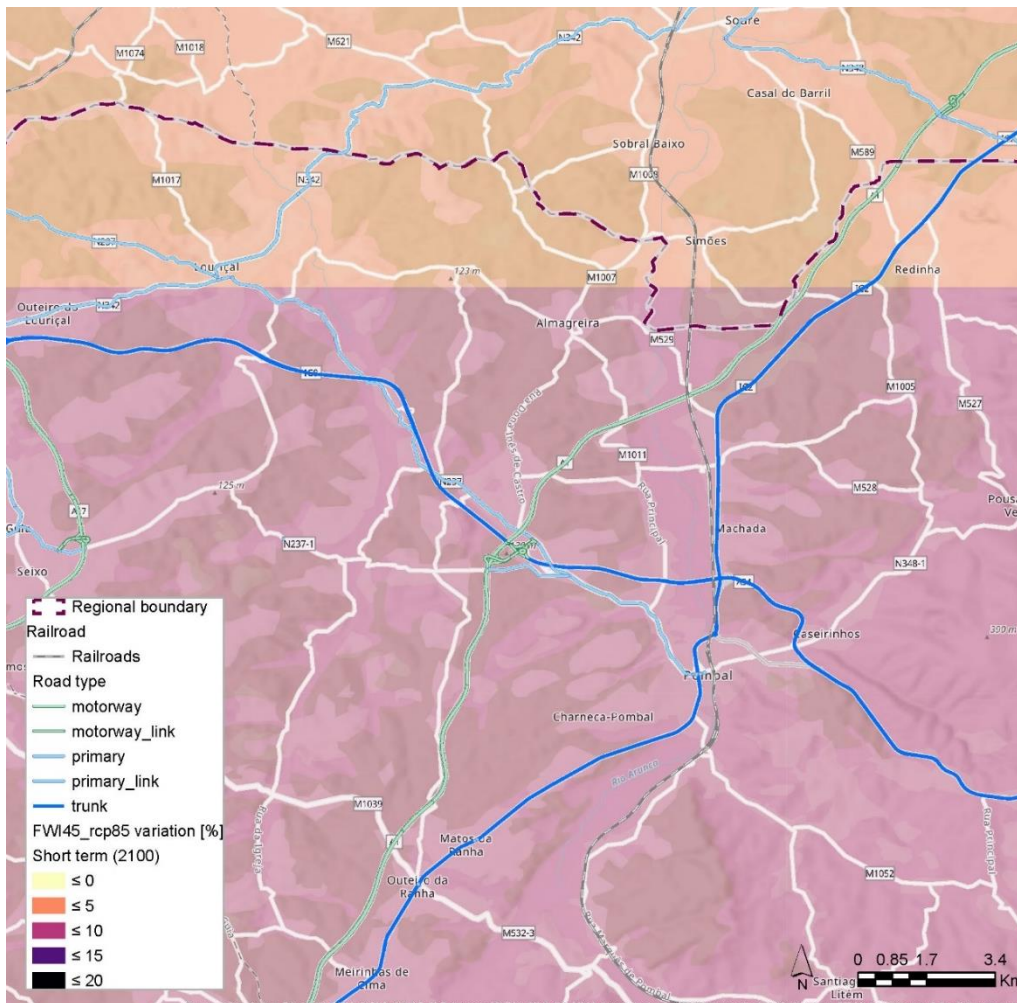


**Figure 67. The exceedance probability variation of the FWI>45 in the future climate period 2071-2100 in Portugal, between Coimbra and Leiria provinces, compared to the past period 1971-2000.**

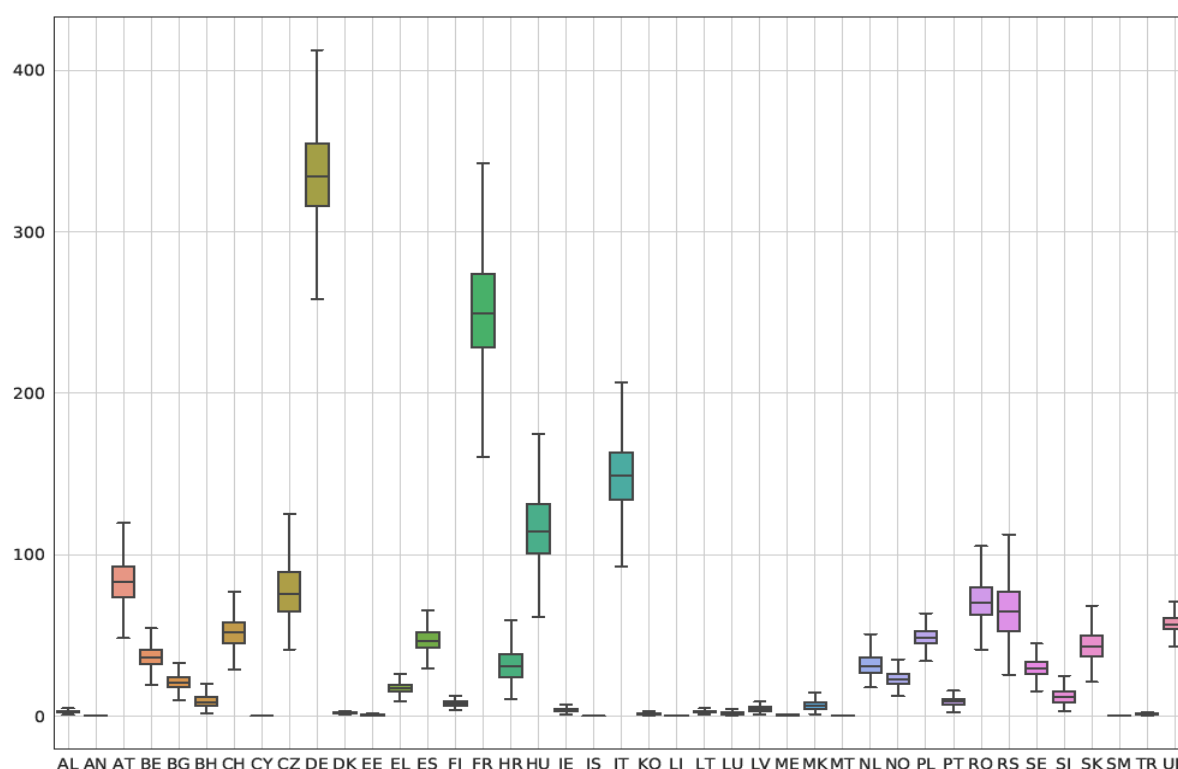
#### **7.1.4 Modelling of direct flood damage in future climate**

The assessment of direct losses has been evaluated also considering a future scenario (in addition to the assessment presented in Section 5.2). Floods maps for 10, 100, 500-year return periods for the RCP 8.5 scenario, assuming no counter measures against climate change, have been considered for the analyses. The maps were derived from the database of the RAIN project (see section 7.1.2). The methodology to perform the analyses is described in Section 5.

Figure 68 show the results of the annual total loss for railways. The results have been presented in box-and-whiskers plots, representing the median, the quartiles (25 and 75), the caps and the whiskers. The highest value for the median annual loss for railway in a future scenario is reached in Germany with ca 330 M€, then France (FR) with ca 250 M€ and Italy (IT) and Hungary (HU), respectively with 150M€ and 110M€.

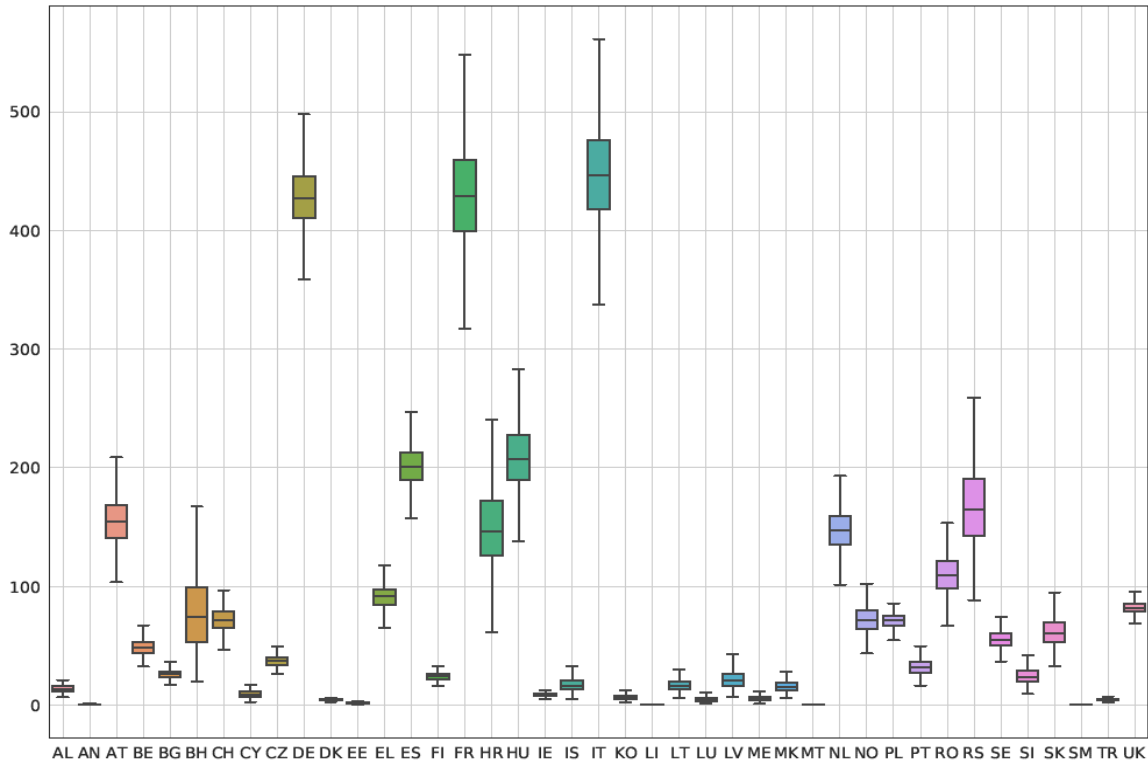
Figure 69 shows the same results but for roads. In this case, for the sake of simplicity, we have merged all the 4 types of roads together. Figure 71 depicts the annual loss for roads in a future scenario. One more time Germany (DE), France (FR) and Italy (IT) show the largest range of the expected annual loss with a median value around 420 M€.

Figure 70 shows the estimated total cost in M€ for railway summed over all countries for future and past scenarios. It is important to mention that the scenario in this setting represents a flooding event striking with equal intensity in all countries. A more likely event that can be assessed through these numbers might be a flooding event striking, say half of the considered countries. The numbers are computed by the Monte Carlo simulations described in Section 5.2.1.5. Note that price levels for each country have not been adjusted to account for differences in GDP per capita. The relative uncertainty of these numbers appears smaller, which is a natural consequence of summing multiple independent random variables. Same type of plot for roads are displayed in Figure 71.



**Figure 68. Expected annual loss for railways in M€ considering flood maps in a future scenario with RCP 8.5.**





**Figure 69. Expected annual loss for roads in M€ considering flood maps in a future scenario with RCP 8.5.**

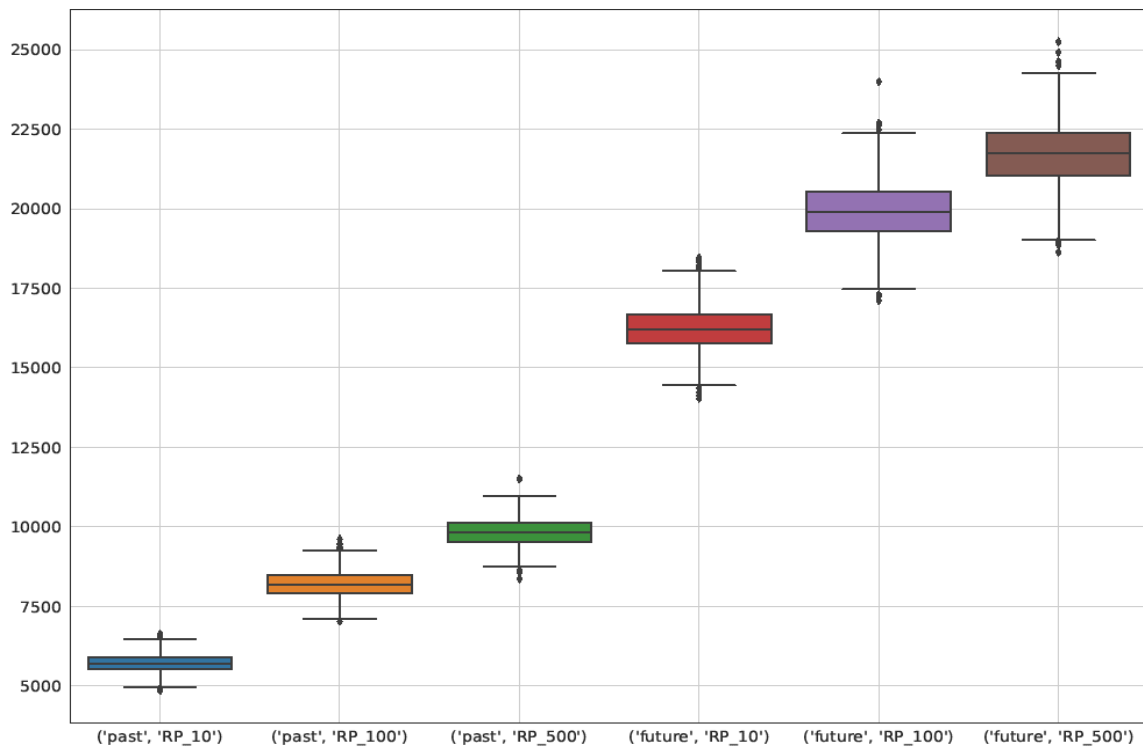


**Figure 70. Estimated total cost for railway by scenario, summed over all countries in M€.**

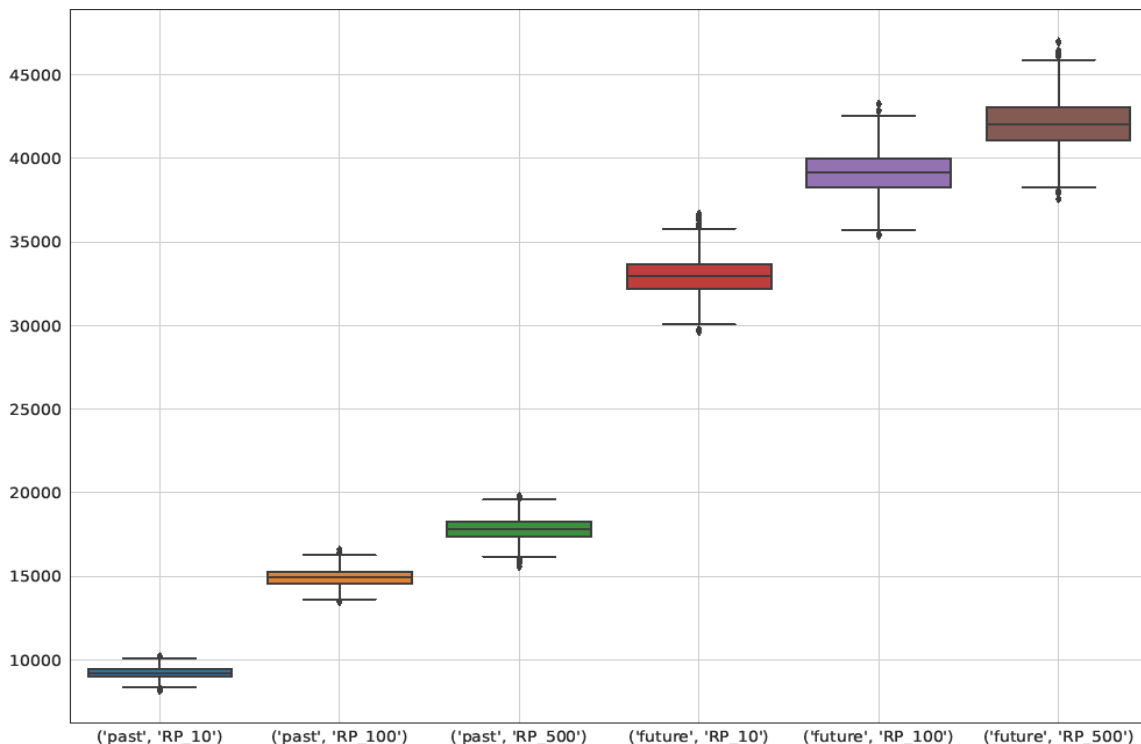


**Figure 71. Estimated total cost for roads by scenario, summed over all countries in M€.**

## 7.2 Population models

Climate change often implies increasing, more frequent, intense, and persistent hazard events affecting populations in growth and with increasing activity. Since the probabilities of adverse events and their potential impacts both increase over time, future economic consequences are multiplicatively enhanced.

However, there are also situations where hazards are less frequent and less severe at the same time as economic activities are diminishing due to population decline. In such cases, the future economic consequences diminish.

The economic performance of resilience measures and policies depend on the situation/conditions at the time of occurrence of the climate related extreme events. The situation/condition refer to the size of the affected populations, resulting activity patterns and values of the assets. It is therefore important to take into account population growth or decline for a proper assessment of the economics of these resilience measures and policies.

### 7.2.1 Future impacts are more heavily discounted

Even with constant population and activity patterns, the timing of future hazards play a role for the economic performance of resilience measures and the benefits of avoiding or reducing damages. Costs and benefits that accrue early in the project period are not discounted as heavily as those that occur later on (note that discounting is always with respect to resulting net present values and has nothing to do with inflation).

Hazards that become less frequent will also tend to occur later in the project period and consequently be more heavily discounted.

### **7.2.2 Monte Carlo modelling of economic indicators**

Since it is unknown exactly when hazards will occur, we model the occurrence of hazard events with different severities as stochastic discrete variables, where the probability of occurrence is specified from previous occurrence statistics. The recurrence rates and distribution can be derived from historic data corrected for predicted expected increases or decreases in probability due to climate changes, and possibly also taking into account changes in the expected probability over time. To derive the expected impacts of hazard events, it is possible to run Monte Carlo simulations where the occurrences of the events are visualized, and the impacts on population, activities, and assets. The sizes of the impacts depend on the set of resilience measures brought into/still in place at the time of simulated occurrence. Given a large number of simulations the discounted value of future expected impacts be calculated at each future time point.

### **7.2.3 Diminishing returns of investments**

Central to the economic analyses of resilience policies is how they depend on context and are instrumental in avoiding or reducing future damages. Due to scarce financial resources, resilience policies require a sequence of investments over time. In such cases the accumulated protective capabilities are also increasing. However, while initial efforts may address stretches where improvements of securing localized gaps or inferior segments produce large benefits with relatively little effort, a diminishing return on investments over time is usual. It becomes subsequently more difficult and costly to gain further advantages. There is consequently a need for modelling the accumulated protective effects of resilience policies at the time of a hazard occurrence and the economic value of the protective capacity gained from the accumulated efforts at that time.

Protective measures that are effective against natural hazards with moderate intensity, may fail completely when water level rises above protective element height. Monte Carlo simulations may provide insights into the net gains of protective measures that have good performance for small and medium sized events but may fail to provide protection for more seldom extreme events.

### **7.2.4 Demographic change in Europe**

Europe's working-age population is shrinking. Total changes in populations are a product of the age distribution, fertility, immigration and emigration. Within each country, rise and decline of industries and services, globalisation, and urbanisation play a role. To provide an overview before looking specifically into the situation in Portugal and the study area, Figure 72 shows the project changes in population at the European member state level until 2100. Portugal is among the countries where the EEA expects one of the steepest drops in population. Only Bulgaria has a larger predicted reduction in population size.

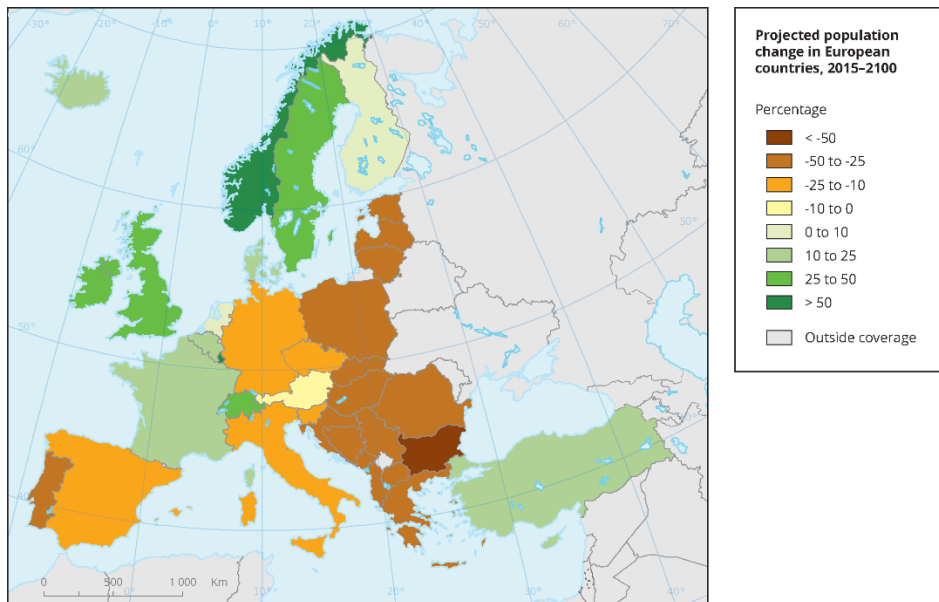


**Figure 72. Estimated changes in European countries 2015-2100 (source: <https://www.eea.europa.eu/data-and-maps/figures/projected-population-change-in-european>)**

The factors driving the changes in overall population size over time, is the age distribution, emigration/immigration, fertility, and mortality. The European population is aging with an expected 30% proportion of citizens being 65+ years old in 2070 vs currently 20%. This is an increase of 33%. The demographic changes are not uniform and vary between countries as well as between more or less developed regions and areas.

The size of the working population relative to the size of the non-working population is an important socio-economic factor. It determines the economic load that each member of the working population needs to carry in addition to him/herself and is an indicator of the growth/decline in the accumulation of wealth/depletion of resources and future prospects.

To view the relative size of the working population relative to the EC average and the composition of non-working segments, it is possible to use a ternary scheme where the proportion of elderly in each country/region are positioned according to the scale on the left edge of a triangle, and the proportion young according to the bottom edge of the triangle (see Figure 73). The size of the working population increases from bottom right to top as the proportion of elderly and young are reduced.

Whereas the proportion of the most elderly is associated with immediate future decline in the population, a smaller young population signals potential future challenges in keeping up the size of the working population.

Portuguese NUTS regions studied in the SAFEWAY project lie in the lower left of the triangle, signifying a higher load on each member of the work force than the EC average, and a lower percentage of youths.

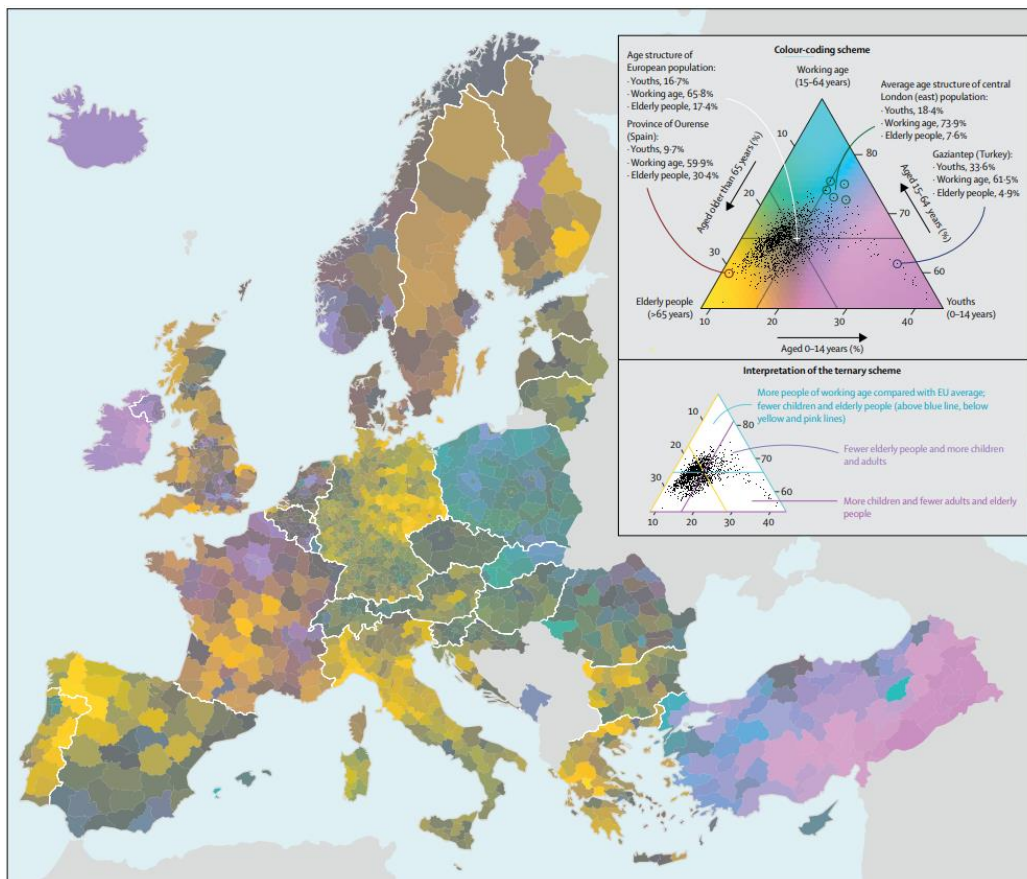
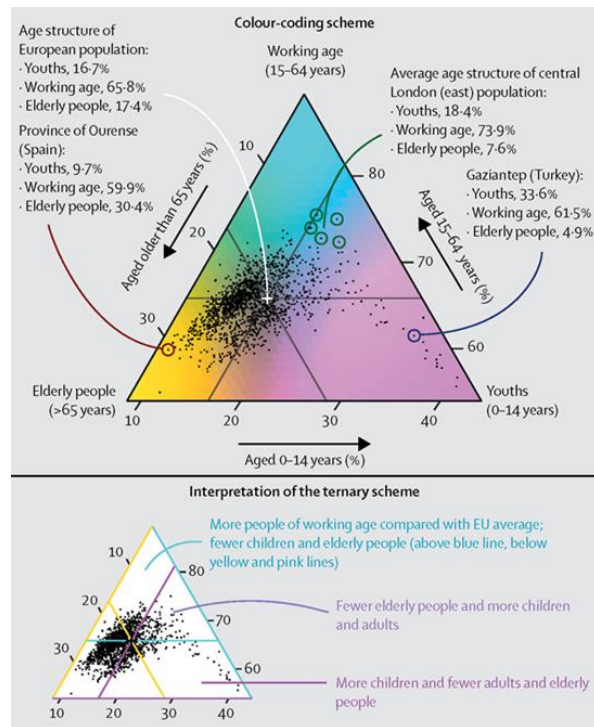


**Figure 73. Visualization of demographic factors characterizing European countries. Upper figure: Zoom-in to show the colour coding scheme of working population in European regions (source: (Kashnitsky and Schöley, 2018))**

### 7.2.5 Predicted population change in demonstration area

Based on an extraction of latest five years crude rates of population change at the NUTS 3 level showing a declining population (see Appendix 4 for full table), the high percentage of elderly and a declining working population, it is seen little reason to not use the current crude rates of change to predict future changes in population. We consequently estimate that the population in the demonstration area will decline between 5 to 10 inhabitants per 1000 per year.

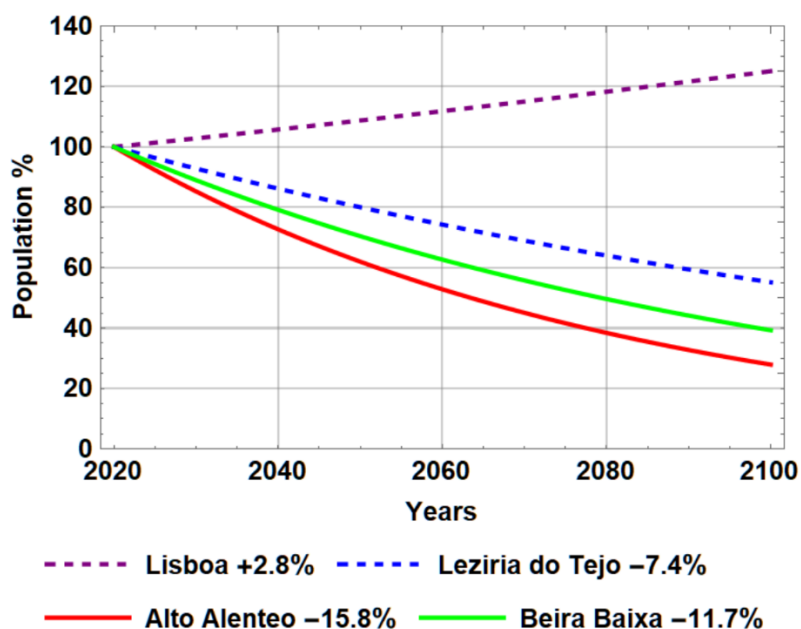


Figure 74. Portugal NUTS 3 with population change rates

Current crude rates of change are determined as the average of the yearly figures for the last 5 years. Changes of this size will over the project horizon result in significant population reductions between 20% and 40% in 2070 (see Figure 75). Lisbon is an exception with a projected population growth of about 17%. Transport between two regions each experiencing 30% reduction in population is expected to diminish by ca. 50% other factors constant. There might be technological and other changes that contribute to fewer trips being necessary in the future. A recent reminder is the changes in workplace locations, increased use of video



conferencing etc. during the COVID crisis. These changes would make parts of society somewhat more robust against transport net disruptions. Future reduction in fuel prices and other travel costs, may contribute to maintain some of the trips.



**Figure 75. Expected population sizes for some of the NUTS3 areas affected by a potential 100-year flooding.**

### 7.3 Time-variant consequence models

Information on population changes over time is one input factor to transport and traffic modelling. Typically, the amount of traffic between an origin and destination point is seen to be proportional to each of their respective population sizes, and inversely related to the “friction” or generalized travel cost between the start and end points.

Based on the NUTS3 rates of change, to obtain the change in transport activities between an origin and destination with declining growth would be to multiply their growth rates. In the case of one NUTS3 area having a crude rate of change of -10 per 1000 and another with -5 per 1000, the resulting change should be  $1 - (1 - 0.01) * (1 - 0.005)$  that results in a crude change in rate of -15 per 1000 or -1.5 percent. To illustrate possible impact of uncertainty in growth rates we suggest adding/subtracting 5 per 1000 to and from the NUTS3 crude rates of population change.

The traffic modelling needs to consider potential future changes in the friction or generalized travel cost in the period. Given improved or less costly transport the number of trips and transport movements will increase. On the other hand, population reductions may lead to a reduction in service provisions with longer waiting times and consequently also an increase in generalized travel costs.

## 8. Conclusions

A dynamic risk-based framework has been proposed in this deliverable, which improves the understanding and the proper modelling of transportation networks. The core of the framework is the three main components of a risk-based methodology, namely the hazard assessment, the infrastructure performance, and the quantification of possible consequences. In addition, real-time data has been introduced into the framework as a means to reducing the uncertainties in the hazard estimation and in the infrastructure asset condition, and to potentially providing support for early warning systems and traffic re-routing for reducing the impacts of extreme event occurrences. Moreover, the importance of accounting for time-variant factors has been stressed in the framework. For instance, socioeconomic factors such as population growth and traffic demands vary over time, and consequently the impacts should be projected at long-term. Finally, hazard projections have been also addressed in the framework to account for future extreme events.

Throughout the deliverable, different methodologies have been reviewed and applied to depict the assessment of each component from the framework, with focus on roadway and railway infrastructures exposed to flooding hazard. First, performance predictive models have been implemented to different infrastructure assets in order to forecast their deterioration. Then, Bayesian inference procedures have been introduced to facilitate the updating of the adopted predictive models based on new collected information. This updated condition is used afterwards to assess the probability of failure of the infrastructures when exposed to extreme hazard events.

Subsequently, methodologies for flood hazard assessment have been reviewed and recommendations have been made depending on the data availability and the scope of the analysis. Flood fragility functions for different infrastructure assets have been also examined, and a framework has been proposed for construction of fragility curves for a portfolio of bridges, which are among the most complex assets given their multiple components and therefore the possible related failure modes. Then, an illustrative example has been presented to demonstrate the methodology and thus facilitate the performance assessment at network level.

Furthermore, the framework has been applied to evaluate the risk of linear transportation infrastructures at European level, by considering direct impacts and vulnerability relations expressing the degree of material damage. The implementation of the approach through a GIS environment has enabled the identification of the exposure of the infrastructures by geographical coincidence. Also, the uncertainties associated to both costs and vulnerability values have been considered through MC sampling, which allows fully risk-informed decisions. On the other hand, methodologies for the quantification of indirect impacts due to the disruption of the transportation service have been also addressed, and a simplified assessment has been carried out with focus on indirect user costs given the probability and duration of a service disruption. This approach offers a preliminary estimation of indirect impacts, yet all the socioeconomic costs which have been broadly reviewed, namely operation costs of travel and external damage costs due

---

to increase traffic flows, remain to be incorporated on more detail qualifications supported by traffic models.

Finally, for the projection of long-term impacts, both the dispersion of future hazards given the modification in the return periods due to climate change, and the situation and conditions of the population affected by these future occurrences have been analysed. A stochastic approach has been proposed to analyse resilience policies against future uncertain hazard impacts. In these analyses, benefits that are dependent on the size and timing of uncertain future events can be calculated through Monte Carlo simulation, and the uncertainties associated with the calculations and their impact on the resulting economic indicators can be visualised.

---

## Acknowledgements

The work described in this deliverable was carried out in the framework of the GIS-Based Infrastructure Management System for Optimized Response to Extreme Events of Terrestrial Transport Networks (SAFEWAY) project, which has received funding from the European Union's Horizon 2020 research and innovation programme under grant agreement No 769255.

## References

- AASHTO (2010) *Bridge Element Inspection Guide Manual*. United States of América.
- ACI 318 CODE (2014) *Building Code Requirements for Structural Concrete and Commentary*.
- Adey, B. T. *et al.* (2016) 'Ensuring acceptable levels of infrastructure related risks due to natural hazards with emphasis on conducting stress tests', in *Proceedings of the 1st International Symposium on Infrastructure Asset Management (SIAM 2016)*.
- Albrecht, P. and Naeemi, A. H. (1984) *Performance of weathering steel in bridges*. Riverdale, Maryland.
- Alfieri, L. *et al.* (2015) 'Global warming increases the frequency of river floods in Europe', *Hydrology and Earth System Sciences*, 19(5), pp. 2247–2260.
- Alvarez, M. A., Rosasco, L. and Lawrence, N. D. (2011) 'Kernels for Vector-Valued Functions: a Review'.
- Amundsen, A. H., Klæboe, R. and Fyhri, A. (2008) 'Annoyance from vehicular air pollution: Exposure--response relationships for Norway', *Atmospheric Environment*, 42(33), pp. 7679–7688.
- Ang, A. H.-S. and Tang, W. H. (1975) *Probability Concepts in Engineering Planning and Design, Basic Principles*. Edited by Wiley.
- APA (2014) *Elaboração de cartografia específica sobre o risco de inundação para Portugal Continental. Agência Portuguesa do Ambiente. Estudos técnicos: AQUALOGUS, ACTION MODULERS*.
- Argyroudis, S. A. *et al.* (2019) 'Fragility of transport assets exposed to multiple hazards: State-of-the-art review toward infrastructural resilience', *Reliability Engineering & System Safety*, 191, p. 106567.
- ARH Tejo (2012) *PLANO DE GESTÃO DA REGIÃO HIDROGRÁFICA DO TEJO*.
- Attina, M. *et al.* (2018) *Assessment of unit costs (standard prices) of rail projects (CAPital Expenditure). Final report, Contract No 2017CE16BAT002*.
- Avent, R. R. and Alawady, M. (2005) 'Bridge scour and substructure deterioration: Case study', *Journal of Bridge Engineering*, 10(3), pp. 247–254.
- Azevêdo, T. M., Nunes, E. and Ramos, C. (2004) 'Some morphological aspects and hydrological characterization of the Tagus floods in the Santarém region, Portugal', *Natural Hazards*, 31(3), pp. 587–601.
- Basner, M. and McGuire, S. (2018) 'WHO environmental noise guidelines for the European region: a systematic review on environmental noise and effects on sleep', *International journal of environmental research and public health*, 15(3), p. 519.
- Bedia, J. *et al.* (2014) 'Forest fire danger projections in the Mediterranean using ENSEMBLES regional climate change scenarios', *Climatic Change*, 122(1), pp. 185–

199.

Benn, J. (2013) 'Railway bridge failure during flooding in the UK and Ireland', *Proceedings of the Institution of Civil Engineers-Forensic Engineering*, 166(4), pp. 163–170.

Beven, K. J. (2011) *Rainfall-runoff modelling: the primer*. John Wiley & Sons.

Beven, K. J. and Hall, J. (2014) *Applied uncertainty analysis for flood risk management*. World Scientific.

Beven, K. J., Leedal, D. T. and McCarthy, S. (2014) 'Framework for assessing uncertainty in fluvial flood risk mapping, CIRIA report C721/2014'.

Birdsall, J. and Hajdin, R. (2008) 'Vulnerability assessment of individual infrastructure objects subjected to natural hazards', *Transportation research circular*, (E-C128), pp. 339–355.

Blöschl, G. *et al.* (2019) 'Changing climate both increases and decreases European river floods', *Nature*, 573(7772), pp. 108–111.

Bocsi, B. *et al.* (2011) 'Learning inverse kinematics with structured prediction', in. Institute of Electrical and Electronics Engineers (IEEE), pp. 698–703. doi: 10.1109/iros.2011.6094666.

Bolukbasi, M., Mohammadi, J. and Arditi, D. (2004) 'Estimating the future condition of highway bridge components using national bridge inventory data', *Practice Periodical on Structural Design and Construction*, 9(1), pp. 16–25.

Briaud, J.-L. *et al.* (2011) *Realtime monitoring of bridge scour using remote monitoring technology*.

Bu, G. *et al.* (2014) 'Development of an integrated method for probabilistic bridge-deterioration modeling', *Journal of Performance of Constructed Facilities*, 28(2), pp. 330–340.

Bukhsh, Z. A. and Stipanovic, I. (2020) 'Predictive Maintenance for Infrastructure Asset Management', *IT Professional*, 22(5), pp. 40–45.

Bundesamt für Strassen ASTRA (2012) 'Naturgefahren auf den Nationalstrassen: Risikokonzept, Methodik für eine risikobasierte Beurteilung, Prävention und Bewältigung von gravitativen Naturgefahren auf Nationalstrassen', *Ausgabe V2.20, ASTRA 89001*.

Burgueño, R., Zhe, L. and others (2008) *Identification of causes and development of strategies for relieving structural distress in bridge abutments*.

Casas, A. *et al.* (2006) 'The topographic data source of digital terrain models as a key element in the accuracy of hydraulic flood modelling', *Earth Surface Processes and Landforms: The Journal of the British Geomorphological Research Group*, 31(4), pp. 444–456.

CEN, E. (2003) '1: Actions on structures-Part 2: Traffic loads on bridges', *EN 1991: 2*, 6, p. 2003.

Chang, H. *et al.* (2010) 'Potential impacts of climate change on flood-induced travel disruptions: a case study of Portland, Oregon, USA', *Annals of the Association of*



---

*American Geographers*, 100(4), pp. 938–952.

Chang, L. and Song, J. (2016) 'Title: Matrix-based System Reliability Analysis of Urban Infrastructure Networks: A Case Study of MLGW Natural Gas Network', in *Fifth China-Japan-US Trilateral Symposium on Lifeline Earthquake Engineering*. Shanghai, China.

Chapados, N. and Bengio, Y. (2007) 'Augmented Functional Time Series Representation and Forecasting with Gaussian Processes', in *Proceedings of the 20th International Conference on Neural Information Processing Systems*, pp. 265–272.

Choe, D. E. *et al.* (2008) 'Probabilistic capacity models and seismic fragility estimates for RC columns subject to corrosion', *Reliability Engineering and System Safety*, 93(3), pp. 383–393. doi: 10.1016/j.ress.2006.12.015.

Conde, B. *et al.* (2020) 'Probabilistic-based structural assessment of a historic stone arch bridge', *Structure and Infrastructure Engineering*, pp. 1–13.

Crotti, G. and Cigada, A. (2019) 'Scour at river bridge piers: Real-time vulnerability assessment through the continuous monitoring of a bridge over the river Po, Italy', *Journal of Civil Structural Health Monitoring*, 9(4), pp. 513–528.

Czarnecki, A. A. and Nowak, A. S. (2006) 'System reliability assessment of steel girder bridges', in *Solid Mechanics and its Applications*. Dordrecht: Springer Netherlands, pp. 699–710. doi: 10.1007/1-4020-4891-2\_59.

D'Ayala, D. *et al.* (2015) 'Fragility functions matrix', *Deliverable D3*, 2.

Denysiuk, R. *et al.* (2016) 'A computational framework for infrastructure asset maintenance scheduling', *Structural Engineering International*, 26(2), pp. 94–102.

DfT (2014) *Transport Resilience Review. A review of the resilience of the transport network to extreme weather events*. London (UK).

Doll, C., van Essen, H. and others (2008) 'Road infrastructure cost and revenue in Europe', *Produced within the study Internalisation Measures and Policies for all external cost of Transport (IMPACT) P Deliverable*, 2, p. 1435.

Dong, Y., Frangopol, D. M. and Saydam, D. (2013) 'Time-variant sustainability assessment of seismically vulnerable bridges subjected to multiple hazards', *Earthquake Engineering & Structural Dynamics*, 42(10), pp. 1451–1467.

Du, Y. G., Clark, L. A. and Chan, A. H. C. (2005) 'Residual capacity of corroded reinforcing bars', *Magazine of Concrete Research*, 57(3), pp. 135–147. doi: 10.1680/mac.2005.57.3.135.

ECA (2013) *Are EU cohesion policy funds well spent on roads, Special Report No 5, European Court of auditors*. Available at: <https://op.europa.eu/en/publication-detail/-/publication/219f40bf-3af4-48d7-9505-67fc99ef26b8/language-en>.

Eidsvig, U., Kristensen, K. and Vangelsten, B. V. (2017) 'Assessing the risk posed by natural hazards to infrastructures'.

Ellingwood, B. R. (2007) 'Structure and Infrastructure Engineering Risk-informed condition assessment of civil infrastructure: state of practice and research issues'. doi: 10.1080/15732470412331289341.

- Ellingwood, B. R. and Mori, Y. (1993) 'Probabilistic methods for condition assessment and life prediction of concrete structures in nuclear power plants', *Nuclear Engineering and Design*, 142(2-3), pp. 155-166. doi: 10.1016/0029-5493(93)90199-J.
- England Jr, J. F. *et al.* (2019) *Guidelines for determining flood flow frequency—Bulletin 17C*.
- Enright, M. P. and Frangopol, D. M. (1998) 'Probabilistic analysis of resistance degradation of reinforced concrete bridge beams under corrosion', *Engineering Structures*, 20(11), pp. 960-971. doi: 10.1016/S0141-0296(97)00190-9.
- Erath, A. L. (2011) *Vulnerability assessment of road transport infrastructure*. ETH Zurich.
- Estes, A. C. (1997) *A system reliability approach to the lifetime optimization of inspection and repair of highway*. University of Colorado.
- Estes, A. C., Foltz, S. D. and McKay, D. T. (2005) 'Estimating Risk from Spillway Gate Systems on Dams Using Condition Assessment Data', (October), pp. 1-97.
- Estes, A. C. and Frangopol, D. M. (1999) 'Repair optimization of highway bridges using system reliability approach', *J. Struct. Eng.*, 125, pp. 766-775.
- Estes, A. C. and Frangopol, D. M. (2003) 'Updating Bridge Reliability Based on Bridge Management Systems Visual Inspection Results', *Journal of Bridge Engineering*, 8(6), pp. 374-382. doi: 10.1061/(ASCE)1084-0702(2003)8:6(374).
- Faleschini, F., Zanini, M. A. and Casas Rius, J. R. (2019) 'State-of-research on performance indicators for bridge quality control and management', *Frontiers in built environment*, 5, pp. 1-20.
- Faturechi, R. and Miller-Hooks, E. (2015) 'Measuring the performance of transportation infrastructure systems in disasters: A comprehensive review', *Journal of infrastructure systems*, 21(1), p. 4014025.
- FEDRO (2012) *Natural hazards on national roads: Risk concept. Methodology for risk-based assessment, prevention and response to gravitative natural hazards on national roads. ASTRA Documentation 89001*.
- Fell, R. *et al.* (2005) 'A framework for landslide risk assessment and management', *Landslide risk management*, pp. 3-25.
- Frangopol, D. M. and Estes, A. C. (1997) 'Lifetime Bridge Maintenance Strategies Based on System Reliability', *Structural Engineering International: Journal of the International Association for Bridge and Structural Engineering (IABSE)*, 7(3), pp. 193-198. doi: 10.2749/101686697780494662.
- Frauenfelder, R. *et al.* (2017) 'Impacts of extreme weather events on transport infrastructure in Norway', *Natural Hazards and Earth System Sciences Discussions*, pp. 1-24.
- Ganesh Prasad, G. and Banerjee, S. (2013) 'The impact of flood-induced scour on seismic fragility characteristics of bridges', *Journal of Earthquake Engineering*, 17(6), pp. 803-828.
- Ghosh, J. and Padgett, J. E. (2010) 'Aging considerations in the development of

- time-dependent seismic fragility curves', *Journal of Structural Engineering*, 136(12), pp. 1497–1511.
- Ghosh, J. and Sood, P. (2016) 'Consideration of time-evolving capacity distributions and improved degradation models for seismic fragility assessment of aging highway bridges', *Reliability Engineering & System Safety*, 154, pp. 197–218.
- Gilbert, M. *et al.* (2019) 'Limit Analysis of Masonry Arch Bridges Using Discontinuity Layout Optimization', in *International Conference on Arch Bridges*, pp. 307–314.
- Guski, R., Schreckenber, D. and Schuemer, R. (2017) 'WHO environmental noise guidelines for the European region: A systematic review on environmental noise and annoyance', *International journal of environmental research and public health*, 14(12), p. 1539.
- Hackl, J. *et al.* (2018) 'Estimating network related risks: A methodology and an application in the transport sector', *Natural Hazards and Earth System Sciences*, 18(8), pp. 2273–2293.
- Hadjidemetriou, G. M., Xie, X. and Parlikad, A. K. (2020) 'Predictive Group Maintenance Model for Networks of Bridges', *Transportation Research Record*, 2674(4), pp. 373–383.
- Hajdin, R., Kusar, M., *et al.* (2018) *WG3 Technical Report: Establishment of a Quality Control Plan*. doi: ISBN: 978-86-7518-200-9.
- Hajdin, R., Kušar, M., *et al.* (2018) 'WG3 technical report: Establishment of a Quality Control Plan of COST Action 1406'.
- Hajdin, R., Casas, J. and Matos, J. (2019) 'Inspection of existing bridges: moving on from condition rating', in *IABSE Symposium Guimarães 2019: Towards a Resilient Built Environment-Risk and Asset Management, March 27-29, 2019, Guimarães, Portugal*, pp. 940–947.
- Hall, W. B. (1988) 'Reliability of Service-Proven Structures', *Journal of Structural Engineering*, 114(3), pp. 608–624. doi: 10.1061/(asce)0733-9445(1988)114:3(608).
- Hazus-MH (2013) *Multi-hazard Loss Estimation Methodology: Flood Model Hazus-MH Technical Manual*.
- Hearn, G. and Frangopol, D. M. (1996) 'Segment-based reporting for element level bridge inspection', in *4th NSF National Workshop on Bridge Research in Progress*. Buffalo, N.Y.: National Science Foundation, Washington, D.C., pp. 33–38.
- Higgins, C. and Farrow, W. C. (2006) 'Tests of reinforced concrete beams with corrosion-damaged stirrups', *ACI Structural Journal*, 103(1), pp. 133–141. doi: 10.14359/15094.
- Holmgren, N. and Fedoryshyn, N. (2015) *Utslipp fra veitrafikk i Norge. Dokumentasjon av beregningsmetoder, data og resultater (Emissions from road traffic in Norway-Method for estimation, input data and emission estimates)*.
- Hulet, K. M., Smith, C. C. and Gilbert, M. (2006) 'Load-carrying capacity of flooded masonry arch bridges', in *Proceedings of the Institution of Civil Engineers-Bridge*

*Engineering*, pp. 97–103.

IP (2017) *Sistema de Gestão de Obras de Arte da IP (SGOA IP)- Bases do Sistema*.

IPCC (2013) 'The physical science basis', *Contribution of Working Group I to the Fifth Assessment Report of the Intergovernmental Panel on Climate Change*. Cambridge University Press Cambridge, pp. 159–254.

IPMA (2020) *Climate monitoring*.

Isailović, D. *et al.* (2020) 'Bridge damage: Detection, IFC-based semantic enrichment and visualization', *Automation in Construction*, 112(December 2019), p. 103088. doi: 10.1016/j.autcon.2020.103088.

ISO (2018) *STANDARD OPERATING GUIDELINES*.

ISSMGE TC32 (2004) *Risk Assessment Glossary of Terms*. Available at: [http://140.112.12.21/issmge/2004Glossary\\_Draft1.pdf](http://140.112.12.21/issmge/2004Glossary_Draft1.pdf).

Jacobsen, J. K. S., Leiren, M. D. and Saarinen, J. (2016) 'Natural hazard experiences and adaptations: A study of winter climate-induced road closures in Norway', *Norsk Geografisk Tidsskrift-Norwegian Journal of Geography*, 70(5), pp. 292–305.

JCSS (2008) 'Risk assessment in engineering, principles, system representation & risk criteria', *Joint Committee on Structural Safety*.

JCSS, J. (2001) 'Probabilistic model code', *Joint Committee on Structural Safety*.

Jnaid, F. and Aboutaha, R. S. (2016) 'Residual flexural strength of corroded reinforced concrete beams', *Engineering Structures*, 119, pp. 198–216. doi: 10.1016/j.engstruct.2016.04.018.

Kaplan, S. and Garrick, B. J. (1981) 'On the quantitative definition of risk', *Risk analysis*, 1(1), pp. 11–27.

Karimzadeh, A. and Shoghli, O. (2020) 'Predictive analytics for roadway maintenance: A review of current models, challenges, and opportunities', *Civil Engineering Journal*, 6(3), pp. 602–625.

Kashnitsky, I. and Schöley, J. (2018) 'Regional population structures at a glance', *The Lancet*, 392(10143), pp. 209–210.

Van Kempen, E. *et al.* (2018) 'WHO environmental noise guidelines for the European region: a systematic review on environmental noise and cardiovascular and metabolic effects: a summary', *International journal of environmental research and public health*, 15(2), p. 379.

Kim, H. *et al.* (2017) 'Flood fragility analysis for bridges with multiple failure modes', *Advances in Mechanical Engineering*, 9(3), p. 1687814017696415.

Klæboe, R., Amundsen, A. H. and Fyhri, A. (2008) 'Annoyance from vehicular air pollution: A comparison of European exposure--response relationships', *Atmospheric Environment*, 42(33), pp. 7689–7694.

Krajzewicz, D. *et al.* (2012) 'Recent development and applications of SUMO-Simulation of Urban MObility', *International journal on advances in systems and measurements*, 5(3&4).

- Lagasse, P. F. *et al.* (2013) 'Risk-based approach for bridge scour prediction', *National Cooperative Highway Research Program Transportation Research Board National Research Council: Washington, DC, USA*, 20.
- Lam, J. and Adey, B. (2016) 'Functional loss assessment and restoration analysis to quantify indirect consequences of hazards', *ASCE-ASME Journal of Risk and Uncertainty in Engineering Systems, Part A: Civil Engineering*, 2(4), p. 4016008.
- Lam, W. H. K. *et al.* (2013) 'Modeling the Effects of Rainfall Intensity on Traffic Speed, Flow, and Density Relationships for Urban Roads', *Journal of Transportation Engineering*, 139(7), pp. 758–770. doi: 10.1061/(ASCE)TE.1943-5436.0000544.
- Lamb, R. *et al.* (2017) 'Vulnerability of bridges to scour: insights from an international expert elicitation workshop', *Nat. Hazards Earth Syst. Sci.*, 17(8).
- Lark, R. and Flaig, K. D. (2005) 'The use of reliability analysis to aid bridge management', *Structural Engineer*, 83(5).
- Le, B. and Andrews, J. (2016) 'Petri net modelling of bridge asset management using maintenance-related state conditions', *Structure and Infrastructure Engineering*, 12(6), pp. 730–751. doi: 10.1080/15732479.2015.1043639.
- Lee, B.-J. (2017) 'Analysis on Inundation Characteristics for Flood Impact Forecasting in Gangnam Drainage Basin', *Atmosphere journal*, 27(2), pp. 189–197. doi: 10.14191/Atmos.2017.27.2.189.
- Van Leeuwen, Z. and Lamb, R. (2014) 'Flood and scour related failure incidents at railway assets between 1846 and 2013', *Railway Safety & Standards Board*.
- LimitState (2019) *LimitState:GEO Manual, Version 3.5 edition*. Available at: <http://www.limitstate.com/geo> (Accessed: 15 December 2020).
- Lin, C. *et al.* (2014) 'Case history analysis of bridge failures due to scour', in *Climatic effects on pavement and geotechnical infrastructure*, pp. 204–216.
- Lindberg, G. (2005) 'Measuring the marginal social cost of transport', *Res. Transport. Econ.*, 14, pp. 155–183.
- Lounis, Z. and McAllister, T. P. (2016) 'Risk-Based Decision Making for Sustainable and Resilient Infrastructure Systems', *Journal of Structural Engineering*, 142(9), p. F4016005. doi: 10.1061/(ASCE)ST.1943-541X.0001545.
- Lu, P., Wang, H. and Tolliver, D. (2019) 'Prediction of Bridge Component Ratings Using Ordinal Logistic Regression Model', *Mathematical Problems in Engineering*, 2019.
- Ludvigsen, J. *et al.* (2012) *Costs and consequences of extreme weather on European freight and logistics industries and supply chains*.
- Ludvigsen, J. and Klæboe, R. (2014) 'Extreme weather impacts on freight railways in Europe', *Natural hazards*, 70(1), pp. 767–787.
- Lynch, S. M. (2007) 'Basics of Bayesian Statistics', in *Introduction to Applied Bayesian Statistics and Estimation for Social Scientists*. Springer New York, pp. 47–75. doi: 10.1007/978-0-387-71265-9\_3.
- Ma, Y. *et al.* (2013) 'Probabilistic prediction with bayesian updating for strength



degradation of RC bridge beams', *Structural Safety*, 44, pp. 102–109. doi: 10.1016/j.strusafe.2013.07.006.

Manning, R. *et al.* (1890) *On the flow of water in open channels and pipes*.

Marshall Institute (2020) *Preventive Maintenance Optimization (PMO) Workshop*. Available at: [https://www.marshallinstitute.com/pdfs/PMO\\_Workshop.pdf](https://www.marshallinstitute.com/pdfs/PMO_Workshop.pdf).

McKenna, G. *et al.* (2020) 'Multiple hazard fragility analysis for granular highway embankments: Moisture ingress and scour', *Transportation Geotechnics*, 26, p. 100431.

McMillan, H., Krueger, T. and Freer, J. (2012) 'Benchmarking observational uncertainties for hydrology: rainfall, river discharge and water quality', *Hydrological Processes*, 26(26), pp. 4078–4111.

Md Ali, A., Solomatine, D. P. and Di Baldassarre, G. (2015) 'Assessing the impact of different sources of topographic data on 1-D hydraulic modelling of floods', *Hydrology and Earth System Sciences*, 19(1), pp. 631–643.

Mekker, M. M. *et al.* (2018) 'Application of LiDAR and connected vehicle data to evaluate the impact of work zone geometry on freeway traffic operations', *Transportation research record*, 2672(16), pp. 1–13.

Melchers, R. E. and Beck, A. T. (2018) *Structural Reliability Analysis and Prediction*. Third Edit. Hoboken: John Wiley & Sons Ltd.

Miedema, H. M. and Oudshoorn, C. G. (2001) 'Annoyance from transportation noise: relationships with exposure metrics DNL and DENL and their confidence intervals.', *Environmental health perspectives*, 109(4), pp. 409–416.

Miller-Hooks, E., Zhang, X. and Faturechi, R. (2012) 'Measuring and maximizing resilience of freight transportation networks', *Computers & Operations Research*, 39(7), pp. 1633–1643.

Mirzaei, Z. *et al.* (2014) *The IABMAS bridge management committee overview of existing bridge management systems*.

Misra, S. *et al.* (2020) 'An expert opinion survey on post-hazard restoration of roadways and bridges: Data and key insights', *Earthquake Spectra*, 36(2), pp. 983–1004.

Mitoulis, S. and Argyroudis, S. (2021) *Survey for bridge restoration after floods*. doi: 10.13140/RG.2.2.13550.23368.

Molarius, R. *et al.* (2012) 'D. 5.1 weather hazards and vulnerabilities for the European transport system—a risk panorama. EWENT project deliverable, VTT, July 2012'.

Mondoro, A. and Frangopol, D. M. (2018) 'Risk-based cost-benefit analysis for the retrofit of bridges exposed to extreme hydrologic events considering multiple failure modes', *Engineering Structures*, 159, pp. 310–319.

Morcous, G. (2011) 'Developing Deterioration Models for Nebraska', 1(July), p. 106. doi: [http://www.royalcommission.vic.gov.au/finaldocuments/summary/PF/VBRC\\_Summary\\_PF.pdf](http://www.royalcommission.vic.gov.au/finaldocuments/summary/PF/VBRC_Summary_PF.pdf).



- Moreira, V. N. *et al.* (2016) 'Reliability-based assessment of existing masonry arch railway bridges', *Construction and Building Materials*, 115, pp. 544–554.
- Morgado, J. *et al.* (2019) 'The Development of Multi-Asset Performance Indicators for the Management of the Portuguese Road and Rail Networks', in *Towards a Resilient Built Environment - Risk and Asset Management*. Guimarães, Portugal, pp. 1643–1650.
- Moriondo, M. *et al.* (2006) 'Potential impact of climate change on fire risk in the Mediterranean area', *Climate research*, 31(1), pp. 85–95.
- Mouillot, F., Rambal, S. and Joffre, R. (2002) 'Simulating climate change impacts on fire frequency and vegetation dynamics in a Mediterranean-type ecosystem', *Global Change Biology*, 8(5), pp. 423–437.
- NCCS (2017) 'Climate in Norway 2100-a knowledge base for climate adaptation. Authors: Hanssen-Bauer I, Førland E J, Haddeland I, Hisdal H, Mayer S, Nesje A, Nilsen J, Sandven S, Sandø A, Sorteberg A', *NCCS report no. 1/2017*, 1, p. 2017. Available at: [www.klimaservicesenter.no](http://www.klimaservicesenter.no).
- Nowak, A. and Collins, K. (2013) *Reliability of Structures, Second Edition* -. Second edi. New York: CRC Press, Taylor & Francis.
- Nowak, A. S. (1995) 'Calibration of LRFD Bridge Code', *Journal of Structural Engineering*, 121(8), pp. 1245–1251. doi: 10.1061/(ASCE)0733-9445(1995)121:8(1245).
- Nowak, A. S. (2004) 'System reliability models for bridge structures', *Bulletin of the Polish Academy of Sciences: Technical Sciences*, 52(4), pp. 321–328. doi: 10.1007/978-3-642-83279-6\_23.
- Oberndorfer, S., Sander, P. and Fuchs, S. (2020) 'Multi-hazard risk assessment for roads: probabilistic versus deterministic approaches', *Natural hazards and earth system sciences*, 20(11), pp. 3135–3160.
- Omar, T. and Nehdi, M. (2018) 'Condition Assessment of Reinforced Concrete Bridges: Current Practice and Research Challenges', *Infrastructures*, 3(3), p. 36.
- on Structural Safety, J. C. (2001) *Probabilistic assessment of existing structures*. RILEM Publ.
- Palau, A. S. *et al.* (2018) 'Recurrent Neural Networks for real-time distributed collaborative prognostics', in *2018 IEEE International Conference on Prognostics and Health Management, ICPHM 2018*. Institute of Electrical and Electronics Engineers Inc. doi: 10.1109/ICPHM.2018.8448622.
- Palsson, R. and Mirza, M. S. (2002) 'Mechanical response of corroded steel reinforcement of abandoned concrete bridge', *ACI Structural Journal*, 99(2), pp. 157–162. doi: 10.14359/11538.
- Penning-Rowsell, E. *et al.* (2005) 'The benefits of flood and coastal risk management: a handbook of assessment techniques', *ISBN 1904750516*.
- Pesti, G. and Brydia, R. E. (2017) 'Work zone impact assessment methods and applications', *Transportation Research Record*, 2617(1), pp. 52–59.
- Pitilakis, K., Crowley, H. and Kaynia, A. M. (2014) 'SYNER-G: typology definition

and fragility functions for physical elements at seismic risk', *Geotechnical, Geological and Earthquake Engineering*, 27.

Portela, M. M., Espinosa, L. A. and Zelenakova, M. (2020) 'Long-Term Rainfall Trends and Their Variability in Mainland Portugal in the Last 106 Years', *Climate*, 8(12), p. 146.

Pregolato, M., Ford, A., Glenis, V., *et al.* (2017) 'Impact of climate change on disruption to urban transport networks from pluvial flooding', *Journal of Infrastructure Systems*, 23(4), p. 4017015.

Pregolato, M., Ford, A., Wilkinson, S. M., *et al.* (2017) 'The impact of flooding on road transport: A depth-disruption function', *Transportation Research Part D: Transport and Environment*, 55, pp. 67–81. doi: 10.1016/j.trd.2017.06.020.

Pregolato, M. (2019) 'Bridge safety is not for granted--a novel approach to bridge management', *Engineering Structures*, 196, p. 109193.

Pyatkova, K. *et al.* (2019) 'Assessing the knock-on effects of flooding on road transportation', *Journal of environmental management*, 244, pp. 48–60.

Rakoczy, A. M. and Nowak, A. S. (2013) 'Reliability-based sensitivity analysis for prestressed concrete girder bridges.', *PCI journal*, 58(4).

Rasmussen, C. E. (2004) 'Gaussian Processes in machine learning', *Lecture Notes in Computer Science (including subseries Lecture Notes in Artificial Intelligence and Lecture Notes in Bioinformatics)*, 3176, pp. 63–71. doi: 10.1007/978-3-540-28650-9\_4.

Richardson, R. R., Osborne, M. A. and Howey, D. A. (2017) 'Gaussian process regression for forecasting battery state of health', *Journal of Power Sources*, 357, pp. 209–219. doi: 10.1016/j.jpowsour.2017.05.004.

Rødseth, K. *et al.* (2019) *The external costs of transport - Marginal damage cost estimates for passenger and freight transport in Norway*. Oslo.

Rosendahl, K. E. (2000) *Helseeffekter og samfunnsøkonomiske kostnader av luftforurensning*. Oslo.

SAFEWAY (2019a) *Deliverable D2.1 European critical hazards (natural)*. Lead Authors: Unni Eidsvig, Luca Piciullo, Kristine Ekseth, Christina Ekeheien.

SAFEWAY (2019b) *Deliverable D2.2 Impact evaluation of human-made hazards on diverse infrastructure types*. Lead authors: Galvão Neryvaldo, Sousa Helder.

SAFEWAY (2019c) *Deliverable D3.1 Data acquisition report*. Lead Authors: Angelo Amodio, Vincenzo Massimi, Belén Riveiro, Mario Soilán.

SAFEWAY (2020) *Deliverable D2.3 Vulnerability and Resilience Factors*. Lead Authors: Eidsvig Unni, Ekeheien Christina, Tanasić Nikola, Hajdin Rade.

Saksena, S. and Merwade, V. (2015) 'Incorporating the effect of DEM resolution and accuracy for improved flood inundation mapping', *Journal of Hydrology*, 530, pp. 180–194.

Sánchez-silva, M. and Klutke, G.-A. (2016) *Reliability Engineering and Life-Cycle Analysis of Deteriorating Systems*. doi: 10.1007/978-3-319-20946-3.

- Santamaria Ariza, M. *et al.* (2020) 'Comparison of forecasting models to predict concrete bridge decks performance', *Structural Concrete*.
- Santamaria, M. *et al.* (2019) 'Reliability analysis of a post-tensioned railway bridge exposed to corrosion effects', in *International Probabilistic Workshop 2019*.
- Santos, P. P. *et al.* (2020) 'A comprehensive approach to understanding flood risk drivers at the municipal level', *Journal of environmental management*, 260, p. 110127.
- Savage, J. T. S. *et al.* (2016) 'When does spatial resolution become spurious in probabilistic flood inundation predictions?', *Hydrological Processes*, 30(13), pp. 2014–2032.
- Saviotti, A. (2014) 'Bridge assessment, management and life cycle analysis', *Modern Applied Science*, 8(3), pp. 167–181. doi: 10.5539/mas.v8n3p167.
- SFT (2005) *Marginale miljøkostnader ved luftforurensning - Skadekostnader og tiltakskostnader*. Oslo.
- Sheppard, D. M. and Renna, R. (2010) 'Bridge scour manual', Tallahassee, FL.
- Silva, A. (2019) 'Maintenance Management of Railway Bridges and Tunnels', in *IABSE Symposium Guimarães 2019: Towards a Resilient Built Environment-Risk and Asset Management*, March 27-29. Guimarães, Portugal, pp. 1015–1019.
- Smith, C. and Gilbert, M. (2007) 'Application of discontinuity layout optimization to plane plasticity problems', *Proceedings of the Royal Society A: Mathematical, Physical and Engineering Sciences*, 463(2086), pp. 2461–2484.
- Sousa, J. J. and Bastos, L. (2013) 'Multi-temporal SAR interferometry reveals acceleration of bridge sinking before collapse', *Natural Hazards and Earth System Sciences*, 13(3), pp. 659–667.
- Stewart, M. G. (2009) 'Mechanical behaviour of pitting corrosion of flexural and shear reinforcement and its effect on structural reliability of corroding RC beams', *Structural Safety*, 31(1), pp. 19–30. doi: 10.1016/j.strusafe.2007.12.001.
- Suarez, P. *et al.* (2005) 'Impacts of flooding and climate change on urban transportation: A systemwide performance assessment of the Boston Metro Area', *Transportation Research Part D: transport and environment*, 10(3), pp. 231–244.
- Sustainable Bridges (2007) 'Guideline for load and resistance assessment of existing European railway bridges: Advices on the use of advanced methods', *Sustainable bridge*, p. 428. Available at: [http://www.sustainablebridges.net/main.php/SB4.2\\_Guideline\\_LRA.pdf?fileitem=14043924](http://www.sustainablebridges.net/main.php/SB4.2_Guideline_LRA.pdf?fileitem=14043924).
- Tanasić, N. (2015) *Vulnerability of reinforced concrete bridges to local scour in bridge management*. University of Belgrade.
- Tanasić, N. and Hajdin, R. (2018) 'Management of bridges with shallow foundations exposed to local scour', *Structure and Infrastructure Engineering*, 14(4), pp. 468–476.
- Tanasić, N., Ilić, V. and Hajdin, R. (2013) 'Vulnerability assessment of bridges exposed to scour', *Transportation research record*, 2360(1), pp. 36–44.

- Taylor, M. A. P., Sekhar, S. V. C. and D'Este, G. M. (2006) 'Application of accessibility based methods for vulnerability analysis of strategic road networks', *Networks and Spatial Economics*, 6(3-4), pp. 267-291.
- Thomas Steven Savage, J. *et al.* (2016) 'Quantifying the importance of spatial resolution and other factors through global sensitivity analysis of a flood inundation model', *Water Resources Research*, 52(11), pp. 9146-9163.
- Tolliver, D. and Lu, P. (2012) 'Analysis of bridge deterioration rates: A case study of the northern plains region', in *Journal of the Transportation Research Forum*.
- Tsubaki, R. *et al.* (2016) 'Development of fragility curves for railway embankment and ballast scour due to overtopping flood flow', *Natural Hazards and Earth System Sciences*, 16(12), p. 2455.
- Tubaldi, E. *et al.* (2017) 'A framework for probabilistic assessment of clear-water scour around bridge piers', *Structural safety*, 69, pp. 11-22.
- Turner, D. (2016) *Fragility assessment of bridge superstructures under hydrodynamic forces*. Colorado State University. Libraries.
- Tuutti, K. (1982) *Corrosion of steel in concrete*. Cement- och betonginst.
- USACE (2016) 'HEC-RAS River Analysis System Hydraulic Reference Manual. Version 5.0'. Hydrologic Engineering Center Davis.
- Varnes, D. J. (1984) *Landslide hazard zonation: a review of principles and practice*.
- Vijayasree, B. A. *et al.* (2019) 'Influence of bridge pier shape on flow field and scour geometry', *International Journal of River Basin Management*, 17(1), pp. 109-129.
- Vu, K. A. T. and Stewart, M. G. (2000) 'Structural reliability of concrete bridges including improved chloride-induced corrosion models', *Structural safety*, 22(4), pp. 313-333.
- Van Wagner, C. E., Forest, P. and others (1987) 'Development and structure of the canadian forest fireweather index system', in *Can. For. Serv., Forestry Tech. Rep.*
- WHO (2013) *Health risks of air pollution in Europe - HRAPIE project. Recommendations for concentration-response functions for cost-benefit analysis of particulate matter, ozone and nitrogen dioxide*. Copenhagen.
- Wisniewski, D., Ferreira, R. M. and Cruz, P. J. S. (2006) *Properties of Ready-Mixed Concretes- Report 06-DEC/E-11*.
- Yang, Y. *et al.* (2019) 'Local Scour at Complex Bridge Piers in Close Proximity under Clear-Water and Live-Bed Flow Regime', *Water*, 11(8), p. 1530.
- Yilmaz, T., Banerjee, S. and Johnson, P. A. (2018) 'Uncertainty in risk of highway bridges assessed for integrated seismic and flood hazards', *Structure and Infrastructure Engineering*, 14(9), pp. 1182-1196.
- Zampieri, P. *et al.* (2017) 'Failure analysis of masonry arch bridges subject to local pier scour', *Engineering failure analysis*, 79, pp. 371-384.
- Zhang, H. and Marsh, D. W. R. (2019) 'Multi-State Deterioration Prediction for

---

Infrastructure Asset: Learning from Uncertain Data, Knowledge and Similar Groups', *Information Sciences*.

Zheng, Y.-J. and Ling, H.-F. (2013) 'Emergency transportation planning in disaster relief supply chain management: a cooperative fuzzy optimization approach', *Soft Computing*, 17(7), pp. 1301–1314.

Zhu, H.-H., Shi, B. and Zhang, C.-C. (2017) 'FBG-based monitoring of geohazards: current status and trends', *Sensors*, 17(3), p. 452.





# SAFEWAY

## GIS-BASED INFRASTRUCTURE MANAGEMENT SYSTEM FOR OPTIMIZED RESPONSE TO EXTREME EVENTS OF TERRESTRIAL TRANSPORT NETWORKS

**Grant Agreement No. 769255**

### **Dynamic Risk-based Predictive Models - Appendices**

WP 5

Predictive Models

|                         |   |
|-------------------------|---|
| <b>Deliverable ID</b>   | <b>D5.1</b>                                 |
| <b>Deliverable name</b> | <b>Dynamic Risk-based Predictive Models</b> |
| Lead partner            | UMINHO                                      |
| Contributors            | NGI, TØI, UCAM, IMC                         |

**PUBLIC**

#### PROPRIETARY RIGHTS STATEMENT

This document contains information, which is proprietary to the SAFEWAY Consortium. Neither this document nor the information contained herein shall be used, duplicated or communicated by any means to any third party, in whole or in parts, except with prior written consent of the SAFEWAY Consortium.



---

## Appendices Content

- **Appendix 1: Deterministic Models**
- **Appendix 2: Stochastic Models**
- **Appendix 3: Fragility Functions**
- **Appendix 4: Population Changes**

## Appendix 1. Deterministic Models

### A.1.1. Correlation analysis for Pavements

The variables considered in the database are summarized in Table 1- 1 with their respective characteristics.

**Table 1- 1. Independent variables**

| Variable                           | Type        | Measure |
|------------------------------------|-------------|---------|
| Inspection Year                    | Numerical   | Scale   |
| Average Daily Truck Traffic (ADTT) | Numerical   | Scale   |
| Average Daily Traffic (ADT)        | Numerical   | Scale   |
| Year built                         | Numerical   | Scale   |
| Age at inspection                  | Numerical   | Scale   |
| Type of road                       | Categorical | Nominal |
| Type of Region                     | Categorical | Nominal |

In order to establish a correlation among different variables with Quality index is necessary to test the variables normality. The normality was verified with Kolmogorov-Smirnov test how is shown in Table 1- 2, with p-values less than the level of significance 5%. Therefore the null hypothesis of normality is rejected, it means, none of the variables follows a normal distribution.

**Table 1- 2. Normality test**

| Variable          | Statistic | df    | Sig.  |
|-------------------|-----------|-------|-------|
| Inspection Year   | 0.156     | 20061 | 0.000 |
| Quality Index     | 0.083     | 20061 | 0.000 |
| tmda2012          | 0.129     | 20061 | 0.000 |
| tmda pes12        | 0.140     | 20061 | 0.000 |
| Year built        | 0.209     | 20061 | 0.000 |
| Age at inspection | 0.131     | 20061 | 0.000 |

Consequently, Spearman's rho correlation is selected to establish the degree of relationship between the variables. Statistical results are summarized in Table 1- 3.

**Table 1- 3. Spearman correlations between Quality Index and other variables**

|                 | Correlation coefficient | Sig. (2-tailed) | N     |
|-----------------|-------------------------|-----------------|-------|
| Inspection Year | -0.004                  | 0.601           | 20270 |
| ADTT            | 0.085**                 | 0.000           | 20270 |
| ADT             | 0.101**                 | 0.000           | 20270 |

|                   |          |       |       |
|-------------------|----------|-------|-------|
| Year built        | -0.143** | 0.000 | 20061 |
| Age at inspection | 0.117**  | 0.000 | 20061 |

\*\* Correlation is significant at the level 0.01 (2-tailed).

The table above shows a minimum level of correlation between QI and the other variables, due to values present for these correlations are less than 0.3. Therefore, it means that there is a minimum dependence for these variables with QI. However, the significances of the established correlations with a p-value lower than 0,01 indicate that the correlations are statistically significant, except for the Inspection Year (p-value > 0.05).

### A.1.2. Regression analysis for Pavements

Since the main objective is to formulate a pavement degradation model over time, the QI and Age at inspection variables will be considered. Simple linear regression analysis was conducted with Quality index as a dependent variable or response (Y) and Age at inspection as an independent or regressor variable. The results obtain for simple linear regression are shown in Table 1- 4.

**Table 1- 4. Regression model for complete database**

| Equation    | Model Summary |        |     |       | Parameter Estimates |       |        |           |
|-------------|---------------|--------|-----|-------|---------------------|-------|--------|-----------|
|             | R Square      | F      | df1 | Sig.  | Constant            | b1    | b2     | b3        |
| Lineal      | 0.064         | 81.385 | 1   | 0.000 | 3.164               | 0.007 |        |           |
| Quadratic   | 0.086         | 74.336 | 2   | 0.000 | 3.121               | 0.022 | -0.001 |           |
| Cubic       | 0.097         | 63.645 | 3   | 0.000 | 3.160               | 0.000 | 0.001  | -5.21E-05 |
| Power       | 0.048         | 46.934 | 1   | 0.000 | 3.103               | 1.002 |        |           |
| Growth      | 0.048         | 46.934 | 1   | 0.000 | 1.132               | 0.002 |        |           |
| Exponential | 0.048         | 46.934 | 1   | 0.000 | 3.103               | 0.002 |        |           |
| Logistic    | 0.048         | 46.934 | 1   | 0.000 | 0.322               | 0.998 |        |           |

Independent variable: Age at Inspection

Dependent variable: Quality Index

However, the R<sup>2</sup> values showed for the different type of equation are low, even when all are statistically significant. It means that the model does not fit well with the data as is shown in Figure 1- 1.

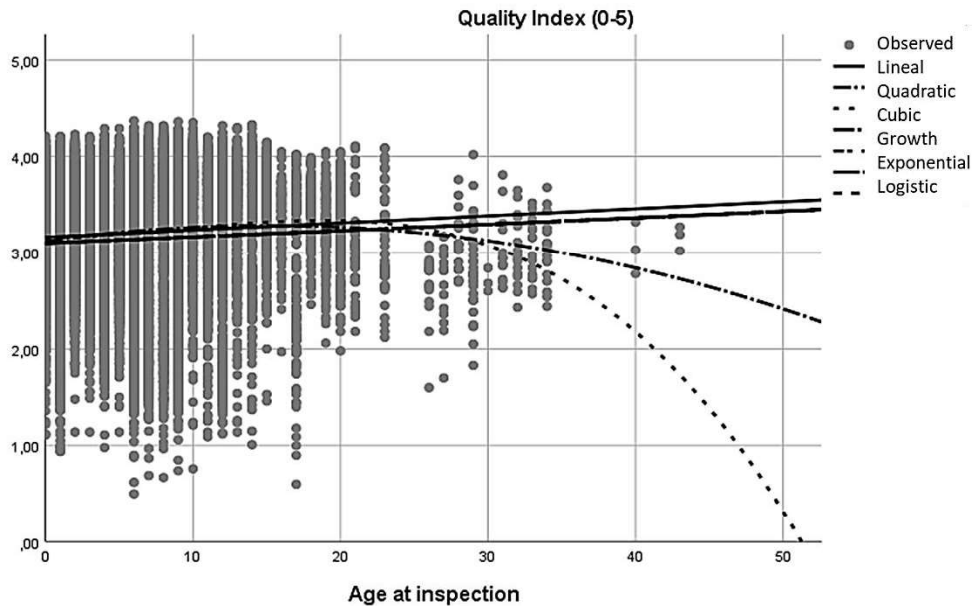


**Figure 1- 1. Regression**

Therefore, in order to obtain predictive models with enough accuracy, several clusters were applied. These filters have the objective of eliminate missing, duplicate or active data with important maintenance actions and obtain a reliable data set for deterioration models. The database was cluster by region, type of road and AADT. Is important to mention that into the AADT classification there are three different ranges AADT>2500, 2500<AADT<7500 and AADT>7500. For a total of 45 combinations, as is shown in Figure 1- 2.



**Figure 1- 2. Different clusters for regression models**

Posterior, model regressions were applied and compared regarding  $R^2$  value, in order to select the model that best fits with the data. Each of the mentioned cases is shown below, summarized in table 1 - 5 to 1 - 22, considering the different types of models, the respective coefficients,  $R^2$  value and F-test value.



**Table 1- 5. Regression models for National road, Coimbra and AADT<2500**

| Equation    | Model Summary |         |     |       | Parameter Estimates |        |       |
|-------------|---------------|---------|-----|-------|---------------------|--------|-------|
|             | R Square      | F       | df1 | Sig.  | Constant            | b1     | b2    |
| Lineal      | 0.962         | 62.580  | 1   | 0.001 | 5.84                | -0.236 |       |
| Quadratic   | 0.982         | 53.707  | 2   | 0.001 | 9.693               | -0.825 | 0.220 |
| Cubic       | 0.982         | 55.554  | 2   | 0.001 | 8.467               | -0.539 | 0.001 |
| Compound    | 0.974         | 93.396  | 1   | 0.000 | 8.448               | 0.916  |       |
| Power       | 0.981         | 125.305 | 1   | 0.000 | 51.859              | -1.156 |       |
| Exponential | 0.974         | 93.396  | 1   | 0.000 | 8.448               | -0.087 |       |
| Logistic    | 0.974         | 93.396  | 1   | 0.000 | 0.118               | 1.091  |       |
| Logarithmic | 0.974         | 94.035  | 1   | 0.000 | 10.798              | -3.146 |       |
| Reverse     | 0.979         | 116.534 | 1   | 0.000 | -0.439              | 40.594 |       |
| Growth      | 0.974         | 93.396  | 1   | 0.000 | 2.134               | -0.087 |       |
| S           | 0.980         | 119.008 | 1   | 0.000 | -0.173              | 14.827 |       |

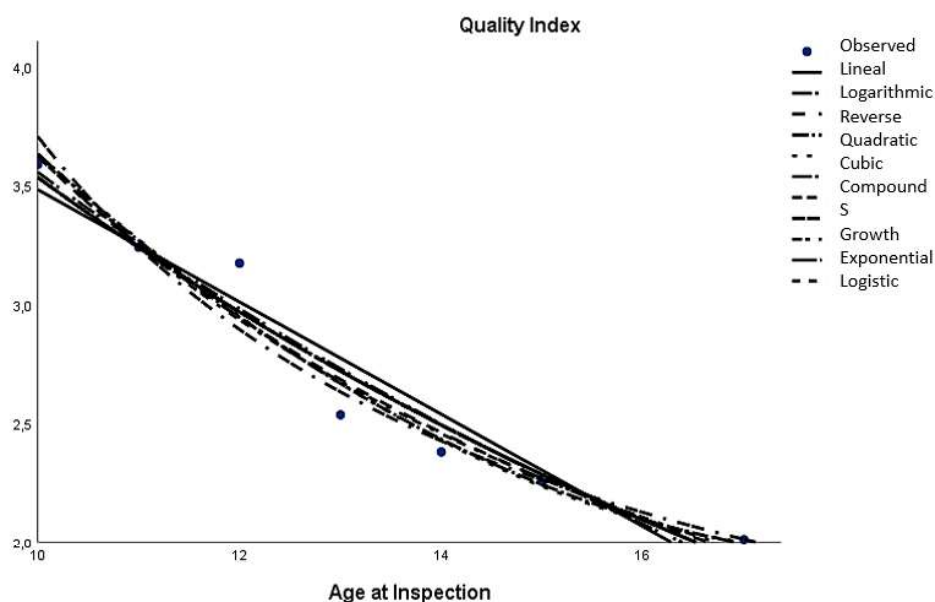


**Table 1- 6. Regression models for National roads, Leiria and AADT<2500**

| Equation    | Model Summary |        |     |       | Parameter Estimates |        |       |        |
|-------------|---------------|--------|-----|-------|---------------------|--------|-------|--------|
|             | R Square      | F      | df1 | Sig.  | Constant            | b1     | b2    | b3     |
| Lineal      | 0.975         | 38.108 | 1   | 0.025 | 3.457               | -0.046 |       |        |
| Quadratic   | 0.996         | 59.664 | 2   | 0.091 | 3.468               | -0.079 | 0.011 |        |
| Cubic       | 1.000         |        | 3   |       | 3.470               | -0.113 | 0.043 | -0.007 |
| Compound    | 0.976         | 40.316 | 1   | 0.024 | 3.457               | 0.986  |       |        |
| Exponential | 0.976         | 40.316 | 1   | 0.024 | 3.457               | -0.014 |       |        |
| logarithmic | 0.976         | 40.316 | 1   | 0.024 | 0.289               | 1.014  |       |        |
| Growth      | 0.976         | 40.316 | 1   | 0.024 | 1.240               | -0.014 |       |        |

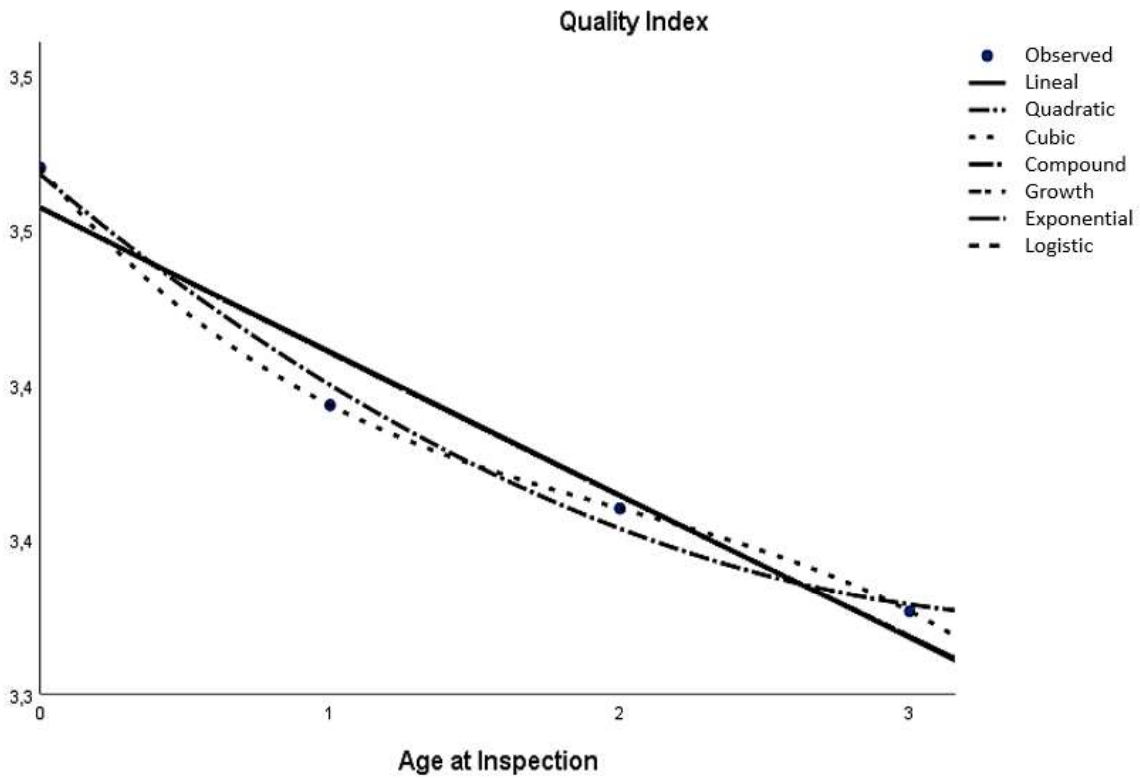


**Table 1- 7. Regression models for National roads, Santarem and AADT<2500**

| Equation    | Model Summary |         |     |       | Parameter Estimates |        |        |       |
|-------------|---------------|---------|-----|-------|---------------------|--------|--------|-------|
|             | R Square      | F       | df1 | Sig.  | Constant            | b1     | b2     | b3    |
| Lineal      | 0.987         | 195.337 | 1   | 0.000 | 3.366               | -0.186 |        |       |
| Quadratic   | 0.989         | 92.962  | 2   | 0.000 | 3.400               | -0.227 | 0.007  |       |
| Cubic       | 0.990         | 48.62   | 3   | 0.005 | 3.387               | -0.186 | -0.012 | 0.002 |
| Compound    | 0.988         | 208.478 | 1   | 0.000 | 3.396               | 0.936  |        |       |
| Exponential | 0.988         | 208.478 | 1   | 0.000 | 3.396               | -0.066 |        |       |
| logarithmic | 0.988         | 208.478 | 1   | 0.000 | 0.294               | 1.069  |        |       |
| Growth      | 0.988         | 208.478 | 1   | 0.000 | 1.223               | -0.066 |        |       |

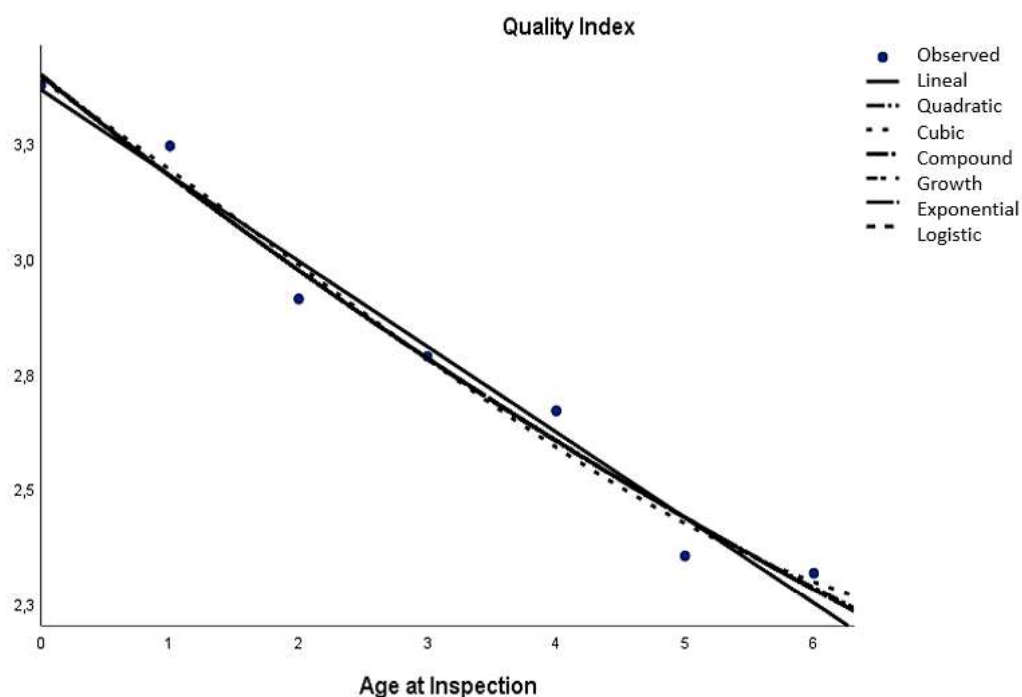


**Table 1- 8. Regression models for National roads, Leiria and 2500 < AADT < 7500**

| Equation    | Model Summary |         |     |       | Parameter Estimates |        |          |
|-------------|---------------|---------|-----|-------|---------------------|--------|----------|
|             | R Square      | F       | df1 | Sig.  | Constant            | b1     | b2       |
| Lineal      | 0.991         | 111.061 | 1   | 0.009 | 5.000               | -0.085 |          |
| Quadratic   | 0.992         | 31.511  | 2   | 0.125 | 6.492               | -0.247 | 0.004    |
| Cubic       | 0.992         | 31.799  | 2   | 0.124 | 6.029               | -0.169 | 8.14E-05 |
| Compound    | 0.991         | 114.28  | 1   | 0.009 | 5.423               | 0.975  |          |
| Exponential | 0.991         | 114.28  | 1   | 0.009 | 5.423               | -0.025 |          |
| logarithmic | 0.992         | 121.25  | 1   | 0.008 | 8.015               | -1.575 |          |
| Growth      | 0.991         | 114.28  | 1   | 0.009 | 1.691               | -0.025 |          |
| Reverse     | 0.992         | 122.503 | 1   | 0.008 | 1.850               | 28.992 |          |
| Power       | 0.992         | 121.785 | 1   | 0.008 | 13.073              | -0.460 |          |
| S           | 0.992         | 119.849 | 1   | 0.008 | 0.771               | 8.461  |          |
| Logistic    | 0.991         | 114.28  | 1   | 0.009 | 0.184               | 1.025  |          |

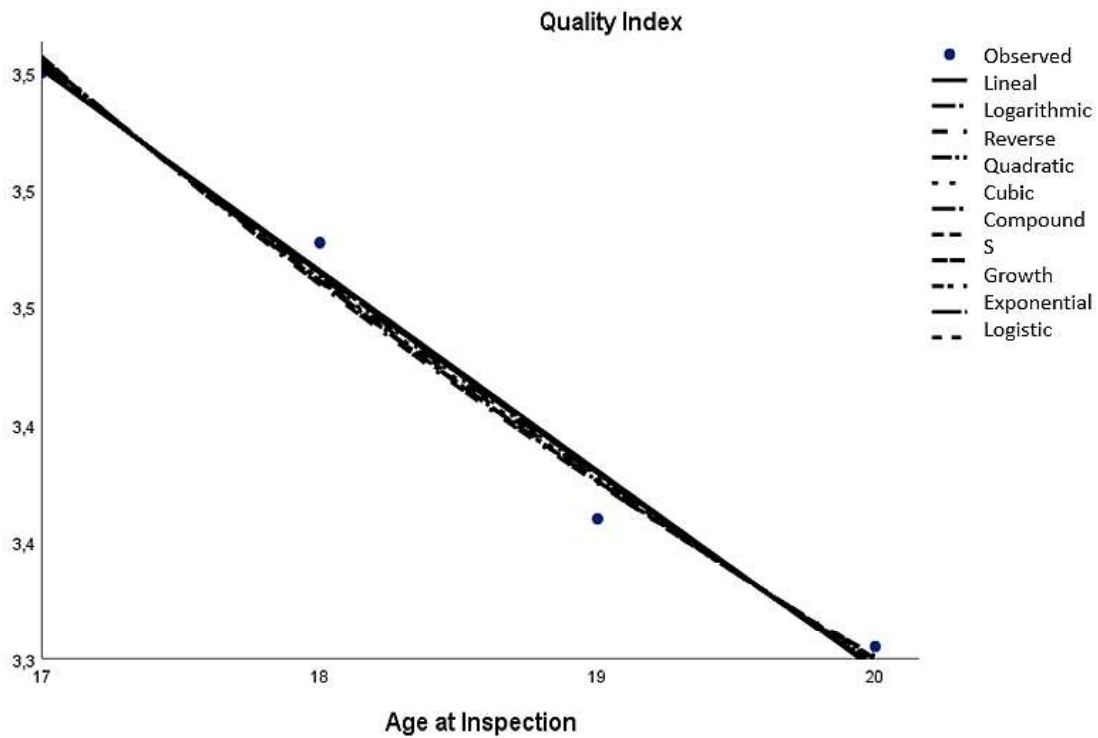


**Table 1- 9. Regression models for National roads, Santarem and 2500 < AADT < 7500**

| Equation    | Model Summary |          |     |       | Parameter Estimates |        |        |          |
|-------------|---------------|----------|-----|-------|---------------------|--------|--------|----------|
|             | R Square      | F        | df1 | Sig.  | Constant            | b1     | b2     | b3       |
| Lineal      | 0.998         | 1616,481 | 1   | 0.000 | 3.397               | -0.087 |        |          |
| Quadratic   | 0.998         | 696.731  | 2   | 0.000 | 3.401               | -0.089 | 0.000  |          |
| Cubic       | 0.998         | 388.242  | 3   | 0.000 | 3.397               | -0.085 | -0.001 | 4.75E-05 |
| Compound    | 0.997         | 1280.328 | 1   | 0.000 | 3.427               | 0.971  |        |          |
| Exponential | 0.997         | 1280.328 | 1   | 0.000 | 3.427               | -0.030 |        |          |
| logarithmic | 0.947         | 60.887   | 1   | 0.000 | 3.426               | -0.330 |        |          |
| Growth      | 0.997         | 1280.328 | 1   | 0.000 | 1.232               | -0.030 |        |          |
| Reverse     | 0.804         | 12.778   | 1   | 0.009 | 2.727               | 0.719  |        |          |
| Power       | 0.935         | 48.534   | 1   | 0.000 | 3.454               | -0.112 |        |          |
| S           | 0.784         | 11.157   | 1   | 0.012 | 1.004               | 0.241  |        |          |
| Logistic    | 0.997         | 1280.328 | 1   | 0.000 | 0.292               | 1.030  |        |          |

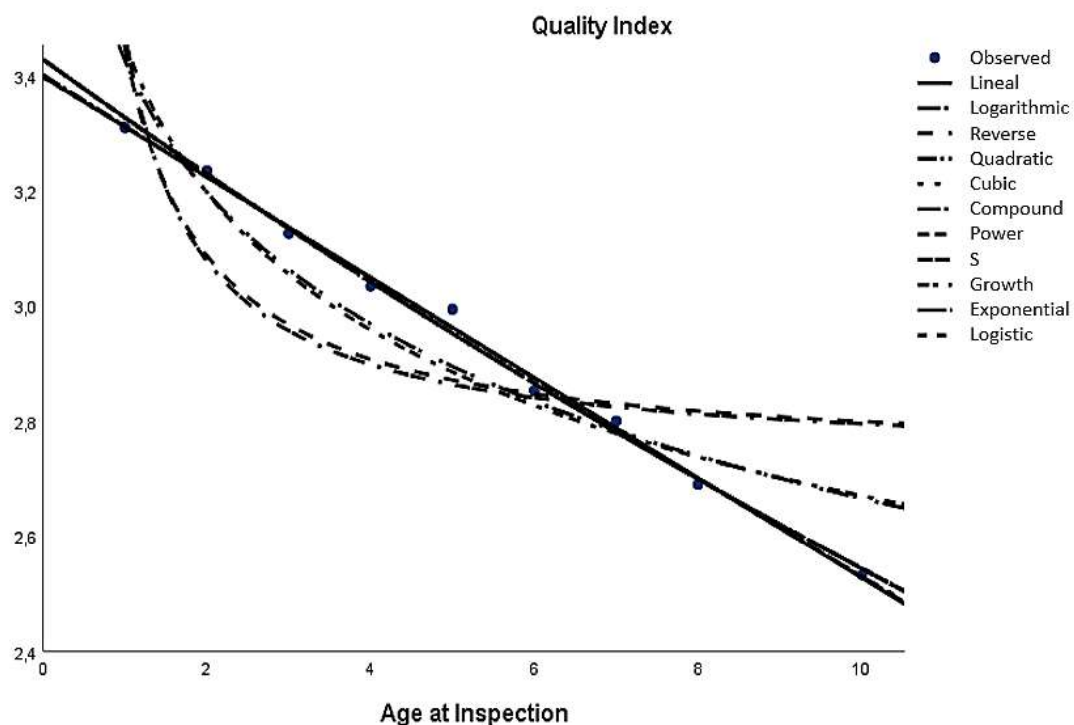


**Table 1- 10. Regression models for National roads, Santarem and AADT>7500**

| Equation    | Model Summary |          |     |       | Parameter Estimates |        |        |        |
|-------------|---------------|----------|-----|-------|---------------------|--------|--------|--------|
|             | R Square      | F        | df1 | Sig.  | Constant            | b1     | b2     | b3     |
| Lineal      | 0.956         | 31.902   | 1   | 0.011 | 3.585               | -0.057 |        |        |
| Quadratic   | 0.996         | 116.324  | 2   | 0.009 | 3.486               | 0.027  | -0.014 |        |
| Cubic       | 1.000         | 3719.259 | 3   | 0.012 | 3.563               | -0.081 | 0.027  | -0.005 |
| Compound    | 0.953         | 29.690   | 1   | 0.012 | 3.589               | 0.983  |        |        |
| Exponential | 0.953         | 29.690   | 1   | 0.012 | 3.589               | -0.017 |        |        |
| logarithmic | 0.874         | 9.670    | 1   | 0.053 | 3.538               | -0.130 |        |        |
| Growth      | 0.953         | 29.690   | 1   | 0.012 | 1.278               | -0.017 |        |        |
| Reverse     | 0.763         | 4.177    | 1   | 0.134 | 3.311               | 0.223  |        |        |
| Power       | 0.869         | 9.257    | 1   | 0.056 | 3.539               | -0.038 |        |        |
| Logistic    | 0.953         | 29.690   | 1   | 0.012 | 0.279               | 1.017  |        |        |

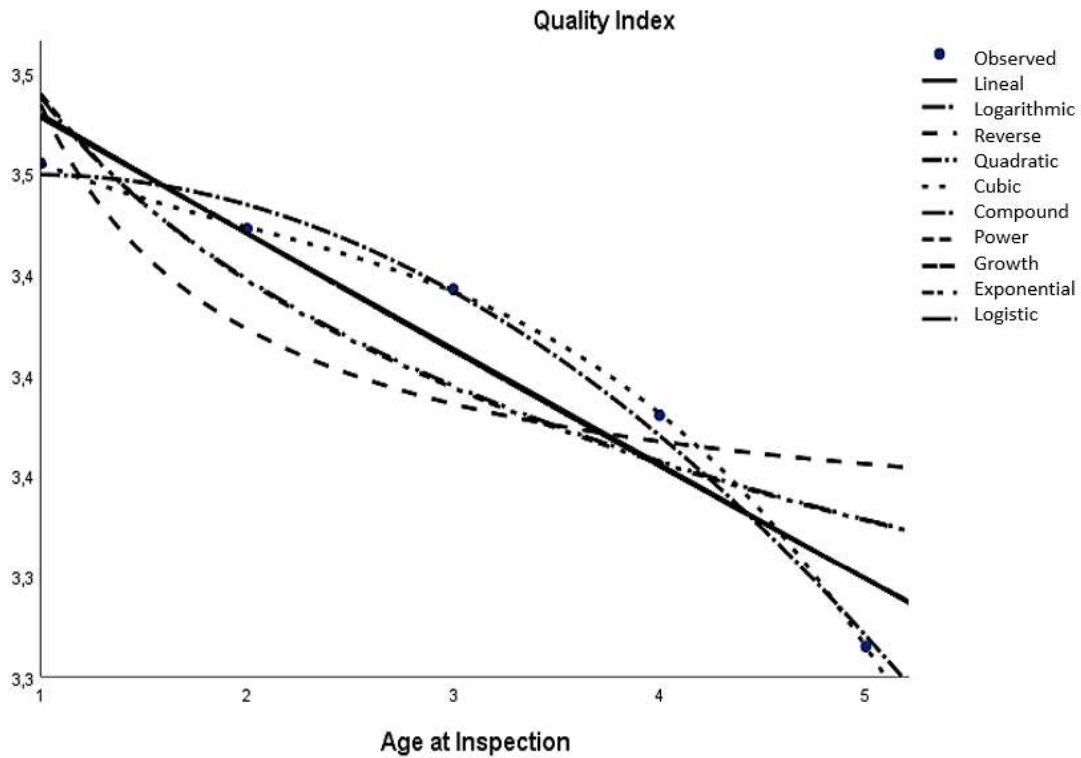


**Table 1- 11. Regression models for disqualified national roads, Santarem and AADT<2500**

| Equation    | Model Summary |        |     |       | Parameter Estimates |        |        |       |
|-------------|---------------|--------|-----|-------|---------------------|--------|--------|-------|
|             | R Square      | F      | df1 | Sig.  | Constant            | b1     | b2     | b3    |
| Lineal      | 0.986         | 69.808 | 1   | 0.014 | 3.200               | -0.053 |        |       |
| Quadratic   | 0.996         | 64.047 | 2   | 0.088 | 3.249               | -0.093 | 0.006  |       |
| Cubic       | 1.000         |        | 3   |       | 3.175               | 0.003  | -0.027 | 0.003 |
| Compound    | 0.987         | 75.891 | 1   | 0.013 | 3.204               | 0.982  |        |       |
| Exponential | 0.987         | 75.891 | 1   | 0.013 | 3.204               | -0.018 |        |       |
| logarithmic | 0.984         | 61.321 | 1   | 0.016 | 3.172               | -0.150 |        |       |
| Growth      | 0.987         | 75.891 | 1   | 0.013 | 1.164               | -0.018 |        |       |
| Reverse     | 0.922         | 11.271 | 1   | 0.078 | 2.885               | 0.296  |        |       |
| Power       | 0.983         | 57.368 | 1   | 0.017 | 3.174               | -0.050 |        |       |
| Logistic    | 0.987         | 75.891 | 1   | 0.013 | 0.312               | 1.018  |        |       |
| S           | 0.919         | 10.800 | 1   | 0.081 | 1.060               | 0.097  |        |       |



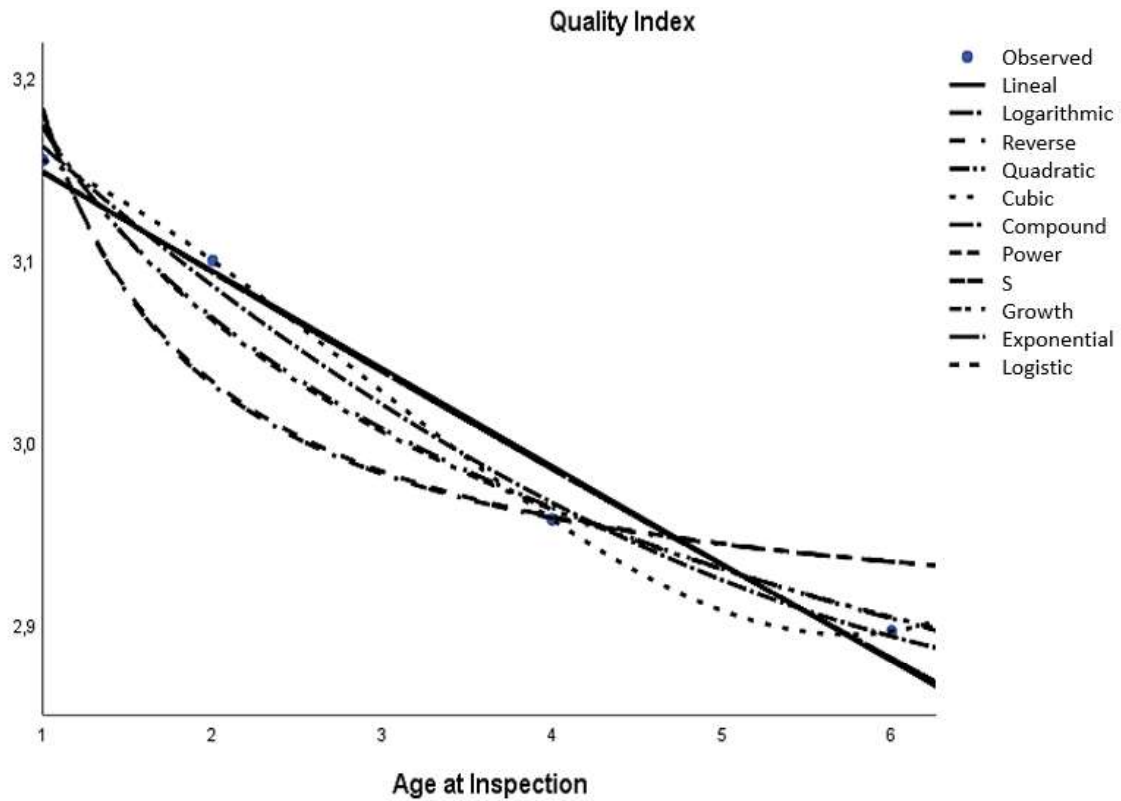


**Table 1- 12. Regression models for disqualified national roads, Santarem and 2500<AADT<7500**

| Equation    | Model Summary |          |     |       | Parameter Estimates |        |        |       |
|-------------|---------------|----------|-----|-------|---------------------|--------|--------|-------|
|             | R Square      | F        | df1 | Sig.  | Constant            | b1     | b2     | b3    |
| Lineal      | 0.998         | 1085.799 | 1   | 0.000 | 3.301               | -0.138 |        |       |
| Quadratic   | 0.998         | 485.218  | 2   | 0.000 | 3.312               | -0.149 | 0.001  |       |
| Cubic       | 1.000         | 3565.285 | 3   | 0.000 | 3.287               | -0.081 | -0.018 | 0.001 |
| Compound    | 0.998         | 927.709  | 1   | 0.000 | 3.333               | 0.950  |        |       |
| Exponential | 0.998         | 927.709  | 1   | 0.000 | 3.333               | -0.051 |        |       |
| Growth      | 0.998         | 927.709  | 1   | 0.000 | 1.204               | -0.051 |        |       |
| Logistic    | 0.998         | 927.709  | 1   | 0.000 | 0.300               | 1.053  |        |       |

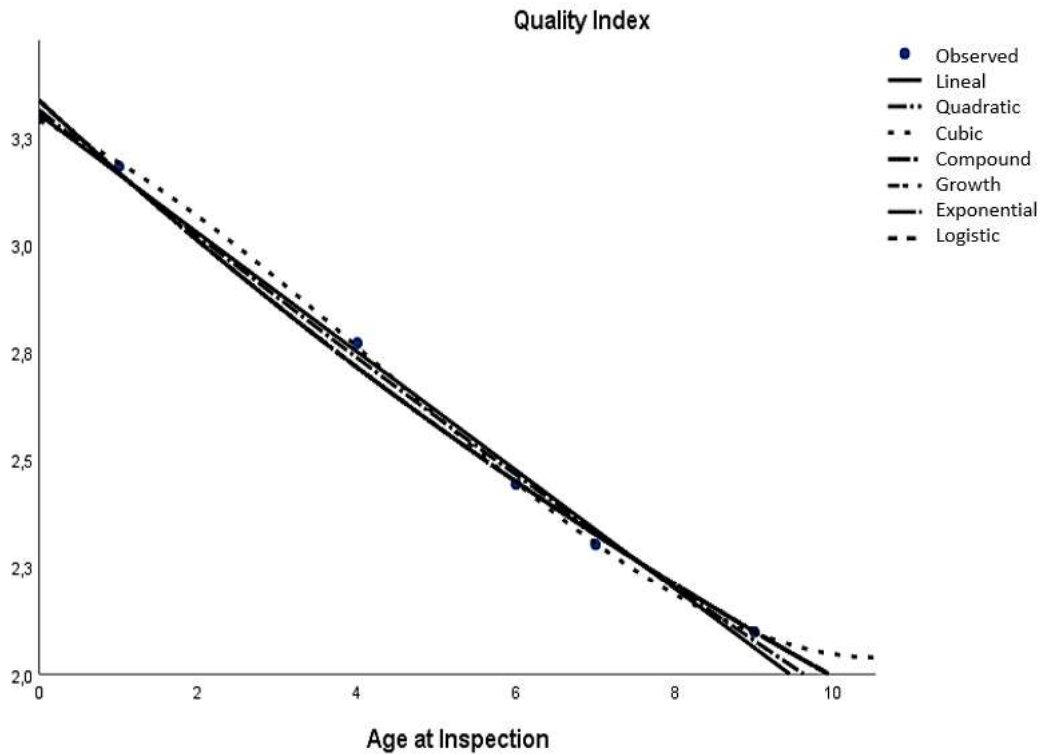


**Table 1- 13. Regression models for disqualified national roads, Santarem and AADT>7500**

| Equation    | Model Summary |         |     |       | Parameter Estimates |        |       |        |
|-------------|---------------|---------|-----|-------|---------------------|--------|-------|--------|
|             | R Square      | F       | df1 | Sig.  | Constant            | b1     | b2    | b3     |
| Lineal      | 0.996         | 238.809 | 1   | 0.004 | 3.779               | -0.058 |       |        |
| Quadratic   | 0.997         | 88.245  | 2   | 0.075 | 3.784               | -0.069 | 0.003 |        |
| Cubic       | 1.000         |         | 3   |       | 3.787               | -0.109 | 0.035 | -0.006 |
| Compound    | 0.996         | 277.761 | 1   | 0.004 | 3.779               | 0.984  |       |        |
| Exponential | 0.996         | 277.761 | 1   | 0.004 | 3.779               | -0.016 |       |        |
| Growth      | 0.996         | 277.761 | 1   | 0.004 | 1.330               | -0.016 |       |        |
| Logistic    | 0.996         | 277.761 | 1   | 0.004 | 0.265               | 1.016  |       |        |

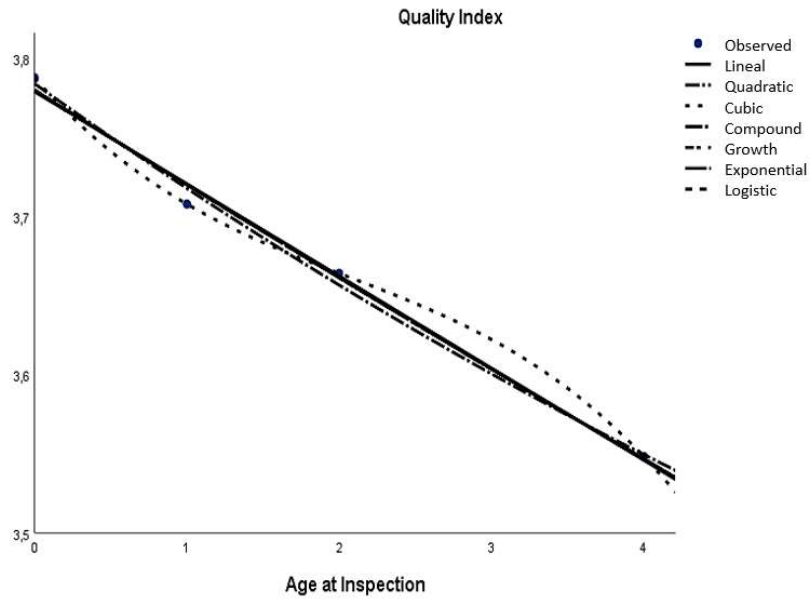


**Table 1- 14. Regression models for Regional roads, Coimbra and AADT<2500**

| Equation    | Model Summary |         |     |       | Parameter Estimates |        |       |
|-------------|---------------|---------|-----|-------|---------------------|--------|-------|
|             | R Square      | F       | df1 | Sig.  | Constant            | b1     | b2    |
| Lineal      | 0.995         | 284.675 | 1   | 0.000 | 2.848               | -0.031 |       |
| Quadratic   | 0.998         | 215.381 | 2   | 0.005 | 2.950               | -0.055 | 0.001 |
| Cubic       | 0.998         | 234.715 | 2   | 0.004 | 2.922               | -0.045 | 0.000 |
| Compound    | 0.996         | 333.495 | 1   | 0.000 | 2.863               | 0.988  |       |
| Exponential | 0.996         | 333.495 | 1   | 0.000 | 2.863               | -0.012 |       |
| logarithmic | 0.996         | 424.735 | 1   | 0.000 | 3.163               | -0.276 |       |
| Growth      | 0.996         | 333.495 | 1   | 0.000 | 1.052               | -0.012 |       |
| Reverse     | 0.985         | 97.940  | 1   | 0.002 | 2.298               | 2.274  |       |
| Power       | 0.996         | 378.098 | 1   | 0.000 | 3.237               | -0.107 |       |
| Logistic    | 0.996         | 333.495 | 1   | 0.000 | 0.349               | 1.012  |       |
| S           | 0.983         | 88.082  | 1   | 0.003 | 0.838               | 0.885  |       |

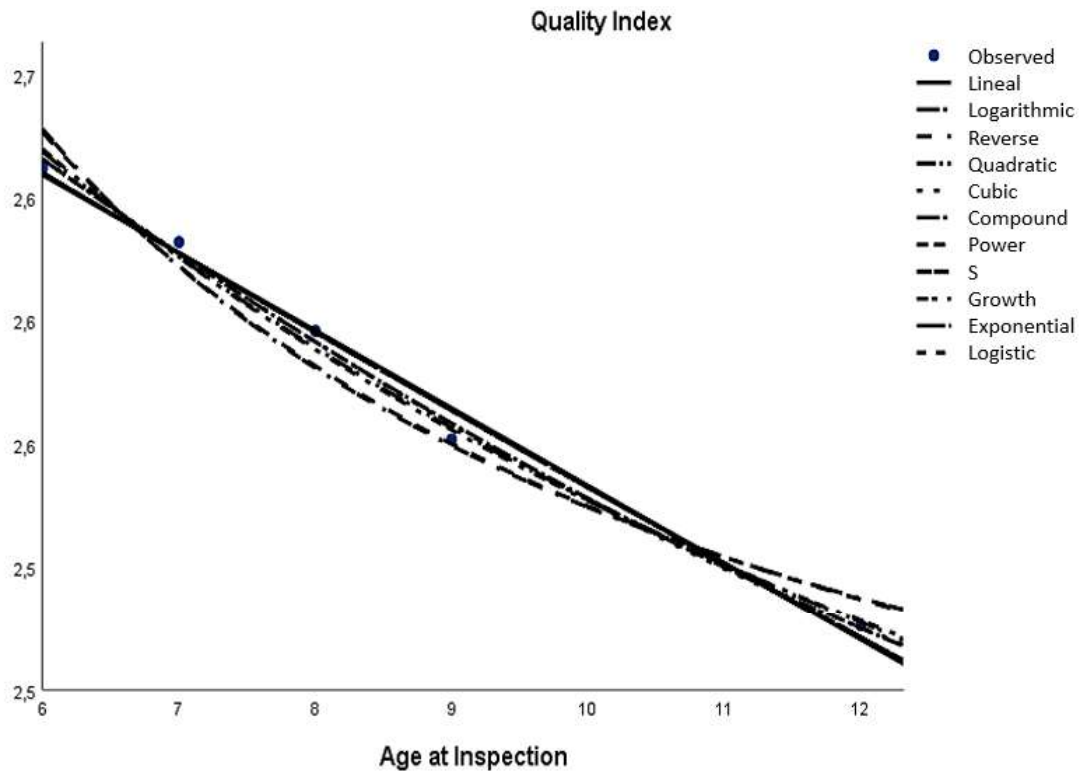


**Table 1- 15. Regression models for Regional roads, Leiria and AADT<2500**

| Equation    | Model Summary |         |     |       | Parameter Estimates |        |       |
|-------------|---------------|---------|-----|-------|---------------------|--------|-------|
|             | R Square      | F       | df1 | Sig.  | Constant            | b1     | b2    |
| Lineal      | 0.997         | 486.961 | 1   | 0.000 | 4.449               | -0.079 |       |
| Quadratic   | 0.997         | 163.101 | 2   | 0.006 | 4.410               | -0.073 | 0.000 |
| Cubic       | 0.997         | 163.101 | 2   | 0.006 | 4.410               | -0.073 | 0.000 |
| Compound    | 0.997         | 489.383 | 1   | 0.000 | 4.619               | 0.977  |       |
| Exponential | 0.997         | 489.383 | 1   | 0.000 | 4.619               | -0.023 |       |
| logarithmic | 0.994         | 229.759 | 1   | 0.001 | 6.005               | -1.012 |       |
| Growth      | 0.997         | 489.383 | 1   | 0.000 | 1.530               | -0.023 |       |
| Reverse     | 0.984         | 92.204  | 1   | 0.002 | 2.427               | 12.612 |       |
| Power       | 0.992         | 188.079 | 1   | 0.001 | 7.282               | -0.296 |       |
| Logistic    | 0.997         | 489.383 | 1   | 0.000 | 0.216               | 1.023  |       |
| S           | 0.981         | 77.827  | 1   | 0.003 | 0.938               | 3.688  |       |

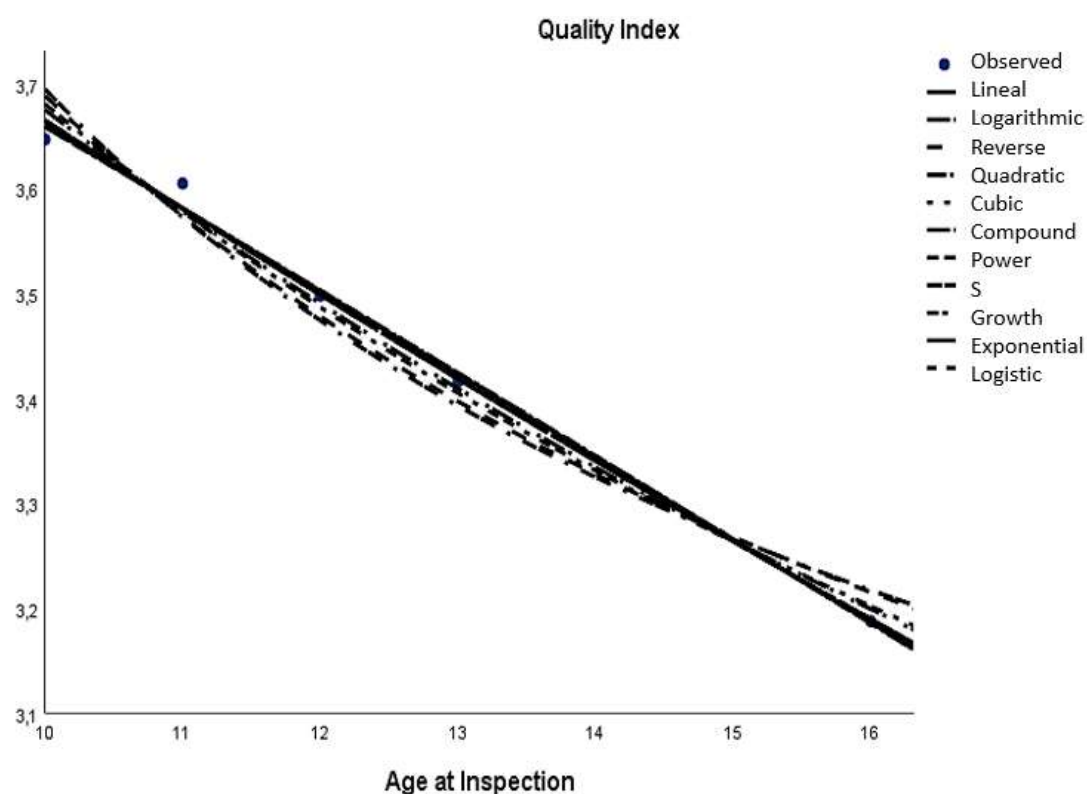


**Table 1- 16. Regression models for Regional roads, Santarem and 2500<AADT<7500**

| Equation    | Model Summary |        |     |       | Parameter Estimates |        |       |
|-------------|---------------|--------|-----|-------|---------------------|--------|-------|
|             | R Square      | F      | df1 | Sig.  | Constant            | b1     | b2    |
| Lineal      | 0.957         | 29.109 | 1   | 0.033 | 3.399               | -0.067 |       |
| Quadratic   | 0.979         | 11.286 | 2   | 0.206 | 3.903               | -0.219 | 0.011 |
| Cubic       | 0.979         | 11.286 | 2   | 0.206 | 3.903               | -0.219 | 0.011 |
| Compound    | 0.970         | 31.752 | 1   | 0.030 | 3.435               | 0.977  |       |
| Exponential | 0.970         | 31.752 | 1   | 0.030 | 3.435               | -0.023 |       |
| logarithmic | 0.977         | 41.935 | 1   | 0.023 | 3.817               | -0.463 |       |
| Growth      | 0.970         | 31.752 | 1   | 0.030 | 1.234               | -0.023 |       |
| Reverse     | 0.983         | 58.517 | 1   | 0.017 | 2.465               | 3.081  |       |
| Power       | 0.979         | 45.027 | 1   | 0.021 | 3.958               | -0.157 |       |
| Logistic    | 0.970         | 31.752 | 1   | 0.030 | 0.291               | 1.023  |       |
| S           | 0.984         | 60.141 | 1   | 0.016 | 0.916               | 1.046  |       |

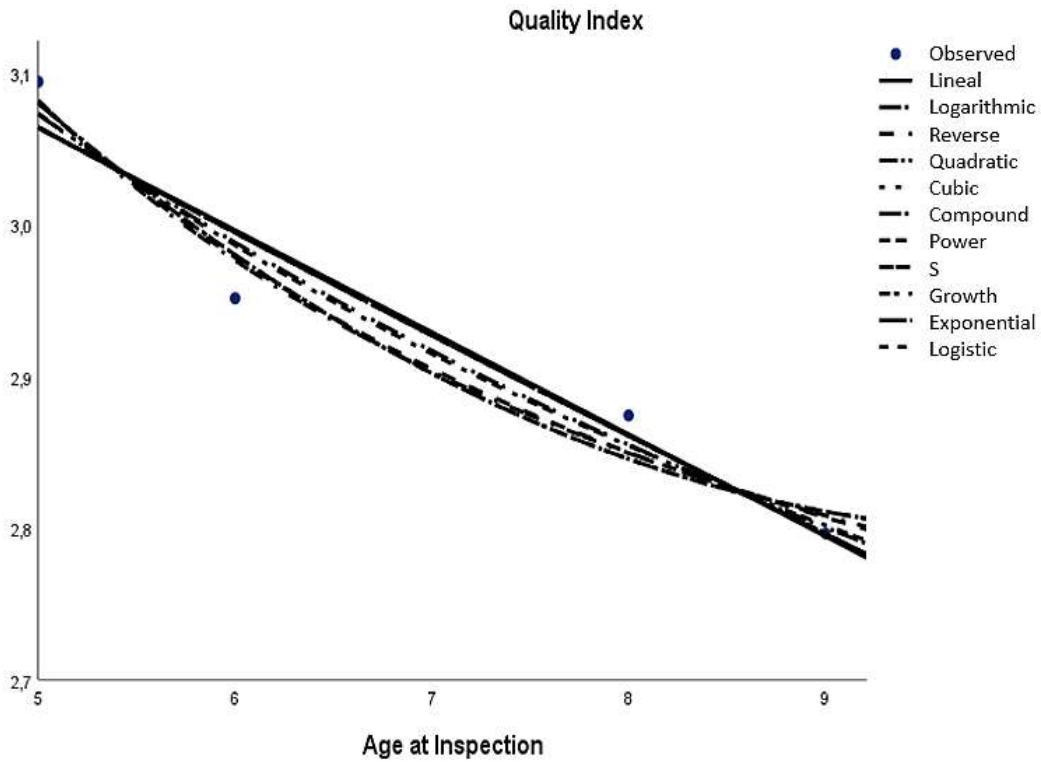


**Table 1- 17. Regression models for complementary routes, Leiria and AADT>7500**

| Equation    | Model Summary |         |     |       | Parameter Estimates |        |       |
|-------------|---------------|---------|-----|-------|---------------------|--------|-------|
|             | R Square      | F       | df1 | Sig.  | Constant            | b1     | b2    |
| Lineal      | 0.994         | 306.311 | 1   | 0.000 | 4.369               | -0.055 |       |
| Quadratic   | 0.994         | 118.978 | 2   | 0.001 | 4.451               | -0.070 | 0.001 |
| Cubic       | 0.994         | 118.978 | 2   | 0.001 | 4.451               | -0.070 | 0.001 |
| Compound    | 0.993         | 303.103 | 1   | 0.000 | 4.418               | 0.986  |       |
| Exponential | 0.993         | 303.103 | 1   | 0.000 | 4.418               | -0.015 |       |
| logarithmic | 0.993         | 268.284 | 1   | 0.000 | 5.172               | -0.591 |       |
| Growth      | 0.993         | 303.103 | 1   | 0.000 | 1.486               | -0.015 |       |
| Reverse     | 0.986         | 137.476 | 1   | 0.000 | 3.185               | 6.165  |       |
| Power       | 0.991         | 232.137 | 1   | 0.000 | 5.467               | -0.157 |       |
| Logistic    | 0.993         | 303.103 | 1   | 0.000 | 0.226               | 1.015  |       |
| S           | 0.984         | 118.658 | 1   | 0.000 | 1.171               | 1.635  |       |

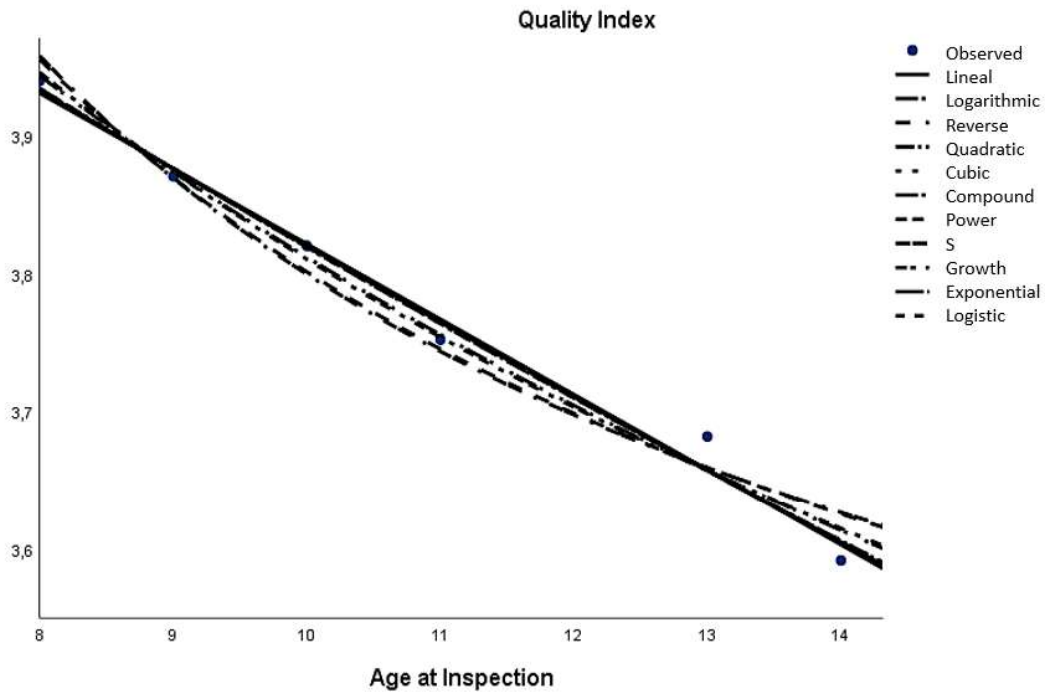


**Table 1- 18. Regression models for complementary routes, Santarem and AADT>7500**

| Equation    | Model Summary |         |     |       | Parameter Estimates |        |        |
|-------------|---------------|---------|-----|-------|---------------------|--------|--------|
|             | R Square      | F       | df1 | Sig.  | Constant            | b1     | b2     |
| Lineal      | 0.987         | 181.749 | 1   | 0.000 | 4.445               | -0.111 |        |
| Quadratic   | 0.995         | 187.206 | 2   | 0.000 | 3.807               | 0.038  | -0.008 |
| Cubic       | 0.995         | 187.206 | 2   | 0.000 | 3.807               | 0.038  | -0.008 |
| Compound    | 0.983         | 140.682 | 1   | 0.000 | 4.609               | 0.968  |        |
| Exponential | 0.983         | 140.682 | 1   | 0.000 | 4.609               | -0.033 |        |
| logarithmic | 0.969         | 76.558  | 1   | 0.000 | 5.505               | -0.949 |        |
| Growth      | 0.983         | 140.682 | 1   | 0.000 | 1.528               | -0.033 |        |
| Reverse     | 0.942         | 39.15   | 1   | 0.002 | 2.543               | 7.690  |        |
| Power       | 0.963         | 63.196  | 1   | 0.001 | 6.279               | -0.278 |        |
| Logistic    | 0.983         | 140.682 | 1   | 0.000 | 0.217               | 1.033  |        |
| S           | 0.933         | 33.731  | 1   | 0.002 | 0.972               | 2.243  |        |



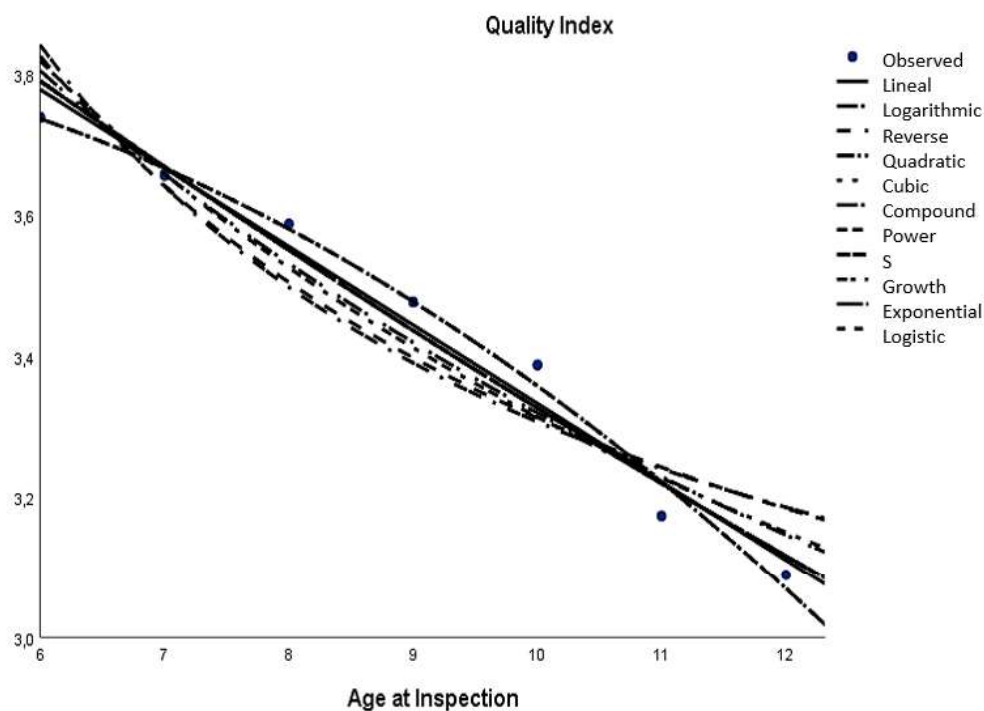


**Table 1- 19. Regression models for complementary routes, Santarem and 7500<AADT<12500**

| Equation    | Model Summary |        |     |       | Parameter Estimates |        |       |
|-------------|---------------|--------|-----|-------|---------------------|--------|-------|
|             | R Square      | F      | df1 | Sig.  | Constant            | b1     | b2    |
| Lineal      | 0.962         | 12.557 | 1   | 0.175 | 2.985               | -0.080 |       |
| Quadratic   | 1.000         |        | 2   |       | 2.998               | -0.157 | 0.039 |
| Cubic       | 1.000         |        |     |       | 2.998               | -0.132 | 0.013 |
| Compound    | 0.964         | 13.113 | 1   | 0.172 | 2.985               | 0.973  |       |
| Exponential | 0.964         | 13.113 | 1   | 0.172 | 2.985               | -0.027 |       |
| Growth      | 0.964         | 13.113 | 1   | 0.172 | 1.094               | -0.027 |       |
| Logistic    | 0.964         | 13.113 | 1   | 0.172 | 0.335               | 1.028  |       |

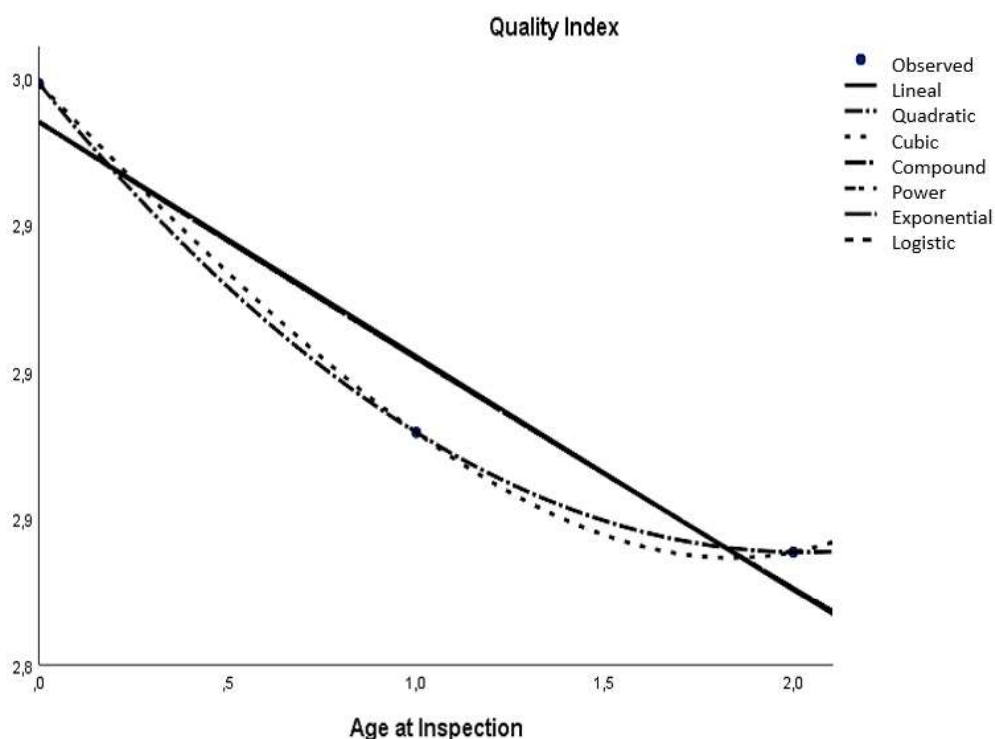


**Table 1- 20. Regression models for complementary routes, Santarem and AADT>12500**

| Equation    | Model Summary |         |     |       | Parameter Estimates |        |        |       |
|-------------|---------------|---------|-----|-------|---------------------|--------|--------|-------|
|             | R Square      | F       | df1 | Sig.  | Constant            | b1     | b2     | b3    |
| Lineal      | 0.984         | 210.759 | 1   | 0.000 | 3.397               | -0.103 |        |       |
| Quadratic   | 0.984         | 90.735  | 2   | 0.000 | 3.402               | -0.108 | 0.001  |       |
| Cubic       | 0.995         | 152.097 | 3   | 0.000 | 3.349               | 0.006  | -0.037 | 0.003 |
| Compound    | 0.984         | 220.500 | 1   | 0.000 | 3.414               | 0.966  |        |       |
| Exponential | 0.984         | 220.500 | 1   | 0.000 | 3.414               | -0.035 |        |       |
| Growth      | 0.984         | 220.500 | 1   | 0.000 | 1.228               | -0.035 |        |       |
| Logistic    | 0.984         | 220.500 | 1   | 0.000 | 0.293               | 1.035  |        |       |

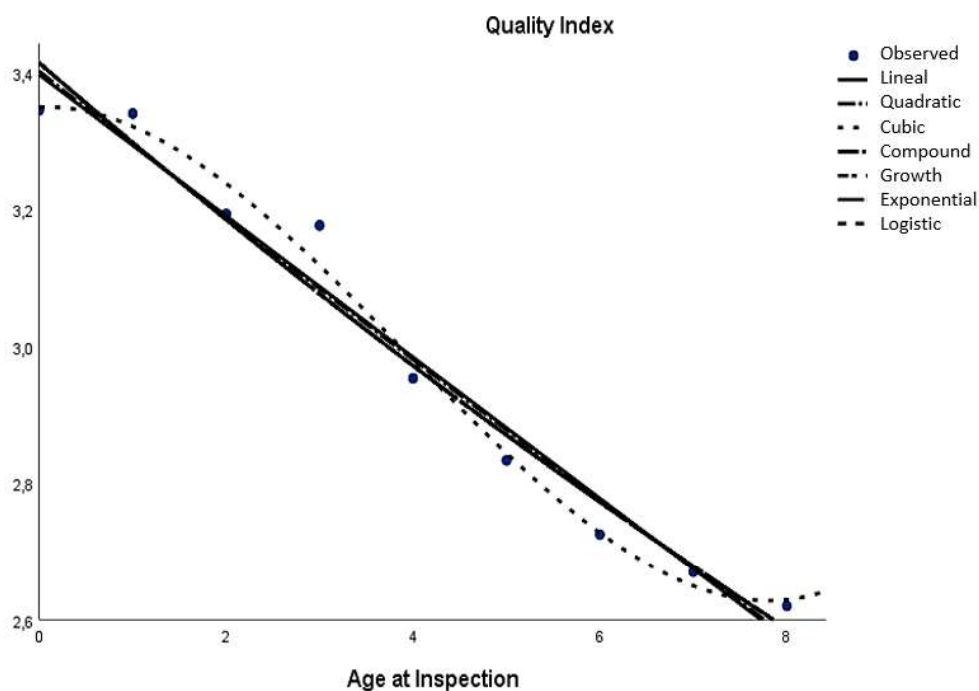


**Table 1- 21. Regression models for Principal routes, Santarem and 7500<AADT<12500**

| Equation    | Model Summary |         |     |       | Parameter Estimates |        |        |       |
|-------------|---------------|---------|-----|-------|---------------------|--------|--------|-------|
|             | R Square      | F       | df1 | Sig.  | Constant            | b1     | b2     | b3    |
| Lineal      | 0.995         | 400.244 | 1   | 0.000 | 3.728               | -0.080 |        |       |
| Quadratic   | 0.997         | 261.591 | 2   | 0.000 | 3.761               | -0.105 | 0.004  |       |
| Cubic       | 0.998         | 153.842 | 3   | 0.006 | 3.722               | -0.055 | -0.013 | 0.002 |
| Compound    | 0.996         | 477.248 | 1   | 0.000 | 3.737               | 0.977  |        |       |
| Exponential | 0.996         | 477.248 | 1   | 0.000 | 3.737               | -0.023 |        |       |
| logarithmic | 0.977         | 83.536  | 1   | 0.001 | 3.691               | -0.221 |        |       |
| Growth      | 0.996         | 477.248 | 1   | 0.000 | 1.318               | -0.023 |        |       |
| Reverse     | 0.899         | 16.872  | 1   | 0.015 | 3.273               | 0.430  |        |       |
| Power       | 0.974         | 73.091  | 1   | 0.001 | 3.696               | -0.064 |        |       |
| Logistic    | 0.996         | 477.248 | 1   | 0.000 | 0.268               | 1.023  |        |       |
| S           | 0.893         | 15.662  | 1   | 0.017 | 1.187               | 0.124  |        |       |

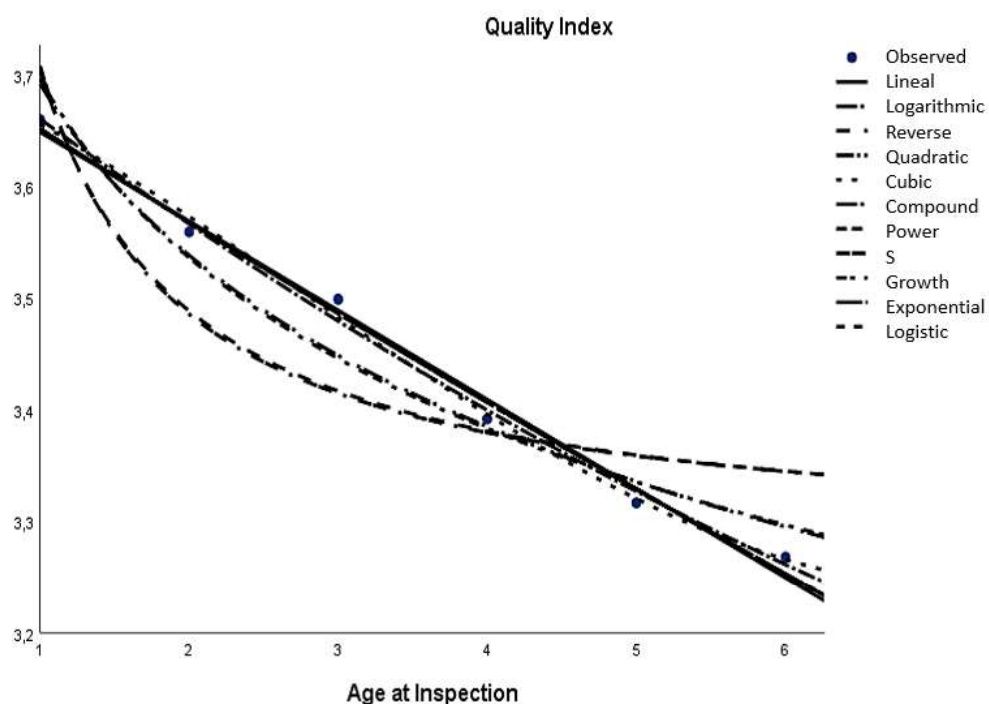
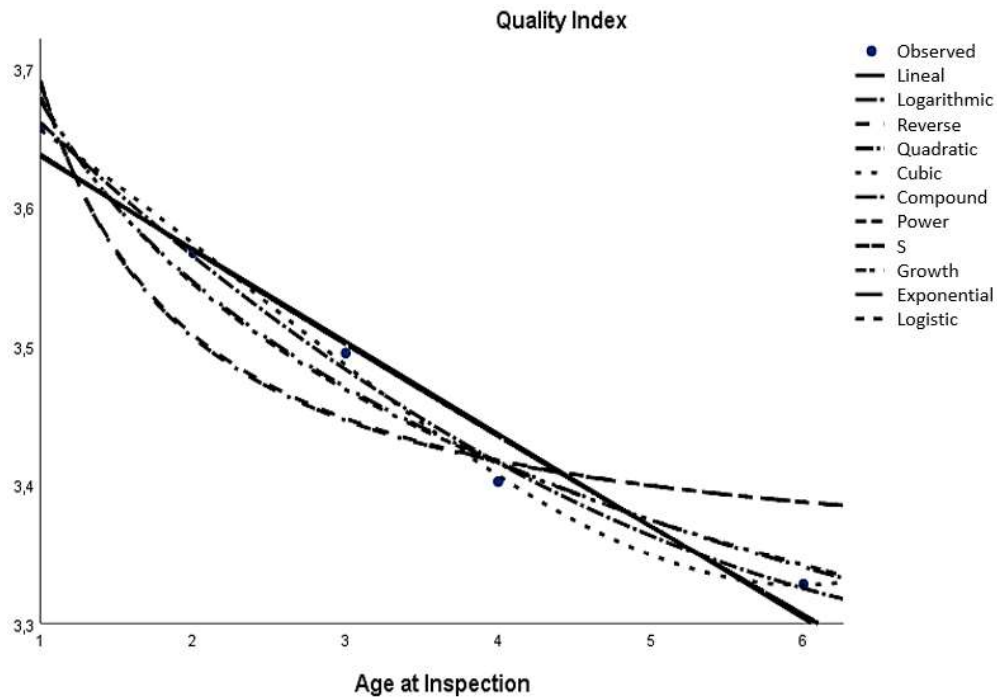


**Table 1- 22. Regression models for Principal routes, Santarem and AADT>12500**

| Equation    | Model Summary |         |     |       | Parameter Estimates |        |        |       |
|-------------|---------------|---------|-----|-------|---------------------|--------|--------|-------|
|             | R Square      | F       | df1 | Sig.  | Constant            | b1     | b2     | b3    |
| Lineal      | 0.983         | 86.130  | 1   | 0.003 | 3.703               | -0.067 |        |       |
| Quadratic   | 0.997         | 190.848 | 2   | 0.005 | 3.771               | -0.118 | 0.007  |       |
| Cubic       | 0.999         | 158.294 | 3   | 0.058 | 3.717               | -0.047 | -0.017 | 0.002 |
| Compound    | 0.985         | 97.485  | 1   | 0.002 | 3.708               | 0.981  |        |       |
| Exponential | 0.985         | 97.485  | 1   | 0.002 | 3.708               | -0.019 |        |       |
| logarithmic | 0.987         | 112.863 | 1   | 0.002 | 3.676               | -0.187 |        |       |
| Growth      | 0.985         | 97.485  | 1   | 0.002 | 1.310               | -0.019 |        |       |
| Reverse     | 0.919         | 16.384  | 1   | 0.027 | 3.327               | 0.361  |        |       |
| Power       | 0.985         | 98.312  | 1   | 0.002 | 3.679               | -0.054 |        |       |
| Logistic    | 0.985         | 97.485  | 1   | 0.002 | 0.270               | 1.019  |        |       |
| S           | 0.914         | 15.260  | 1   | 0.030 | 1.203               | 0.103  |        |       |



After verifying the assumptions for each model. The models suggested for pavement degradation model over time are summarized in table 1- 23.

**Table 1- 23. Regression models for Quality Index degradation**

| ID            | Model Summary |          |          | Parameter Estimates |        |        |
|---------------|---------------|----------|----------|---------------------|--------|--------|
|               | Equation      | R Square | Constant | b1                  | b2     | b3     |
| NR-C<2.5      | Cubic         | 0.982    | 8.467    | -0.539              | 0.001  |        |
| NR-L<2.5      | Cubic         | 1.000    | 3.470    | -0.113              | 0.043  | -0.007 |
| NR-S<2.5      | Exponential   | 0.988    | 3.396    | -0.066              |        |        |
| NR-L-2.5-7.5  | Lineal        | 0.991    | 0.991    | 5.000               | -0.085 |        |
| NR-S-2.5-7.5  | Exponential   | 0.997    | 3.427    | -0.030              |        |        |
| NR-S>7.5      | Cubic         | 1.000    | 3.563    | -0.081              | 0.027  | -0.005 |
| DnR-S<2.5     | Lineal        | 0.986    | 3.200    | -0.053              |        |        |
| DnR-S-2.5-7.5 | Lineal        | 0.998    | 3.301    | -0.138              |        |        |
| DnR-S>7.5     | Exponential   | 0.996    | 3.779    | -0.016              |        |        |
| RR-C<2.5      | Exponential   | 0.996    | 2.863    | -0.012              |        |        |
| RR-L<2.5      | Quadratic     | 0.997    | 4.410    | -0.073              | 0.000  |        |
| RR-S-2.5-7.5  | Cubic         | 7.708    | -1.931   | 0.261               | -0.012 |        |
| CR-L>7.5      | Exponential   | 0.993    | 4.418    | -0.015              |        |        |
| CR-S>7.5      | Quadratic     | 0.995    | 3.807    | 0.038               | -0.008 |        |
| CR-S-7.5-12.5 | Cubic         | 1.000    | 3.357    | -0.316              | 0.136  | 0.0183 |
| CR-S>12.5     | Exponential   | 0.984    | 3.414    | -0.035              |        |        |
| PR-S-7.5-12.5 | Exponential   | 0.996    | 3.737    | -0.023              |        |        |
| PR-S>12.5     | Exponential   | 0.985    | 3.708    | -0.019              |        |        |

## Appendix 2. Stochastic Models

The complementary results obtained from the application of the Markov Chains predictive model to the roadway and railway databases described in Chapter 2.1.1 are herein presented for each bridge component.

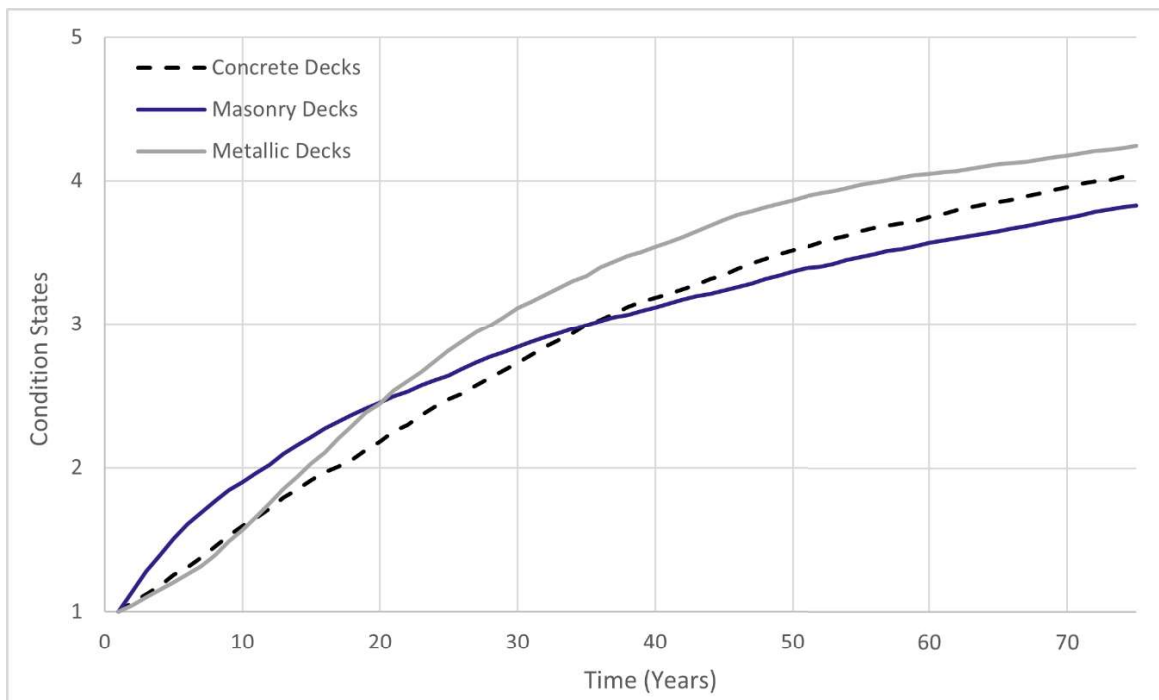


**Figure 2- 1 Performance Prediction of railway bridge decks through MC models**

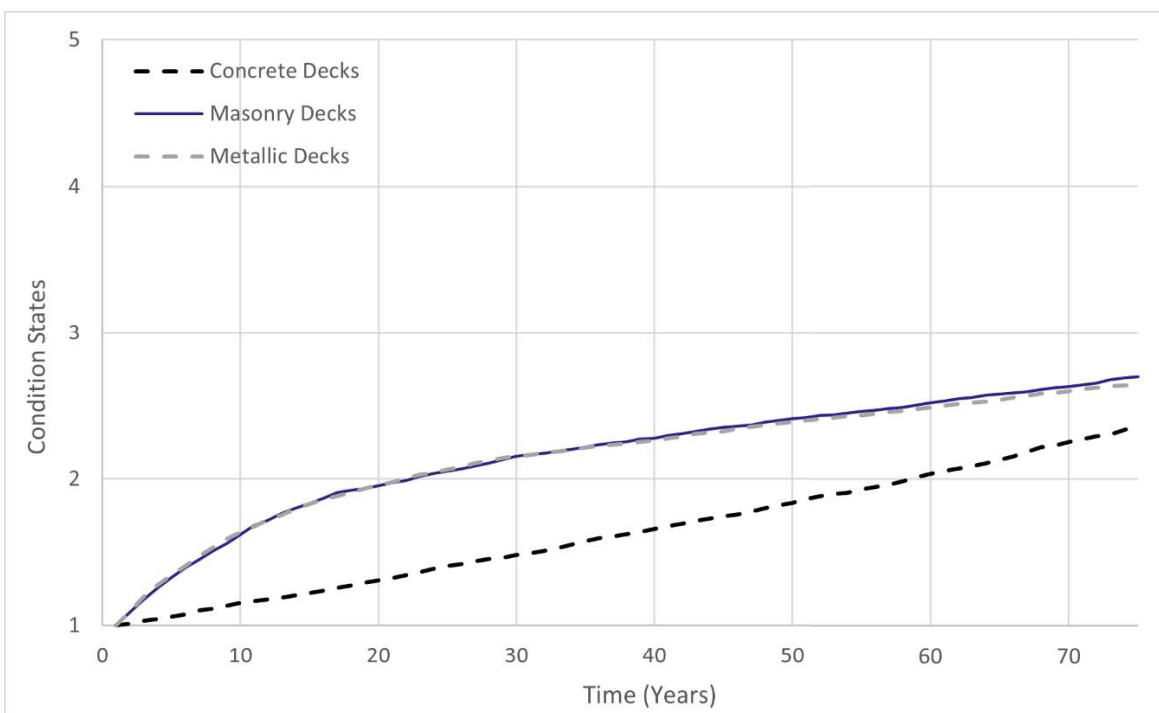


**Figure 2- 2 Performance Prediction of roadway bridge decks through MC models**

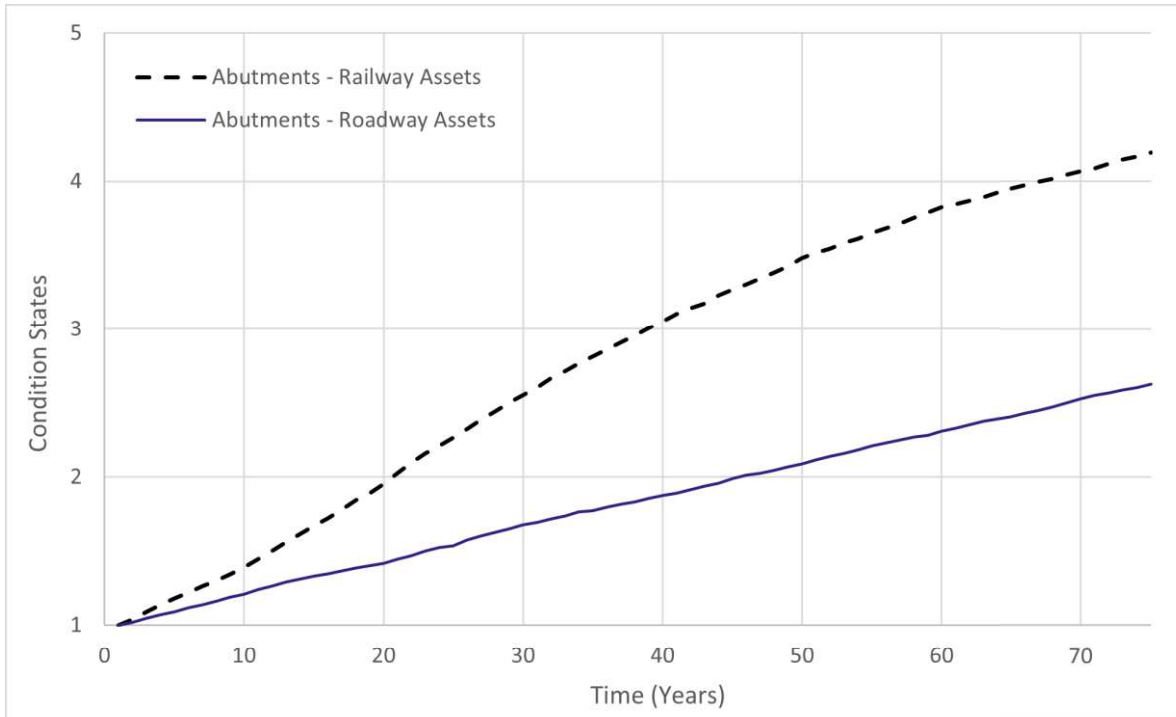


**Figure 2- 3 Performance Prediction of bridge abutments through MC models**

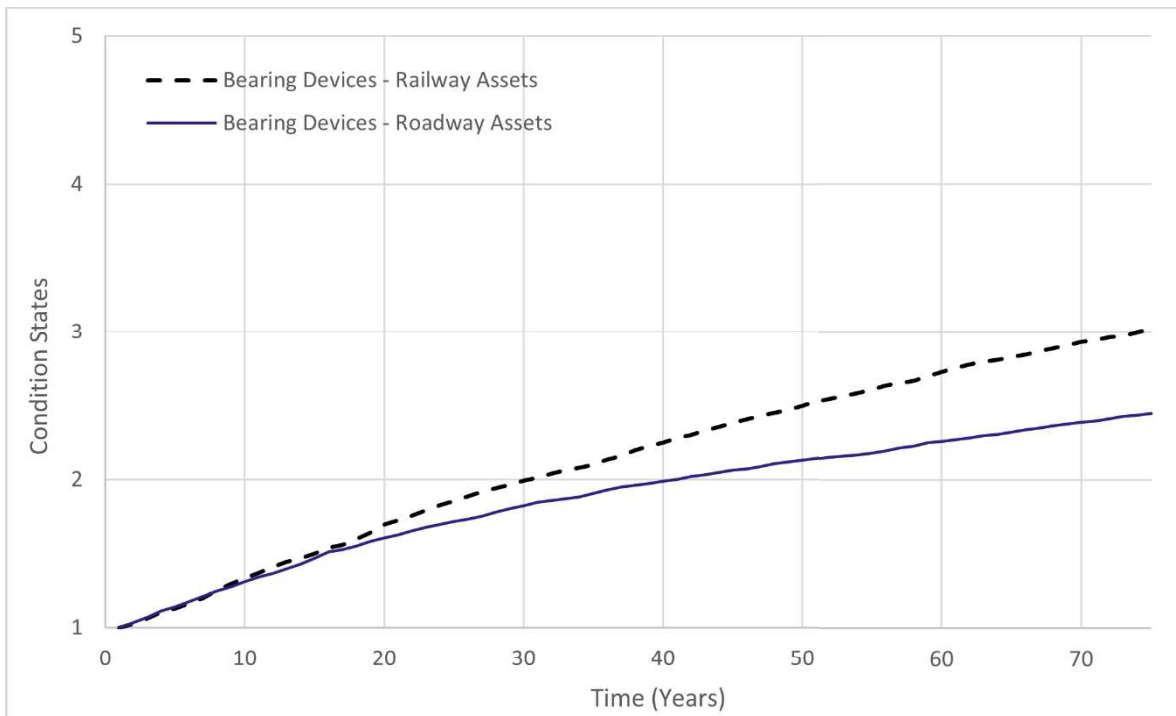


**Figure 2- 4 Performance Prediction of bridge bearing devices through MC models**



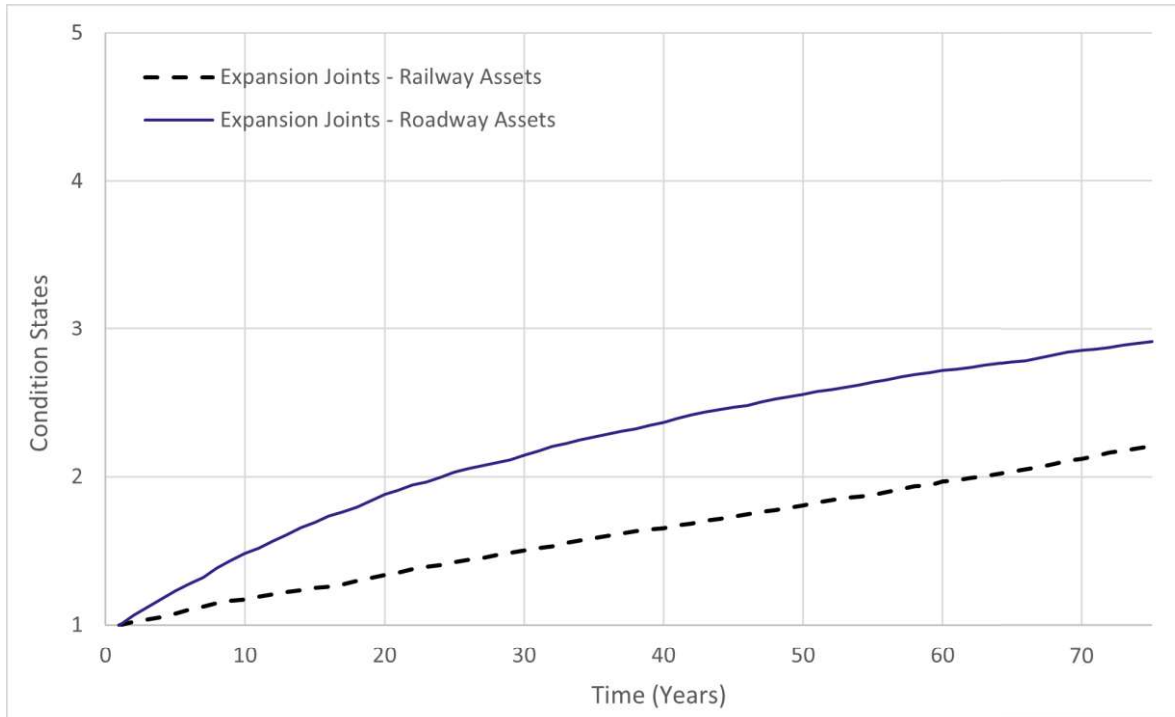


**Figure 2- 5 Performance Prediction of bridge expansion joints through MC models**

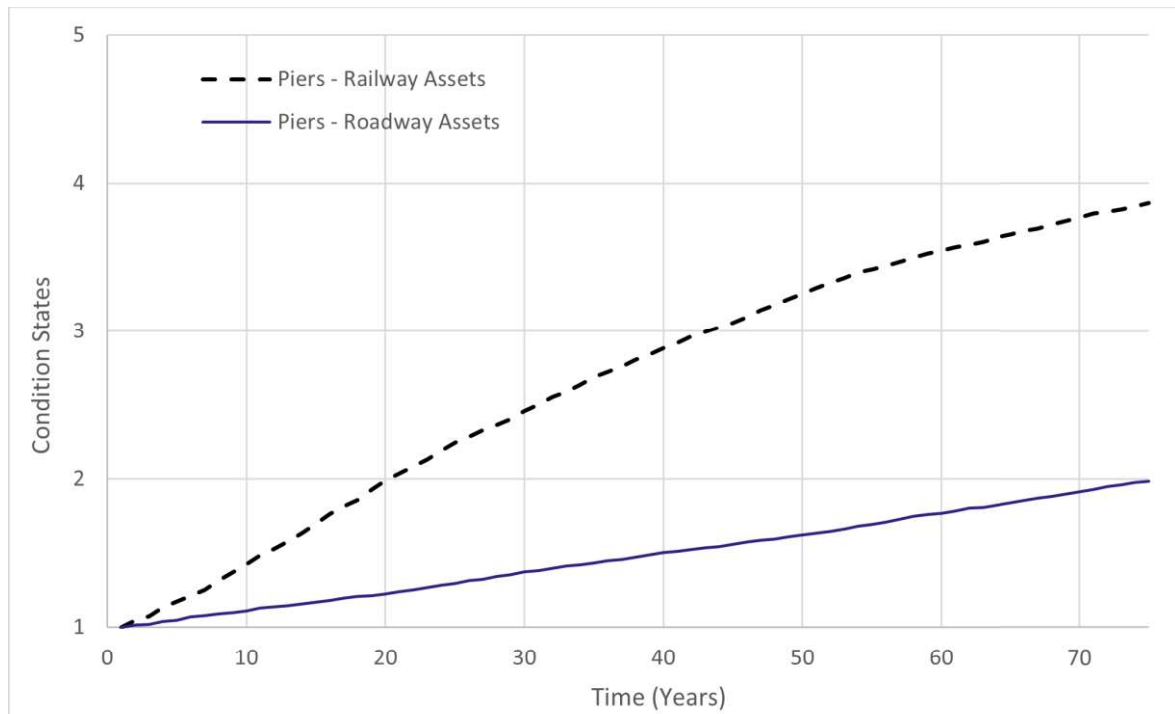


**Figure 2- 6 Performance Prediction of bridge piers through MC models**

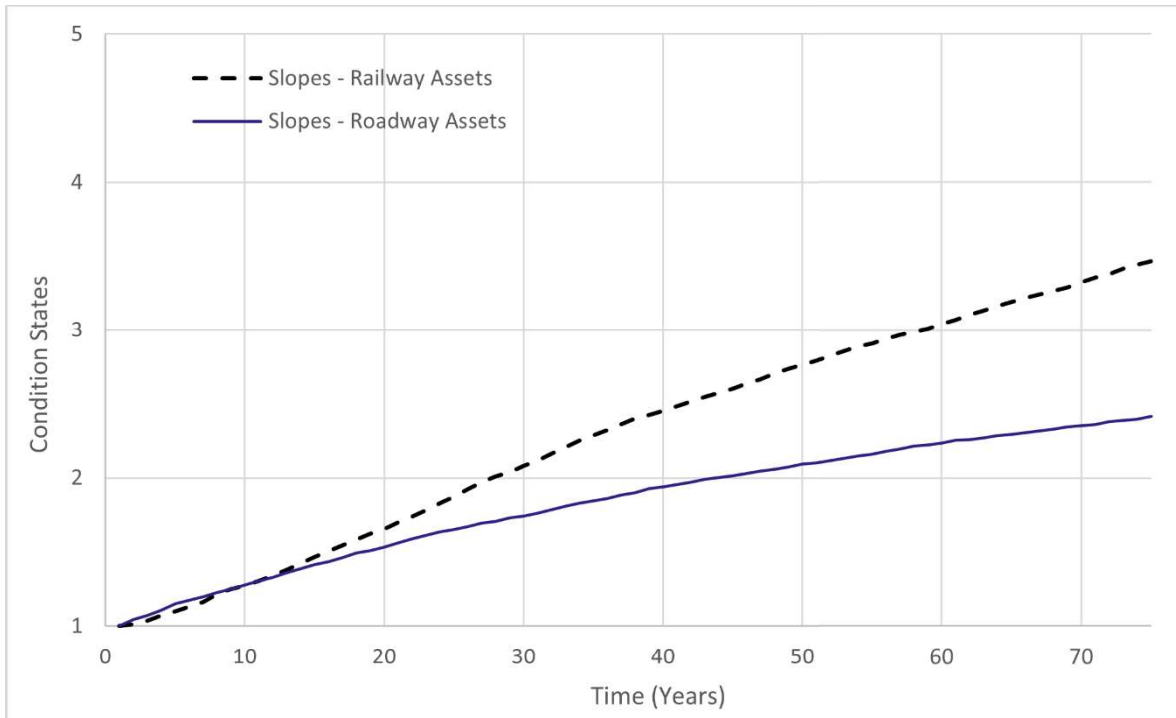


**Figure 2- 7 Performance Prediction of bridge slopes through MC models**

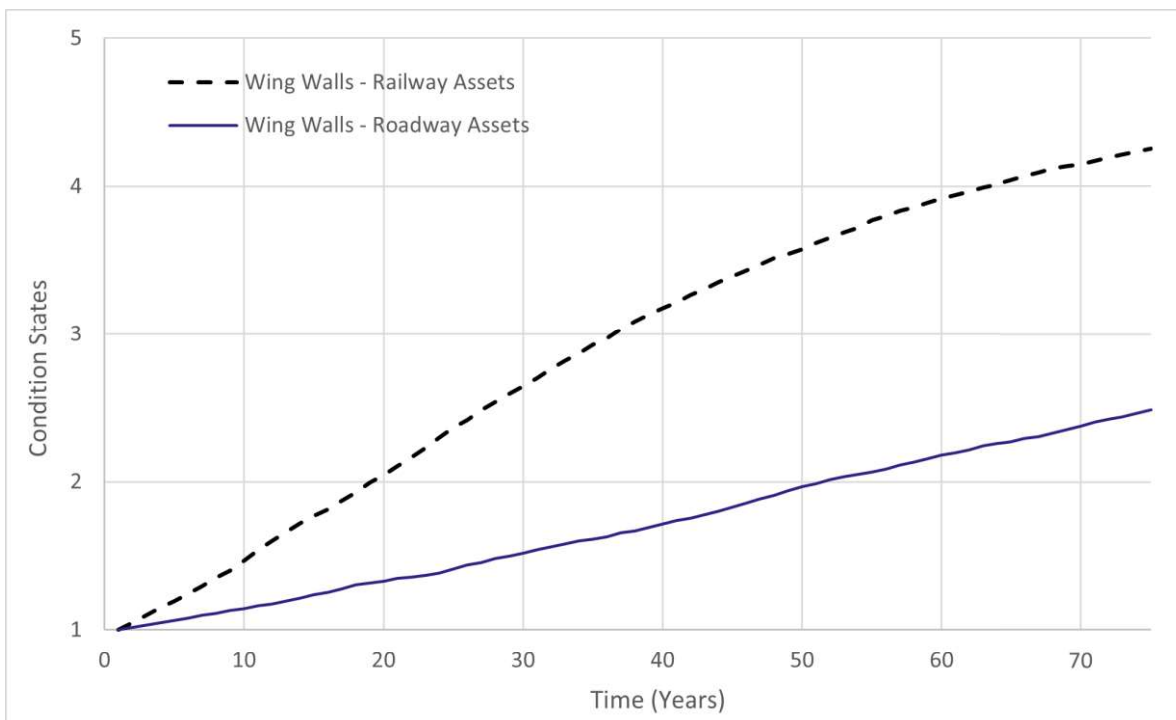


**Figure 2- 8 Performance Prediction of bridge wing walls through MC models**

## Appendix 3. Fragility functions

**Table 3- 1. Probabilistic parameters of RVs for the capacity (Moreira et al., 2016)**

| Material        | Parameter                            | Mean value              | CoV (%) | Distribution |
|-----------------|--------------------------------------|-------------------------|---------|--------------|
| Masonry units   | Unit weight ( $\gamma_m$ )           | 25 [kN/m <sup>3</sup> ] | 10      | Normal       |
|                 | Compressive strength ( $f_m$ )       | 20 [MPa]                | 20      | Normal       |
| Masonry joints  | Internal friction angle ( $\phi$ )   | 32.6 [°]                | 20      | Normal       |
| Soil backfill   | Unit weight ( $\gamma_s$ )           | 20 [kN/m <sup>3</sup> ] | 10      | Normal       |
|                 | Internal friction angle ( $\phi$ )   | 30 [°]                  | 20      | Normal       |
| Foundation soil | Unit weight ( $\gamma_s$ )           | 14 [kN/m <sup>3</sup> ] | 10      | Normal       |
|                 | Saturated unit weight ( $\gamma_s$ ) | 19 [kN/m <sup>3</sup> ] |         |              |
|                 | Internal friction angle ( $\phi$ )   | 28 [°]                  | 20      | Normal       |

**Table 3- 2. Probabilistic parameters of RVs for the determination of the flood demand (Lagasse et al., 2013)**

| Category             | Parameter                             | Mean value                  | CoV (%) | Distribution |
|----------------------|---------------------------------------|-----------------------------|---------|--------------|
| Hydraulic parameters | Manning roughness coefficient ( $n$ ) | 0.020 [s/m <sup>1/3</sup> ] | 1.5     | Lognormal    |
|                      | Channel bed slope ( $S_0$ )           | 0.01 [m/m]                  | 10      | Normal       |
| Local scour          | Mean size diameter ( $D_{50}$ )       | 64 [mm]                     | 10      | Lognormal    |
|                      | Peak flood duration ( $t$ )           | 8 [hours]                   | 10      | Normal       |
|                      | Model uncertainty ( $\theta_{sc}$ )   | 0.78                        | 20      | Normal       |

## Appendix 4. Population Changes

**Population change - Demographic balance and crude rates at regional level (NUTS 3)**

Last update: 14-05-2020

Table Customization [hide](#)

Labeling:  Codes  Labels  Both  Dimension specific

Cell Formatting:  1,234,56  1,234.56  1 234.56

Hide empty lines  Hide flags/footnotes

TIME GEO

|                              | 2014                | 2015                 | 2016  | 2017  | 2018  |
|------------------------------|---------------------|----------------------|-------|-------|-------|
| Continente                   | -4.9                | -3.1 <sup>(E)</sup>  | -3.0  | -1.7  | -1.3  |
| Norte                        | -6.2                | -5.0 <sup>(E)</sup>  | -5.3  | -2.3  | -1.0  |
| Alto Minho                   | -8.9                | -7.3 <sup>(E)</sup>  | -10.5 | -7.0  | -5.3  |
| Cávado                       | -3.5                | -2.2 <sup>(E)</sup>  | -4.6  | -1.8  | -0.2  |
| Ave                          | -5.0                | -3.4 <sup>(E)</sup>  | -6.6  | -4.4  | -2.9  |
| Area Metropolitana do Porto  | -5.5                | -4.5 <sup>(E)</sup>  | -2.7  | 0.4   | 1.6   |
| Portugal                     | -5.0 <sup>(E)</sup> | -3.2 <sup>(E)</sup>  | -3.1  | -1.8  | -1.4  |
| Alto Tâmega                  | -11.6               | -10.6 <sup>(E)</sup> | -14.9 | -9.0  | -8.0  |
| Tâmega e Sousa               | -5.8                | -4.5 <sup>(E)</sup>  | -6.7  | -5.0  | -3.6  |
| Douro                        | -11.0               | -10.0 <sup>(E)</sup> | -10.5 | -6.0  | -4.9  |
| Terras de Trás-os-Montes     | -12.4               | -12.7 <sup>(E)</sup> | -12.3 | -7.9  | -6.3  |
| Algarve                      | -2.0                | 1.0 <sup>(E)</sup>   | -1.0  | -4.2  | -1.7  |
| Algarve                      | -2.0                | 1.0 <sup>(E)</sup>   | -1.0  | -4.2  | -1.7  |
| Centro (PT)                  | -7.6                | -3.4 <sup>(E)</sup>  | -5.5  | -5.6  | -6.6  |
| Oeste                        | -4.6                | 0.4 <sup>(E)</sup>   | -1.6  | -0.9  | -2.6  |
| Região de Aveiro             | -4.5                | -0.4 <sup>(E)</sup>  | -1.5  | -1.8  | -2.7  |
| Região de Coimbra            | -8.8                | -4.8 <sup>(E)</sup>  | -5.4  | -5.8  | -6.7  |
| Região de Leiria             | -5.7                | -0.8 <sup>(E)</sup>  | -5.0  | -5.1  | -6.4  |
| Viseu Dão Lafões             | -7.9                | -3.4 <sup>(E)</sup>  | -8.7  | -9.0  | -9.5  |
| Beira Baixa                  | -14.0               | -9.9 <sup>(E)</sup>  | -10.8 | -11.1 | -12.7 |
| Médio Tejo                   | -9.3                | -5.8 <sup>(E)</sup>  | -6.6  | -6.8  | -7.7  |
| Beiras e Serra da Estrela    | -12.6               | -9.6 <sup>(E)</sup>  | -12.7 | -12.7 | -13.3 |
| Area Metropolitana de Lisboa | 0.6                 | 1.2 <sup>(E)</sup>   | 3.1   | 4.4   | 4.5   |
| Area Metropolitana de Lisboa | 0.6                 | 1.2 <sup>(E)</sup>   | 3.1   | 4.4   | 4.5   |
| Alentejo                     | -13.5               | -12.3 <sup>(E)</sup> | -8.7  | -8.6  | -9.1  |
| Alentejo Litoral             | -11.2               | -11.2 <sup>(E)</sup> | -6.2  | -5.5  | -5.5  |
| Baixo Alentejo               | -14.2               | -14.3 <sup>(E)</sup> | -9.2  | -9.8  | -11.2 |
| Lezíria do Tejo              | -10.6               | -9.1 <sup>(E)</sup>  | -5.9  | -5.3  | -5.9  |
| Alto Alentejo                | -18.2               | -16.6 <sup>(E)</sup> | -15.1 | -14.2 | -14.8 |
| Alentejo Central             | -15.3               | -13.3 <sup>(E)</sup> | -9.8  | -10.8 | -10.9 |
| Região Autónoma dos Açores   | -4.4                | -2.4 <sup>(E)</sup>  | -2.0  | -5.8  | -4.2  |
| Região Autónoma dos Açores   | -4.4                | -2.4 <sup>(E)</sup>  | -2.0  | -5.8  | -4.2  |
| Região Autónoma dos Açores   | -4.4                | -2.4 <sup>(E)</sup>  | -2.0  | -5.8  | -4.2  |
| Região Autónoma da Madeira   | -10.1               | -8.8 <sup>(E)</sup>  | -6.1  | -2.0  | -1.7  |
| Região Autónoma da Madeira   | -10.1               | -8.8 <sup>(E)</sup>  | -6.1  | -2.0  | -1.7  |
| Região Autónoma da Madeira   | -10.1               | -8.8 <sup>(E)</sup>  | -6.1  | -2.0  | -1.7  |

Figure 4- 1. Extraction of data from Eurostat

**Table 4- 1. Calculation of the relevant NUTS3-level 5-year averages**

| <b>GEO/TIME</b>                 | <b>2014</b> | <b>2015</b> | <b>2016</b> | <b>2017</b> | <b>2018</b> | <b>5 Year</b> | <b>Average</b> |
|---------------------------------|-------------|-------------|-------------|-------------|-------------|---------------|----------------|
| Portugal                        | -5.0        | -3.2        | -3.1        | -1.8        | -1.4        | -14.5         | -2.9           |
| Continente                      | -4.9        | -3.1        | -3.0        | -1.7        | -1.3        | -14.0         | -2.8           |
| Norte                           | -6.2        | -5.0        | -5.3        | -2.3        | -1.0        | -19.8         | -3.96          |
| Alto Minho                      | -8.9        | -7.3        | -10.5       | -7.0        | -5.3        | -39.0         | -7.8           |
| Cávado                          | -3.5        | -2.2        | -4.6        | -1.8        | -0.2        | -12.3         | -2.46          |
| Ave                             | -5.0        | -3.4        | -6.6        | -4.4        | -2.9        | -22.3         | -4.46          |
| Área Metropolitana do Porto     | -5.5        | -4.5        | -2.7        | 0.4         | 1.6         | -10.7         | -2.14          |
| Alto Tâmega                     | -11.6       | -10.6       | -14.9       | -9.0        | -8.0        | -54.1         | -10.82         |
| Tâmega e Sousa                  | -5.8        | -4.5        | -6.7        | -5.0        | -3.6        | -25.6         | -5.12          |
| Douro                           | -11.0       | -10.0       | -10.5       | -6.0        | -4.9        | -42.4         | -8.48          |
| Terras de Trás-os-Montes        | -12.4       | -12.7       | -12.3       | -7.9        | -6.3        | -51.6         | -10.32         |
| Algarve                         | -2.0        | 1.0         | -1.0        | -4.2        | -1.7        | -7.9          | -1.58          |
| Algarve                         | -2.0        | 1.0         | -1.0        | -4.2        | -1.7        | -7.9          | -1.58          |
| Centro (PT)                     | -7.6        | -3.4        | -5.5        | -5.6        | -6.6        | -28.7         | -5.74          |
| Oeste                           | -4.6        | 0.4         | -1.6        | -0.9        | -2.6        | -9.3          | -1.86          |
| Região de Aveiro                | -4.5        | -0.4        | -1.5        | -1.8        | -2.7        | -10.9         | -2.18          |
| Região de Coimbra               | -8.8        | -4.8        | -5.4        | -5.8        | -6.7        | -31.5         | -6.3           |
| Região de Leiria                | -5.7        | -0.8        | -5.0        | -5.1        | -6.4        | -23.0         | -4.6           |
| Viseu Dão Lafões                | -7.9        | -3.4        | -8.7        | -9.0        | -9.5        | -38.5         | -7.7           |
| Beira Baixa                     | -14.0       | -9.9        | -10.8       | -11.1       | -12.7       | -58.5         | -11.7          |
| Médio Tejo                      | -9.3        | -5.8        | -6.6        | -6.8        | -7.7        | -36.2         | -7.24          |
| Beiras e Serra da Estrela       | -12.6       | -9.6        | -12.7       | -12.7       | -13.3       | -60.9         | -12.18         |
| Área Metropolitana de Lisboa    | 0.6         | 1.2         | 3.1         | 4.4         | 4.5         | 13.8          | 2.76           |
| Área Metropolitana de Lisboa    | 0.6         | 1.2         | 3.1         | 4.4         | 4.5         | 13.8          | 2.76           |
| Alentejo                        | -13.5       | -12.3       | -8.7        | -8.6        | -9.1        | -52.2         | -10.44         |
| Alentejo Litoral                | -11.2       | -11.2       | -6.2        | -5.5        | -5.5        | -39.6         | -7.92          |
| Baixo Alentejo                  | -14.2       | -14.3       | -9.2        | -9.8        | -11.2       | -58.7         | -11.74         |
| Lezíria do Tejo                 | -10.6       | -9.1        | -5.9        | -5.3        | -5.9        | -36.8         | -7.36          |
| Alto Alentejo                   | -18.2       | -16.6       | -15.1       | -14.2       | -14.8       | -78.9         | -15.78         |
| Alentejo Central                | -15.3       | -13.3       | -9.8        | -10.8       | -10.9       | -60.1         | -12.02         |
| Região Autónoma dos Açores (PT) | -4.4        | -2.4        | -2.0        | -5.8        | -4.2        | -18.8         | -3.76          |

| <b>GEO/TIME</b>                 | <b>2014</b> | <b>2015</b> | <b>2016</b> | <b>2017</b> | <b>2018</b> | <b>5 Year</b> | <b>Average</b> |
|---------------------------------|-------------|-------------|-------------|-------------|-------------|---------------|----------------|
| Região Autónoma dos Açores (PT) | -4.4        | -2.4        | -2.0        | -5.8        | -4.2        | -18.8         | -3.76          |
| Região Autónoma dos Açores (PT) | -4.4        | -2.4        | -2.0        | -5.8        | -4.2        | -18.8         | -3.76          |
| Região Autónoma da Madeira (PT) | -10.1       | -8.8        | -6.1        | -2.0        | -1.7        | -28.7         | -5.74          |
| Região Autónoma da Madeira (PT) | -10.1       | -8.8        | -6.1        | -2.0        | -1.7        | -28.7         | -5.74          |
| Região Autónoma da Madeira (PT) | -10.1       | -8.8        | -6.1        | -2.0        | -1.7        | -28.7         | -5.74          |